



4D EVOLUTION OF THE OROGENIC GOLD DISTRICT OF

SIGUIRI, GUINEA (WEST AFRICA)

ERWANN O. LEBRUN

M.SCI, Université du Québec à Montréal and Institut des Sciences de la Terre d'Orléans

This thesis is presented for the degree of Doctor of Philosophy.



Centre for Exploration Targeting
ARC Centre for Core to Crust Fluid Systems (CCFS)
School of Earth and Environment
University of Western Australia

July 2015

Supervisors:
Dr Nicolas Thébaud (coordinating)
Dr Stanislav Ulrich
Professor John Miller
Professor T. Campbell McCuaig



All work presented in this thesis is original, and that of the candidate, unless otherwise acknowledged, specified or referenced

.....
Erwann LEBRUN
24th July 2015

We hereby declare the individual authors have granted permission to the candidate (Erwann LEBRUN) to use the results presented in the publications

Candidate

Signature Date

Name

Coordinating Supervisor

Signature Date

Name

À maman et Jean-Luc.
Ça y est, c'est enfin *l'heure des mamans* !

ABSTRACT

The West African Craton hosts some of the biggest gold deposits in the world such as Obuasi, Sadiola, Morila or Siguiri. However, the Craton is still largely unexplored and its formation, evolution and how and when the gold deposits it hosts developed during the Eburnean orogeny remain unclear. The Siguiri district is one of West Africa's largest Paleoproterozoic sedimentary basins and sits in the northern part of the Siguiri Basin. The district and its hosting Basin have received limited attention from the scientific community to date. This thesis makes use of a multi-scale and multi-disciplinary approach in order to constrain the evolution of the Siguiri district and Siguiri Basin architecture and hydrothermal activity through time. The objective is to provide the backbone of future exploration strategies for orogenic gold deposits in the Siguiri Basin and, potentially, in the rest of the West African Craton.

Fieldwork was undertaken in eleven deposits of the Siguiri district. Particular attention was given to the Sintroko PB1, Kosise, Kami, Bidini and Sanu Tinti deposits due to their structural complexity, lithostratigraphic position, outcropping conditions and accessibility. Work was focused on structural mapping, lithofacies recognition, core logging, geochemical sampling, GIS and 3D modelling. In addition to the data collected in the Siguiri district, regional fieldwork was also carried out in the rest of the Siguiri Basin for geochronological sampling and regional mapping.

Regional and district scale geochronological sampling and lithofacies observations indicate that the central Siguiri Basin is of Lower Tarkwa Group age (ca. 2015 Ma) and deposited late during the Eburnean orogeny. Lithostratigraphic observations from the Siguiri district indicate that the district is hosted in three distinct sedimentary Formations (the Balato, Fatoya and Kintinian Formations). Stacks of polymict conglomerate in the Kintinian Formation, interpreted to be olistostrome deposits, were interpreted as marking the onset of the Eburnean compression and highlight the early architecture and fundamental structures

controlling the morphology of the Siguiri Basin. These fundamental structures are viewed as the first order structures controlling the location of the world-class Siguiri district in the eponym Basin.

District to deposit scale structural work indicates that the Siguiri district underwent four deformation events: a N-S compression (D_{1S}), an E-W compression (D_{2S}) progressively evolving into a transpression and later on into a transtension (early- and late- D_{3S} respectively), and a NW-SE compression (D_{4S}). While D_{1S} deformation is cryptic and commonly expressed as F_{1S} recumbent folds with E-W to NW-SE and NE-SW striking axial traces, D_{2S} is typically characterised by F_{2S} upright folds with NNE-SSW to NNW-SSE striking axial planes that refolds F_{1S} folds and are responsible for the bulk of the deformation and structural grain observed in the Siguiri district and Siguiri Basin. The F_{2S} folds are overprinted by four main orientations of structures that develop (or are reactivated) during the early stages of D_{3S} deformation and are consistent with a transpressional deformation: N-S thrusts, E-W normal faults, NE-SW dextral shear zones and WNW-ESE sinistral shear zones. In field exposures and in drill core, these structures are typically discreet and only expressed as sub-vertical damage zones ten to fifteen meters wide and characterised by an increase in vein density or by disseminated pyrite. The veins that developed along these structures are commonly found to be conjugate and their orientation is consistent with a transtensional deformation. These late- D_{3S} veins are overprinted by the sub-vertical NE-SW striking S_{4S} cleavage that characterises the D_{4S} deformation event. Based on finite strain analysis of D_{2S} structural elements and paleo stress-field reconstruction from early- D_{3S} faults and late- D_{3S} conjugate veins, two stress-switches were identified in the Siguiri district. These stress-switches are also documented at a regional scale and highlight the homogenisation of the stress-tensor prior to gold mineralisation. This process is postulated to occur in numerous orogenic gold deposits around the world and may be a pre-requisite for orogenic gold mineralisation.

Deposit to microscopic scale work indicate that hydrothermal activity in the Siguiri district was polyphase and that gold mineralisation developed over three distinct periods. Gold

was first found to be associated with early ankerite-pyrite veins, developed late during D_{3S} deformation. In these veins, LA-ICP-MS data shows that gold is locked in the pyrite crystal lattice. The second and main episode of mineralisation also occurs late during D_{3S} deformation and is associated with the later quartz-ankerite-arsenopyrite-(pyrite) veins, which crosscut the early ankerite-pyrite veins and are coeval with pyrite dissemination in conglomerate layers. Gold is either found native in the veins or invisible and locked in the vein-hosted arsenopyrite crystal lattice. The last gold event is associated with the D_{4S} deformation, which fractures previously developed sulphides and precipitate free gold in their fractures. The geochemical footprint of gold mineralisation in the Siguiri district was recognised to be associated with a wide halo of at least fifteen meters, enriched in: Ag, Au, As, Bi, Co, LOI, Mo, Sb, Se, SO₃, Te and W, typical of orogenic gold mineralisation. Comparison of the characteristics and timing of gold mineralisation in the Siguiri district with other gold deposits from the West African Craton indicates that gold mineralisation in Siguiri is coeval with mineralisation in other gold deposits. However, other orogenic gold deposits in the West African Craton are associated with later gold events that may have formed economic concentrations in the rest of the Siguiri Basin.

The conclusions from this multi-scale multi-disciplinary work have implications for exploration targeting in and around the Siguiri Basin. This thesis highlights the importance of the early architecture as a first order control on orogenic gold systems. The expression of the second and third order structures controlling the mineralisation are thought to develop in response to regional stress-switches that can be recognised in the field. Finally, at a deposit scale, high grade zones can be targeted by geochemistry. This thesis hence shows the power of multiscale and multi-disciplinary studies to unravel the complexity of mineral systems and provide a critical understanding that can be used as a foundation for new exploration strategies.

TABLE OF CONTENTS

<i>Section</i>	<i>Page</i>
ABSTRACT	5
TABLE OF CONTENTS	9
TABLE OF FIGURES	13
ACKNOWLEDGEMENTS	25
CHAPTER 1: INTRODUCTION	29
PREAMBLE AND KNOWLEDGE GAPS	29
AIMS OF THESIS	33
GENERAL METHODOLOGY	34
Fieldwork and sampling	34
Analytical techniques	36
ORGANISATION OF THIS THESIS	37
JUSTIFICATION OF THESIS FORMAT AND AUTHORSHIP	39
SUPPORTING REFERENCES	41
Publications	41
Peer reviewed extended abstracts	41
Short communications	41
REFERENCES	42
CHAPTER 2: PAPER ONE	49
Abstract:	51
Introduction	53
Geological context	54
Regional Geology	54
Structural framework	57
Methodology	58
Fieldwork and sample selection	58
Geophysical data	58
Geochronology	61
Results	62
The Siguiri district lithostratigraphy	62

Geological map and regional stratigraphic integration	69
U-Pb detrital zircon geochronology	71
Discussion	80
Depositional environments of the Siguiri district	80
The Siguiri district geochronology in the West African context	83
The Kintinian Formation – a Tarkwa Group sequence?	86
Early architecture of the Siguiri Basin and orogenic gold systems	87
Conclusion	89
Acknowledgements	89
References	90
 CHAPTER 3: PAPER TWO	 100
 Abstract:	 102
 Introduction	 104
 Geological context and exploration history	 105
 Methodology	 110
 Key deposits of the Siguiri district	 111
Bidini	111
Sanu Tinti	121
Kami and Kosise	122
Sintroko PB1	126
 Discussion	 128
Structural event history	128
Mineralization	135
Stress-field evolution during D _{2S} and early-D _{3S}	139
Transpressional model for the Siguiri District	140
Localized stress switches associated with late-D _{3S} mineralized veining	142
Stress-switches, precursors or triggers to mineralization	143
Geodynamic interpretation and drivers of stress-switches	144
 Conclusion	 146
 Acknowledgements	 147
 References	 147
 CHAPTER 4: PAPER THREE	 156
 Abstract:	 158
 Introduction	 160
 Geological context	 161

Methodology	167
Field approach and sampling	167
Analytical work and data processing	168
Results	172
Bidini	172
Sintroko PB1	179
Kosise	183
Whole-rock multi-element geochemistry	186
LA-ICP-MS and EPMA	191
Discussion	194
Polyphase hydrothermal activity and gold mineralisation	194
Geochemical footprint of the ore shoots	198
Mineralising fluids	199
Comparison with other West African orogenic gold deposits	200
Conclusion	203
Acknowledgements	205
References	205
CHAPTER 5: CONCLUSIONS	214
LITHOSTRATIGRAPHY AND TECTONICS	215
DEFORMATION EVENTS	216
HYDROTHERMAL ACTIVITY, MINERALISATION AND GEOCHEMISTRY	217
CONCLUDING REMARKS AND FUTURE WORK	218
ELECTRONIC APPENDICES	221

TABLE OF FIGURES

<i>Figure number and figure caption</i>	<i>Page</i>
FIGURE 1: GEOLOGICAL MAP OF A) THE WEST AFRICAN CRATON AND ITS GOLD DEPOSITS (RED DISKS), AND; B) THE SIGUIRI BASIN. MODIFIED FROM MILÉSI ET AL. (1989) AND MILLER ET AL. (2013).	30
FIGURE 2: GEOLOGY MAP OF THE SIGUIRI DISTRICT AND ITS DEPOSITS. AFTER CHAPTER 3.	35
FIGURE 3: A) GEOLOGICAL MAP OF THE WEST AFRICAN CRATON. OROGENIC GOLD DEPOSITS ARE DISPLAYED AS SMALL RED DISCS. B) GEOLOGICAL MAP OF THE SIGUIRI BASIN. LOCATION OF THE SIGUIRI DISTRICT MAP IN RED. LOCATION OF THE SARAYA GEOCHRONOLOGICAL SAMPLE, SI326, IN WHITE. MODIFIED FROM MILÉSI ET AL. (1989) AND MILLER ET AL. (2013).	55
FIGURE 4: STRUCTURAL SCHEME OF THE DEFORMATION HISTORY OBSERVED IN THE SIGUIRI DISTRICT. THE E-W COMPRESSION D _{2S} EVOLVES PROGRESSIVELY TO A TRANSTENSION RESPONSIBLE FOR GOLD MINERALISATION IN SIGURI, D _{3S} . AFTER THE WORK FROM LEBRUN ET AL. (IN REVIEW 2015); CHAPTER 3.	57
FIGURE 5: A) GEOLOGICAL MAP OF THE SIGUIRI DISTRICT TENEMENT AS INTERPRETED FROM THE SPECTREM AEM TAU PRODUCTS. DEPOSITS ARE STRUCTURALLY CONTROLLED AND MOSTLY HOSTED IN THE FATOYA FORMATION (LEBRUN ET AL., IN REVIEW 2015; CHAPTER 3). THE LOCATION OF EACH GEOCHRONOLOGICAL SAMPLE IS REPORTED ON THE MAP. SAMPLE SI326 WAS SAMPLED FURTHER WEST (FIGURE 3B). THE BLUE OUTLINE REPRESENTS THE SIGUIRI TENEMENT BOUNDARIES. B) SPECTREM LATE-TIME TAU OF THE Z-COMPONENT (MAXIMUM TAU FOR Z-CHANNEL 5-8) WITH OVERLAIN SEDIMENTARY FORMATION BOUNDARIES, FAULTS AND SIGUIRI TENEMENT BOUNDARIES.	59
FIGURE 6: CORE PHOTOGRAPHS FROM: THE BALATO FORMATION (A), SHOWING MASSIVE, DARK GREY SHALES; THE FATOYA FORMATION (B, C, D) SHOWING THIN-BEDDED, FINING-UPWARD TURBIDITES WITH MASSIVE TO CROSS-LAMINATED GREYWACKE BASES GRADING TO SILTSTONE AND MUDSTONE (T _{C-E} OF THE BOUMA SEQUENCE); THE KINTINIAN FORMATION, SHOWING (E) THE BASAL POLYMICT CONGLOMERATES OBSERVED IN THE SANU TINTI DEPOSIT AND (F) THE	

UPPER MASSIVE DARK-GREEN SHALES WITH CM-THICK, LIMESTONE INTERBEDS. C: CLAST; L: LIMESTONE INTERBEDS; M: MATRIX; QV: QUARTZ VEIN. 63

FIGURE 7: FIELD PHOTOGRAPHS OF (A) RIPPLE MARKS IN THE KAMI DEPOSIT, FATOYA FORMATION; (B) RIP-UP CLASTS OF SHALE AT THE BASE OF A TURBIDITE (GREYWACKE) BED IN THE FATOYA FORMATION; (C) CM TO DM-THICK BEDDED GREYWACKE TURBIDITES IN THE FATOYA FORMATION ASSOCIATED WITH BASAL EROSIONAL (SCOUR) SURFACES (WHITE ARROWS);(D) BASAL CONGLOMERATE OF THE KINTINIAN FORMATION SHOWING THE POLYMICT, POORLY-SORTED, ANGULAR TO SUB-ROUNDED CLASTS DOMINATED BY GREYWACKE/SHALE INTERBEDS AND SHALE (LIKELY SOURCED FROM THE BALATO AND FATOYA FORMATIONS). 64

FIGURE 8: PHOTOGRAPHS OF A) THE SARAYA VOLCANIC BRECCIA; B) MARBLES FROM THE MARBLE HILL LOCATION; AND C) THE CONTACT BETWEEN THE FATOYA AND THE KINTINIAN FORMATION IN THE SEGUELEN DEPOSIT. 65

FIGURE 9: LITHOSTRATIGRAPHIC COLUMN OF THE SIGURI DISTRICT. THIS SYNTHETIC LOG WAS CONSTRUCTED USING SIX DIFFERENT DRILL HOLES SPREAD ACROSS THE DISTRICT. TRUE THICKNESS OF EACH SEDIMENTARY FORMATION IS UNKNOWN. 68

FIGURE 10: GEOLOGICAL MAP OF THE SIGURI BASIN OVERLAIN BY THE MAGNETICS ANALYTICAL SIGNAL AND SHOWING THE SPATIAL CONTINUITY OF THE MAGNETIC CONGLOMERATES THROUGHOUT THE BASIN (HIGHLIGHTED IN RED). THE WSW-STRIKING AND WNW-STRIKING MAGNETIC HIGHS, RESPECTIVELY FOUND IN THE NORTHERN AND SOUTHERN PARTS OF THE BASIN ARE DYKES (FIGURE 4). 70

FIGURE 11: CATHODOLUMINESCENCE IMAGES OF THE REPRESENTATIVE ZIRCONS FOR EACH AGE POPULATION FOR EACH SAMPLE. THESE IMAGES WERE TAKEN AT AN ACCELERATION VOLTAGE OF 10 KV AND WORKING DISTANCE AROUND 14.5 TO 15 MM. 72

FIGURE 12: CONCORDIA PLOTS AND DISTRIBUTION HISTOGRAMS FOR ANALYSED SAMPLES SKRCDD040 237 (A AND B), KMRCDD113 224.5 (C AND D) AND SI241 (E AND F). DATA IN BLACK ARE WITHIN -2 AND +5% DISCORDANCE. EACH COLOUR REPRESENTS A DIFFERENT DETRITAL AGE POPULATION. DISTRIBUTION HISTOGRAM FOR CONCORDANT AND SEMI-CONCORDANT DATA ONLY. 73

FIGURE 13: CONCORDIA PLOTS AND DISTRIBUTION HISTOGRAMS FOR ANALYSED SAMPLES ST1 (A AND B), BDRCDD009 402 (C AND D) AND Si327 (E AND F). DATA IN BLACK ARE WITHIN -2 AND +5% DISCORDANCE. EACH COLOUR REPRESENTS A DIFFERENT DETRITAL AGE POPULATION. DISTRIBUTION HISTOGRAM FOR CONCORDANT AND SEMI-CONCORDANT DATA ONLY.

77

FIGURE 14: SUMMARY DIAGRAM OF THE MAXIMUM DEPOSITION AGES OF EACH DETRITAL SAMPLE AND THE CRYSTALLISATION AGE OF SAMPLE Si326. ALL DETRITAL SAMPLE AGES PLOT AROUND CA. 2105-2130 Ma WHILE SAMPLE Si326 IS CONSISTENT WITH OTHER LATE EBURNEAN MAGMATIC AGES (EGAL ET AL., 1999).

80

FIGURE 15: SIMPLIFIED LITHOSTRATIGRAPHIC AND GEOCHRONOLOGICAL CHART OF SOME KEY AREAS OF THE WEST AFRICAN CRATON. AGES FROM THE SIGUIRI DISTRICT AND SARAYA ARE REPORTED IN THE LEFT COLUMN. MODIFIED FROM: BARATOUX ET AL. (2011), DAVIS ET AL. (2015), LAHONDRE ET AL. (2002), LEBRUN ET AL. (IN REVIEW 2015), PARRA-AVILA ET AL. (THIS VOLUME), PERROUTI ET AL. (2012).

85

FIGURE 16: A) SIMPLIFIED GEOLOGY MAP OF THE SOUTHERN WEST AFRICAN CRATON. RED BOX HIGHLIGHTS THE SIGUIRI BASIN SHOWN IN B. THE SASSANDRA FAULT, BORDERING THE ARCHEAN DOMAIN AND THE SIGUIRI BASIN IS SHOWN AS A THICK BLACK LINE; B) GEOLOGY MAP OF THE SIGUIRI BASIN. RED BOX HIGHLIGHTS THE SIGUIRI DISTRICT SHOWN IN FIGURE 17. RED LINES INDICATE THE SEGMENTS OF THE REGIONAL COMPOSITE CROSS-SECTION (FIGURE 18A). DASHED BLACK LINES REPRESENT THE INTERPRETED REGIONAL EXTENSION OF THE N-S AND WNW-ESE FAULTS CONTROLLING MINERALIZATION IN THE SIGUIRI DISTRICT. MODIFIED FROM MILÉSI ET AL. (1989) AND MILLER ET AL. (2013). C) SIMPLIFIED COMPOSITE E-W CROSS-SECTIONS OF THE SIGUIRI BASIN AND ITS EASTERN BORDER. INTERPRETED CONFORMABLE CONTACTS ARE SYMBOLIZED BY FULL BLACK LINES, UNCONFORMABLE AND UNKNOWN CONTACTS BY DASHED LINES.

106

FIGURE 17: A) FORM LINE MAP, AND; B) STRUCTURAL MAP OF THE SIGUIRI GOLD DISTRICT AND ITS DIFFERENT DEPOSITS CONSTRAINED BY AEROMAGNETICS, MAGNETICS, GRAVIMETRY, DRILL CORE AND FIELD OBSERVATIONS. THE THREE STRUCTURAL DOMAINS FOLLOW THE LITHOSTRATIGRAPHY. RED LINES INDICATE THE SEGMENTS OF THE DISTRICT COMPOSITE CROSS-SECTION SHOWN IN C. C) SIMPLIFIED COMPOSITE E-W CROSS-SECTIONS OF THE SIGUIRI DISTRICT

(DEPOSIT CROSS-SECTIONS IN FIGURE 18). INTERPRETED CONFORMABLE CONTACTS ARE SYMBOLIZED BY FULL BLACK LINES, UNCONFORMABLE AND UNKNOWN CONTACTS BY DASHED LINES.

108

FIGURE 18: DETAILED STRUCTURAL FORM LINE MAPS OF THE A) BIDINI AND SANU TINTI DEPOSITS; B) KAMI DEPOSIT, C) KOSISE DEPOSIT, AND; D) SINTROKO PB1 DEPOSIT. EACH MAP IS ACCCOMPANIED BY THE DEPOSIT CROSS-SECTION, DENOTED IN RED LETTERS. DAMAGE ZONES, DISTINCT AND INCIPENT STRUCTURES ARE ALL REPRESENTED BY A THICK BLACK LINE.

113

FIGURE 19: PHOTOGRAPHS OF FOLDS FROM THE SIGUIRI DISTRICT WITH CORRESPONDING STEREOGRAMS OF STRUCTURAL DATA. ON THE PHOTOGRAPHS, BEDDING IS REPRESENTED BY FULL BLACK LINES, FOLD AXIAL PLANES BY SHORT-DASHED BLACK LINES AND SHEAR ZONE BOUNDARIES BY LONG-DASHED BLACK LINES. IN THE STEREOGRAMS, BEDDING IS REPRESENTED BY BLACK POLES OR FULL BLACK GREAT CIRCLES, CONSTRUCTED FOLD AXIAL PLANES ARE REPRESENTED BY DASHED BLACK GREAT CIRCLES AND CONSTRUCTED FOLD AXES ARE IN YELLOW. FROM TOP-LEFT TO BOTTOM RIGHT: RECUMBENT F_{1s} FOLDS FROM A) BIDINI (THE TRACE OF THE OBSERVED AXIAL PLANAR S_{1s} CLEAVAGE IS ALSO REPRESENTED) AND B) EUREKA NORTH; C) F_{2s} FOLD IN BIDINI; D) THE KOZAN F_{2s} SYNCLINE, THOUGHT TO BE STRUCTURALLY ADJACENT TO THE KOSISE F_{2s} SYNCLINE; E) UPRIGHT F_{2s} FOLD WITH STEEPLY PLUNGING FOLD AXIS FROM SINTROKO PB1. NOTE THE CONSISTENT ORIENTATION OF THE VEINS MINED BY LOCALS (VERTICAL CAVITIES IN WALL) AND THE RHEOLOGICAL CONTROL ON MINERALIZATION (SEAL CAP OF SHALES, IN DARK GREY, WITH STRONG VEINING RESTRICTED TO UNDERLYING SANDSTONES).

114

FIGURE 20: PHOTOGRAPHS OF THE DIFFERENT VEIN GENERATIONS OBSERVED IN SIGUIRI. A) EN-ECHELON BARREN QUARTZ V_{2s} VEINS. THE PROJECTED POLES FROM THE ENTIRE KOSISE DEPOSIT OF BEDDING, V_{2s} BEDDING-PARALLEL AND V_{2s} EN-ECHELON VEINS, HIGHLIGHT THAT ORIENTATIONS AND SIGMOIDAL CHARACTER OF V_{2s} VEINS ARE CONSISTENT WITH THEIR FORMATION BY FLEXURAL SLIP ALONG BEDDING DURING F_{2s} FOLDING. IN THE EQUAL AREA STEREOGRAM/SCHMIDT PROJECTION STEREOGRAM, BEDDING IS REPRESENTED BY BLACK POLES, THE CONSTRUCTED FOLD AXIAL PLANE IS REPRESENTED BY A DASHED BLACK GREAT CIRCLE AND THE CONSTRUCTED FOLD AXIS BY A LARGE YELLOW DISK. BEDDING-PARALLEL VEINS ARE REPRESENTED BY ORANGE POLES, EN-ECHELON ARE IN PURPLE; B) GOLD BEARING ANKERITE-PYRITE V_{3A} VEINS DEVELOPED AS A BRECCIATED VEIN. IN THE EQUAL AREA STEREOGRAM/SCHMIDT PROJECTION STEREOGRAM, V_{3A} POLES ARE IN YELLOW AND A GREAT CIRCLE WAS CONSTRUCTED IN BLUE FROM THEIR AVERAGE ORIENTATIONS; C) SHALLOW V_{3B} VEIN CUTTING ACROSS MULTIPLE ANKERITE-PYRITE V_{3A} VEINS; D) STEEP QUARTZ-ANKERITE V_{3B}

MINERALIZED VEINS WITH ARSENOPYRITE CRYSTAL HALO. THE ARSENOPYRITE TYPICALLY CRYSTALLIZES ALONG THE EDGES OF THE VEIN OR IN THE HOST ROCK AROUND, BUT RARELY IN THE VEIN ITSELF. THE VEIN TO THE LEFT DISPLAYS A UNITAXIAL GEOMETRY, CHARACTERISTIC OF THE CRACK-SEAL GROWTH MECHANISM (PASSCHIER AND TROUW, 2005). BOTH VEINS ARE REPRESENTED AS RED GREAT CIRCLES IN THE EQUAL ANGLE STEREONET/WULFF PROJECTION STEREOGRAM; E) VISIBLE GOLD IN A QUARTZ-ANKERITE V_{3B} MINERALIZED VEIN.

115

FIGURE 21: PHOTOGRAPHS OF CONJUGATE V_{3B} VEIN SETS. FROM TOP LEFT TO BOTTOM RIGHT: A) SANU TINTI EXTENSION DEPOSIT; B) BIDINI (WITH SUB-HORIZONTAL BEDDING, IN BLACK); C) SEGUELEN AND; D) SINTROKO PB1 DEPOSIT. IN THE EQUAL ANGLE STEREONET/WULFF PROJECTION STEREOGRAMS, BEDDING IS REPRESENTED AS BLACK GREAT CIRCLES, V_{3B} VEINS ARE REPRESENTED AS RED GREAT CIRCLES, AND THE S_{4S} CLEAVAGE AS A GREEN GREAT CIRCLE.

117

FIGURE 22: A) PHOTOGRAPH OF A STEEP MINERALIZED V_{3B} VEIN IN KAMI DEPOSIT OVERPRINTED BY THE S_{4S} CLEAVAGE. THE VEIN (RED IN STEREOGRAM) AND MEASURED FOLD AXES FROM OTHER FOLDED MINED VEINS (RED POLES) ARE INDICATIVE OF A NW-SE COMPRESSION (S_{4S} CLEAVAGE IN GREEN); B) CORE FROM BIDINI SHOWING MULTIPLE ARSENOPYRITE CRYSTALS AROUND A V_{3B} MINERALIZED VEIN (BOTTOM; ORIENTATION OF THE VEINS IN THE UPPER PART OF THE PHOTO UNCONSTRAINED). THE CRYSTALS DISPLAY PRESSURE SHADOWS (PS; ORANGE ARROWS) PARALLEL TO THE S_{4S} CLEAVAGE (IN GREEN); C) MICROPHOTOGRAPH FROM THE CORE SHOWN IN B) OF A V_{3B} TWINNED ARSENOPYRITE UNDER CROSS-POLARIZED REFLECTED LIGHT, DEVELOPING PRESSURE SHADOWS DUE TO S_{4S} CLEAVAGE. ASPY: ARSENOPYRITE, QTZ: QUARTZ. STEREOGRAMS: S_0 IN BLACK, MINED VEINS AS RED GREAT CIRCLES, MINED VEIN FOLD AXES AS RED POLES AND S_{4S} IN GREEN; EQUAL ANGLE (WULFF) PROJECTION.

118

FIGURE 23: PHOTOGRAPHS OF VARIOUS STRUCTURAL ELEMENTS LINKED TO MINERALIZATION. A) DOMAL STRUCTURES IN THE KAMI DEPOSIT. THE V_{3B} VEINS, MINED BY LOCAL VILLAGERS, CAN BE SEEN FOCUSED IN THE DOME AND FOLLOWING COMPETENT BEDS. EACH BENCH IS ABOUT 7 METERS HIGH. B) CONJUGATE VEIN GEOMETRY AT DEPOSIT-SCALE. C) MINOR DAMAGE ZONE IN SINTROKO PB1 DISPLAYING MUTUALLY CROSSCUTTING V_{3B} STEEP AND SHALLOW CONJUGATE VEIN SETS; D) CONJUGATE V_{3B} VEIN GEOMETRY AT OUTCROP-SCALE. E) CORE FROM THE BIDINI DEPOSIT DISPLAYING METER-WIDE CARBONATE ALTERATION HALOES (BLEACHED) AROUND V_{3B} VEINS; F) MICROPHOTOGRAPH OF A SANU TINTI DISSEMINATED PYRITE. FREE GOLD IS ASSOCIATED WITH CHALCOPYRITE AND DISPLAYS TRIANGULAR TEXTURES CHARACTERISTIC OF INFILL CRYSTALLIZATION (TAYLOR, 2010). G) PLAN VIEW OF C/C' STRUCTURES AFFECTING THE S_{4S}

CLEAVAGE (HIGHLIGHTED BY QUARTZ; BEDDING PARALLEL TO S_{4S}). THE KINEMATICS INDICATE SINISTRAL MOVEMENT ALONG THE S_{4S} CLEAVAGE, WHICH OVERPRINTS MINERALIZATION. 120

FIGURE 24: PHOTOGRAPHS OF SOME OF THE ORE CONTROLLING STRUCTURES IN VARIOUS DEPOSITS OF THE SIGUIRI DISTRICT.

THESE STRUCTURES ARE ENHANCED DUE TO THE VERY DEEP WEATHERING. A) AND B) INCIPENT STRUCTURE IN SINTROKO PB1 MARKED BY AN INCREASE IN QUARTZ VEIN (V_{3B}) VEIN DENSITY. THE MINERALIZED VEINS (DOTTED LINES IN B), MINED BY LOCAL VILLAGERS, KEEP A CONSISTENT ORIENTATION AND CUT ACROSS THE F_{2S} FOLD. MINERALIZATION DEVELOPS AROUND THE INCIPENT STRUCTURE, AND IS ALSO CONTROLLED BY THE RHEOLOGY OF THE SEDIMENTARY UNITS. C), D) AND E) NE-SW DEXTRAL SHEAR ZONE. INTERSECTIONS BETWEEN NE-SW DEXTRAL SHEAR ZONES AND N-S THRUST FAULTS ARE TYPICALLY HIGHLY MINERALIZED, SUCH AS IN KOSISE (FIGURE 19C). MINOR FAULTS REPRESENTED BY DASHED LINES IN E). STEREOGRAMS: S_0 IN BLACK, CALCULATED F_{2S} FOLD AXES IN YELLOW, STRUCTURES IN BLUE, MINED VEIN IN RED AND S_{4S} IN GREEN; EQUAL ANGLE (WULFF) PROJECTION. 124

FIGURE 25: SUMMARY TABLE OF THE DEFORMATION EVENTS AND TIMING OF THE STRUCTURAL FEATURES RECOGNIZED AT SIGUIRI IN THIS STUDY WITH THE WORK FROM MILÉSI ET AL. (1989, 1992), MILLER ET AL. (2013) AND STEYN (2012). 128

FIGURE 26: STEREOGRAMS OF THE STRUCTURAL DATA COLLECTED OVER THE SIGUIRI DISTRICT DIVIDED INTO FOUR MINE AREAS, FROM NORTH TO SOUTH (BLACK DEPOSIT OUTLINES ON MAPS AT LEFT). BEDDING POLES IN BLACK. MEASURED F_{1S} FOLD AXES IN BLUE, MEASURED F_{2S} FOLD AXES IN RED AND CONSTRUCTED FOLD AXES (POLE OF A GREAT CIRCLE FITTING THE BEDDING POLES OF AN OBSERVED FOLD) IN YELLOW. MEASURED FOLD AXIAL PLANES REPRESENTED AS BLACK GREAT CIRCLES. CLEAVAGES ARE COLORED ACCORDING TO THEIR INTERPRETED GENERATION: S_{1S} IN BLUE, LATE S_{4S} IN GREEN. MINERALIZED V_{3B} VEIN SETS REPRESENTED AS RED POLES. UNLESS SPECIFIED, ALL STEREOGRAMS USE EQUAL ANGLE (WULFF) PROJECTION. 129

FIGURE 27: SCHEMATIC EVOLUTION OF THE EARLY- D_{2S} COMPRESSION AND OF THE MODE OF FORMATION OF THE BEDDING PARALLEL AND EN-ECHELON V_{2S} VEINS ASSOCIATED WITH FLEXURAL SLIP. 131

FIGURE 28: SUMMARY FIGURE OF THE DIFFERENT CONTROLS ON D_{3S} MINERALIZATION FOUND IN THE OROGENIC GOLD SIGUIRI DISTRICT. 136

FIGURE 29: SIMPLIFIED STRESS-STRAIN REPRESENTATION OF THE EVOLUTION OF D_{2S} DEFORMATION FROM A) EARLY-D_{2S} COMPRESSION AND FOLDING TO; B) LATE-D_{2S} TRANSPRESSION AND FRACTURING AND; C) SYN-V_{3B} MINERALIZED VEINING. RELATIVE SCALE BARS.

140

FIGURE 30: IDEALIZED BLOCK MODELS OF DIFFERENT TYPES OF TRANSPRESSION (MODIFIED FROM [HTTP://MAPS.UNOMAHA.EDU/](http://MAPS.UNOMAHA.EDU/)) AND FAULTS RELATIONSHIPS DURING TRANSPRESSION. A) CLASSIC FLOWER STRUCTURE (SANDERSON AND MARCHINI, 1984) SHOWING A COUPLING BETWEEN STRUCTURES ACCOMMODATING PURE AND SIMPLE SHEAR; B) BLOC MODEL OF AN IDEALIZED DECOUPLED TRANSPRESSION. PURE AND SIMPLE SHEAR ARE ACCOMMODATED ALONG DISTINCT THRUST FAULTS AND STRIKE-SLIP FAULTS, RESPECTIVELY; C) SIMPLIFIED MAP VIEW OF THE DECOUPLED EARLY-D_{3S} TRANSPRESSION OBSERVED IN THE SIGUIRI DISTRICT. FORMATION AND DEPOSIT COLORS AS IN FIGURE 17.

141

FIGURE 31: STEREOPRISMATIC PROJECTIONS OF THE CALCULATED ORIENTATION OF THE PRINCIPAL STRESS AXES DURING THE LATE-D_{3S} TRANSTENSION BASED ON CONJUGATE MINERALIZED V_{3B} VEINS. RESPECTIVELY FROM LEFT TO RIGHT: Σ_1 , Σ_2 AND Σ_3 ORIENTATION. SIGMA 1 AND Σ_2 ORIENTATIONS VARY AND PLOT ON THE SAME GIRDLE WHEREAS Σ_3 ORIENTATION REMAINS CONSTANT.

142

FIGURE 32: GEOLOGICAL MAP OF THE SIGUIRI BASIN. LOCATION OF THE SIGUIRI DISTRICT MAP IN RED. AFTER MILLER ET AL., 2013, MILÉSI ET AL. (1989) AND LEBRUN ET AL., (IN REVIEW 2015B); CHAPTER 2.

162

FIGURE 33: FORM LINE MAP OF THE SIGUIRI GOLD DISTRICT AND ITS DIFFERENT DEPOSITS. LOCATIONS OF THE LOGGED DRILL HOLES AND AREAS OF INTEREST HIGHLIGHTED IN RED. AFTER LEBRUN ET AL., (IN REVIEW 2015A); CHAPTER 3.

164

FIGURE 34: PHOTOGRAPHS OF A) VEINING AND ALTERATION ASSOCIATED WITH A HIGH GRADE ZONE IN THE KOSISE DEPOSIT (HOLE KSDD024); B) EXAMPLE OF AN UNALTERED AND UNMINERALISED ZONE FROM THE KOSISE DEPOSIT (HOLE KSDD024, SAMPLE O); C) EXAMPLE OF V_{3A} CARBONATE-PYRITE BRECCIA VEINS. ONLY MINOR PYRITE WAS FOUND IN THIS SAMPLE BUT ABUNDANT CHLORITE WAS FOUND INSTEAD; D) SANU TINTI STYLE OF MINERALISATION SHOWING DISSEMINATED PYRITE IN A CONGLOMERATE INTERBED (HOLE BDRCDD009); E) DRILL CORE FROM KOSISE SHOWING THE CROSCUTTING RELATIONSHIP BETWEEN V_{2S}, V_{3A} AND V_{3B} VEIN SETS; F) NATIVE GOLD FOUND IN THE CENTRE OF AN

ANTITAXIAL V_{3B} QUARTZ-ANKERITE-ARSENOPYRITE VEIN; G) NATIVE GOLD IN AN ANTITAXIAL V_{3B} QUARTZ-ANKERITE-ARSENOPYRITE VEIN OVERPRINTING A V_{2S} QUARTZ-(CARBONATE) VEIN. CHLORITE IS PARTIALLY REPLACING THE FE-CARBONATES. VG: VISIBLE GOLD.

166

FIGURE 35: SIMPLIFIED STRUCTURAL MAPS AND CROSS-SECTIONS OF KEY DEPOSITS FROM THE SIGUIRI DISTRICT (LOCATION MAP ON FIGURE 33). A) SANU TINTI AND BIDINI; B) KOSISE, AND; C) SINTROKO PB1. LOCATIONS OF THE DRILL HOLES AND COLLECTED SAMPLES HIGHLIGHTED.

173

FIGURE 36: LOG OF HOLE BDRCDD009 (LOCATION MAP ON FIGURE 34). THE LOG HAS BEEN OVERTURNED TO ACCOUNT FOR THE STRATIGRAPHY, THE KINTINIAN FORMATION BEING YOUNGER THAN THE FATOYA FORMATION (LEBRUN ET AL., IN REVIEW 2015B; CHAPTER 2). THE ALTERATION INTENSITY SECTION DISPLAYS CARBONATE ALTERATION IN LIGHT BROWN AND ALBITISATION IN LIGHT PINK. WAY-UP INDICATORS IN RED ARE BASED ON GRADED BEDDING RIPPLE MARKS AND RIP-UP CLASTS. POSITION OF THE COLLECTED SAMPLES REPORTED AS COLOURED DISKS (CONGLOMERATE SAMPLES IN RED, SHALE IN BLUE AND GREYWACKE IN ORANGE).

174

FIGURE 37: PHOTOGRAPHS OF THE MAIN STRUCTURAL ELEMENTS FROM THE BIDINI AND SANU TINTI DEPOSITS. A) OVERVIEW OF THE BIDINI DEPOSIT. IN THE FOREGROUND, 5 TO 20 M-DEEP HOLES DUG BY LOCAL VILLAGERS ARE USED TO REACH V_{3B} VEINS IN ONE OF THE HIGH GRADE ZONES ALONG WHICH THE DEPOSIT SITS. A SECOND HIGH GRADE ZONE IS VISIBLE ON THE RIGHT (JUST BELOW THE (SE) SYMBOL). B) CONJUGATE RELATIONSHIPS BETWEEN V_{3B} VEINS. C) FOLDED V_{3B} VEIN AND AXIAL PLANAR S_{4S} CLEAVAGE. D) PYRITE DEVELOPED ALONG THE S_{4S} CLEAVAGE. E) CLOSE-UP PHOTOGRAPH OF THE POLYMIXT CONGLOMERATE FROM THE KINTINIAN FORMATION FOUND BELOW THE BIDINI DEPOSIT AND IN THE SANU TINTI DEPOSIT. F) STRUCTURAL CONTACT (FAULT) BETWEEN THE KINTINIAN AND FATOYA FORMATIONS IN THE SANU TINTI DEPOSIT.

175

FIGURE 38: MICROPHOTOGRAPHS OF A) SIDERITE NODULES BEING PSEUDOMORPHOSED BY V_{3B} PYRITE; B) A V_{3B} ARSENOPYRITE FRACTURED AND SHOWING GOLD-CHALCOPYRITE-(GALENA) INFILLS; C) SANU TINTI STYLE V_{3B} PYRITE FRACTURED AND SHOWING GOLD-CHALCOPYRITE INFILLS; D) SANU TINTI STYLE V_{3B} PYRITE OVERPRINTED BY CHALCOPYRITE VEINLETS; E) V_{3B} ARSENOPYRITE SHOWING QUARTZ STRAIN FRINGES ASSOCIATED WITH THE DEVELOPMENT OF THE S_{4S} PENETRATIVE CLEAVAGE. THIS CLEAVAGE IS ALSO RESPONSIBLE FOR THE PREFERENTIAL ORIENTATION OF THE SERICITE AND THE STRAIN SHADOWS DEVELOPING AROUND THE SIDERITE NODULES; F) COEVAL V_{3A}

PYRITE AND ARSENOPYRITE CRYSTALS; G) BACKSCATTERED ELECTRON IMAGE OF V_{3A} PYRITE DISPLAYING AS-RICH AND AS-POOR GROWTH RINGS AND BEING CROSSCUT BY GOLD INFILLED FRACTURES; H) HEMATITE INCLUSIONS IN V_{3A} PYRITE ASSOCIATED WITH GOLD. HEMATITE LATHS SEEM TO FOLLOW THE PYRITE CRYSTAL LATTICE WHILE GOLD DISPLAY TRIANGULAR TEXTURES TYPICAL OF OPEN SPACE INFILL (TAYLOR, 2010). ASPY: ARSENOPYRITE, AU: GOLD, CCP: CHALCOPYRITE, GN: GALENA, HEM: HEMATITE, PY: PYRITE, QTZ: QUARTZ, SER: SERICITE, SID: SIDERITE.

178

FIGURE 39: PHOTOGRAPHS OF THE MAIN STRUCTURAL ELEMENTS FOUND IN THE SINTROKO PB1 DEPOSIT. A) OVERVIEW OF THE DEPOSIT. THE MAIN ORE SHOOT FOUND IN THIS DEPOSIT FOLLOWS THE BLACK SHALE LAYER (LEFT) AND CROSSCUT THE F_{2S} SUB-VERTICAL FOLD FOUND ON THE EASTERN SIDE OF THE DEPOSIT (RIGHT). B) PHOTOGRAPH OF AN ORE SHOOT, EXPRESSED AS A SUB-VERTICAL DAMAGE ZONE ASSOCIATED WITH DENSE V_{3S} VEINING. C) ANOTHER EXAMPLE OF A HIGH GRADE DAMAGE ZONE AND OF THE LARGE SCALE CONJUGATE GEOMETRY DISPLAYED BY THE V_{3B} VEINS. D) REFRACTION OF V_{3B} VEIN ORIENTATIONS BETWEEN BEDS OF GREYWACKE AND SHALE. E) STRAIN SHADOWS AROUND ARSENOPYRITE CRYSTALS DEVELOPED AROUND A V_{3B} VEIN (CRUMPLED DOWN ON THE RIGHT) BY THE S_{4S} CLEAVAGE. F) CONJUGATE RELATIONSHIP OF THE V_{3B} VEINS AT THE OUTCROP SCALE.

180

FIGURE 40: LOG OF HOLE SKRCDD040 (LOCATION MAP ON FIGURE 39). THIS LOG HIGHLIGHTS THE STRONG LINK BETWEEN BRITTLE DEFORMATION, VEINING, SULPHIDATION AND CARBONATE ALTERATION WITH GOLD. THE ALTERATION INTENSITY SECTION DISPLAYS CARBONATE ALTERATION IN LIGHT BROWN AND OVERPRINTING CHLORITISATION IN GREEN. WAY-UP INDICATORS IN RED ARE BASED ON GRADED BEDDING RIPPLE MARKS AND RIP-UP CLASTS. POSITION OF THE COLLECTED SAMPLES REPORTED AS COLOURED DISKS (SHALE SAMPLES IN BLUE, GREYWACKE IN ORANGE).

182

FIGURE 41: PHOTOGRAPHS OF THE MAIN STRUCTURAL ELEMENTS FOUND IN THE SINTROKO PB1 DEPOSIT. A) OVERVIEW OF THE DEPOSIT. THE NORTHERN PART OF THE DEPOSIT (CENTRE) HOSTS A BEDDING PARALLEL THRUST FAULT THAT DEVELOP INTENSE V_{3S} VEINING (B). B) VEINING DEVELOPED IN THE NORTHERN PART OF THE DEPOSIT. THE V_{3B} VEINS ARE STRATIGRAPHICALLY CONTROLLED AND MAINLY HOSTED IN THE GREYWACKE AND SANDSTONE BEDS. C) CLOSE-UP PHOTOGRAPH OF ONE OF THE RARE DISCRETE STRUCTURES CONTROLLING GOLD GRADES IN THE SIGUIRI DISTRICT, A DEXTRAL NE-SW SHEAR ZONE. GOLD GRADES ACROSS THIS SHEAR ZONE ARE OVER 100 G/T AU. D) SIDERITE NODULES DEVELOPED AROUND THE ORE SHOOTS. THE SUB-VERTICAL S_{4S} CLEAVAGE OVERPRINTS THESE NODULES.

184

FIGURE 42: GEOCHEMICAL SPIDER-DIAGRAMS OF THE A) LEAST ALTERED SAMPLES COLLECTED IN THE SIGUIRI DISTRICT AND NORMALISED TO LEAST ALTERED FATOYA GREYWACKE SAMPLE (SAMPLE O, COLLECTED IN THE KOSISE DEPOSIT), REPRESENTATIVE OF THE LITHOLOGIES HOSTING THE BULK OF THE MINERALISATION IN SIGUIRI. KINTINIAN CONGLOMERATE IN RED, FATOYA SAMPLES IN BLUE, BALATO SAMPLES IN GREEN, SHALE SAMPLES AS DASHED LINES, GREYWACKE SAMPLES AS SOLID LINES; B) KINTINIAN CONGLOMERATE SAMPLES NORMALISED TO THE LEAST ALTERED SAMPLE; C) FATOYA SHALE SAMPLES AND KINTINIAN SHALE SAMPLE NORMALISED TO THE LEAST ALTERED FATOYA SHALE SAMPLE; D) BALATO SHALE SAMPLES NORMALISED TO THE LEAST ALTERED SAMPLE; E) FATOYA GREYWACKE SAMPLES AND KINTINIAN GREYWACKE SAMPLE NORMALISED TO THE LEAST ALTERED FATOYA SHALE SAMPLE, AND; F) BALATO GREYWACKE SAMPLES NORMALISED TO THE LEAST ALTERED SAMPLE.

187

FIGURE 43: NORMAL PROBABILITY PLOTS OF THE WHOLE-ROCK GEOCHEMICAL SAMPLES FROM THE BALATO (IN GREEN), FATOYA (IN BLUE) AND KINTINIAN FORMATIONS (IN RED). THE VALUES PLOTTED ALONG THE X AXIS ARE IN UNITS OF STANDARD DEVIATION (MEAN = 0 AND A STANDARD DEVIATION = 1). THESE PLOTS STATISTICALLY SEPARATE EACH DATASET INTO MULTIPLE POPULATIONS BASED ON THEIR INDIVIDUAL VALUES AND REPRESENTATION IN THE DATASET.

188

FIGURE 44: COMPOSITE LOG AND GEOCHEMICAL CROSS-SECTION FROM THE KOSISE DEPOSIT. TWO MINERALISED ZONES WERE IDENTIFIED (AROUND SAMPLES J, K, L, M AND SAMPLES A, B, C, D) AND ARE IN CLOSE PROXIMITY TO SHEAR ZONES AND A THRUST FAULT (FIGURE 42 AND 43). THE MAIN MINERALISED ZONE (SAMPLES J, K, L, M) IS ASSOCIATED WITH TYPICAL OROGENIC GOLD ENRICHMENTS IN Au-As-Sb-Te AND W. EACH GEOCHEMICAL SAMPLE WAS NORMALISED TO THE CORRESPONDING GREYWACKE OR SHALE LEAST ALTERED SAMPLE (O AND F, RESPECTIVELY). THE COMPOSITE GEOCHEMICAL CROSS-SECTIONS ALSO SHOW ENRICHMENTS IN Bi, Mo AND S AROUND THE MAIN MINERALISED ZONE (SAMPLES J, K, L, M). CA INCREASES AWAY FROM THE MAIN MINERALISED ZONE AND IS INTERPRETED TO REPRESENT THE REACTION FRONT. THE FACT THAT Si DOES NOT SHOW ANY VARIATION ACROSS THE ORE SHOOTS IS ATTRIBUTED TO THE REMOVAL OF THE VEINS IN EACH SAMPLE (HOST ROCK CHARACTERIZATION ONLY). MOLAR AND NORMALISED 3K/Al AND Na/Al SATURATION INDICES (KISHIDA AND KERRICH, 1987) BOTH HIGHLIGHT BOTH MINERALISED ZONES. EACH GEOCHEMICAL SAMPLE WAS NORMALISED TO THE CORRESPONDING GREYWACKE OR SHALE LEAST ALTERED SAMPLE (O AND F, RESPECTIVELY).

191

FIGURE 45: LA-ICP-MS AND EPMA DATA FROM THE DIFFERENT GENERATIONS OF PYRITE AND ARSENOPYRITE OBSERVED IN THE SIGUIRI DISTRICT. V_{2S} PYRITE (A) IS REPRESENTED IN ORANGE. V_{3A} PYRITE (B) IS REPRESENTED IN RED. V_{3B} PYRITE IS REPRESENTED IN BLUE AND V_{3B} ARSENOPYRITE IN PINK (C). D_{4S} PYRITE IS REPRESENTED IN GREEN (D) AND FINALLY, SANU TINTI STYLE DISSEMINATED PYRITE IS REPRESENTED IN BLACK. REGRESSION LINES ARE IN BLACK FOR PYRITE AND PINK FOR ARSENOPYRITE IN E) AND I).

192

FIGURE 46: PARAGENETIC SEQUENCE FOR THE SIGUIRI DISTRICT.

195

FIGURE 47: SYNTHETIC TIME CHART COMPARISON OF SOME KEY LATE EBURNEAN GOLD MINERALISATION EVENTS AND THEIR TIMING. FROM DIA ET AL. (1997), FOUGEROUSE ET AL. (2015), HIRDES AND DAVIS (2002), LAWRENCE ET AL. (2013A), LAWRENCE ET AL. (2013B), LEBRUN ET AL. (IN REVIEW 2015A); CHAPTER 3, LEBRUN ET AL. (IN REVIEW 2015B); CHAPTER 2, MASUREL ET AL. (IN PRESS), MCFARLANE ET AL. (2011), MILLER ET AL. (IN REVIEW 2015), PARRA-AVILA (2015), PARRA-AVILA ET AL., (IN REVIEW 2015).

202

ACKNOWLEDGEMENTS

The sum of knowledge and expertise required to complete this project being much greater than my own, I would like to acknowledge the help and support of the many people who contributed in so many ways to this adventure. From the ping-pong break talks to the one-on-one masterclasses on sedimentology, all these persons rendered this work achievable.

Firstly, I would like to thank my supervisors, Nicolas Thébaud, Stanislav Ulrich, John Miller and Campbell McCuaig. They recruited me while my English skills were outrageously imperfect, believed in me and gave me the opportunity to prove them right. It all started around a coffee in Paris with Nicolas Thébaud and it is only natural that I thank him first. He guided me throughout most of this journey and advised me on more aspects of the research enterprise than I could have ever hoped for. Thanks to Stanislav Ulrich, who was my first supervisor and whose views and comments have always made my work progress. I thank him also for making himself available and for the discussions we had even after he left the Centre for Exploration Targeting (CET). Many thanks to John, for his great guidance, his insightful ideas and for the time he spent conveying them to me. His skills both on the field and in a conference room have always been a source of inspiration for me. Thanks to Cam who opened me the doors of the CET and for teaching me new and efficient ways of looking at maps or geological problems: I am now confident I get the big picture.

Outside the CET, other geoscientists from AngloGold Ashanti, the University of Western Australia (UWA) and from Curtin University contributed to the collection of quality data and to the maturation of ideas. I thank deeply Eddie Connell, Shawn Kitt and Katharina Wulff for their support, inspiring discussions and many good laughs during epic squash games after a long day on the field. I also thank Craig Duvel and the whole of the brownfield geologists in general for providing site access and advices. Seydou Kante and Juan Steyn for bringing me along on the various greenfield projects and providing me with regional scale information to get a grasp on the big picture. Thanks also to Yacouba Djikite, who helped in

more than one occasion to get things going for me at the core yard. At UWA, I thank Professor and friend Julien Bourget for his precious help regarding the description and interpretation of sediments and sedimentary facies. I also acknowledge the facilities, and the scientific and technical assistance of the Australian Microscopy & Microanalysis Research Facility at the Centre for Microscopy, Characterisation & Analysis (CMCA), a facility at UWA funded by the University, State and Commonwealth Governments. In particular, I thank Janet Muhling and Malcolm Roberts from the CMCA for their help on the delicate machines the SEM and microprobe are. At Curtin, Hao Gao and Cristina Talavera are thanked for their incredible patience and determination to make the SHRIMP operate smoothly. I thank Noreen Evans and Brad McDonald for their help and expertise in the collection of quality LA-ICP-MS data.

In addition to these colleagues and fellow researchers, the admin and research staff/student at the CET were an irreplaceable support in the success of this project. Specifically, Matt Hill, Luis Parra, Quentin Masurel, Thomas Angerer, Ana-Sophie Hensler and Christian Schindler are thanked for reminding me that a PhD was also the occasion to meet great people and share good moments around a beer (or two maybe). Cindy Dunjey, Susie Cass, Estelle Dawes, Emily Denham, Wendy Carter, Gillian Evans and Hayley Newberry are thanked for handling the financial and administrative side of the research.

Regarding financial support, this project is funded by AngloGold Ashanti, which I thank, and is associated with an ARC Linkage Grant: "Four dimensional lithospheric evolution and controls on mineral system distribution in Neoarchean to Paleoproterozoic terranes" (LP110100667), and in collaboration with the AMIRA P934A project "West African Exploration Initiative- Stage 2".

Outside the academic world, my friends and family were the strong pillars that supported me all along, cheered me up when things were looking dire and have always been a welcomed distraction when I was meant to work hard. In particular, I thank my spearfishing buddies and dear friends Mael Coret, Craig McPhilimey and Jacques Wittig for accompanying me on our regular underwater escapes in the cold waters around Albany and the warm depths

of Indonesia. I would also like to thank my friend Raphaël Doutre. Our friendship has been long lasting, following each other from the slopes of French volcanoes to the forests of Canada, the sandy beaches of Australia, and supporting one another for many years. I sincerely hope it will stay this way for the years to come (you may have to get out of your office every now and then for this to happen though!). I also thank Jasmin Pierucci, for being by my side during the harsher times of this journey, coping with the accumulated stress I could not evacuate at the gym and supporting me in my enterprise. Thank you for being my best reason to take time off.

Finally, and most importantly, I thank my parents: Martine and Jean-Luc. I hope I made them at least half proud of me than I am proud of having been raised by the both of them. They supported me for the past twenty-seven years and taught me the utmost important thing I needed to complete this long journey: determination.

CHAPTER 1: INTRODUCTION

4D EVOLUTION OF THE OROGENIC GOLD DISTRICT OF SIGUIRI, GUINEA (WEST AFRICA)

PREAMBLE AND KNOWLEDGE GAPS

The West African Craton (WAC) is also known as the Leo-Man Shield. It is made of two distinct terranes: the Archean Kénéma-Man domain to the south-west, and the Paleoproterozoic Baoulé-Mossi domain (Figure 1A). The Archean domain is dominated by gneiss dated between ca. 3540 and 2750 Ma (Kouamelan et al., 1997; Thiéblemont et al., 2001) while the Paleoproterozoic domain displays an assemblage of volcano-sedimentary belts and felsic intrusives, ranging in age from ca. 2250 to 2040 Ma (Davis et al., 2015; Parra-Avila, 2015; Tshibubudze et al., 2013). A large part of the Baoulé-Mossi domain is overlain unconformably by the Neoproterozoic sediments of the Taoudení Basin (Begg et al., 2009; Lawrence et al., 2013a; Villeneuve and Cornée, 1994). The Baoulé-Mossi domain was accreted against the Kénéma-Man domain during the Eburnean orogeny (ca. 2210-2040 Ma; Abouchami et al., 1990; Egal et al. 2002; Thiéblemont et al., 2004; Lahondère et al., 2002; Parra-Avila, 2015; Davis et al., 2015). This orogeny is associated with the development of numerous world-class gold deposits across the West African Craton. These deposits formed at different times during the Eburnean orogeny and display a wide range of mineralization styles ranging from: intrusion related gold (e.g. Morila; McFarlane et al., 2011), orogenic gold (e.g. Obuasi, Sadiola and Loulo; Fougerouse et al., in press; Masurel et al., in press 2015; Lawrence et al., 2013a; Lawrence et al., 2013b), atypical orogenic gold (e.g. Masawa deposit; Treloar et al., 2015),

residuum gold (e.g. Yatela; Hanssen et al., 2004) and placer type deposits (e.g. Tarkwa; Sestini, 1973; Pigois et al., 2003). Amongst this breadth of gold mineral systems, the Siguiri gold district in north-eastern Guinea is the only large gold deposit (> 50 t Au; AngloGold Ashanti Ltd., 2013) hosted in the Siguiri Basin (Figure 1B) and one of the largest gold mineral systems in the West African Craton.

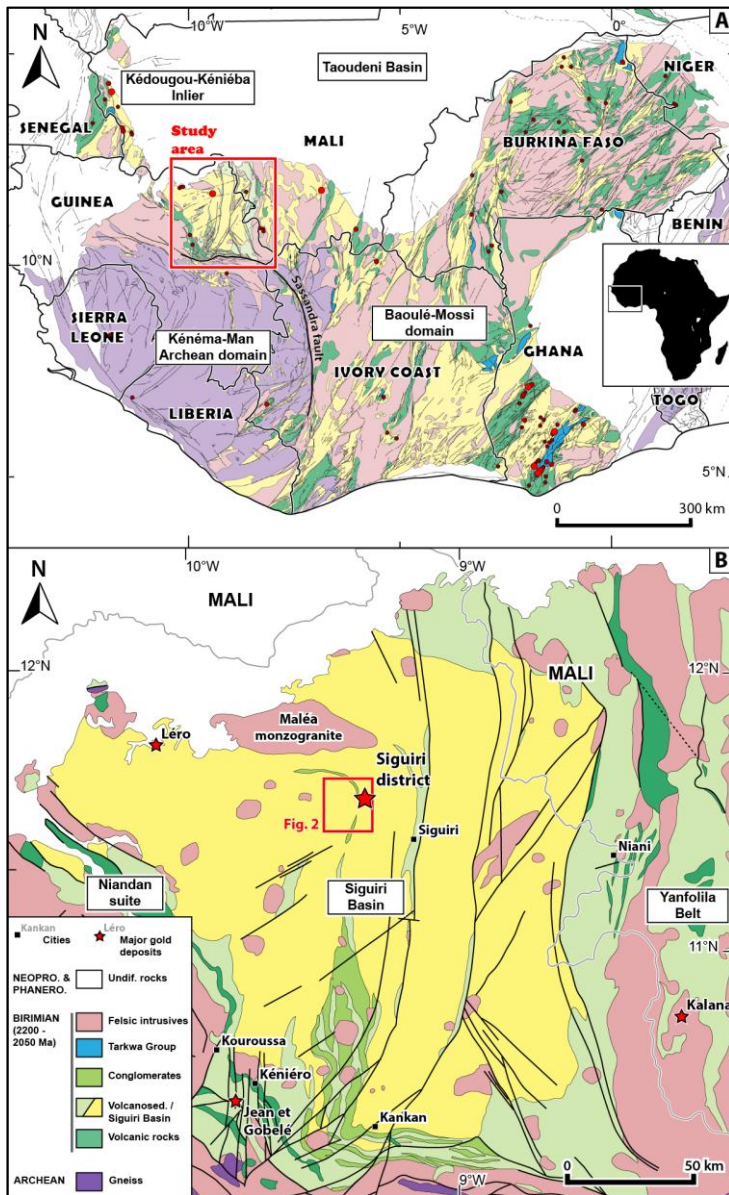


Figure 1: Geological map of A) the West African Craton and its gold deposits (red disks), and; B) the Siguiri Basin.

Modified from Milési et al. (1989) and Miller et al. (2013).

The Siguiri Basin is located in the Baoulé-Mossi domain, directly north of the Archean Kénema-Man domain (Figure 1A). The Basin spreads over more than 40,000 km², mostly in north-eastern Guinea but also in southern Mali, and is one of the largest sedimentary basins of

the West African Craton. The Siguiri Basin rocks were described has Lower Birimian sediments by Milési et al. (1989) and Egal et al. (1999). These sediments are metamorphosed to sub-greenschist facies and were interpreted to derive from Paleoproterozoic volcanic rocks and felsic intrusions that were emplaced during the early stages of the Eburnean orogeny (Milési et al., 1989; Begg et al., 2009; Feybesse and Milési, 1994). The Niandan ultramafics and the Kéniéro Range mafics and felsic volcanic rocks border the Siguiri Basin to the west and southwest (Figure 1B). The felsic volcanic rocks were dated at ca. 2095 Ma Feybesse et al. (1999). Bordering the Basin to the east, the Yanfolila Belt displays an assemblage of sedimentary and mafic to intermediate volcanic rocks intruded by felsic magmas. In the west of the Yanfolila Belt, intermediate to felsic calc-alkaline volcanic rocks from the Niani suite were dated at ca. 2210 Ma and interpreted to be arc-related and derived from subduction of a young and hot oceanic plate (Lahondère et al., 2002). To the south, the Siguiri Basin is bordered by a series of late Eburnean intrusives (ca. 2090-2070 Ma) and by the Sassandra fault separating the Basin sediments from the Archean Kénéma-Man gneiss (Egal et al., 2002). The Archean banded iron formations of the Simandou also outcrop south of the Siguiri Basin (Egal et al., 1999). Finally, to the north, the Siguiri Basin is unconformably overlain by the Neoproterozoic sediments of the Taoudeni Basin. The Siguiri Basin sediments are intruded by a number of late Eburnean monzogranite and biotite granite intrusions dated at ca. 2090-2070 Ma such as the Malea monzogranite, outcropping in the northernmost part of the Basin, 50 km north of the Siguiri district (Egal et al., 2002; Parra-Avila, 2015). A series of Mesozoic dolerite sills, ENE-striking dolerite dykes and basaltic lava flows, all related to the South Atlantic Ocean opening, intrude and overlie the Basin sedimentary rocks (Abouchami et al. 1990; Paranhos, 2008; Egal et al., 1999; Egal et al., 2002). On the basis of this regional framework the age of the Siguiri Basin is loosely constrained between ca. 2210 and 2093 Ma (Egal et al., 1999; Lahondère et al., 2002). This large age bracket highlights an important knowledge gap in the understanding of the lithostratigraphic position and tectonic significance of the Siguiri Basin within the Eburnean orogeny.

The Siguiri Basin, has been known for its gold endowment since the 12th century and potentially as early as the 3rd century, and is associated with a prolonged and ongoing artisanal mining history (Watts, 2010). Over the last 84 years, gold in the Basin has been produced at an industrial scale by various international mining companies including by a French company starting the production in 1931, a Russian company from 1960 to 1963, and North American and British companies in the 1980s. In 2002, the world-class Siguiri gold district was bought by AngloGold Ashanti Ltd. (Watts, 2010). Gold mineralisation in the Siguiri district have been discussed by a MSc student (Steyn, 2012) and contractors, but descriptions and interpretations differ greatly. For instance, typology of gold mineralisation in the district has been ascribed to a variety of styles ranging from epithermal lode (Paranhos, 2008), orogenic (Holcombe, 2007) to paleoplacers overprinted by mineralised veins (Watts, 2010). Even though all these studies propose that gold mineralisation in Siguiri is dominantly controlled by veins, no consensus was reached by the authors on what controls the location of the Siguiri gold district at the scale of the Siguiri Basin or what controls the extent of the ore shoots at the district and deposit scales.

To further the understanding of the characteristics, geometry and genesis of gold mineralisation in the Siguiri district, a multi-scale and multidisciplinary approach was employed. This approach addresses the various scales at which geological processes work in gold mineral systems. Modern gold exploration strategies increasingly rely on such an approach, involving integration of fieldwork, geophysics, and geochemistry among other techniques, used at different scales (McCuaig and Hronsky, 2014; McCuaig et al., 2010; Robert et al., 2005; Miller et al., 2010; Williams and Currie, 1993; McIntyre and Martyn, 2005; Blewett et al., 2010; Goldfarb et al., 2005; Groves et al., 2003; Groves et al., 2000; Neumayr et al., 2008; Eilu and Groves, 2001; Eilu et al., 1999). At a province scale, numerous studies highlight the role of early architecture as a primary control on gold mineralisation (Robert et al., 2005; Miller et al., 2010; McIntyre and Martyn, 2005; Chapter two). Down one scale at the district level, secondary structures control and/or host gold mineralisation (Blewett et al., 2010;

Goldfarb et al., 2001; Goldfarb et al., 2005; Miller et al., 2010; Chapter three). Province- and district-scale controlling structures are typically delineated using geophysical datasets (Blewett et al., 2010; Chapter two) but can also be exposed by exploration geochemistry, especially at smaller scale (e.g. deposit scale; Eilu and Groves, 2001; Eilu et al., 1999; Chapter four).

The present study thus focuses on the detailed description of the geology and regional framework of gold mineralisation in the world-class Siguiri gold district. The results of this study presents the 4D (space-time) evolution of the Siguiri district lithostratigraphic record, structural architecture, and mineral alteration. Collectively, the data recorded during the course of this study provides an insight into the tectonic context, genetic processes and the geochemical footprint of gold mineralisation in the Siguiri district. All these elements define the knowledge base to improve exploration strategies in and around the Siguiri Basin as well as in the broader West African Craton.

AIMS OF THESIS

Based on background information and knowledge gaps identified in the Siguiri Basin and Siguiri district, the principal objectives of this study are to:

- 1) Characterise the lithostratigraphy and tectonic significance of the Siguiri district and Siguiri Basin sediments in the context of the Eburnean orogeny;
- 2) Use this newly developed understanding to highlight the early architecture of the Siguiri Basin and the large scale structures which may have played a fundamental role in the location of the Siguiri district;
- 3) Characterise the structural evolution of the district, attributing relative timing to the major structures and deformation events in the context of previous structural work conducted in West Africa;
- 4) Develop an integrated model for the control on the geometry and mineralisation processes within the Siguiri district at the ore shoot, ore body and district scales;

- 5) Characterise the mineral assemblage, its evolution and the geochemical footprint left by the gold mineralisation in the metasediments of the Siguiri district;

GENERAL METHODOLOGY

This section briefly details the different methods and techniques used to meet the defined objectives of this study.

Fieldwork and sampling

In order to achieve the objectives identified in the previous section, fieldwork was conducted in and around the Siguiri district. A total of 22 weeks were spent in the field over the course of this study. Fieldwork was focused on geological and structural mapping, core logging and sampling in the different deposits of the district but was also conducted around the district and outside of the Siguiri Basin.

Thirteen deposits from the Siguiri district were accessible over the course of this study. From south to north: Sintroko PB1, Sintroko PB2C, Sintroko PB3A, Sintroko North, Kosise, Kami, Kozan, Kalamagna PB1, Tubani, Bidini, Sanu Tinti, Eureka North and Seguelen (Figure 2). These deposits are spread along an average WNW-ESE trend across the three different sedimentary Formations hosting the district: the Kintinian, Fatoya and Balato Formations (Figure 2; Watts, 2010). Fieldwork was undertaken in all these deposits but the greater part of the work was focused on Sintroko PB1, Kosise, Kami, Bidini and Sanu Tinti. This choice was based on the:

- 1) importance of the gold mineralisation in the deposit;
- 2) hosting Formation;
- 3) proximity to contact with another Formation;
- 4) outcropping quality of the deposit, and;
- 5) density of drill cores in the deposit.

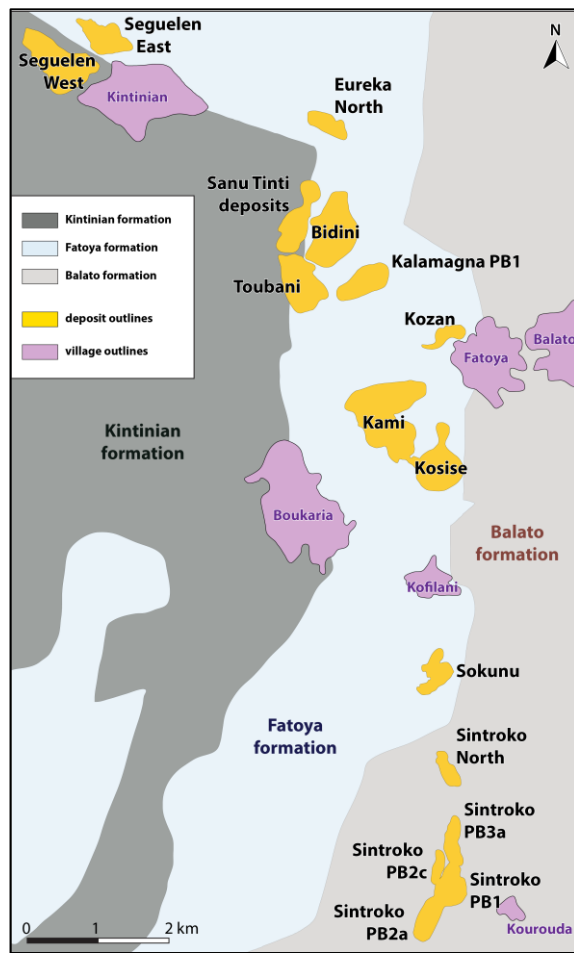


Figure 2: Geology map of the Siguiri district and its deposits. After Chapter 3.

Sampling was focused in these five key deposits and organised to cover the main lithotypes (greywacke, shale and conglomerate) inside and outside of the ore zones. Sampling for whole-rock multi-element geochemistry was focused in the Kosise deposit. For more details on sampling, see the methodology sections of Chapters two and four.

Regional fieldwork was first conducted in the first hundred kilometres around the Siguiri district. Two main regions were targeted for structural and lithostratigraphic observations and sampling: the Maléa monzogranite region, ~30 km north of the district, and the Saraya greenfield project ~50 km to the west of the district. The Maléa site was chosen because this monzogranite represents the closest and largest mapped pluton intruding the sediments of the Siguiri Basin. Dating of this intrusive hence gives a minimum age for the Siguiri Basin sediments. Additionally, structural observations from this site would get an

absolute timing constraint that could later be used to relate the overall deformation history in Siguiri to that of the overall West African Craton during the Eburnean orogeny. The second site, Saraya, was chosen for its peculiar lithostratigraphy, displaying volcanic rocks not encountered in the district. This site was also selected for dating, lithostratigraphic and structural observations. In addition to these two regional localities, a transect from Siguiri to the Archean Kénéma-Man Craton was completed. This transect focused on the lithostratigraphic and structural characterisation of the Siguiri Basin sediments, extrusives and intrusives rocks as well as the igneous and gneissic rocks located along and beyond the Sassandra fault. For more details on how structural readings were taken during fieldwork, see the methodology section of Chapter three.

Analytical techniques

PETROGRAPHY AND IMAGING

Petrographic observations of polished thin-sections were undertaken at the Centre for Exploration Targeting (CET) in Perth, Western Australia. These observations were complemented by Secondary Electron Microscope (SEM) imaging on a Tescan Vega 3 at the Centre for Microscopy, Characterisation and Analysis (CMCA) at the University of Western Australia (UWA). For more details on the SEM imaging, see the methodology section of Chapter four.

U-Pb SHRIMP GEOCHRONOLOGY

U-Pb SHRIMP II geochronology on detrital and igneous zircons was carried out at the John de Laeter Centre for Isotope Research (JdL) at Curtin University in Perth, Western Australia. The use of an ion microprobe was essential for the high precision and small beam size required, as well as for logistical reasons. This technique spatial resolution (20 µm ablation diameter versus 30-60 µm for LA-ICP-MS) allows for the very small detrital zircons and highly damaged igneous zircons collected to be analysed while avoiding cracked, damaged or

metamict areas. This technique was the most appropriate for this study. For more details on this technique and sample preparation, see the methodology section of Chapter two.

WHOLE-ROCK MULTI-ELEMENT GEOCHEMISTRY

Samples for whole-rock geochemistry were analysed for major and minor elements at the Intertek Genalysis laboratory in Perth, Western Australia. Major elements were obtained by X-Ray fluorescence spectrometry (XRF) and trace elements by Inductively Coupled Plasma Mass Spectrometry (ICP-MS) and Inductively Coupled Plasma Optical Emission Spectrometry (ICP-OES). The loss on ignition (LOI) was determined by gravimetry. For more details on the geochemistry techniques used, see the methodology section of Chapter four.

GIS AND 3D MODELLING

Data integration, spatial analysis and 3D modelling were carried out in ArcGIS and LeapFrog Mining 3D computer programs.

ORGANISATION OF THIS THESIS

This thesis is presented as a series of three refereed journal publications tied together by an introduction and a conclusion chapter, following the University of Western Australia regulations outlined in the Postgraduate Research and Scholarships Handbook. Regulation 30.(1)(b) states that: "A typescript may be structured in any of a range of ways, including, but not limited to: a monograph; a paper or series of papers suitable for publication in scholarly journals; or a combination of published and unpublished work ". This thesis includes:

- 1) an introduction (Chapter one) that presents the current state of knowledge, the gaps this thesis aims to address and details the approach used to address these knowledge gaps;
- 2) one paper submitted to a special issue on West Africa of the journal Precambrian Research (Chapter two). This paper presents the lithostratigraphy and

geochronology of the central Siguiri Basin rocks. It revises the lithostratigraphic and tectonic position of the Siguiri Basin in the evolution of the Eburnean orogeny. It also discusses the early architecture of the Basin, thus highlighting the first order structural controls at play in the Siguiri district and in the rest of the Basin;

- 3) one paper submitted to a special issue on West Africa of the journal Economic Geology (Chapter three). This paper presents the structural evolution of the Siguiri district and the second and third order structures hosting the mineralisation. It also discusses the mode of emplacement and stress-field variations associated with the veins hosting the bulk of the mineralisation in Siguiri;
- 4) one paper submitted to Mineralium Deposita (Chapter four). This paper presents the petrographic and geochemical characteristics of the mineral assemblages observed in the Siguiri district. It also discusses the use of laser ablation to constrain the timing of mineralisation and the polyphase nature of hydrothermal activity and gold mineralisation in the Siguiri district and in the rest of the West African Craton;
- 5) a conclusion (Chapter five) that summarizes the main findings of this thesis and introduces the remaining questions to answer and possible future work.

The three papers form the separate parts of a coherent study on the Siguiri district litho-structural and hydrothermal evolution and that of its host basin in the context of the West African craton and the Eburnean orogeny. The overall scope of this study zooms in from a regional scale in Chapter two, to a district scale in Chapter three, to a deposit scale in Chapter four, emphasizing the multi-scale approach of this work. Each chapter is linked to the previous by a brief introductory paragraph explaining how the overall study evolves and benefits from the following work.

JUSTIFICATION OF THESIS FORMAT AND AUTHORSHIP

This PhD project combines the resources and personnel at the Centre for Exploration Targeting at UWA, at the John de Laeter centre at Curtin University, and at AngloGold Ashanti Limited. As a result, a number of collaborators from these institutions contributed to the studies presented in this thesis. Collaborative work has been properly acknowledged and all co-authors gave their permission for me to include the results of our collaboration in this thesis. According to UWA regulations 29.(1) and 29.(3), I declare that all the material presented in this thesis has not been presented in part or full for a degree at any other university. In accordance with regulation 30.(2)(a) stating that: "the work done by the student must be clearly indicated and certified as such by the co-authors", the contribution of the candidate and all co-authors for the papers presented in Chapter two, three and four is listed below.

The manuscript presented in Chapter two is first authored by the candidate and co-authored by Nicolas Thébaud, John Miller, Stanislav Ulrich, Julien Bourget, and Ockert Terblanche. The candidate undertook all sampling, sample preparation, geochronological analyses and writing of the manuscript. Drs Nicolas Thébaud, John Miller, Stanislav Ulrich all went on the field with the candidate on numerous occasions and contributed to the gathering of geological observations presented in the manuscript. Dr Nicolas Thébaud also helped with SHRIMP data processing. Dr Nicolas Thébaud and Dr John Miller assisted in the development of the overall idea of the paper and provided many fruitful discussions. Dr John Miller also provided numerous datasets and a base for the making of the Siguiri Basin GIS map undertaken by the candidate and attached to the manuscript. Dr Stanislav Ulrich communicated numerous observations from both district and regional scale that helped synthesizing the lithostratigraphy of the Siguiri Basin. Dr Julien Bourget assisted with sedimentary facies interpretation and sedimentary vocabulary check of the manuscript. Ockert Terblanche processed the geophysical data and produced the images attached to the

manuscript as well as detailing the techniques he used in the methodology section of the manuscript.

The manuscript presented in Chapter three is first authored by the candidate and co-authored by John Miller, Nicolas Thébaud, Stanislav Ulrich, and Campbell T. McCuaig. The candidate developed the idea behind the paper and is responsible for the entire writing of the manuscript. Drs Stanislav Ulrich, John Miller, Nicolas Thébaud, and Campbell T. McCuaig all contributed to structural data collection on the field. Dr Stanislav Ulrich spent the most time with the candidate on the field and contributed to the overall interpretation of the structural evolution of the Siguiri district. Dr John Miller also contributed to this interpretation and provided numerous fruitful discussions regarding stress-switches in orogenic gold deposits. Drs Nicolas Thébaud, and Campbell T. McCuaig also largely contributed in the revisions done to the manuscript and by providing insightful discussions.

The manuscript presented in Chapter four is first authored by the candidate and co-authored by Nicolas Thébaud, John Miller, Malcolm Roberts and Noreen Evans. The candidate undertook all sampling, sample preparation, optical microscopy, whole-rock geochemical analyses and writing of the manuscript. Drs Nicolas Thébaud and John Miller provided numerous tips to help sampling and numerous editorial comments. Dr Malcolm Roberts assisted with the Electron Probe Micro-Analyzer (EPMA) data collection on sulphides, data processing and numerous fruitful discussions. Dr Noreen Evans assisted with the Laser Ablation Inductively Coupled Plasma Mass Spectrometry (LA-ICP-MS) data collection and first-pass data processing.

SUPPORTING REFERENCES

In addition to the three journal publications submitted forming the main chapters of this thesis, the PhD candidate Lebrun wrote another submitted publication and six abstracts and extended abstracts for a number of international conferences:

Publications

Lebrun, E., Ulrich, S., Miller, J., Thébaud, N. and T. McCuaig, C., in review 2015, The world-class orogenic gold Siguiri district, Siguiri Basin (Guinea, West Africa): Ore Geology Review.

Peer reviewed extended abstracts

Lebrun, E., Thébaud, N., Miller, J., T. McCuaig, C., 2014, Polyphase gold mineralization in the Siguiri district, Guinea (West Africa): Extended abstract in proceeding of: SEG 2014 conference.

Lebrun, E., Ulrich, S., Miller, J., Thébaud, N. and T. McCuaig, C., 2013, Structural framework and evolution of the world class Siguiri orogenic gold district (Guinea, West Africa): Extended abstract in proceeding of: SGA- 12th biennial meeting, vol. 3, p 1136-1140.

Short communications

Lebrun, E., Miller, J., Thébaud, N., Ulrich, S. and T. McCuaig, C., 2014, Understanding the Role and Origin of Stress-Field Variations in Orogenic Gold Systems: A Case Study of the World-Class Siguiri District, Siguiri Basin, Guinea, West Africa: Abstract in proceeding of: Gold14@Kalgoorlie International Symposium, n° 59, p 74-75.

Lebrun, E., Thébaud, N., Miller, J. and T. McCuaig, C., 2014, Geochronology and lithostratigraphy of a major Birimian sedimentary basin: insight into the tectonostratigraphic evolution and gold mineralisation controls of the Siguiri Basin,

Guinea (West Africa): Abstract in proceeding of: AESC- 22nd Australian Geological Convention, vol. 110, p 84-85.

Lebrun, E., Miller, J., Thébaud, N., Ulrich, S. and T. McCuaig, C., 2013, Structural framework and evolution of the world class Siguiri orogenic gold district (Guinea, West Africa): CET Sponsors' Day.

Lebrun, E., Miller, J., Thébaud, N., Ulrich, S. and T. McCuaig, C., 2013, Structural framework and evolution of the world class Siguiri orogenic gold district (Guinea, West Africa): CCFS conference.

REFERENCES

Abouchami, W., Boher, M., Michard, A., and Albarede, F., 1990, A Major 2.1 Ga Event of Mafic Magmatism in West Africa - an Early Stage of Crustal Accretion: Journal of Geophysical Research-Solid Earth and Planets, v. 95, p. 17605-17629.

AngloGold Ashanti Ltd., 2013, Mineral resource and ore reserve report, Available from:
<www.agr-reports.com/13/download/AGA-RR13.pdf>, [10 October 2014].

Begg, G. C., Griffin, W. L., Natapov, L. M., O'Reilly, S. Y., Grand, S. P., O'Neill, C. J., Hronsky, J. M. A., Djomani, Y. P., Swain, C. J., Deen, T., and Bowden, P., 2009, The lithospheric architecture of Africa: Seismic tomography, mantle petrology, and tectonic evolution: *Geosphere*, v. 5, p. 23-50.

Blewett, R., Czarnota, K., and Henson, P., 2010, Structural-event framework for the eastern Yilgarn Craton, Western Australia, and its implications for orogenic gold: *Precambrian Research*, v. 183, p. 203-229.

Davis, J., Miller, J., Thébaud, N., McCuaig, C., Begg, G., Jessel, M., Hein, K., Baratoux, L., 2015, Craton-scale lithostratigraphic correlation as an insight for the geodynamic evolution of the South West African Craton: *Proceedings of the 50th SGA conference*.

- Egal, E., Lahondere, D., Costea, A. C., Diabate, B., Diallo, A., Diallo, A. B., Diallo, S., Gaye, F., Iliescu, D., and Minthe, D., 1999, Carte géologique de la Guinée à 1/200 000; Feuille Sigiri, BRGM.
- Egal, E., Thiéblemont, D., Lahondère, D., Guerrot, C., Costea, C. A., Iliescu, D., Delor, C., Goujou, J., Lafon, J., Tegyey, M., Diaby, S., and Kolie, P., 2002, Late Eburnean granitization and tectonics along the western and northwestern margin of the Archean Kénéma–Man domain (Guinea, West African Craton): Precambrian Research, v. 117, p. 57-84.
- Eilu, P., and Groves, D., 2001, Primary alteration and geochemical dispersion haloes of Archaean orogenic gold deposits in the Yilgarn Craton: the pre-weathering scenario: Geochemistry: Exploration, Environment, Analysis, v. 1, p. 183-200.
- Eilu, P. S., Mathison, C. I., Groves, D. I., and Allardyce, W. J., 1999, Atlas of alteration assemblages, styles and zoning in orogenic lode-gold deposits in a variety of host rock and metamorphic settings, Geology and Geophysics Department (Centre for Strategic Mineral Deposits) & UWA Extension, The University of Western Australia, Publication 30, 50 p.
- Feybesse, J., Bangoura, A., Billa, M., Costea, A., Diabaté, B., Diaby, S., Diallo, A., Diallo, S., Diallo, A., and Egal, E., 1999, Notice explicative de la Carte géologique de la Guinée à 1/200 000, Feuille no. 19, Kankan: BRGM, DNRGH, Ministère des Mines, de la Géologie et de l'Environnement, Conakry, Guinée, p. 27.
- Feybesse, J.-L., and Milési, J.-P., 1994, The Archean/Proterozoic contact zone in West Africa: a mountain belt of décollement thrusting and folding on a continental margin related to 2.1 Ga convergence of Archean cratons?: Precambrian Research, v. 69, p. 199-227.
- Fougerouse, D., Micklethwaite, S., Ulrich, S., Miller, J., Godel, B., Adams, D. T. and McCuaig, T. C., in press, Evidence for Two Stages of Mineralization in West Africa's Largest Gold Deposit: Obuasi, Ghana: Economic Geology
- Goldfarb, R., Groves, D., and Gardoll, S., 2001, Orogenic gold and geologic time: a global synthesis: Ore geology reviews, v. 18, p. 1-75.

Goldfarb, R. J., Baker, T., Dube, B., Groves, D. I., Hart, C. J., and Gosselin, P., 2005, Distribution, character, and genesis of gold deposits in metamorphic terranes: Economic Geology 100th Anniversary Volume, p. 407-450.

Groves, D. I., Goldfarb, R. J., Knox-Robinson, C. M., Ojala, J., Gardoll, S., Yun, G. Y., and Holyland, P., 2000, Late-kinematic timing of orogenic gold deposits and significance for computer-based exploration techniques with emphasis on the Yilgarn Block, Western Australia: Ore Geology Reviews, v. 17, p. 1-38.

Groves, D. I., Goldfarb, R. J., Robert, F., and Hart, C. J., 2003, Gold deposits in metamorphic belts: overview of current understanding, outstanding problems, future research, and exploration significance: Economic Geology, v. 98, p. 1-29.

Guj, P., Fallon, M., McCuaig, T. C., and Fagan, R., 2011, A Time-Series Audit of Zipf's Law as a Measure of Terrane Endowment and Maturity in Mineral Exploration: Economic Geology, v. 106, p. 241-259.

Hanssen, E., Kaisin, J. and Tessougue, S., 2004, The Yatela gold mine, Western Mali: Supergene enrichment of lower Proterozoic gold mineralization in a surficial karst: Abstract in proceeding of: CIM Annual Meeting.

Holcombe, R., 2007, Structural framework - Siguiri gold mine, Guinea, unpublished.

Jaireth, S., and Huston, D., 2010, Metal endowment of cratons, terranes and districts: Insights from a quantitative analysis of regions with giant and super-giant deposits: Ore Geology Reviews, v. 38, p. 288-303.

Kouamelan, A. N., Delor, C., and Peucat, J.-J., 1997, Geochronological evidence for reworking of Archean terrains during the early Proterozoic (2.1 Ga) in the western Cote d'Ivoire (Man Rise-West African Craton): Precambrian Research, v. 86, p. 177-199.

Lahondère, D., Thiéblemont, D., Tegyey, M., Guerrot, C., and Diabate, B., 2002, First evidence of early Birimian (2.21 Ga) volcanic activity in Upper Guinea: the volcanics and associated rocks of the Niani suite: Journal of African Earth Sciences, v. 35, p. 417-431.

Lawrence, D. M., Treloar, P. J., Rankin, A. H., Harbridge, P., and Holliday, J., 2013a, The geology

and mineralogy of the Loulo Mining District, Mali, West Africa: evidence for two distinct styles of orogenic gold mineralization: *Economic Geology*, v. 108, p. 199-227.

Lawrence, D. M., Treloar, P. J., Rankin, A. H., Boyce, A., and Harbridge, P., 2013b, A fluid inclusion and stable isotope study at the Loulo mining district, Mali, West Africa: Implications for multifluid sources in the generation of orogenic gold deposits: *Economic Geology*, v. 108, p. 229-257.

Masurel, Q., Thébaud, N., Miller, J., Ulrich, S., Hein, K.A.A., Cameron, G., Béziat, D. and Bruguier, O., in press 2015, Sadiola Hill: a world-class gold deposit in Mali, West Africa: *Economic Geology*.

McCuaig, T. C., Beresford, S., and Hronsky, J., 2010, Translating the mineral systems approach into an effective exploration targeting system: *Ore Geology Reviews*, v. 38, p. 128-138.

McCuaig, T. C., and Hronsky, J. M. A., 2014, The Mineral System Concept: The Key to Exploration Targeting: *Economic Geology - Special Publication*, v. 18, p. 153-175.

McFarlane, C. R. M., Mavrogenes, J., Lentz, D., King, K., Allibone, A., and Holcombe, R., 2011, Geology and Intrusion-Related Affinity of the Morila Gold Mine, Southeast Mali: *Economic Geology*, v. 106, p. 727-750.

McIntyre, J., and Martyn, J., 2005, Early extension in the Late Archaean northeastern Eastern Goldfields Province, Yilgarn Craton, Western Australia: *Australian Journal of Earth Sciences*, v. 52, p. 975-992.

Milési, J. P., Feybesse, J. L., Ledru, P., Dommange, A., Ouedraogo, M. F., Marcoux, E., Prost, A., Vinchon, C., Sylvain, J. P., Johan, V., Teguey, M., Calvez, J. Y., and Lagney, P., 1989, Les minéralisations aurifères de l'Afrique de l'Ouest. Leurs relations avec l'évolution lithostructurale au Protérozoïque inférieur: *Chronique de la recherche minière*, v. 497, p. 3-98.

Miller, J., Blewett, R., Tunjic, J., and Connors, K., 2010, The role of early formed structures on the development of the world class St Ives Goldfield, Yilgarn, WA: Precambrian Research, v. 183, p. 292-315.

Miller, J. M., Davis, J., Baratoux, L., McCuaig, T. C., Metelka, V. and Jessel, M., 2013, Evolution of gold systems in Guinea, southern Mali and western Burkina Faso: AMIRA International Ltd P934A - West African Exploration Initiative - Stage 2 Final report, Appendix D1, confidential

Neumayr, P., Walshe, J., Hagemann, S., Petersen, K., Roache, A., Frikken, P., Horn, L., and Halley, S., 2008, Oxidized and reduced mineral assemblages in greenstone belt rocks of the St. Ives gold camp, Western Australia: vectors to high-grade ore bodies in Archaean gold deposits?: Mineralium Deposita, v. 43, p. 363-371.

Paranhos, C. J., 2008, Siguiri gold mine - State of knowledge of the main geological controls of gold mineralization, unpublished, p. 40.

Parra-Avila, L. A., 2015, 4D Evolution of the Paleoproterozoic Baoulé-Mossi Domain of the West African Craton: PhD thesis, University of Western Australia

Pigois, J.-P., Groves, D. I., Fletcher, I. R., McNaughton, N. J., and Snee, L. W., 2003, Age constraints on Tarkwaian palaeoplacer and lode-gold formation in the Tarkwa-Damang district, SW Ghana: Mineralium Deposita, v. 38, p. 695-714.

Robert, F., Poulsen, K. H., Cassidy, K. F., and Hodgson, C. J., 2005, Gold metallogeny of the Superior and Yilgarn cratons: Economic geology, v. 100, p. 1001-1033.

Sestini, G., 1973, Sedimentology of a Paleoplacer: The Gold-bearing Tarkwaian of Ghana, Ores in Sediments, Springer, p. 275-305.

Steyn, J. G., 2012, Structural geology and controls of gold mineralization in the Siguiri Mine, Guinea, West Africa, Stellenbosch University.

Thiéblemont, D., Delor, C., Cocherie, A., Lafon, J. M., Goujou, J. C., Baldé, A., Bah, M., Sané, H., and Fanning, C. M., 2001, A 3.5 Ga granite–gneiss basement in Guinea: further

- evidence for early archean accretion within the West African Craton: Precambrian Research, v. 108, p. 179-194.
- Thiéblemont, D., Goujou, J. C., Egal, E., Cocherie, A., Delor, C., Lafon, J. M., and Fanning, C. M., 2004, Archean evolution of the Leo Rise and its Eburnean reworking: Journal of African Earth Sciences, v. 39, p. 97-104.
- Treloar, P., Lawrence, D., Senghor, D., Boyce, A., and Harbridge, P., 2015, The Massawa gold deposit, Eastern Senegal, West Africa: an orogenic gold deposit sourced from magmatically derived fluids?: Geological Society, London, Special Publications, v. 393, p. 135-160.
- Tshibubudze, A., Hein, K. A. A., Peters, L. F. H., Woolfe, A. J., and McCuaig, T. C., 2013, Oldest U-PB crystallisation age for the West African Craton from the Oudalan-Gorouol Belt of Burkina Faso: South African Journal of Geology, v. 116, p. 169-181.
- Villeneuve, M., and Cornée, J., 1994, Structure, evolution and palaeogeography of the West African craton and bordering belts during the Neoproterozoic: Precambrian Research, v. 69, p. 307-326.
- Watts, M., 2010, An introduction to the geology of Siguiri gold mine and the economic potential of the fresh rock in block 1, unpublished, p. 139.
- Williams, P., and Currie, K., 1993, Character and regional implications of the sheared Archaean granite-greenstone contact near Leonora, Western Australia: Precambrian research, v. 62, p. 343-365.
- West Africa: A Look at Gold Mining in Ghana, Mali and Burkina Faso, 2014, Available from: <<http://goldinvestingnews.com/46088/africa-ghana-mali-burkina-faso-iamgold-roxgold-true-gold-randgold-perseus-askano.html>>, [15 July 2015].

CHAPTER 2: PAPER ONE

GEOCHRONOLOGY AND LITHOSTRATIGRAPHY OF THE SIGUIRI DISTRICT: IMPLICATIONS FOR GOLD MINERALISATION IN THE SIGUIRI BASIN (GUINEA, WEST AFRICA)

The Siguiri district sits alone in the central Siguiri Basin, one of the biggest sedimentary basins of the West African Craton. The following paper presents the lithostratigraphy and geochronology of the central part of the Siguiri Basin. The study is based on field observations and geophysical datasets from the whole Siguiri Basin. This work constitutes the first integrated study of the Siguiri Basin lithostratigraphy and geochronology. A total of six new U-Pb ages were determined from three sedimentary Formations (four ages) and two igneous rocks.

The Siguiri Basin sediments were deposited around ca. 2015 Ma, making the Siguiri Basin relatively young compared to most West African sedimentary basins. A major change in the lithostratigraphy observed across the entire Siguiri Basin in geophysical datasets and ground-truthed in the field, is interpreted to represent olistostrome deposits that mark a change in the Basin opening dynamics and the onset of the Eburnean compression. The morphology of this olistostrome is controlled by faults interpreted as fundamental structures associated with the early architecture of the Siguiri Basin and viewed as the first order controls on the location of the Siguiri district. These conclusions make the Siguiri Basin and the Siguiri

district key locations for the understanding of the Eburnean orogeny and gold mineralisation in this part of the West African Craton.

This chapter was submitted to Precambrian Research and is hence formatted in this style. It was revised a number of times by all co-authors and by two reviewers from the Precambrian Research journal before resubmission.

Geochronology and lithostratigraphy of the Siguiri district: implications for gold mineralisation in the Siguiri Basin (Guinea, West Africa)

Erwann Lebrun^{1*}, Nicolas Thébaud¹, John Miller¹, Stanislav Ulrich², Julien Bourget³, Ockert Terblanche²

¹: Centre for Exploration Targeting and ARC Centre of Excellence for Core to Crust Fluid Systems, School of Earth and Environment, Robert Street Building, M006, The University of Western Australia, 35 Stirling Highway, Crawley, WA, 6009, Australia

²: AngloGold Ashanti Ltd - Brownfields Exploration Technical Hub - Continental Africa Region, 44 St George Terrace, Perth, WA, 6000, Australia

³: Centre for Petroleum Geoscience and CO₂ Sequestration, School of Earth and Environment, M004, The University of Western Australia, 35 Stirling Highway, Crawley, WA, 6009, Australia

*: Corresponding author. Phone: (+61) 8 6488 7152 Email: erwann.lebrun@gmail.com

Abstract:

Geochronology and lithostratigraphic characterisation of the Siguiri district in the Paleoproterozoic Birimian terrane of West Africa has provided a reappraisal of the Siguiri Basin stratigraphy. This new insight into the evolution of the central part of the Basin further highlights first order controls on the location of the world class Siguiri orogenic gold district. Three metasedimentary Formations occur in the Siguiri district, namely: the Balato, Fatoya and Kintinian Formations. These consist of fine-grained organic-rich shales, mudstone and siltstone/greywacke/limestone interbeds, decimetre to metre-thick graded greywacke beds and debris flow deposits. The Balato Formation displays low-energy, hemipelagic marine or

lake sediments, while the Fatoya Formation consists of distal turbidite deposits (thin-bedded turbidites and channel-fill deposits). Altogether they form a basal regressive sequence. The over-lying Kintinian Formation is shale-rich, and displays up to a 100 metre-thick stack of polymict conglomeratic interbeds observed in the basal part of the Formation in the Siguiri district. These conglomerates transect the whole Siguiri Basin and are interpreted as the product of repeated subaqueous debris flow deposits and to representolistostromes (or mélanges of sedimentary origin) with various autochthonous and allochthonous clasts. The Balato, Fatoya and Kintinian Formations maximum age of deposition was dated at 2113 ± 10 , 2113 ± 5 Ma and 2124 ± 7 Ma respectively. The minimum age of deposition of these sediments is constrained by a crosscutting volcanic breccia dated at 2092 ± 5 Ma, and by the Maléa monzogranite intrusion dated at 2089 ± 12 Ma. Comparison of the sedimentary facies and geochronology of the Siguiri sediments with other metasedimentary basins in the West African Craton, suggests that the Kintinian Formation is part of the Lower Tarkwa Group sediments commonly described as “late orogenic basin” sediments. The Kintinian olistostromes are inferred to highlight the onset of renewed tectonic activity associated with the first phases of compression during the Eburnean orogeny in the Siguiri Basin at ca. 2115 Ma. The peculiar morphology of this olistostrome, compared to the bulk of the Siguiri Basin sediments, illustrates a major change in lithofacies. This change is interpreted to have developed along WNW-ESE, N-S and NE-SW oriented fundamental basement structures, controlling the early architecture of the Siguiri Basin as well as the location of world-class gold mineralisation in the Siguiri district. These WNW-ESE, N-S and NE-SW fundamental structures are thought to have acted as the first order fluid pathways during the E-W progressive compressional event responsible for orogenic gold mineralisation in the Siguiri district.

Keywords: West Africa, Siguiri Basin, geochronology, lithostratigraphy, early architecture, gold

Introduction

A comprehensive understanding of the lithostratigraphy is a fundamental part of defining the regional structural framework of any mineralized province. Lithostratigraphic syntheses of Precambrian terranes have highlighted how the early architecture and fundamental structures controlling the lithostratigraphic record can be delineated (e.g. Robert et al., 2005; Williams and Currie, 1993; McIntyre and Martyn, 2005; Blewett et al., 2010). These early structures are often proposed to apply a multiscale control on mineralisation, as highlighted by the mineral system concept (McCuig and Hronsky, 2014). This early architecture is often cryptic and consists of incipient structures hidden away undercover (Lebrun et al., in review 2015; Chapter 3; "vertical accretive growth" structures of McCuaig and Hronsky, 2014). Later reactivations of these structures to the regional stress-field by overpressured fluids (Sibson et al., 1988; Sibson and Scott, 1998), develops veining in, around and above these structures, often following lithostratigraphic interfaces (Robert et al., 2005; Miller et al., 2010).

As an example, numerous orogenic gold deposits hosted in sedimentary basins around the world are interpreted to be sitting on early structures highlighted in the field through lithofacies variations. For example, the Kirkland Lake deposit hosted along the Kirkland-Lake Cadillac fault that marks the unconformity between the Timiskaming sediments and the Abitibi Supergroup in Canada (Hyde, 1980). Similarly in the Western Australian Yilgarn craton, gold deposits such as Ant Hill, Bullant, Porphyry and Wattlebird are hosted along the Ballard-Zuleika Shear Zone and highlighted by the Kurrawang Group sediments (Robert et al., 2005; Mueller et al., 1996; Weinberg et al., n.d.). In the West African Craton, the giant Obuasi deposit in Ghana is hosted along the Ashanti fault separating the Birimian sediments from the "late orogenic" Tarkwaian sediments of the Ashanti Belt (Perrouty et al., 2012; Sestini, 1973).

Also located in the West African Craton, the world-class orogenic gold district of Siguiri (Steyn, 2012; Lebrun et al., in review 2015; Chapter 3) is hosted in the north of the Siguiri Basin (Guinea), about 200 km south-west of Bamako in Mali and 150 km north of Kankan, the second

largest city in Guinea. The district measured resources were 21.08 t Au indicated resources from ore averaging 2.35 g/t as of the 31st of December 2013 (inclusive non-attributable resources only) and produced an estimated cumulative total of 240 t Au (AngloGold Ashanti Ltd., n.d.; Lebrun et al., in review 2015; Chapter 3).

Due to its very poor outcropping quality, the lithostratigraphy of the Siguiri Basin has received little attention, and existing studies have mostly focused on the importance of magmatism during the Eburnean orogeny (Egal et al., 2002). Early regional mapping from the French Geological Survey (BRGM) described the Siguiri Basin as an homogeneous package of undifferentiated fine sedimentary rocks (Egal et al., 1999; Feybesse et al., 1999).

This paper presents a multi-disciplinary study combining sedimentological, geochronological and geophysical analyses over the Siguiri district that allows for further discrimination of the Siguiri Basin sedimentary record. Used collectively, the datasets constrain the lithostratigraphic succession of the central Siguiri Basin and permit the drafting of a new geological map for this critical region. The results of this study allow to: 1) enhance our understanding of the fundamental lithofacies and architecture of the Siguiri Basin, and its tectonic position in the West African Craton evolution, 2) explain that the location of the world-class orogenic gold Siguiri district is controlled by the early architecture of the Basin, and 3) provide a fundamental targeting criteria for orogenic gold systems in the West African Craton.

Geological context

Regional Geology

The Siguiri Basin is located in the north-western part of the Paleoproterozoic Baoulé-Mossi domain, which covers western Guinea, southern Mali, most of Burkina Faso, western Niger, south-east Liberia, Ivory Coast and western Ghana; the Kédougou-Kéniéba inlier, in eastern Senegal, being the western-most expression of these Birimian terranes (ca. 2050-2200 Ma; Figure 3A). The Paleoproterozoic Baoulé-Mossi domain was accreted against the Archean

Kénéma-Man domain, in the south-west of the West African Craton, during the Eburnean orogeny (ca. 2100-2000 Ma; Abouchami et al., 1990; Egal et al. 2002; Thiéblemont et al. 2004). The Neoproterozoic sediments of the Taoudeni Basin overlie both these domains unconformably.

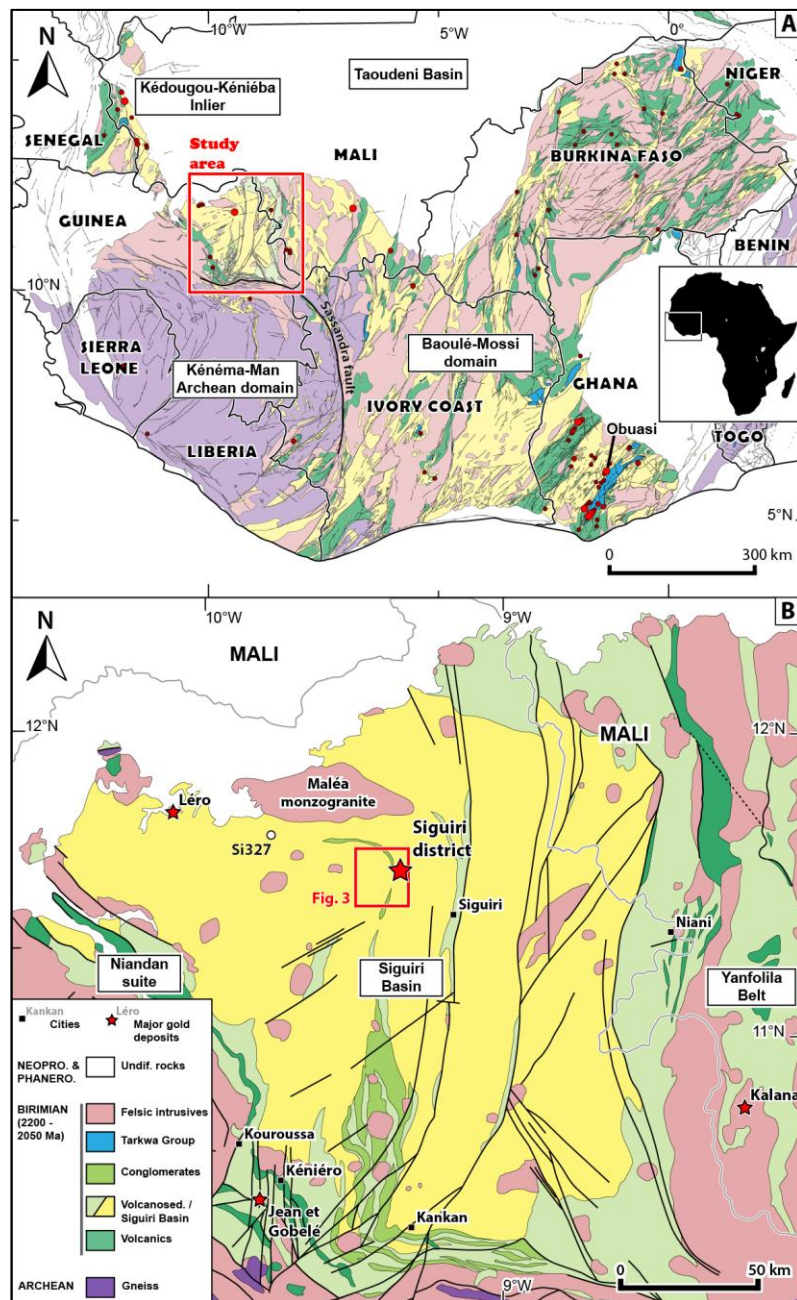


Figure 3: A) Geological map of the West African Craton. Orogenic gold deposits are displayed as small red discs. B) Geological map of the Siguiri Basin. Location of the Siguiri district map in red. Location of the Saraya geochronological sample, Si326, in white. Modified from Milési et al. (1989) and Miller et al. (2013).

The Siguiri Basin is bordered to the west and south by the mafic to felsic volcanic rocks of the Kéniéro Range (dated at 2093 ± 2 Ma; Feybesse et al., 1999), the komatiite suite of Niandan, and by a large volume of granodiorite (ca. 2090-2070 Ma, Egal et al., 2002; Figure 3B). To the south the Sassandra fault separates the Siguiri Basin from the Kénéma-Man Archean domain (Egal et al., 2002), host to the Archean Simandou banded iron formations. To the east, the Siguiri Basin is bordered by the intermediate to felsic calc-alkaline Niani suite, dated at 2212 ± 6 Ma, and by the Yanfolila greenstone belt which has an intercalation of volcanoclastic sedimentary rocks and dominantly mafic to intermediate volcanics. To the north, the Siguiri Basin is overlain unconformably by the flat-lying sandstones of the Neoproterozoic Taoudeni Basin. Mesozoic sills, volcanic flows and ENE-WSW dykes related to the south Atlantic opening also cut across or overlie the Siguiri Basin (Abouchami et al. 1990; Egal et al., 1999; Egal et al., 2002; Paranhos 2008, unpublished). Localised Archean banded iron formations also outcrop to the north-west and south of the Siguiri Basin.

The lithostratigraphy of the West Africa Craton has received little attention since its early description and craton-scale correlations by Milési et al. (1989), Milési et al. (1992) and Feybesse and Milési (1994). Hirdes et al. (1992), Hirdes and Davis (1998), Loh and Hirdes (1999) and Taylor et al. (1992) provided further geochronological constraints. Most recent regional reconstructions have systematically used geochronological and geophysical constraints when delineating lithological distributions across a study area (Baratoux et al., 2011; Davis et al., 2015; Parra-Avila et al., this volume; Perrouty et al., 2012; Perrouty et al., 2014).

Goloubinow (1936), Villeneuve (1992) together with the BRGM, mapped the Siguiri Basin as a homogeneous package of undifferentiated fine sediments derived from erosion of Paleoproterozoic granitoids that were emplaced during the earliest stages of the Eburnean orogeny (Egal et al., 1999; Milési et al. 1989). The Siguiri Basin sediments are interpreted to have deposited during the Lower Birimian and be accompanied by volcanic rocks, later

intruded by monzogranites and biotite granites at ca. 2075 Ma (Egal et al., 1999; Egal et al., 2002; Feybesse and Milési 1994; Feybesse et al., 1999; Milési et al. 1989).

Structural framework

A protracted deformation history for the Siguiri Basin has been recently compiled on the basis of the Siguiri district study (Steyn, 2012; Lebrun et al., in review 2015; Chapter 3). This deformation history is characterized by three folding episodes associated with: a N-S compression, D_{1s} , followed by an E-W compression, D_{2s} (that progressively evolved into a transpression and then a transtension during D_{3s}), and a late NW-SE compression, D_{4s} (Figure 4).

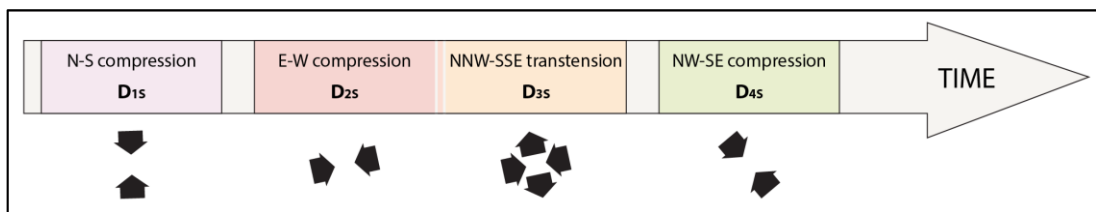


Figure 4: Structural scheme of the deformation history observed in the Siguiri district. The E-W compression D_{2s} evolves progressively to a transtension responsible for gold mineralisation in Siguiri, D_{3s} . After the work from Lebrun et al. (in review 2015); Chapter 3.

While D_{1s} deformation is cryptic and its E-W folds discreet, D_{2s} E-W compression is associated with the bulk of the deformation observed in the Siguiri district and is responsible for the N-S structural grain of the Siguiri Basin. Finite strain analysis of the ductile and brittle structural elements associated with D_{2s} and D_{3s} (e.g. folds, faults, veins) indicates multiple stress-switches. The early- D_{2s} E-W compression is interpreted to have evolved into an early- D_{3s} E-W transpression before the stress-field switched to a late- D_{3s} NNW-SSE transtensional deformation responsible for the development of gold mineralisation. Ore shoots are controlled by four main orientations of structures formed late during D_{2s} (N-S thrusts and E-W normal faults) and early- D_{3s} (NE-SW to ENE-WSW dextral shear zones and WNW-ESE sinistral shear zones), but all reactivated late- D_{3s} . These structures are characterised in the field by an increase in gold bearing vein density. These veins are made of quartz-carbonate-arsenopyrite,

are consistently oriented NE-SW across the entire Siguiri district and are typically steeply dipping to the SE. Overprinting all earlier structures, the D_{4S} NW-SE compression develops a penetrative steep cleavage, S_{4S}, that is parallel to the sub-solidus magmatic fabric found in the Maléa monzogranite which intrudes the Siguiri Basin sediments a few kilometres north of the Siguiri district (Figure 2B).

Methodology

Fieldwork and sample selection

Twenty-two weeks of fieldwork in the Siguiri Basin were conducted over 2 years starting in April 2011. Fieldwork campaigns, of about a month length each, were mainly focused on the Siguiri district tenement (Figure 5), with 2 weeks of regional field transects undertaken. Observations and description of the stratigraphy, lithofacies associations and geochronological sampling were conducted directly on outcrop and drill core. These observations, integrated with geophysical data, were compiled on a geology map of the district (Figure 5).

Seven diamond drill cores were logged, allowing the creation of a synthetic lithostratigraphic column. This column was constrained by sedimentary descriptions and interpretations (Figures 6 to 8), as well as structural work (e.g. fold vergence). The stratigraphic column (Figure 9) was constructed by detailed logging of bedsets in the selected cores and stacking each log according to field observations of geopetal indicators or structural relationships.

Geophysical data

The Siguiri gold district is characterised by lateritic profile of up to 200 m thick. To compensate for this thick cover and link district-scale and regional-scale interpretations over the Siguiri Basin lithostratigraphy, multiple geophysical datasets were used. The airborne electromagnetics (AEM) response of each individual lithostratigraphic Formation was

particularly useful in the making of the district-scale geological map (Figure 5), regional correlations were constrained by the magnetics datasets.

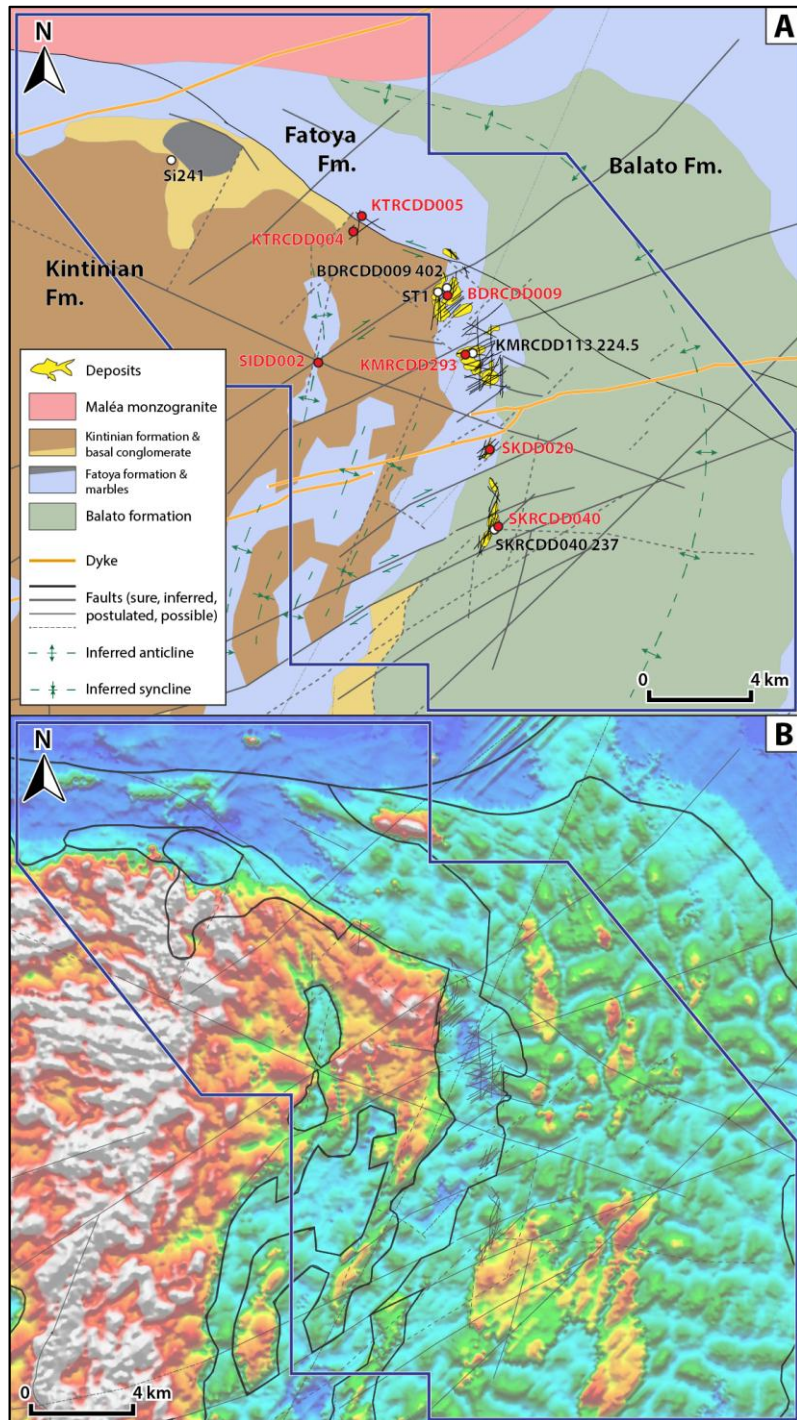


Figure 5: A) Geological map of the Siguiri district tenement as interpreted from the Spectrem AEM Tau products. Deposits are structurally controlled and mostly hosted in the Fatoya formation (Lebrun et al., *in review* 2015; Chapter 3). The location of each geochronological sample is reported on the map. Sample Si326 was sampled further west (Figure 3B). The blue outline represents the Siguiri tenement boundaries. B) SPECTREM Late-Time Tau of the Z-component (maximum Tau for Z-channel 5-8) with overlain sedimentary formation boundaries, faults and Siguiri tenement boundaries.

The AEM system employed is the fixed-wing SPECTREM platform that simultaneously measures electromagnetic, total field magnetic and radiometric response. Both the electromagnetic and magnetic sensors are towed (as “birds”) behind the aircraft in the slingram configuration, while the radiometric crystals are installed inside the cabin. The SPECTREM system has a 100% duty cycle with a base frequency of 75Hz, a 400 000 A.m² RMS dipole moment, the X & Z components are measured and the AEM data is binned into 8 channels or windows. The survey was completed in 2007 using 200 m line-spacing at 45° and a nominal aircraft altitude of 90 m.

The mineral exploration community has historically applied AEM as a “bump detector” for bedrock conductors. Another application of AEM is the ability to discriminate or map individual lithologies or lithostratigraphic packages within a sedimentary terrain. Due to the sedimentary facies variations of the Balato, Fatoya and Kintinian Formations (as described in §4.1); the Kintinian will generally be more conductive and the Fatoya the most resistive of the three units (Figure 5). Because of the large depth of weathering both mid-time and late-time Tau-Z products have been used to ensure bedrock variations are being highlighted. The use of the Tau products also minimises severe terrain-clearance effects that are evident on the Z-channel grids within isolated areas.

The study used airborne magnetic data, with the analytical signal being one of the key data sets (Roest et al., 1992). This is a function related to magnetic fields by a combination of derivatives. While the analytical signal is not a measurable parameter it is useful for interpretation purpose as it is completely independent of the Earth’s magnetic field. This means that all geological bodies displaying a similar geometry, exhibit the same analytical signal. Furthermore as the peaks of analytic signal functions are symmetrical and occur directly above the edges of wide geological entities, interpretation of analytical signal maps and images can provide simple indications of magnetic source geometry. It is a useful dataset to delineate various geological entities, lithologies or lithostratigraphic packages.

Geochronology

A total of six rock samples were collected in the Sigiri Basin. Five representative detrital samples were selected for each interpreted lithostratigraphic Formation encountered in the Sigiri district (Figure 5). An extra sample from a crosscutting volcanic lithology was also sampled to the west of the district (Figure 3). Samples were collected from pit exposures, field outcrop or drill core. Around 3 to 5 kg of material were taken for most samples, but conglomerate and brecciated samples had 10 kg of material sampled to compensate for their larger grain-size. While most samples came from ore zone vicinities, each one was taken within the least hydrothermally altered and weathered areas. All samples had their weathered area trimmed off prior to being crushed.

The zircons were separated using standard heavy liquid and magnetic techniques by GeoTrack International laboratories in Melbourne (Australia). Mineral concentrates were then sent to MinSep Laboratories in Denmark (Australia), where zircons were hand-picked, mounted and polished for SHRIMP analysis. Mount imaging was conducted on a Nikon Eclipse LV100 POL at the Centre for Exploration Targeting (CET) in Perth (Australia). SEM imaging was conducted on a TESCAN VEGA3 at the Centre for Microscopy, Characterization and Analysis (CMCA) of the University of Western Australia, also in Perth. Each mount, containing 2 to 3 samples, was cleaned according to the standard protocol described by Wingate and Kirkland (2014). Gold coating was conducted at the John de Laeter Centre for Isotope Research of Curtin University, in Perth.

All mounts were analysed by Sensitivity High Resolution Ion Microprobe (SHRIMP II) at the John de Laeter Centre for Isotope Research of Curtin University, in Perth (Australia). Analytical conditions and operational procedures are standard (Claoue-Long, 1995; Compston et al., 1984; Wingate and Kirkland, 2013). For each sample, an average of fifteen analyses of the standard BR266 (559 Ma, 903 ppm U; Stern, 2001) or M257 (561 Ma, 840 ppm U; Nasdala et al., 2008) was carried out over the twenty-four hour SHRIMP session. Raw data reduction was completed following Wingate and Kirkland, (2013) directions using SQUID (Ludwig, 2000).

Corrections for common Pb were based on measured ^{204}Pb , assuming an average crustal composition fitting the age of the mineral (Stacey and Kramers, 1975). Calibration uncertainties and error of mean were used for the error calculation of the $^{238}\text{U}/^{206}\text{Pb}$ ratios. This in turn provided the way to merge multiple raw data files from different SHRIMP sessions of the same rock sample, increasing the statistical validity of the reduction. Merging was conducted for samples: 1) KMRCDD113 224.5 (two mounts); and 2) Si241 (three mounts). Limit values for the analyses of unknowns were as follow: 1) common Pb < 1.0%; and 2) -2 % \leq discordance \leq 5%. Analyses on zircons with high crack density or strong metamict damage were discarded.

Results

The Siguiri district lithostratigraphy

The Siguiri district lithostratigraphy consists of a thick (>400 m) sedimentary sequence metamorphosed to sub-greenschist facies. Overall, the metasediments mostly consist of normally graded to massive, dm to m-thick greywacke beds interbedded with claystone-siltstone, and shale (Figure 6, 7, 8, 9).

In detail, the lithostratigraphy of the Siguiri district was divided into three distinct sedimentary Formations (Figure 9; Watts, 2010). These Formations are, from older to younger: the Balato, Fatoya and Kintinian Formations. A schematic log representing the lithostratigraphic column of the Siguiri gold district is presented on Figure 9.

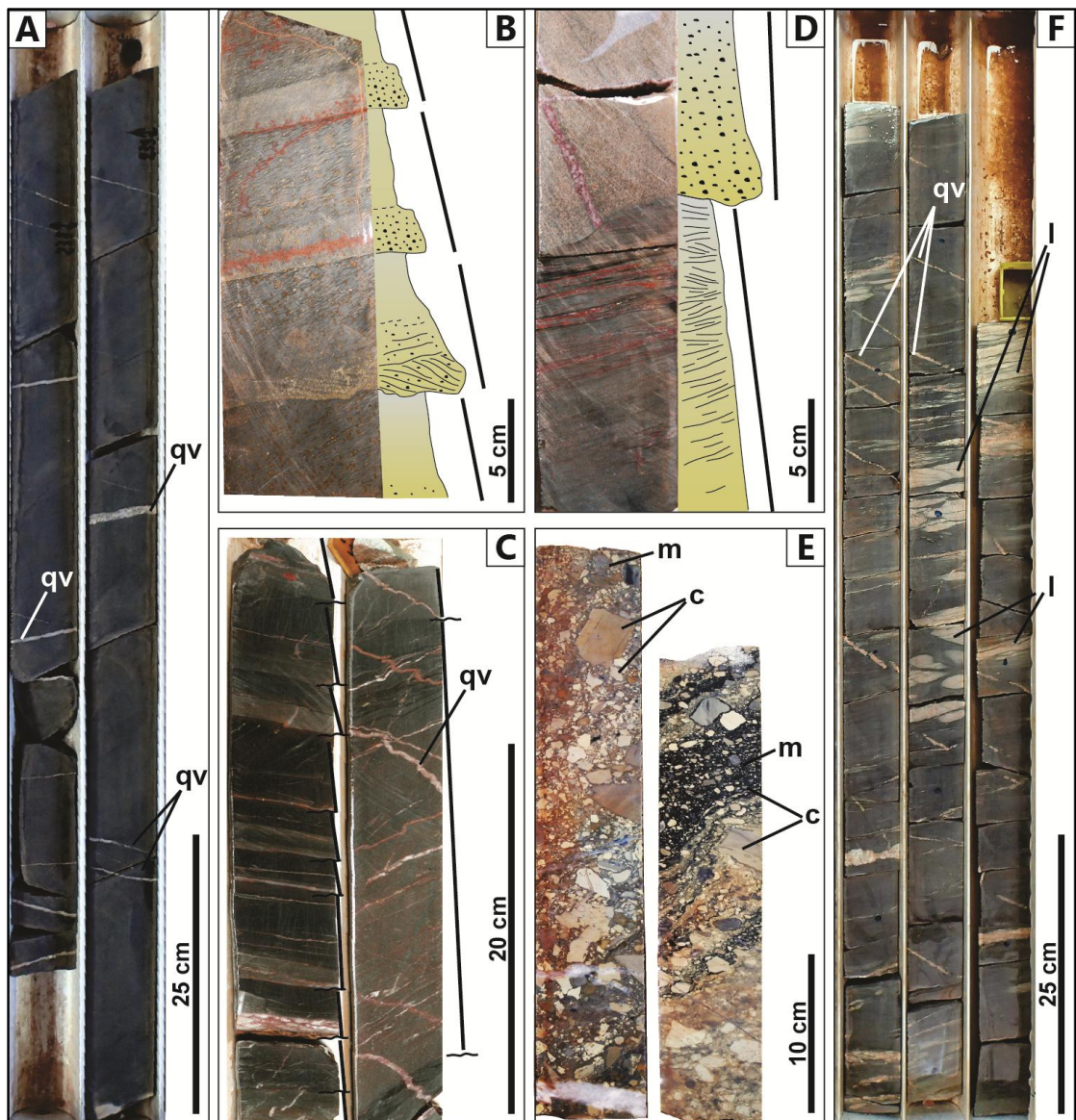


Figure 6: Core photographs from: the Balato formation (A), showing massive, dark grey shales; the Fatoya formation (B, C, D) showing thin-bedded, fining-upward turbidites with massive to cross-laminated greywacke bases grading to siltstone and mudstone (T_c-e of the Bouma sequence); the Kintinian formation, showing (E) the basal polymict conglomerates observed in the Sanu Tinti deposit and (F) the upper massive dark-green shales with cm-thick, limestone interbeds. c: clast; l: limestone interbeds; m: matrix; qv: quartz vein.

The Balato Formation is dominated by dark grey to light grey massive siltstone beds grading upwards to shale, alternating with cm-thick shale-siltstone and rare fine greywacke interbeds (Figure 6A). The unit is relatively incompetent, is intensely deformed, and displays isoclinal folding. Only the top of this Formation is sampled by the existing drilling and the thickness of the Balato Formation is difficult to evaluate. The contact between the Balato and overlying Fatoya Formation was not observed in the drill-core or on the field.

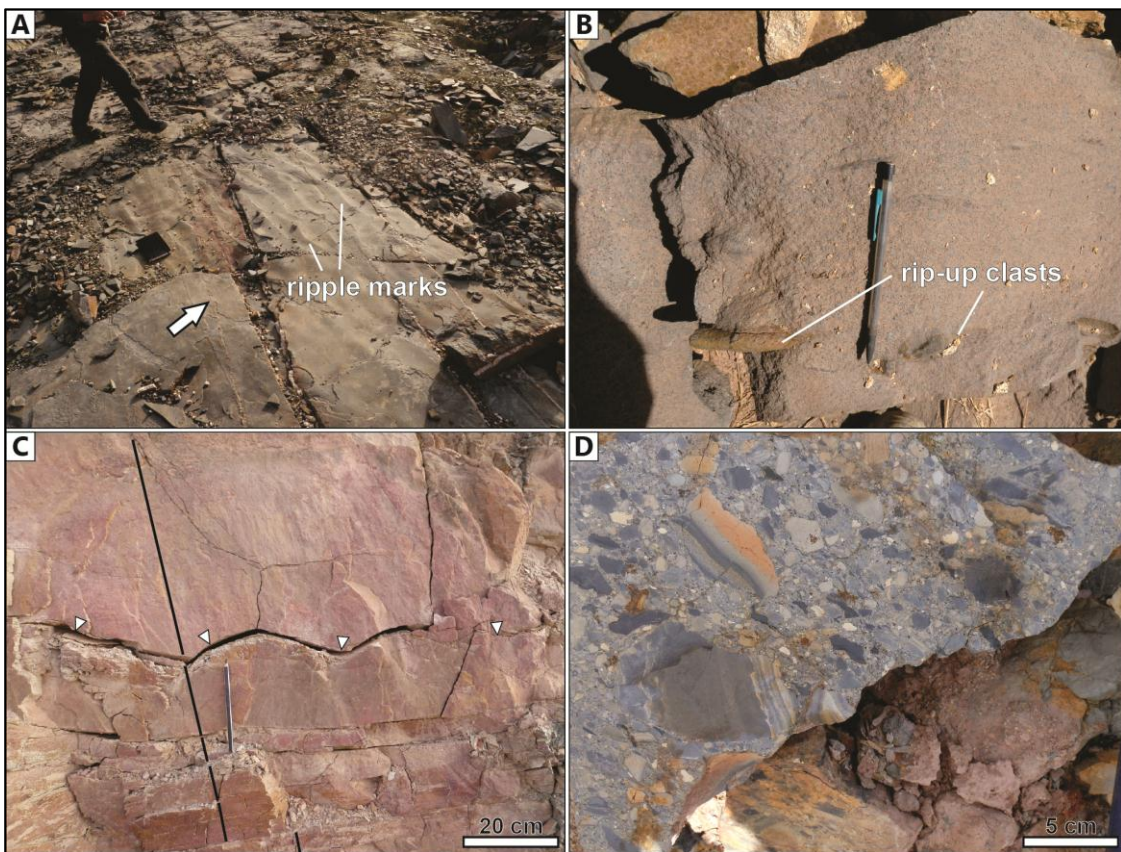


Figure 7: Field photographs of (A) ripple marks in the Kami deposit, Fatoya formation; (B) rip-up clasts of shale at the base of a turbidite (greywacke) bed in the Fatoya formation; (C) cm to dm-thick bedded greywacke turbidites in the Fatoya formation associated with basal erosional (scour) surfaces (white arrows); (D) basal conglomerate of the Kintinian formation showing the polymict, poorly-sorted, angular to sub-rounded clasts dominated by greywacke/shale interbeds and shale (likely sourced from the Balato and Fatoya formations).

The Fatoya Formation is dominated by normally-graded (fining-upward), dm to m-thick beds of medium to coarse-grained greywacke grading upwards to siltstone and mudstone (Figure 5C, 5D, 6B). Beds are highlighted by sharp to erosional (scoured) basal surfaces (Figure 6D and 7C). Sub-angular to sub-rounded rip-up clasts of siltstone, mudstone and shale can be observed in some instances (Figure 7B), suggesting that the fining-upward greywacke beds were the product of erosional flows. High to low-angle cross-lamination is commonly observed highlighting the deposition of current ripples in lower flow regime conditions (Figure 6B and 6D). Asymmetric ripple marks are also observed in the field (Figure 7A). Pyrite is abundant in the upper, finer-grained layers of the beds (Figure 6B). Although difficult to evaluate because of the poor overlap between the drill-holes logged, the minimum thickness of the Fatoya

Formation is estimated at ~400m (Figure 9). Field observations of the contact between the Fatoya and Kintinian Formation clearly put the latter stratigraphically on top of the former. In the Seguelen deposit further to the north, the contact between the two Formations is sharp and disconformable (Figure 8C).

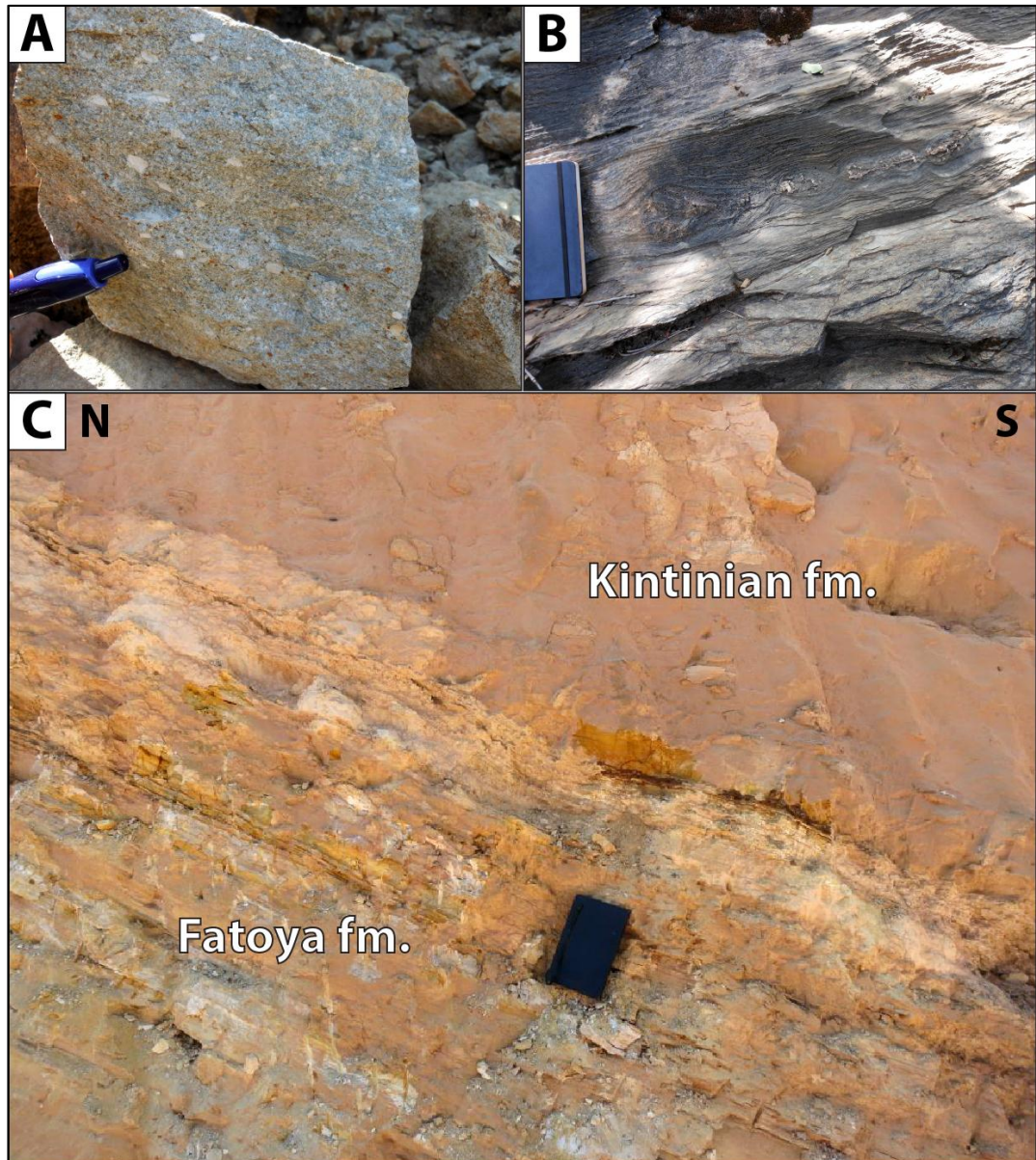


Figure 8: Photographs of A) the Saraya volcanic breccia; B) marbles from the Marble Hill location; and C) the contact between the Fatoya and the Kintinian formation in the Seguelen deposit.

The Kintinian Formation is a >400 m thick Formation dominated by massive dark-green shale with cm-thick, boudinaged limestone interbeds (Figure 6F). Thin beds of siltstone or fine graded greywacke are also observed. The most striking feature of the Kintinian Formation is the presence of a thick sequence (~ 100 m) of at least two stacked conglomeratic layers

observed interbedded within the Formation (Figure 6E and 7D). These conglomerates consist of dominantly clast-supported deposits with 5 to 30 vol% of fine-grained (mudstone to fine greywacke) matrix (Figure 6E). The clasts are angular to sub-rounded and poorly sorted, ranging in size from a few millimetres up to a meter but average 2-3 centimetres (Figure 7D). Based on field and core observations, thin-sections and photographs, clast lithologies in the Siguiri district include:

- shale. These commonly massive clasts sometimes show fine laminations or are interbedded with siltstone and greywacke. They are dark grey to light brown when not altered, and represent about 85 vol% of the clasts observed;
- limestone. These clasts are commonly white to light cream and show a massive to laminated texture. They represent an average of about 10 vol% of the clasts observed but can also represent the bulk of the clasts, such as in drill core SIDD002;
- felsic volcanics. These clasts can be confused with limestone clasts because of their colour but show a hardness close that of quartz to the scribe pen. They typically show a massive texture and are thought to represent less than 1 vol% of the clasts observed;
- felsic intrusive. These clasts are difficult to recognize since carbonatation spotting and albitisation can sometimes be confused with their granular texture. Clasts mineralogy comprises quartz, feldspar and biotite. They may represent about 1 vol% of the clasts observed and were mostly found in darker intersects of conglomerate;
- banded iron formation (BIF). These black clasts are only rarely observed in thin-section (below 1 vol%), where they show a discrete banding and a mineralogy made of hematite, quartz, plagioclase and biotite;
- possible mafic volcanics. These black massive clasts are typically more rounded and show an aphanitic texture in cores. They may represent up to 4 vol% of the observed clasts.

The thickness of individual conglomerate beds and their stacking patterns is difficult to determine from drill cores, as larger clasts might be mistaken for major breaks in the

sedimentation. However, available data show that the Kintinian conglomerates occur as thick (~10-15 m) deposits overlain by thin (<50 cm) shale to mudstone intervals. The conglomerates were observed at the contact with Fatoya greywackes, above a thrust fault in the Sanu Tinti deposit, and reworking meta-limestone/marble in drill cores from the Silakoro area. Based on the current data, the conglomeratic layers sit near the base of the Kintinian Formation, are overlain by mudstone and boudinaged limestone interbeds representing the bulk of the Kintinian Formation (Figure 6F), and their true thickness varies across the map and in cores.

In order to integrate the observations from the Siguiri district in the broader Siguiri basin framework, two additional localities were investigated: the Marble Hill and the Saraya area (Figure 3B and 5A). Located between the Kintinian and the Fatoya Formations in map view (area around sample Si241 on Figure 5A), the Marble Hill displays conglomerate and greywacke sitting on top of strongly foliated meta-limestone beds (Figure 6D). This is the only place in the Siguiri district where *in situ* beds of meta-limestone were observed. The conglomerate layers found in the Marble Hill are similar to the ones hosted in the Kintinian Formation and observed in the Sanu Tinti deposit. However, in the conglomerate units in and around the Marble Hill, limestone clasts increase in proportion (drill-hole SIDD002; Figure 5A). The Marble Hill conglomerates are viewed as a locally sourced lateral variation of the Kintinian conglomerate found in the Sanu Tinti deposit. The meta-limestone beds are therefore considered to represent the overturned stratigraphic top of the Fatoya Formation or base of the Kintinian Formation (Figure 9). Even though not enough zircons could be separated from the meta-limestone, meta-greywacke from the top of the Marble Hill were sampled successfully for SHRIMP dating (sample Si241; Figure 5A).

The Saraya area is located ~50 km west of the Siguiri district (area around sample Si327 on Figure 3B). The lithostratigraphy in the Saraya area is similar to that of the district, displaying fine micaceous greywacke, siltstone and shale beds alike of those of the Balato, Fatoya and Kintinian Formations. In AEM, the Saraya area shows a low response similar to that of the Fatoya Formation. The Saraya metasediments are however overlain unconformably by

volcaniclastic rocks of andesitic composition displaying cm to dm-sized subangular felsic clasts (Figure 6A) alternating with black chert lenses and meter-thick layers of tuff (Cayn, 2011). These volcaniclastic units are estimated to be over 400 m thick and were sampled for SHRIMP dating (sample Si327; Figure 3B).

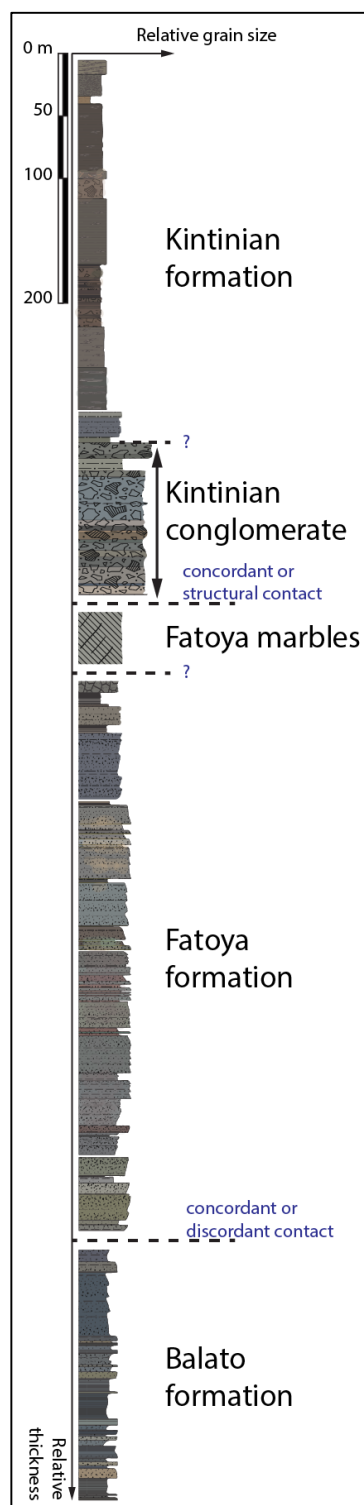


Figure 9: Lithostratigraphic column of the Siguiri district. This synthetic log was constructed using six different drill holes spread across the district. True thickness of each sedimentary formation is unknown.

Geological map and regional stratigraphic integration

The field and drill core observations were integrated with the geophysical datasets available over the Siguiri district.

Airborne electromagnetic dataset (AEM):

The variation in the amount of conductive material (e.g. shale) in the different units has resulted in some important contrasts in the AEM response of the three major sedimentary Formations observed in the district. The Kintinian Formation, dominated by shale is the most responsive (conductive) in AEM, while the greywacke-dominated Fatoya Formation shows a very low response (least conductive). The Balato Formation AEM response returns an intermediate signal between that of the Fatoya and Kintinian Formation. Using these contrasts, a revised map of the Siguiri district was made (Figure 5A). The highly conductive Kintinian Formation dominates the western side of the map. The medium AEM response of the Balato sedimentary rocks takes most of the eastern side, slightly rotating around a N-S orientation (Figure 5B). A strip of the low response Fatoya Formation separates the two, dominating the central and northern parts of the map. The Maléa monzogranite, is resistive and was delineated to the north.

In detail, isolated windows of the Fatoya Formation can also be found in the Kintinian Formation. Most notably, the region of Silakoro (core SIDD002 on Figure 5A) displays numerous marble and conglomeratic drill core intersects which appear to be at the contact between AEM responses analogous to those of the Fatoya and Kintinian Formations. Multiple fold successions were also identified using AEM response between these two Formations in the central-lower part of the district, as well as faults and dykes (Figure 5A).

Magnetic dataset:

The magnetic datasets, were used to delineate regional features but were of no use to distinguish between the three sedimentary Formations at the scale of the Siguiri district. At a regional scale, the magnetic datasets were used to highlight dykes, structures and to follow the conglomeratic base of the Kintinian Formation throughout the entire Siguiri Basin (Figure 10).

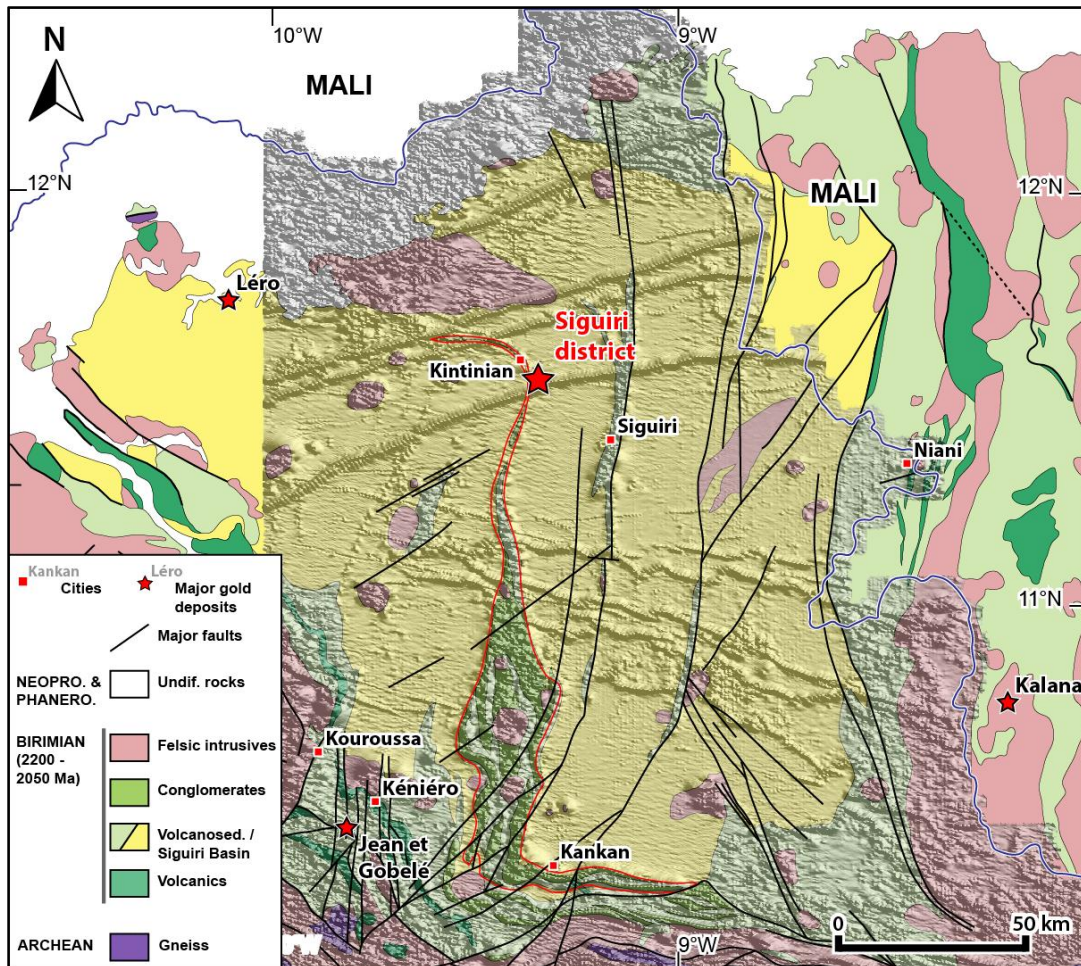


Figure 10: Geological map of the Siguiri Basin overlain by the magnetics analytical signal and showing the spatial continuity of the magnetic conglomerates throughout the Basin (highlighted in red). The WSW-striking and WNW-striking magnetic highs, respectively found in the northern and southern parts of the Basin are dykes (Figure 4).

This unit shows a stronger magnetic response than the rest of the Siguiri Basin sedimentary rocks and forms a distinctive "Z"-shape from the Siguiri district to the south of the city of Kankan (Figure 10). Ground-truthing of this geophysical observation indicates a strong magnetite alteration of the conglomerate in the southern part of the Siguiri Basin and lateral

compositional variation across the Basin, consistent with the local geology. For instance, limestone clasts were observed in the conglomerate from the Marble Hill location (Figure 5), north-west of the Siguiri district is dominated by shale and greywacke from the Fatoya and Balato Formations.

U-Pb detrital zircon geochronology

Few geochronological constraints exist over the study area and the broader Siguiri Basin area (Egal et al., 1999; Egal et al., 2002; Feybesse et al., 1999). Sample details and analytical data for each sample are below and in Table 1 (in Electronic Appendices).

Sample SKRCDD040 236.5, meta-greywacke (WGS84, UTM 29N, East.: 462781, North.: 1271072, Elev.: 364 m)

This sample is a fine-grained, massive, equigranular, dark grey greywacke (~60 vol% matrix) at sub-greenschist facies from the Balato Formation (Sintroko PB1 deposit). Modal composition for quartz, albite and white micas of around 20, 25 and 20 vol% respectively. Carbonates and chamosite make most of the remaining volume. The zircons sampled from this sample are mostly colourless or faded brown. Crystals are usually heavily fractured but remain subhedral with a prismatic habit and present typical crystal size of 80x100 µm. CL imaging shows that grains exhibit oscillatory zoning (Figure 11E).

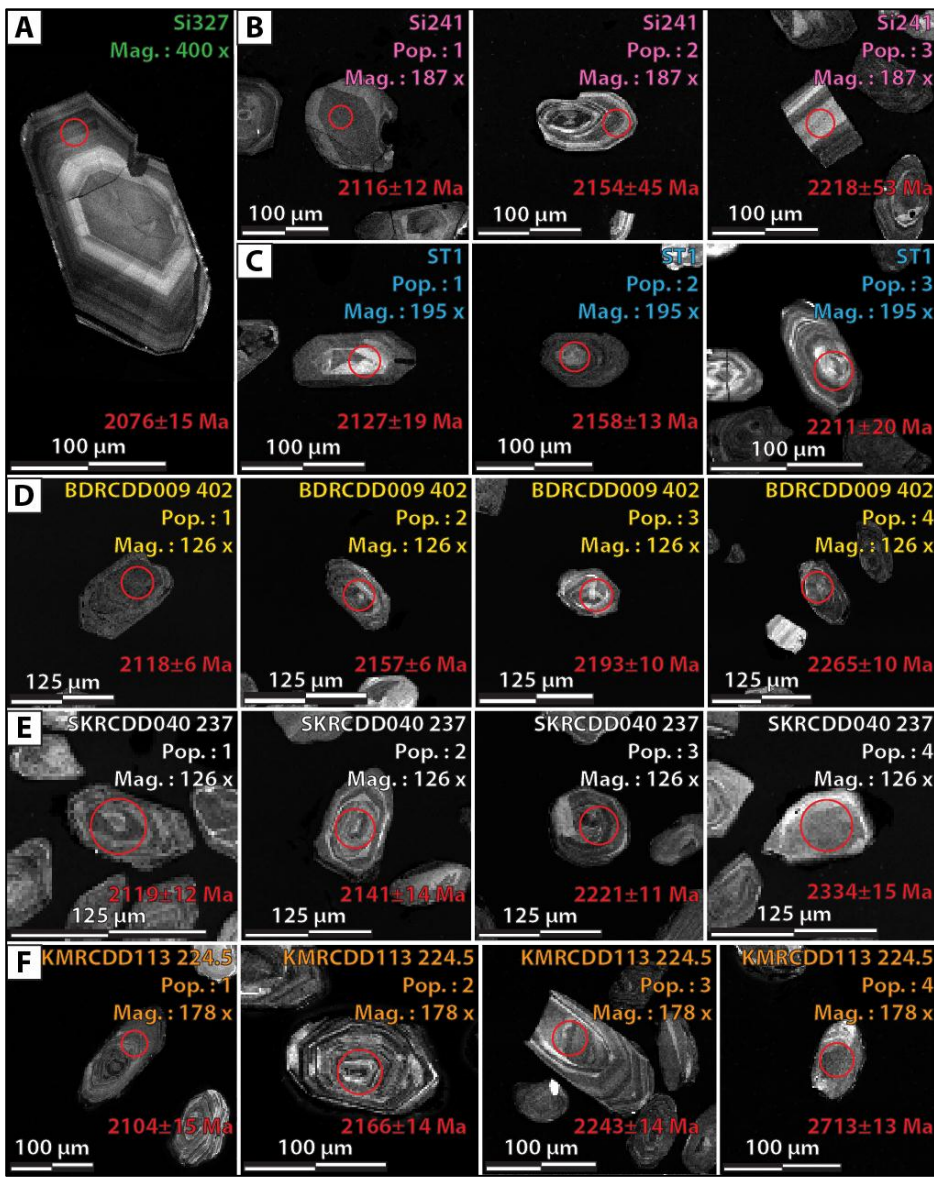


Figure 11: Cathodoluminescence images of the representative zircons for each age population for each sample.

These images were taken at an acceleration voltage of 10 kV and working distance around 14.5 to 15 mm.

Fifty-three analyses were obtained from 53 zircons (external spot-to-spot uncertainty: 0.00% (1σ error); error of mean: 0.14% (1σ error)). Ten analyses >5% discordant and four analyses >2% reversely discordant were not included in the age calculation. Six additional analyses were rejected from the age calculation because morphological defects (e.g. cavities, fractures) over the spots analysed. The remaining 33 concordant to slightly discordant analyses yield two prominent detrital populations (Figure 12A and 12B): 2113 ± 10 Ma (MSWD = 0.83; n = 8; average U content: 138 ppm) and 2143 ± 6 Ma (MSWD = 1.03; n = 23; average U content: 172 ppm), plus individual zircons of: 2221 ± 11 Ma (U content: 199 ppm) and 2334 ± 15 Ma (U

content: 109 ppm). Eight analyses of the youngest population yielded a weighted mean $^{207}\text{Pb}^*/^{206}\text{Pb}^*$ age of 2113 ± 10 Ma (2σ , MSWD = 0.83) which provides a maximum deposition age for the Balato Formation.

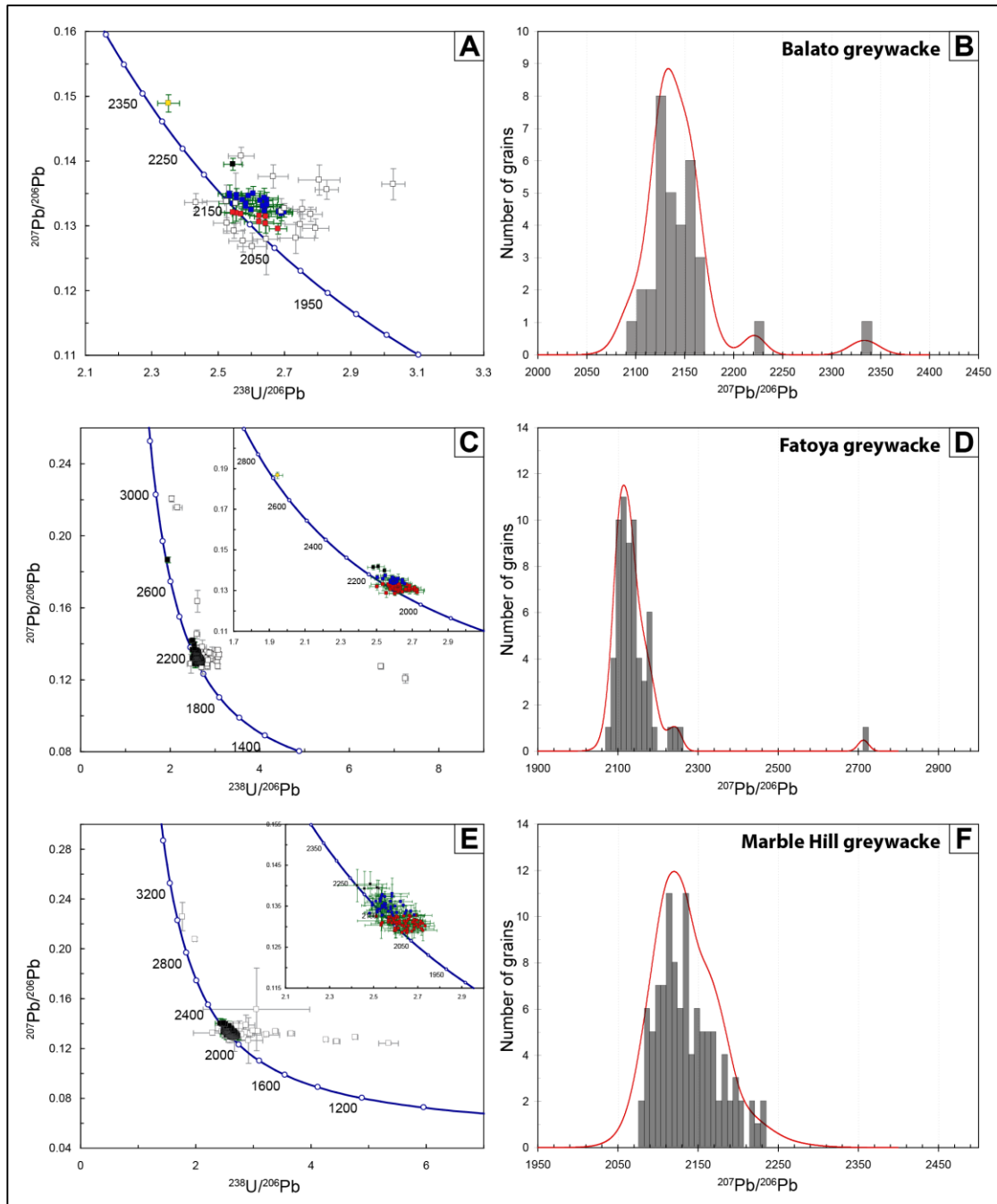


Figure 12: Concordia plots and distribution histograms for analysed samples SKRCDD040 237 (A and B), KMRCDD113 224.5 (C and D) and Si241 (E and F). Data in black are within -2 and +5% discordance. Each colour represents a different detrital age population. Distribution histogram for concordant and semi-concordant data only.

Sample KMRCDD113 224.5, meta-greywacke (WGS84, UTM 29N, East.: 461552, North.: 1277874, Elev.: 400 m)

This sample is a massive, coarse-grained dark grey feldspathic greywacke (~50 vol% matrix) at sub-greenschist facies from the Fatoya Formation (Kami deposit). Its modal composition is similar to sample SKRCDD040 236.5 (20 vol% quartz, 25 vol% albite, 20 vol% white micas) and traces of pyrite were also found. Zircon yield from Geotrack Pty Ltd was abundant and the average crystal size was 60x80 µm. The zircons are mostly colourless or pale brown, subhedral and heavily fractured. CL imaging shows that grains exhibit oscillatory zoning (Figure 11F).

The sample was mounted and dated on two separate mounts and over two sessions. The respective external spot-to-spot uncertainty (1σ error) for each mount was: 0.49, and 0.00%; and the errors of mean (1σ error): 0.18 and 0.17%. A total of 108 analyses were obtained from 105 zircons. Forty-two analyses >5% discordant and one analysis >2% reverse discordant were rejected in the age calculation. Two additional analyses were rejected from the age calculation because of morphological defects over the spots analysed. The remaining 63 analyses are concordant to slightly discordant and yielded four detrital populations (Figure 12C and 12D): 2113 ± 5 Ma (MSWD = 1.00; n = 43; average U content: 102 ppm), 2167 ± 9 Ma (MSWD = 0.88; n = 16; average U content: 89 ppm), 2239 ± 16 Ma (MSWD = 0.88; n = 3; average U content: 127 ppm) and a single zircon dated at 2713 ± 13 Ma (U content: 68 ppm). Forty-three analyses of the youngest population yielded a weighted mean $^{207}\text{Pb}^*/^{206}\text{Pb}^*$ age of 2113 ± 5 Ma (2σ , MSWD = 1.00) which provides a maximum deposition age for the Fatoya Formation.

Sample Si241, meta-greywacke (WGS84, UTM 29N, East.: 449911, North.: 1285773, Elev.: 574 m)

This sample is a strongly foliated, very coarse-grained, dark green feldspathic greywacke at sub-greenschist facies displaying ~30% of matrix. It comes from the Marble Hill location, a hill made of marbles, conglomerate and greywacke sedimentary rocks. The modal composition of this sample is similar to the previous greywacke, with about 20 vol% quartz, 25 vol% albite and 20 vol% white micas. The proportion of clasts is however higher than in the other greywacke samples. Zircons are medium to dark brown, display an average crystal size of 50x70 μm , are reasonably fractured and mostly subhedral to anhedral. The vast majority of grains exhibit a strong oscillatory zoning (Figure 11B).

The sample was mounted and dated on three separate mounts. The external spot-to-spot uncertainty (1σ error) for each respective mount was: 0.65, 0.51 and 1.02%; and the respective errors of mean (1σ error): 0.23, 0.20 and 0.38%. A total of 158 analyses were conducted on this sample on 145 zircons. Forty-two analyses >5% discordant and 8 analyses >2% reverse discordant were rejected for the age calculation. Two extra analyses were also rejected due to fractures at the spot of the analyses. The remaining 106 concordant to slightly discordant analyses yielded three detrital-zircon age populations (Figure 12E and 12F): 2111 \pm 4 Ma (MSWD = 1.00; n = 60; average U content: 99 ppm), 2162 \pm 5 Ma (MSWD = 1.00; n = 41; average U content: 75 ppm) and 2222 \pm 28 Ma (MSWD = 0.03; n = 5; average U content: 56 ppm).

The sixty analyses of the youngest population yielded a weighted mean $^{207}\text{Pb}^*/^{206}\text{Pb}^*$ age of 2111 \pm 4 Ma (2σ , MSWD = 1.00) which provides a maximum deposition age for the Marble Hill greywacke.

Sample ST1, conglomerate (WGS84, UTM 29N, East.: 460252, North.: 1280352, Elev.: 400 m)

This sample is a clast-supported polymict conglomerate coming from the Sanu Tinti deposit, at the base of the Kintinian Formation. Clasts are angular and their nature is dominated by carbonates, but clasts of mafic volcanic, felsic intrusive and even banded iron formation (BIF) could also be found. This conglomerate can be extremely porous as attested by large amounts of disseminated pyrite and the strong hydrothermal alteration in some other samples. Similar conglomerates were found across the Siguiri Basin. The cement is dominated by quartz, feldspaths and white micas as per the previous detrital samples. The zircons display an average crystal size of 40x60 μm , are mostly colourless or light-brown, heavily fractured but remains subhedral with a prismatic habit and a strong oscillatory zoning (Figure 11C).

Fourty-eight analyses were collected from 48 zircons (external spot-to-spot uncertainty: 0.67% (1σ error); error of mean: 0.26% (1σ error)). Eighteen analyses >5% discordant and 2 analyses >2% reverse discordant were rejected for the age calculation. One extra analysis was also rejected due to fractures at the spot of the analyses. The remaining 27 analyses display three detrital-zircon age populations (Figure 13A and 13B): 2124 \pm 7 Ma (MSWD = 0.63; n = 14; average U content: 155 ppm), 2154 \pm 8 Ma (MSWD = 0.36; n = 9; average U content: 175 ppm) and 2205 \pm 15 Ma (MSWD = 0.42; n = 4; average U content: 102 ppm). The fourteen analyses of the youngest population yielded a weighted mean $^{207}\text{Pb}^*/^{206}\text{Pb}^*$ age of 2124 \pm 7 Ma (2σ , MSWD = 0.63) which provides a maximum deposition age for the Kintinian conglomerate.

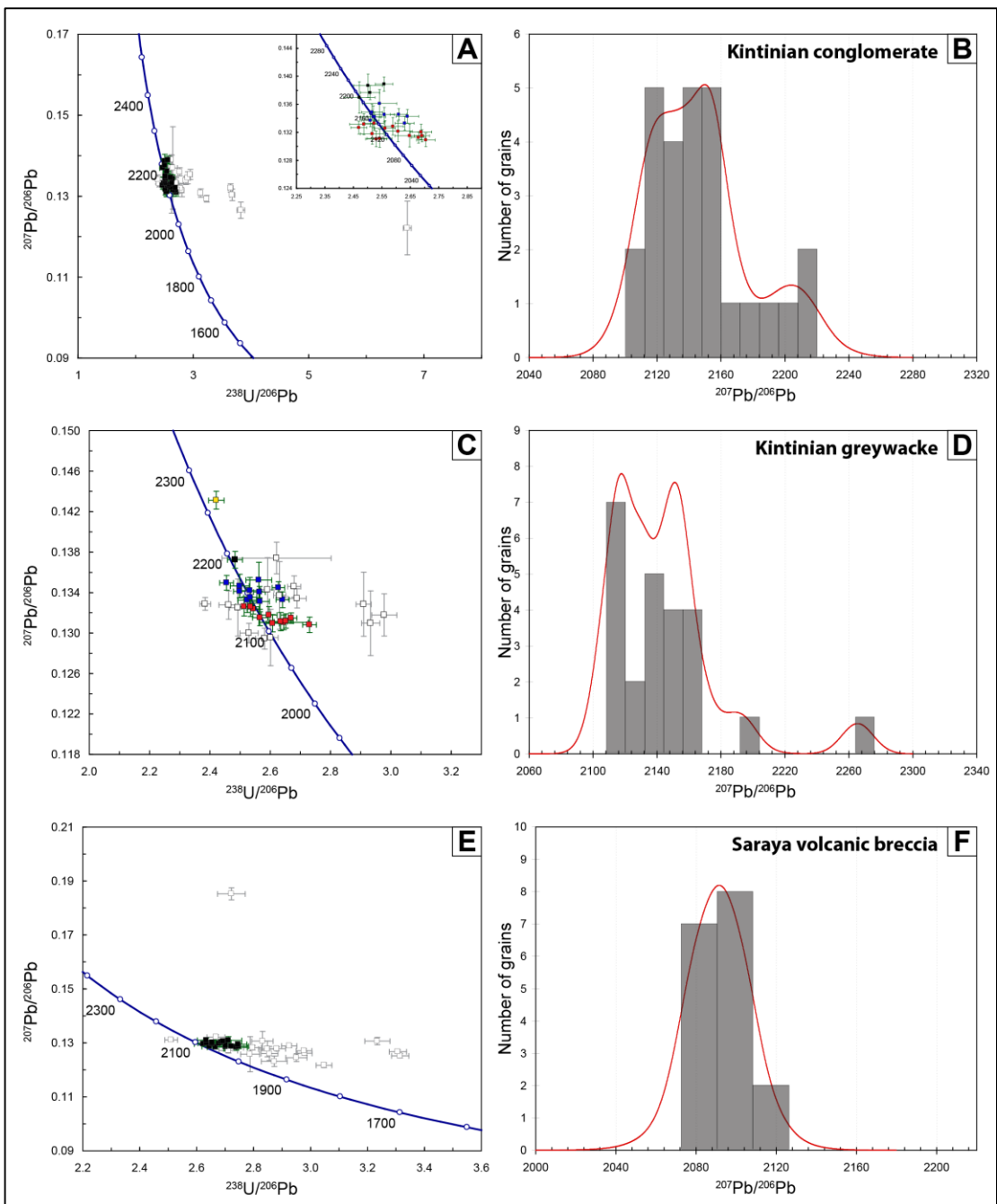


Figure 13: Concordia plots and distribution histograms for analysed samples ST1 (A and B), BDRCDD009 402 (C and D) and Si327 (E and F). Data in black are within -2 and +5% discordance. Each colour represents a different detrital age population. Distribution histogram for concordant and semi-concordant data only.

Sample BDRCDD009 402, meta-greywacke (WGS84, UTM 29N, East.: 460946, North.: 1280579, Elev.: 352 m)

This sample comes from the base of the Kintinian Formation, below the Bidini deposit. It is a medium-grained, equigranular, massive, feldspathic greywacke (~50 vol% matrix) at sub-greenschist facies. Petrographic observations indicate that its modal composition is around: 20 vol% quartz, 25 vol% albite, 20 vol% white micas. Zircon yield was low and the average crystal size is 60x80 μm . The zircons are mostly colourless and fractured but remain subhedral to euhedral with a prismatic habit. CL imaging shows that grain exhibit oscillatory zoning (Figure 11D).

Thirsty-eight analyses from 37 zircons were obtained from sample BDRCDD009 402 (external spot-to-spot uncertainty: 0.51% (1σ error); error of mean: 0.23% (1σ error)). Six analyses >5% discordant and 3 analyses >2% reverse discordant were not taken into account for the age calculation. Five additional analyses were rejected form the age calculation because of morphological defects over the spots analysed. The remaining 24 analyses are concordant to slightly discordant and yielded four detrital populations (Figure 13C and 13D): 2120 ± 5 Ma (MSWD = 0.93; n = 11; average U content: 194 ppm), 2152 ± 6 Ma (MSWD = 0.68; n = 11; average U content: 141 ppm), as well as two monozircon detrital ages: 2193 ± 10 Ma (U content: 119 ppm) and 2265 ± 10 Ma (U content: 98 ppm). The eleven analyses of the youngest population yielded a weighted mean $^{207}\text{Pb}^*/^{206}\text{Pb}^*$ age of 2120 ± 5 Ma (2σ , MSWD = 0.93) which provides a maximum deposition age for the Kintinian Formation, and a possible minimum age for the underlying Fatoya Formation.

Sample Si327, volcanic breccia (WGS84, UTM 29N, East.: 415178, North.: 1290080, Elev.: 371 m)

This sample, from the Saraya region (west of the Siguiri district), is a strongly foliated silica-rich volcanic breccia displaying numerous dark grey and brown sedimentary clasts of quartzitic nature (chert) and of carbonates. Centimeter to multicentimeter subangular clasts of light-pink pumice or tuff can also be found in the cream-pink groundmass. All minerals are interlocked (no or little porosity or matrix) and the matrix displays a granular texture. The mineralogy is characteristic of an intermediate to felsic composition (Cayn, 2011). Zircon yield was low (20+) and large amounts of pyrite was also found in the concentrates. Zircons are pale brown with an average crystal size of 80x100 µm. Crystals are fractured but remains subhedral with a prismatic habit and a strong oscillatory zoning (Figure 11A).

Thirty-six analyses were obtained from 32 zircons (external spot-to-spot uncertainty: 0.65% (1σ error); error of mean: 0.22% (1σ error)). Fourteen analyses >5% discordant and one analysis >2% reverse discordant were rejected for the age calculation. Four extra analyses were also rejected due to the presence of inclusions and fractures at the spot of the analyses. The remaining 17 concordant to slightly discordant analyses display one magmatic-zircon age population at 2092 ± 5 Ma (MSWD = 1.2; n = 17; average U content: 110 ppm; Figure 13E and 13F). The weighted mean $^{207}\text{Pb}^*/^{206}\text{Pb}^*$ age of crystallisation for the Saraya volcanic breccia is 2092 ± 5 Ma (2σ ; MSWD = 1.2).

All five detrital SHRIMP samples display a polymodal detrital zircon age distribution. The magmatic sample from Saraya does not show any inheritance (one age population). Mean U content remains relatively constant and around 100-150 ppm for all samples, except for the sedimentary rocks from Marble Hill, where values are slightly lower. All maximum ages of deposition and the magmatic age are compiled on Figure 14.

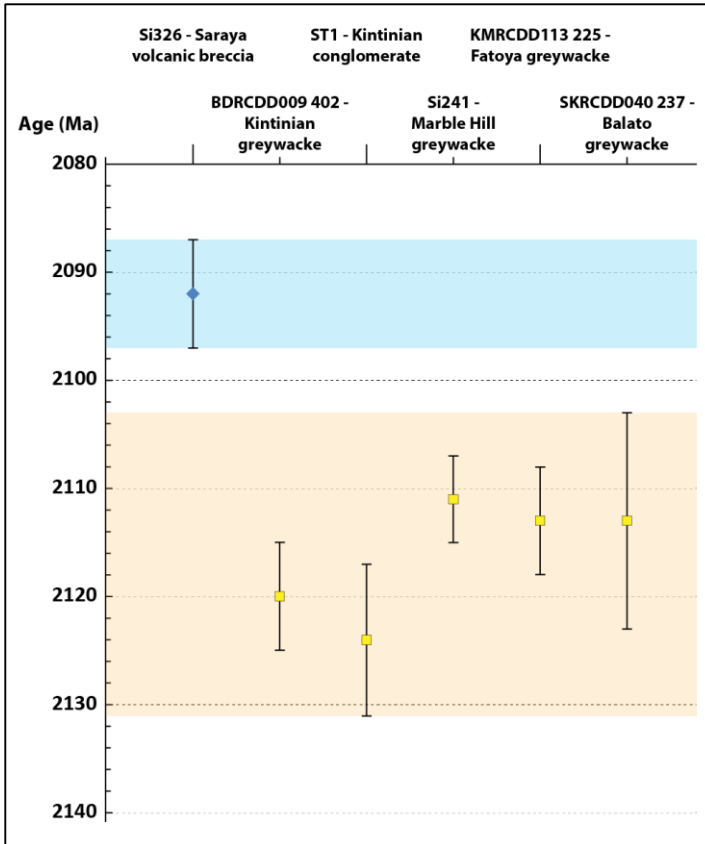


Figure 14: Summary diagram of the maximum deposition ages of each detrital sample and the crystallisation age of sample Si326. All detrital sample ages plot around ca. 2105-2130 Ma while sample Si326 is consistent with other late Eburnean magmatic ages (Egal et al., 1999).

Discussion

Depositional environments of the Siquiri district

The very fine-grained size of the Balato Formation deposits suggests deposition in a low energy, marine or lake setting. The dominantly dark colour of the Balato shales suggests high content in organic material and deposition in reduced water oxygenation and circulation (relatively quiescent phase of sedimentation).

The sedimentary rocks of the Fatoya Formation are interpreted as the product of submarine, sediment-laden gravity flows waning through time (Mulder and Alexander, 2001). The normally-graded greywacke to mudstone beds are interpreted as the Ta/b (coarser-grained, massive greywacke with basal rip-up clasts), Tc/d (current ripples) and Td/Te (siltstone and mudstone) terms of the Bouma sequence (Bouma, 1962). The Fatoya Formation is

therefore interpreted as a marine or deep lake sequence formed by turbidity current deposits. The relatively fine-grained, thin-bedded turbidites suggest a rather distal depositional setting, such as the outer part of a channel-levee system (Piper and Deptuck, 1997) and/or a distal turbidite lobe setting (e.g. Gervais et al., 2006; Bourget et al., 2010). In contrast, the presence of thick beds (up to ~5 m-thick) of massive medium to fine-grained greywacke in drill cores suggest deposition in a low-relief, channelized depositional environment such as lobe distributaries (Gervais et al., 2006; Bourget et al., 2010). The meta-limestone/marbles, reworked by the Kintinian conglomerates, are interpreted to lay at the top of the Fatoya Formation or base of the Kintinian Formation.

The Kintinian Formation strongly contrasts with the other sedimentary Formations recognized in the Siguiri district. The stacked conglomerates sitting near its base are interpreted as the products of subaqueous, cohesive debris flows (Mulder and Alexander, 2001). They incorporated relatively local clasts, as highlighted by the clast angularity, sorting and the along-strike variations in their origin. This is exemplified by the shale-dominated clasts eroded along the marine (or lake) slope from the older Balato and Fatoya Formations in the Siguiri district while limestone clasts dominates in the conglomerates observed closer to the Marble Hill location. The rest of the Kintinian is interpreted as a return to a low energy marine or lake depositional setting with fluctuating water geochemistry and conditions at the origin of the organic-rich shales / limestone interbeds (Figure 6F).

Overall, the Siguiri district sediments are interpreted as marine or lake sedimentary deposits. They initially form a regressive (coarsening-upward) sequence showing a transition from (Figure 9):

- 1) low-energy marine (or lake) organic-rich shales (lower Balato Formation);
- 2) onset of gravity-flow deposits and distal turbidite deposition (possibly turbidite lobe complex including distributary channel fills), and;

3) onset of high-energy debris flow deposition (basal Kintinian conglomerates). The sequence then fines up to the upper Kintinian Formation, which is associated with a return to lower energy marine (or lake) deposits as a result of either a shutdown of the coarse-grained siliciclastic input in the basin and/or a relative increase in water depth (e.g. transgression).

This interpretation is relatively consistent with the observations of “a succession of mudstones and siltstones Formations” made by Egal et al. (1999) and their interpretation of the Siguiri Basin sediments as “fine marine sediments”.

The stacked Kintinian conglomerates (which were also previously described by Egal et al., (1999) and Feybesse et al. (1999)) can be considered as olistostrome deposits with various autochthonous and allochthonous clasts (Flores, 1955; Neuendorf et al., 2005). Olistostromes (or mélanges of sedimentary origin) are interpreted as the product of submarine debris flow triggered by slope failure (Dalrymple and James, 2010; Prothero and Schwab, 2004), possibly associated with earthquake-induced faulting events (Chang et al., 2001; Cieszkowski et al., 2009; Moore et al., 1976; Wendorff, 2005). The basal Kintinian olistostrome can be followed throughout the entire Siguiri Basin (Figure 10). These basal conglomerates contrast strongly with the rest of the Siguiri Basin “fine sediments” described by Egal et al., (1999) and Feybesse et al. (1999), and mark an abrupt change in depositional energy and tectonic context.

The Siguiri Basin is hence viewed as much more complex than previously described. The presence of olistostrome near the base of the Kintinian Formation is regarded as a major change in lithofacies (Figure 3B), marking a change in the dynamics of the Siguiri Basin opening and tectonic activity. This change is marked by the transition from a relatively quiescent marine or deep lake sequence formed in rather distal depositional setting (Balato and Fatoya Formations) to a period accompanied by enhanced faulting and mass-wasting events along the paleo-marine slope, resulting in over-steepening, erosion, and deposition of a stack of conglomerates from repeated debris-flow events (Kintinian Formation).

The Siguiri district geochronology in the West African context

Geochronological constraints on sedimentary rocks are typically limited by the mechanisms that generate them, including erosion, transport and deposition. Zircons analysed in this study can be zoned and have a variety of origins (igneous, metamorphic or hydrothermal). The age obtained from these zircons can therefore reflect the age of crystallisation of a magma, the age of a metamorphism or that of an hydrothermal event. The prismatic habit and strong oscillatory zoning displayed by the vast majority of zircons analysed in this study is suggestive of magmatic zircons. The ages considered in this study are crystallisation ages of eroded or deposited igneous rocks and may thus represent maximum depositional ages only. The fact that all five detrital samples display a polymodal distribution of detrital zircon ages, reflects the existence of multiple sources or of a polymict source.

The maximum ages of deposition for the Siguiri district sediments are all within error of each other and average at ca. 2117 Ma (Figure 14). Currently, the only constraint on the minimum deposition age is provided by the crystallisation age of the Saraya volcanic breccia (2092 ± 5 Ma), sitting on top of the siliciclastic sedimentary rocks of the Siguiri district. This volcanic unit is coeval with the intrusion of the Maléa monzogranite, whose crystallisation age was dated by Parra-Avila et al. (this volume) at 2089 ± 12 Ma.

Based on a recent regional synthesis Davis et al. (2015), proposes that the lithostratigraphic succession of the Baoule-Mossi domain exhibit three distinct sedimentary units including from bottom to top:

- Lower Birimian basins dominated by pyroclastics, volcanoclastics and associated with extensive volcanism dated between ca. 2190 to ca. 2140 Ma;
- Upper Birimian basins unconformably overlying the Lower Birimian sediments and dominated by greywacke, argilite and some volcanoclastics dated between ca. 2130 and ca. 2110, and;

- Tarkwa Group basins, dominated by sandstone, greywacke and conglomerate and dated between ca. 2110 and ca. 2095 Ma. These basins are less common compared to the other two.

When put into the regional context of the West African Craton, the maximum sedimentation ages observed in the Siguiri district appear younger than the Lower Birimian rocks (Figure 15). For example, the Sefwi Formation in Ghana (Perrouti et al., 2012), which is dominated by pyroclastics and volcanoclastics, has an age of crystallisation/deposition of 2162 ± 6 Ma (Loh et al., 1999) and is associated with important basaltic and andesitic volcanism dated from around ca. 2200 up to ca. 2140 Ma (Adadey et al., 2009; Davis et al., 2015; Davis et al., 1994; Hirde and Davis, 1998; Taylor et al., 1992). The Sefwi Formation displays similar facies and ages as the Fetekoro sediments and its equivalents in the Boromo, Houndé and Banfora belts of Burkina Faso (Davis et al., 2015; Baratoux et al., 2011). In Burkina Faso, the Boromo, Houndé and Banfora sedimentary rocks have been described as tuffs, epiclastic volcano-sediments, volcaniclastics, argilites and wackes with occasional intercalations of andesites (Baratoux et al., 2011). The Komana sedimentary rocks in the Yanfolila Belt of Mali, are another example interpreted by Davis et al. (2015) to be a lateral equivalent of the Sefwi Formation (Figure 15).

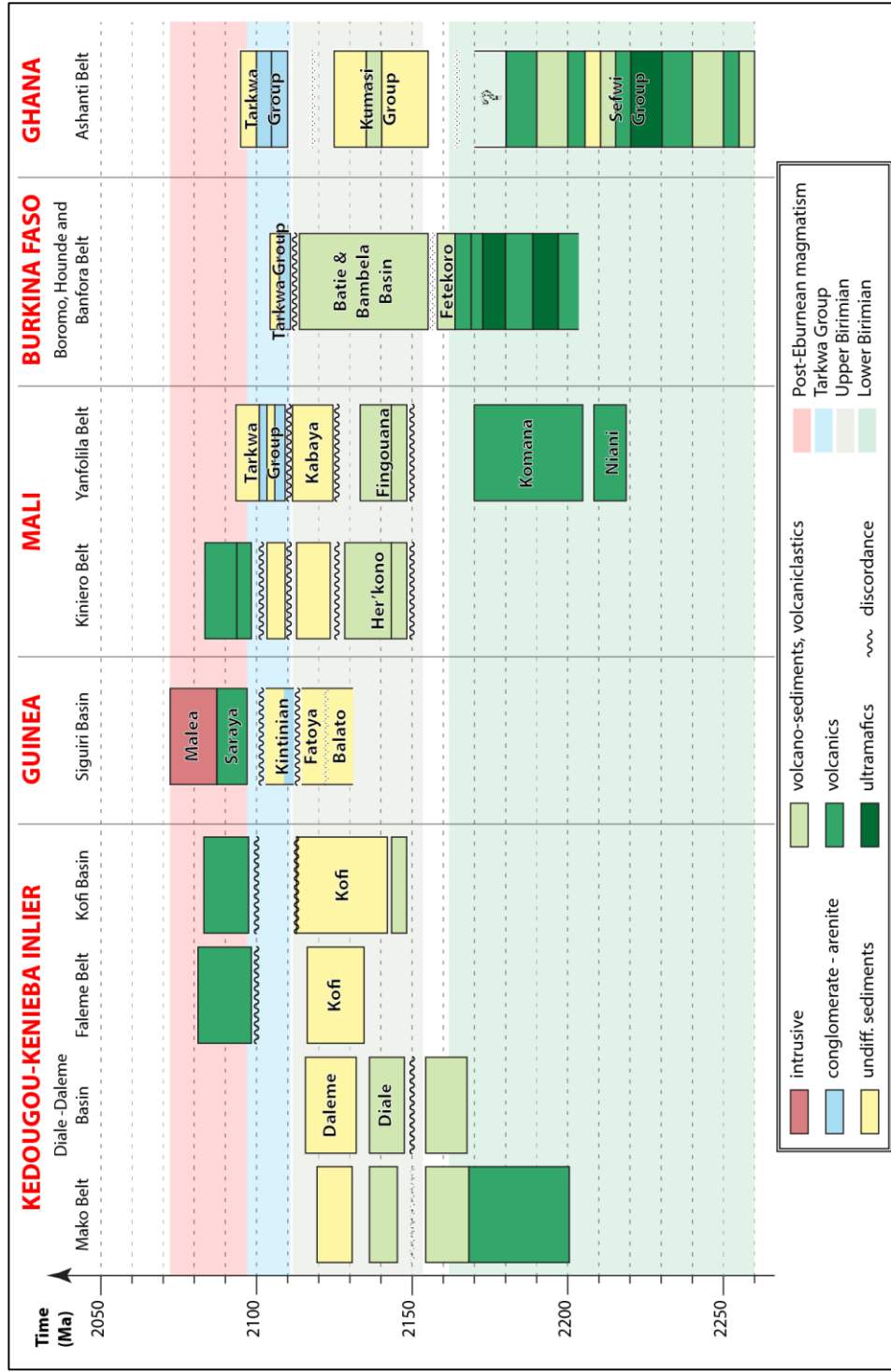


Figure 15: Simplified lithostratigraphic and geochronological chart of some key areas of the West African Craton.

Ages from the Siguiri district and Saraya are reported in the left column. Modified from: Baratoux et al. (2011), Davis et al. (2015), Lahondère et al. (2002), Lebrun et al. (in review 2015); Chapter 3, Parra-Avila et al. (this volume), Perrouti et al. (2012).

In contrast, the deposition ages of the Siguiri Basin sediments compare with those of the Upper Birimian and Tarkwa Group rocks such as the Kumasi Formations (Ghana), Batie

Formation and Bambela Basin sediments in Burkina Faso, and Fingouana, Kabaya and Her'kono Formations in Mali. All these sedimentary rocks are dominated by flysch-like metasediments (e.g. greywacke, argillite) deposited at ca. 2120 Ma (Figure 15; Davis et al., 2015). The Siguiri district sedimentary rocks are therefore interpreted to have deposited at the same time than that of the Lower Tarkwa Group deposited between 2110 and ca. 2095 Ma, or to represent the last expression of Upper Birimian sedimentation dated as 2130-2110 Ma (Davis et al., 2015).

The Kintinian Formation – a Tarkwa Group sequence?

With the sole base of the geochronological record it remains difficult to determine whether the Siguiri district sediments belong to the Upper Birimian or Tarkwa Group. The first detailed study of the Tarkwaian sedimentary rocks lithotype in Ghana, defining the Tarkwa Group, was conducted over 40 years ago by Sestini (1973). The Tarkwaian consists of intercalations of conglomerates, sandstones and phyllites. The conglomeratic layers display Birimian quartz pebbles and volcanic clasts and were interpreted to represent piedmont-type deposits (short transport in an environment of active continental erosion; Bossière et al., 1996; Mueller et al., 1996), similar to that found on the southern foot of the Alps and the Himalayas (Hirdes and Nunoo, 1994; Sestini, 1973). Since this early work, sedimentary rocks from the Tarkwa Group have been described in other parts of the West African Craton. Tarkwa Group rocks were all deposited late during the Eburnean lithostratigraphic evolution and are also referred to as “Tarkwa-like” by some authors (Baratoux et al., 2011).

The Tarkwa Group, are “late orogenic basin”-type sedimentary rocks. These types of rocks were deposited in other cratons throughout the Earth geological history. The Timiskaming sedimentary rocks and the rest of the Duperquet Basin in Canada, as well as the Kurrawang Group in the Eastern Goldfields of Western Australia, are Archean examples (Krapež et al., 2000; Mueller et al., 1996). The Hanmer Basin, a foreland sedimentary basin in New Zealand, is a modern example of these “late orogenic basin” sediments (Wood et al., 1994). These sediments may be associated with early phases of orogenic contraction (Robert

et al., 2005; Ledru et al., 1994), as pull-apart basins developed in transpressive environments (e.g. Krapež and Pickard, 2010), or alternatively, as extensional basins developed during regional extension (e.g. Blewett et al., 2010).

The sedimentary facies of the Kintinian Formation strongly contrasts with that of the Balato and Fatoya formations. The Kintinian Formation conglomerate, that contains banded iron formation clasts interpreted to be sourced from the Archean Simandou, compares well with Tarkwa Group sediments. Together, the age overlap and peculiar facies of the Kintinian Formation suggests that this Formation may belong to the Lower Tarkwa Group (Figure 15), as defined by Davis et al. (2015). We suggest that the Kintinian Formation formed late during the Eburnean orogeny lithostratigraphic evolution as distal turbiditic lobes in deep water and olistostromes typical of an early stage of “late basin” sedimentation. The Kintinian Formation sediments would hence be associated with the onset of the Eburnean convergence.

Early architecture of the Siquiri Basin and orogenic gold systems

Regardless of the timing of mineralisation, it has been demonstrated in several terranes of varying age that the structural framework associated with mineralisation is intimately controlled by the early architecture (Dörling et al., 1996; Love et al., 2004; Garwin et al., 2005; Lund, 2008; Miller et al., 2010). Early architecture is crucial for exploration targeting and major stratigraphic boundaries are commonly used in orogenic gold exploration (Robert et al., 2005). These boundaries and variations within a basin are typically controlled by, and therefore highlight, fundamental structures that were active at the time of the basin formation (Ersoy et al., 2014; Collins et al., in press; Gindre et al., 2012; Hajná et al., 2011). These fundamental structures are commonly reactivated multiple times and will act as important fluid pathways, focusing fluids produced from deep-seated sources (e.g. magmatic, mantle derived, metamorphic). The early architecture and associated structures are often cryptic and difficult to recognize on the field. These structures may be visible in large-scale geophysical datasets, and highlighted in the field by lithological variations (e.g. Miller et al., 2010).

The basal Kintinian olistostrome marks the interface between the Fatoya and Kintinian Formations and can be traced in regional magnetic datasets and by field mapping as a narrow N-S belt across the entire Siguiri Basin (Figure 10). The prominence of this N-S trend in other major volcano-sedimentary belts across the West African Craton, parallel to the central Siguiri Basin (e.g. Yanfolila Belt; Figure 3A), indicates probable basement structure reactivation. Bends in the Kintinian olistostrome and in the rest of the lithostratigraphy defined in the Siguiri district can be observed both at the scale of the district (Figure 5) and at the regional scale where the olistostrome forms a "Z"-shaped unit recognized across the entire Siguiri Basin (Figure 3B and 10). The peculiar shape of the Kintinian olistostrome recognized across the Siguiri Basin originated from the first phases of orogenic contraction affecting the Basin, such as D_{1S} N-S compression. The WNW-ESE, N-S and NE-SW structures that bound the Kintinian olistostrome across the Siguiri Basin (Figure 3B, 5 and 10) are therefore considered to represent fundamental deeper basement structures that controlled the thickness and morphology of this unit at the time of its deposition.

The location of the Siguiri district, previously hosted amidst an undifferentiated package of sediments, now falls at the intersection between early WNW-ESE and N-S faults highlighted by the Kintinian olistostrome and also recognized in geophysics by Markov et al. (this volume). These fundamental structures also intersect with the locations of other smaller deposits hosted in and around the Siguiri Basin (e.g. Léro, Jean et Gobelé, Kalana). We propose that the WNW-ESE, N-S and NE-SW faults defining the early architecture of the Siguiri Basin, applied a first-order structural control on the location of gold mineralization in the Basin as well as magmatic intrusions (Figure 3B) and regional magnetite alteration (Figure 10).

Overall, the link between basin morphology and the later orogenic gold mineralisation is a major exploration targeting tool for orogenic gold systems. In the West African Craton, the association between "late orogenic basins" and gold mineralisation is also exemplified by the Tarkwa Basin in Ghana where numerous deposits, including the giant Obuasi deposit, are hosted along structures controlling the morphology of the Tarkwa Basin (Figure 3B).

Conclusion

The lithostratigraphy and geochronology of the Siguiri Basin, and of the Siguiri district in particular indicates that:

- 1) The Siguiri Basin is not a uniform package of undifferentiated fine sedimentary rocks, but has a complex lithostratigraphy. This lithostratigraphy includes (from top to bottom) the Kintinian, Fatoya and Balato sedimentary Formations;
- 2) In the context of the West African Craton, the central Siguiri Basin and sedimentary rocks from the Siguiri district are interpreted as spanning the transition from Upper Birimian to Lower Tarkwa Group sedimentation. The Tarkwa Group sediments are “late basin”-type sediments associated with margin convergence and the central Siguiri Basin sediments signal the onset of a period of orogenic compression.
- 3) The polymict conglomerates of the Kintinian Formation are interpreted as an olistostrome with various autochthonous and allochthonous clasts. It marks a major change in lithofacies of the Siguiri district and was deposited as a linear belt crossing the entire Siguiri Basin;
- 4) The morphology of this stratigraphic boundary highlights the early architecture of the Siguiri Basin and fundamental structures that controlled the deposition of the Kintinian Formation at the time of the Basin opening;
- 5) The early architecture of the Siguiri Basin is characterized by WNW-ESE, N-S and NE-SW early structures that control the location of the Siguiri gold district and of its ore shoots within the Basin and can be targeted for orogenic gold systems.
- 6) Delineation of similar Tarkwa Group sediments is viewed as a key targeting tool for orogenic gold in the rest of the West African Craton.

Acknowledgements

This project is funded by AngloGold Ashanti Limited. Eddie Connell, Shawn Kitt, Katharina Wulff and Craig Duvel are acknowledged for providing site access, support and

inspiring discussions. Doctor-to-be Luis Parra-Avila is also thanked for the help provided regarding all SHRIMP-related encountered difficulties. The authors also acknowledge the facilities, and the scientific and technical assistance of the Australian Microscopy & Microanalysis Research Facility at the Centre for Microscopy, Characterisation & Analysis, the John de Laeter Centre for Isotope Research, The University of Western Australia and Curtin University. Finally, thanks to Michel Villeneuve, Raphael Doutre and the other anonymous person for reviewing this paper, as well as everyone I could not mention here above.

References

- Abouchami, W., Boher, M., Michard, A., and Albarede, F., 1990, A Major 2.1 Ga Event of Mafic Magmatism in West Africa - an Early Stage of Crustal Accretion: *Journal of Geophysical Research-Solid Earth and Planets*, v. 95, p. 17605-17629.
- Adadey, K., Clarke, B., Théveniaut, H., Urien, P., Delor, C., Roig, J., and Feybesse, J., 2009, Geological map explanation—map sheet 0503 B (1: 100 000), CGS/BRGM/Geomar, Geological Survey Department of Ghana (GSD). No, MSSP/2005/GSD/5a.
- AngloGold Ashanti Ltd., 2013, Mineral resource and ore reserve report: Available from:
www.ag-a-reports.com/13/download/AGA-RR13.pdf. [12/05/2015]
- AngloGold Ashanti Ltd., n.d., Reports: Available from:
<http://www.anglogoldashanti.com/en/Media/Pages/reports.aspx>. [15/05/2015]
- Baratoux, L., Metelka, V., Naba, S., Jessell, M. W., Grégoire, M., and Ganne, J., 2011, Juvenile Paleoproterozoic crust evolution during the Eburnean orogeny (~ 2.2–2.0 Ga), western Burkina Faso: *Precambrian Research*, v. 191, p. 18-45.
- Blewett, R., Czarnota, K., and Henson, P., 2010, Structural-event framework for the eastern Yilgarn Craton, Western Australia, and its implications for orogenic gold: *Precambrian Research*, v. 183, p. 203-229.

- Bossière, G., Bonkoungou, I., Peucat, J.-J., and Pupin, J.-P., 1996, Origin and age of Paleoproterozoic conglomerates and sandstones of the Tarkwaian Group in Burkina Faso, West Africa: Precambrian Research, v. 80, p. 153-172.
- Bouma, A. H., 1962, Sedimentology of some Flysch deposits: A graphic approach to facies interpretation, 168 p.
- Bourget, J., Zaragosi, S., Mulder, T., Schneider, J.-L., Garlan, T., Van Toer, A., Mas, V., and Ellouz-Zimmermann, N., 2010, Hyperpycnal-fed turbidite lobe architecture and recent sedimentary processes: A case study from the Al Batha turbidite system, Oman margin: Sedimentary Geology, v. 229, p. 144-159.
- Cayn, J.-A., 2011, Petrographic analysis in the Paleoproterozoic (Birimian) volcano-sedimentary sequence of Siguiri basin, northeastern Guinea, unpublished.
- Chang, C., Angelier, J., Huang, C., and Liu, C., 2001, Structural evolution and significance of a mélange in a collision belt: the Lichi Mélange and the Taiwan arc-continent collision: Geological Magazine, v. 138, p. 633-651.
- Cieszkowski, M., Golonka, J., Krobicki, M., Slaczka, A., Oszczypko, N., Waskowska, A., and Wendorff, M., 2009, The Northern Carpathians plate tectonic evolutionary stages and origin of olistoliths and olistostromes: Geodinamica Acta, v. 22, p. 101-126.
- Claoué-Long, J. C., 1995, Two Carboniferous ages: a comparison of SHRIMP zircon dating with conventional zircon ages and 40Ar/39Ar analysis.
- Collins, A. S., Patranabis-Deb, S., Alexander, E., Bertram, C. N., Falster, G. M., Gore, R. J., Mackintosh, J., Dhang, P. C., Saha, D., Payne, J. L., Jourdan, F., Backé, G., Halverson, G. P., and Wade, B. P., in press, Detrital mineral age, radiogenic isotopic stratigraphy and tectonic significance of the Cuddapah Basin, India: Gondwana Research.
- Compston, W., Williams, I., and Meyer, C., 1984, U-Pb geochronology of zircons from lunar breccia 73217 using a sensitive high mass-resolution ion microprobe: Journal of Geophysical Research: Solid Earth (1978–2012), v. 89, p. B525-B534.

Dalrymple, R. W., James, N. P., and Geological Association of C., 2010, Facies models 4: St. John's, Nfld., Geological Association of Canada.

Davis, J., Miller, J., Thébaud, N., McCuaig, C., Begg, G., Jessel, M., Hein, K., Baratoux, L., 2015, Craton-scale lithostratigraphic correlation as an insight for the geodynamic evolution of the South West African Craton: Proceedings of the 50th SGA conference.

Davis, D., Hirdes, W., Schaltegger, U., and Nunoo, E., 1994, U-Pb age constraints on deposition and provenance of Birimian and gold-bearing Tarkwaian sediments in Ghana, West Africa: Precambrian Research, v. 67, p. 89-107.

Dörling, S., Dentith, M., Groves, D., and Vearncombe, J., 1996, Mississippi Valley-type deposits of the southeast Lennard Shelf: an example of the interplay of extensional deformation, sedimentation and mineralization: Carbonate-Hosted Lead Deposits: Society of Economic Geologists Special Publication, v. 4, p. 96-111.

Egal, E., Lahondere, D., Costea, A. C., Diabate, B., Diallo, A., Diallo, A. B., Diallo, S., Gaye, F., Iliescu, D., and Minthe, D., 1999, Carte géologique de la Guinée à 1/200 000; Feuille Sigiri, BRGM.

Egal, E., Thiéblemont, D., Lahondère, D., Guerrot, C., Costea, C. A., Iliescu, D., Delor, C., Goujou, J., Lafon, J., Tegyey, M., Diaby, S., and Kolie, P., 2002, Late Eburnean granitization and tectonics along the western and northwestern margin of the Archean Kénéma–Man domain (Guinea, West African Craton): Precambrian Research, v. 117, p. 57-84.

Ersoy, E. Y., Çemen, İ., Helvacı, C., and Billor, Z., 2014, Tectono-stratigraphy of the Neogene basins in Western Turkey: Implications for tectonic evolution of the Aegean Extended Region: Tectonophysics, v. 635, p. 33-58.

Feybesse, J., Bangoura, A., Billa, M., Costea, A., Diabaté, B., Diaby, S., Diallo, A., Diallo, S., Diallo, A., and Egal, E., 1999, Notice explicative de la Carte géologique de la Guinée à 1/200 000, Feuille no. 19, Kankan: BRGM, DNRGH, Ministère des Mines, de la Géologie et de l'Environnement, Conakry, Guinée, 27p.

Feybesse, J.-L., and Milési, J.-P., 1994, The Archean/Proterozoic contact zone in West Africa: a mountain belt of décollement thrusting and folding on a continental margin related to 2.1 Ga convergence of Archean cratons?: Precambrian Research, v. 69, p. 199-227.

Flores, G., 1955, Definition of “olistostrome”. Forth World Petroleum Congress: Proceedings, Sec. I, p. 122.

Garwin, S., Hall, R., and Watanabe, Y., 2005, Tectonic setting, geology, and gold and copper mineralization in Cenozoic magmatic arcs of Southeast Asia and the West Pacific: Economic Geology 100th Anniversary Volume, p. 891-930.

Gervais, A., Mulder, T., Savoye, B., and Gonthier, E., 2006, Sediment distribution and evolution of sedimentary processes in a small sandy turbidite system (Golo system, Mediterranean Sea): implications for various geometries based on core framework: Geo-Marine Letters, v. 26, p. 373-395.

Gindre, L., Le Heron, D., and Bjørnseth, H. M., 2012, High resolution facies analysis and sequence stratigraphy of the Siluro-Devonian succession of Al Kufrah basin (SE Libya): Journal of African Earth Sciences, v. 76, p. 8-26.

Goloubinow, R., 1936, Géologie et ressources en or de la Guinée française: thesis, Université de Nancy, 142p.

Hajná, J., Žák, J., and Kachlík, V., 2011, Structure and stratigraphy of the Teplá–Barrandian Neoproterozoic, Bohemian Massif: A new plate-tectonic reinterpretation: Gondwana Research, v. 19, p. 495-508.

Hirdes, W., Davis, D., and Eisenlohr, B., 1992, Reassessment of Proterozoic granitoid ages in Ghana on the basis of U/Pb zircon and monazite dating: Precambrian Research, v. 56, p. 89-96.

Hirdes, W., and Davis, D. W., 1998, First U-Pb zircon age of extrusive volcanism in the Birimian Supergroup of Ghana/West Africa: Journal of African Earth Sciences, v. 27, p. 291-294.

Hirdes, W., and Nunoo, B., 1994, The Proterozoic paleoplacers at Tarkwa gold mine, SW Ghana; sedimentology, mineralogy, and precise age dating of the Main Reef and West Reef,

and bearing of the investigations on source area aspects: *Geologisches Jahrbuch D*, v. 100, p. 247-311.

Hyde, R. S., 1980, Sedimentary facies in the Archean Timiskaming Group and their tectonic implications, Abitibi greenstone belt, Northeastern Ontario, Canada: *Precambrian Research*, v. 12, p. 161-195.

Krapež, B., Brown, S., Hand, J., Barley, M., and Cas, R., 2000, Age constraints on recycled crustal and supracrustal sources of Archaean metasedimentary sequences, Eastern Goldfields Province, Western Australia: evidence from SHRIMP zircon dating: *Tectonophysics*, v. 322, p. 89-133.

Krapež, B., and Pickard, A. L., 2010, Detrital-zircon age-spectra for Late Archaean synorogenic basins of the Eastern Goldfields Superterrane, Western Australia: *Precambrian Research*, v. 178, p. 91-118.

Lebrun, E., Miller, J., Thébaud, N., Ulrich, S., and McCuaig, C., in review 2015, Structural controls on an orogenic gold system: The world-class Siguiri gold district, Siguiri Basin, Guinea, West Africa: *Economic Geology*.

Ledru, P., Johan, V., Milési, J. P., and Tegyey, M., 1994, Markers of the last stages of the Palaeoproterozoic collision: evidence for a 2 Ga continent involving circum-South Atlantic provinces: *Precambrian Research*, v. 69, p. 169-191.

Loh, G., Hirdes, W., 1999, Explanatory notes for the geological map of southwest Ghana, 1:100000—Sekondi (0402A) and Axim (0403B) Sheets, *Geologisches Jahrbuch*, B 93, 149p.

Loh, G., Hirdes, W., Anani, C., Davis, D. W., and Vetter, U. K., 1999, Explanatory notes for the geological map of Southwest Ghana 1: 100,000, *Geologisches Jahrbuch*, Reihe B, Heft 93, 150 p.

Love, D. A., Clark, A. H., and Glover, J. K., 2004, The lithologic, stratigraphic, and structural setting of the giant Antamina copper-zinc skarn deposit, Ancash, Peru: *Economic Geology*, v. 99, p. 887-916.

Ludwig, K., 2000, SQUID 1.00. A User's Manual, Berkeley Geochronology: Center Spec. Publ, p. 19.

Lund, K., 2008, Geometry of the Neoproterozoic and Paleozoic rift margin of western Laurentia: Implications for mineral deposit settings: *Geosphere*, v. 4, p. 429-444.

Markov, J., Dentith, M., Aitken, A., Jessell, M., and Miller, J., this volume, The Structure of the Siguiri Basin, Guinea, West Africa: Interpretation of Magnetic and Gravity Data: Precambrian Research.

McCuig, T. C., and Hronsky, J. M. A., 2014, The Mineral System Concept: The Key to Exploration Targeting: *Economic Geology - Special Publication*, v. 18, p. 153-175.

McIntyre, J., and Martyn, J., 2005, Early extension in the Late Archaean northeastern Eastern Goldfields Province, Yilgarn Craton, Western Australia: *Australian Journal of Earth Sciences*, v. 52, p. 975-992.

Milési, J. P., Feybesse, J. L., Ledru, P., Dommangeat, A., Ouedraogo, M. F., Marcoux, E., Prost, A., Vinchon, C., Sylvain, J. P., Johan, V., Teguey, M., Calvez, J. Y., and Lagny, P., 1989, Les minéralisations aurifères de l'Afrique de l'Ouest. Leurs relations avec l'évolution lithostructurale au Protérozoïque inférieur: *Chronique de la recherche minière*, v. 497, p. 3-98.

Milési, J.-P., Ledru, P., Feybesse, J.-L., Dommangeat, A., and Marcoux, E., 1992, Early Proterozoic ore deposits and tectonics of the Birimian orogenic belt, West Africa: *Precambrian Research*, v. 58, p. 305-344.

Miller, J., Blewett, R., Tunjic, J., and Connors, K., 2010, The role of early formed structures on the development of the world class St Ives Goldfield, Yilgarn, WA: *Precambrian Research*, v. 183, p. 292-315.

Miller, J. M., Davis, J., Baratoux, L., McCuaig, T. C., Metelka, V. and Jessel, M., 2013, Evolution of gold systems in Guinea, southern Mali and western Burkina Faso: AMIRA International Ltd P934A - West African Exploration Initiative - Stage 2 Final report, Appendix D1, unpublished.

Moore, D. G., Curray, J. R., and Emmel, F. J., 1976, Large submarine slide (olistostrome) associated with Sunda Arc subduction zone, northeast Indian Ocean: Marine Geology, v. 21, p. 211-226.

Mueller, W., Daigneault, R., Mortensen, J., and Chown, E., 1996, Archean terrane docking: upper crust collision tectonics, Abitibi greenstone belt, Quebec, Canada: Tectonophysics, v. 265, p. 127-150.

Mulder, T., and Alexander, J., 2001, The physical character of subaqueous sedimentary density flows and their deposits: Sedimentology, v. 48, p. 269-299.

Nasdala, L., Hofmeister, W., Norberg, N., Martinson, J. M., Corfu, F., Dörr, W., Kamo, S. L., Kennedy, A. K., Kronz, A., and Reiners, P. W., 2008, Zircon M257-a Homogeneous Natural Reference Material for the Ion Microprobe U-Pb Analysis of Zircon: Geostandards and Geoanalytical Research, v. 32, p. 247-265.

Neuendorf, K. K., Mehl, J. P., and Jackson, J. A., 2005, Glossary of geology, Springer.

Paranhos, C. J., 2008, Siguiri gold mine - State of knowledge of the main geological controls of gold mineralization, unpublished.

Parra-Avila, L. A., Belousova, E., Fiorentini, M. L., Baratoux, L., Davis, J., Miller, J., and McCuaig, T. C., this volume, Crustal Evolution of the Paleoproterozoic Birimian terranes of the Baoulé-Mossi domain, southern West African Craton: U-Pb and Hf-isotope studies of detrital zircons: Precambrian Research.

Perrouty, S., Aillères, L., Jessell, M. W., Baratoux, L., Bourassa, Y., and Crawford, B., 2012, Revised Eburnean geodynamic evolution of the gold-rich southern Ashanti Belt, Ghana, with new field and geophysical evidence of pre-Tarkwaian deformations: Precambrian Research, v. 204, p. 12-39.

Perrouty, S., Lindsay, M., Jessell, M., Aillères, L., Martin, R., and Bourassa, Y., 2014, 3D modeling of the Ashanti Belt, southwest Ghana: Evidence for a litho-stratigraphic control on gold occurrences within the Birimian Sefwi Group: Ore Geology Reviews.

- Piper, D. J., and Deptuck, M., 1997, Fine-grained turbidites of the Amazon Fan: facies characterization and interpretation: Proceedings of the Ocean Drilling Program. Scientific Results, 1997, p. 79-108.
- Prothero, D. R., and Schwab, F., 2004, Sedimentary Geology: W. H. Freeman.
- Robert, F., Poulsen, K. H., Cassidy, K. F., and Hodgson, C. J., 2005, Gold metallogeny of the Superior and Yilgarn cratons: Economic geology, v. 100, p. 1001-1033.
- Roest, W. R., Verhoef, J., and Pilkington, M., 1992, Magnetic interpretation using the 3-D analytic signal: Geophysics, v. 57, p. 116-125.
- Sestini, G., 1973, Sedimentology of a Paleoplacer: The Gold-bearing Tarkwaian of Ghana, Ores in Sediments, Springer, p. 275-305.
- Sibson, R. H., and Scott, J., 1998, Stress/fault controls on the containment and release of overpressured fluids: Example from gold-quartz vein systems in Juneau, Alaska; Victoria, Australia and Otago, New Zealand: Ore Geology Reviews, v. 13, p. 293-306.
- Sibson, R. H., Robert, F., and Poulsen, K. H., 1988, High-angle reverse faults, fluid-pressure cycling, and mesothermal gold-quartz deposits: Geology, v. 16, p. 551-555.
- Stacey, J. t., and Kramers, J., 1975, Approximation of terrestrial lead isotope evolution by a two-stage model: Earth and Planetary Science Letters, v. 26, p. 207-221.
- Stern, R. A., 2001, A new isotopic and trace-element standard for the ion microprobe: preliminary thermal ionization mass spectrometry (TIMS) U-Pb and electron-microprobe data, Ressources naturelles Canada.
- Steyn, J. G., 2012, Structural geology and controls of gold mineralization in the Sigiri Mine, Guinea, West Africa: MSc thesis, Stellenbosch University.
- Taylor, P. N., Moorbat, S., Leube, A., and Hirde, W., 1992, Early Proterozoic crustal evolution in the Birimian of Ghana: constraints from geochronology and isotope geochemistry: Precambrian Research, v. 56, p. 97-111.

Thiéblemont, D., Goujou, J. C., Egal, E., Cocherie, A., Delor, C., Lafon, J. M., and Fanning, C. M., 2004, Archean evolution of the Leo Rise and its Eburnean reworking: Journal of African Earth Sciences, v. 39, p. 97-104.

Villeneuve, M., 1992, Données nouvelles sur le Birimien du Nord-Est de la Guinée (Afrique de l'Ouest: UNESCO, Geology for Economic development, Newsletter 9, p. 195-202.

Watts, M., 2010, An introduction to the geology of Siguiri gold mine and the economic potential of the fresh rock in block 1, unpublished.

Weinberg, R. F., Groves, D. I., Hodkiewicz, P. and van der Borgh, P., n.d., Hydrothermal Systems, Giant Ore Deposits: Yilgarn Atlas Volume III UWA Gold Module, Part 1, AMIRA

Project P511. Available online from:

<http://users.monash.edu.au/~weinberg/Pages/Yilgarn/Yilgarn_GODS/Zuleika.pdf>.

[15/05/2015]

Wendorff, M., 2005, Evolution of Neoproterozoic–Lower Palaeozoic Lufilian arc, Central Africa: a new model based on syntectonic conglomerates: Journal of the Geological Society, v. 162, p. 5-8.

Williams, P., and Currie, K., 1993, Character and regional implications of the sheared Archaean granite-greenstone contact near Leonora, Western Australia: Precambrian research, v. 62, p. 343-365.

Wingate, MTD and Kirkland, CL 2014, Introduction to geochronology information released in 2014: Geological Survey of Western Australia, 5p.

Wood, R. A., Pettinga, J. R., Bannister, S., Lamarche, G., and McMorran, T. J., 1994, Structure of the Hanmer strike-slip basin, Hope fault, New Zealand: Geological Society of America Bulletin, v. 106, p. 1459-1473.

CHAPTER 3: PAPER TWO

STRUCTURAL CONTROLS ON THE WORLD-CLASS SIGUIRI GOLD DISTRICT, SIGUIRI BASIN, GUINEA, WEST AFRICA

The following paper presents the structural framework associated with the Siguiri gold district and its evolution through the Eburnean orogeny. The study is based on field observations, geophysical datasets, drill core logging and petrographic observations. This work focuses on district and deposit-scale observations of the second and third order structures controlling gold mineralisation. It describes the different structural features encountered in the Siguiri district and the link they have with gold mineralisation. This paper discusses the deformation history of the Siguiri district, the development of gold mineralisation in the district and the stress-field variations associated with this mineralisation. Based on this work, four deformation events were recognized to affect the Siguiri district sediments: a N-S compression (D_{1S}), an E-W compression (D_{2S}) interpreted to progressively evolve into transpression and then transtension (D_{3S}), and a NW-SE compression (D_{4S}). Gold mineralisation was interpreted to occur late during D_{3S} around ca. 2100 Ma and be associated with stress-field variations happening at a regional scale. This deformation scheme matches that of the deformation history previously described for the West African Craton.

Not only is this work crucial for the understanding of the deformation events that affected the Siguiri district, but is also critical to highlight the role stress-field variations have as a process leading to orogenic gold mineralisation.

This chapter was submitted to Economic Geology and is hence formatted accordingly. It was revised a number of times by all co-authors and twice by reviewers from the Economic Geology journal before resubmission.

Structural controls on an orogenic gold system: The world-class Siguiri gold district, Siguiri Basin, Guinea, West Africa

Erwann Lebrun¹, John Miller¹, Nicolas Thébaud¹, Stanislav Ulrich², T. Campbell McCuaig¹

¹: Centre for Exploration Targeting and ARC Centre of Excellence for Core to Crust Fluid Systems, School of Earth and Environment, Robert Street Building, M006, The University of Western Australia, 35 Stirling Highway, Crawley, WA, 6009, Australia

²: AngloGold Ashanti Ltd - Assets Development - Brownfields, 44 St George Terrace, Perth, WA, 6000, Australia

Abstract:

Ore bodies in the Siguiri district, a world-class Paleoproterozoic orogenic gold camp located in the Birimian of north-eastern Guinea, are typically represented by cryptic sub-vertical damage zones only expressed by a high density of mineralized veins. Observations from five representative deposits of the Siguiri district (Sanu Tinti, Bidini, Kami, Kosise and Sintroko PB1) show that these ore bodies are structurally controlled by incipient structures and spread across three distinct structural and lithostratigraphic domains. Two shale-dominated peripheral domains adjoin a central domain whose lithostratigraphy is dominated by medium to coarse-grained greywacke and this domain hosts the bulk of the gold endowment of the district. The three domains exhibit similar structural elements that can be described within a four-stage deformation scheme. The first deformation event (D_{1S}) is poorly constrained and interpreted to have been a N-S compressional event. It developed minor folds with W to WNW gently plunging fold axes without a clear axial planar cleavage. The main and second deformation event (D_{2S}) is interpreted to have been associated with E-W to ENE-WSW directed compression. D_{2S} was responsible for forming the dominant N-trending structural grain of the district and creating interference patterns between F_{1S} and F_{2S} folds. The third event (D_{3S}) is

develops progressively from D_{2S} compression into an early-D_{3S} E-W to ENE-WSW directed transpression and a late-D_{3S} NNW-SSE directed transtension characterized by the development of the bulk of the veining observed in the Siguiri district. The fourth and last event (D_{4S}) was a NW-SE oriented compressional event responsible for the localized overprinting of veining by a steep to shallowly dipping NNE-SSW ductile cleavage.

Gold mineralization formed along sub-vertical early-D_{3S} N-S thrusts, NE-trending dextral shear zones, WNW-trending sinistral faults and E-trending normal relay faults. Mineralization is expressed as localized mineralized shear zones or sub-vertical damage zones, characterized by a 10-15 metre-wide zone of dense quartz-carbonate-sulfide veining or disseminated gold-bearing sulfides. The mineralized veins consistently strikes to the ENE-WSW, are steeply dipping, and commonly have a conjugate geometry at the meso-scale. Finite strain analysis on folds, faults and conjugate mineralized vein sets is consistent with an initial stress-switch from a compressional (D_{2S}) to transpressional deformation (termed early-D_{3S}). Results of paleostress analysis on conjugate vein sets on mineralized vein sets that formed late during D_{3S} indicate that the stress-field ranged from extensional to strike-slip, sometimes within the same vein locality. The late-D_{3S} deformation is interpreted to have been a transtensional event. The first change in the principal stress axes orientation is interpreted to be related to a continuous switch from a far field-dominated to a body force-dominated stress field reducing the deviatoric component on the stress tensor. The second change in the principal stress axes orientation from early-D_{3S} transpression to late-D_{3S} transtension, suggests that σ1 and σ2 were close in magnitude, which is inferred to have facilitated localized stress-switches. In the Siguiri district, the early-D_{3S} and late-D_{3S} stress-switches which occurred at both a local and regional scale, have enhanced fracture permeability and are seen as a critical element for the establishment of active fluid pathways leading to the formation of a world-class gold system.

Keywords: West Africa; Siguiri; orogenic gold; tectonics; stress-switch

Introduction

Orogenic gold mineralization is common across the Paleoproterozoic Birimian rocks of the West African Craton e.g. Lawrence et al., (2013a); Milési et al. (1989); Milési et al., (1992). The location of orogenic gold deposits is typically controlled by complex regional-scale fault networks (Goldfarb et al., 2001; Groves et al., 2000). In West Africa, the Ashanti fault system in Ghana, is one example of such a network, and its many faults host some of the biggest vein-hosted and fault-vein-hosted orogenic gold deposits (e.g., Obuasi, Allibone et al., 2002; Fougerouse et al., this volume). The Siguiri district (240 t/7.9 Moz; AngloGold Ashanti Ltd., 2013; AngloGold Ashanti Ltd., n.d.) is unusual in West Africa because it is not located on a recognized large regional scale fault system. Instead it is located in the center of a large sedimentary basin in the Paleoproterozoic Baoulé-Mossi domain of the West African Craton. The Siguiri gold district currently consists of eleven accessible deposits, and is the only large gold district (> 50 t Au) in the weakly metamorphosed rocks of the Siguiri Basin (Egal et al., 1999).

Previous work on the district have recognized grade trends but have struggled to put the geology together and highlight the incipient structures that control gold mineralization at a deposit, district and regional-scale. Most notably, a study on the structural controls of auriferous quartz veining in eight of the deposits of the district was conducted by Steyn (2012). Steyn (2012) concluded that mineralization is hosted by veins, mainly controlled by competent lithologies and associated with N-S to NW-SE fold hinges and N-S to NE-SW shear zones developed during ENE-WSW transpression. This paper builds onto the observations made by Steyn (2012) and describes the different brittle, ductile and brittle-ductile structures observed in the district, including the different vein generations from five representative deposits including Sanu Tinti, Bidini, Kami, Kosise and Sintroko PB1.

Based on this dataset this paper 1) documents the local deformation history and 2) characterizes the structural controls on gold mineralization. The world-class Siguiri orogenic gold district displays a series of structural features that are used to constrain the stress-field

paleo-orientation before, during and after gold mineralization. In turn, these paleo-orientations are used to assess the role stress-switches have had on mineralization. This paper is the first study to put the geology of the Siguiri district together and to highlight the structures that control gold mineralization at a deposit and district-scale and that may represent local expressions of more fundamental structures controlling the location of the Siguiri district within the Siguiri Basin.

Geological context and exploration history

The Siguiri district is located in the north-western part of the Paleoproterozoic Baoulé-Mossi domain, which covers the majority of the Man-Leo shield in West Africa. The Birimian terranes (ca. 2210-2040 Ma; Davis et al., 2015; Figure 16) of the Paleoproterozoic Baoulé-Mossi domain were accreted against the Archean Kénéma-Man domain, in the south-western part of the West African Craton, during the Eburnean orogeny (ca. 2210-2040 Ma; Abouchami et al., 1990; Egal et al. 2002; Thiéblemont et al. 2004; Lahondère et al., 2002; Davis et al., 2015). Both domains are unconformably overlain by the Neoproterozoic Taoudeni Basin, which covers a large part of the craton (Begg et al., 2009; Lawrence et al., 2013a; Villeneuve and Cornée, 1994).

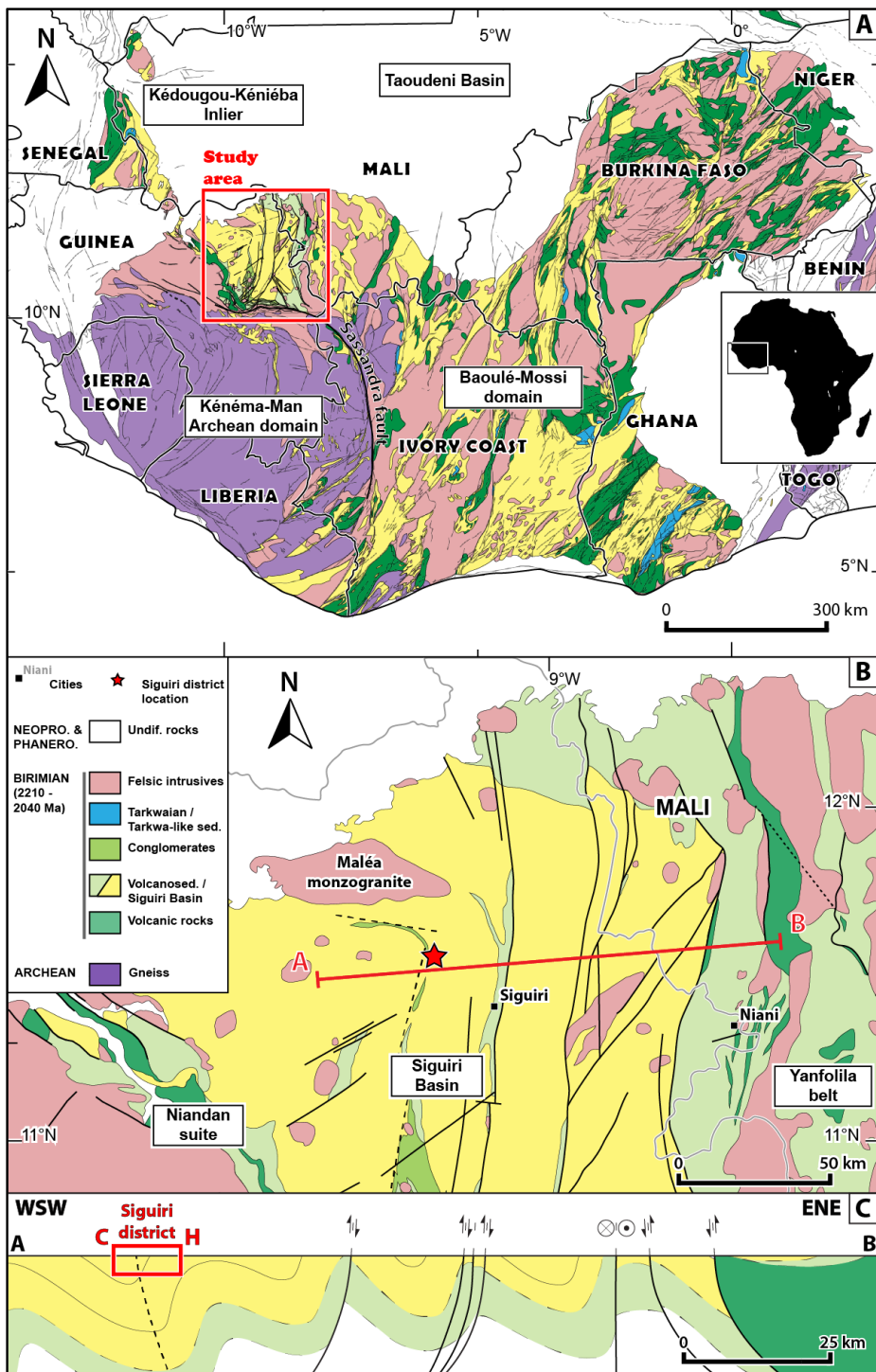


Figure 16: A) Simplified geology map of the Southern West African Craton. Red box highlights the Siguiri Basin shown in B. The Sassandra fault, bordering the Archean domain and the Siguiri Basin is shown as a thick black line; B) Geology map of the Siguiri Basin. Red box highlights the Siguiri district shown in Figure 17. Red lines indicate the segments of the regional composite cross-section (Figure 18A). Dashed black lines represent the interpreted regional extension of the N-S and WNW-ESE faults controlling mineralization in the Siguiri district. Modified from Milési et al. (1989) and Miller et al. (2013). C) Simplified composite E-W cross-sections of the Siguiri Basin and its eastern border. Interpreted conformable contacts are symbolized by full black lines, unconformable and unknown contacts by dashed lines.

The Siguiri Basin covers about 40,000 km² in Guinea and adjacent Mali. It consists of upper Birimian sedimentary, volcanioclastic and volcanic rocks and intrusive rocks. The upper Birimian sediments were derived from Paleoproterozoic volcanic rocks and felsic intrusions that were emplaced during the early stages of the Eburnean orogeny (Milési et al. 1989; Begg et al. 2009; Feybesse and Milési 1994). The Siguiri Basin is bordered to the south-west by the Niandan komatiite suite and the mafic to felsic volcanic rocks of the Kéniéro Range (not shown on map), dated at ca. 2095 Ma by Feybesse et al. (1999). To the south, the Sassandra fault puts rocks of the Kénéma-Man Archean domain in contact with those of the Siguiri Basin (Figure 16A, Egal et al., 2002). To the east, the Siguiri Basin is bordered by the Yanfolila granite-greenstone belt, which consists of volcanioclastic sedimentary and mafic to intermediate volcanic rocks. Finally, to the north, the flat-lying sandstones of the Neoproterozoic Taoudeni Basin unconformably overlie rocks of the Siguiri Basin. Paleoproterozoic intrusive rocks crosscut the Siguiri Basin sediments, such as the Maléa monzogranite (Parra-Avila et al., in press), outcropping north of the Siguiri district (Figure 16B). Mesozoic sills, lava flows and ENE-striking dikes, which are related to the opening of the South Atlantic Ocean, also cut or overlie rocks of the basin (Abouchami et al. 1990; Paranhos 2008, unpublished; Egal et al., 1999; Egal et al., 2002).

The Siguiri district is hosted in fine-grained organic-rich shale, siltstone, greywacke interbeds, graded greywacke beds and rare conglomerate. Based on aeromagnetics, magnetics, gravimetry, drill core and field observations, 3 formations were recognized, namely: the Balato, Fatoya and Kintinian Formations (Figure 17). The Balato Formation is dominated by dark grey siltstone beds grading upwards to shale. The contact between the Balato and the overlying Fatoya Formation was not observed. The Fatoya Formation is dominated by meter-thick beds of medium- to coarse-grained greywacke beds fining upwards to siltstone and shale. The Kintinian Formation, overlies the Fatoya Formation and is dominated by massive dark-green shale with centimeter-thick interbeds of limestone. The Kintinian Formation is also characterized towards its base by a stack of polymict clast-

supported conglomerate beds. In the Sanu Tinti deposit, detailed further in the results, a thrust fault marks the contact between the Fatoya and the Kintinian Formation.

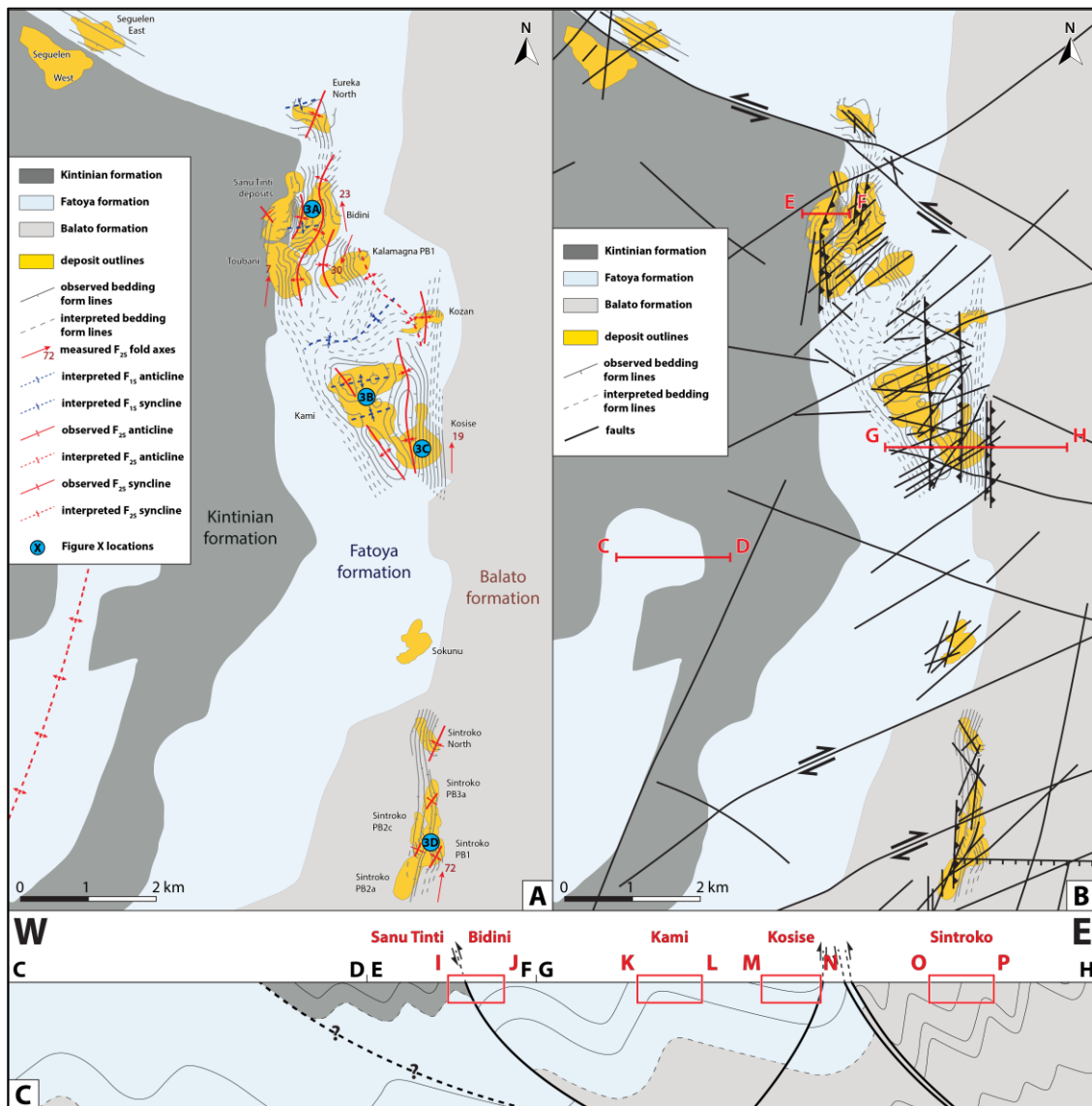


Figure 17: A) Form line map, and; B) structural map of the Siguiri gold district and its different deposits constrained by aeromagnetics, magnetics, gravimetry, drill core and field observations. The three structural domains follow the lithostratigraphy. Red lines indicate the segments of the district composite cross-section shown in C. C) Simplified composite E-W cross-sections of the Siguiri district (deposit cross-sections in Figure 18). Interpreted conformable contacts are symbolized by full black lines, unconformable and unknown contacts by dashed lines.

The Siguiri gold district has been recognized for many years (first gold produced in 1931 by the French; AngloGold Ashanti Ltd., 2013), however, only one publically available research study has been conducted by Steyn (2012). This study detailed the different brittle, ductile and brittle-ductile structures observed in the district and described the structural

controls on auriferous quartz veining in 8 of the deposits of the district. Based on bedding-fabric-vein-fault relationships, Steyn (2012) identified 3 deformation events in the Siguiri district: D1, D2 and D3. One gold event was recognized in the district and is associated with steeply dipping syn-D2 quartz-carbonate-sulfide veins striking to the N-S to NE-SW and commonly displaying conjugate relationships. These veins are accompanied by carbonate alteration in the form of millimeter-sized nodules overgrowing the quartz-albite-sericite host rock mineralogy. Based on bedding-fabric-vein-fault relationships, Steyn (2012) concluded that auriferous veining in the Siguiri district is dominantly controlled by competent lithologies, N-S to NW-SE F2 fold hinges and N-S to NE-SW shear zones developed during D2 in an ENE-WSW dextral transpressive environment.

The Siguiri region has been long recognized for its endowment and has been producing gold for centuries. In the 3rd century, the Sarakolle Kingdom was already familiar with the widespread gold endowment from Senegal to the Niger River. Production of gold from this region is thought to have continued through the 12th and 13th centuries in areas controlled by the Mindingo Kingdom, whose capital Niani is near the present eastern border between Guinea and Mali, less than 100 km from Siguiri. Continued gold production included its use as tribute by the Mali Empire during the 17th century. In the late 19th and early 20th century, minor extraction and prospecting in the Siguiri area was started by the French. Industrial production of gold from the Siguiri district started in 1931 (nearly 75 t reported between 1931 and 1951) (AngloGold Ashanti Ltd., 2013). Between 1960 and 1963 a Russian state company was actively mining in the region, focusing their operations on placer-type deposits. In the 1980s, North American and British companies conducted reconnaissance mapping, traversing, and sampling. In the early 1990s, Société Aurifère de Guinée followed up this work and reported a production of 1.1 t Au. In 1995, Golden Shamrock started a pre-feasibility study of the Siguiri district, before merging with Ashanti Goldfields (now AngloGold Ashanti Ltd) in 1996. Since 2004, the Siguiri mine has been owned 85% by AngloGold Ashanti Ltd and 15% by

the Guinean government. The district measured resources were 21.08 t Au indicated resources from ore averaging 2.35 g/t and inferred resources of 59.09 t of gold from ore averaging 0.8 g/t as of the end of 2013 (AngloGold Ashanti Ltd., 2013). Since AngloGold Ashanti took over the operations, production at the Siguiri district has been approximately 10 t/year for an estimated cumulative production of 105.5 t Au in 2014 (Table 2 in Electronic Appendices; AngloGold Ashanti Ltd., n.d.). Therefore, the cumulative production from the Siguiri district is ca. 160 t Au (5.3 Moz), with resources of ca 80 t Au (2.6 Moz), making the district world class according to the classification of Schodde and Hronsky (2006). AngloGold Ashanti has been focusing its mining and exploration activity in the Siguiri district on the oxidized upper part of the deposits. Minor free gold concentrations are still being extracted by local miners from localized Phanerozoic paleo-placers and from hydromorphic reconcentration in and below the mottled zone of the lateritic profile. Individual gold nuggets of up to several kilograms in weight have been found near regolith surface (Watts, 2010).

Methodology

For the purpose of this paper, each of the eleven open pits is considered a deposit, they are collectively termed the Siguiri district, and the overall district is considered world-class (>6 Moz Au; Schodde and Hronsky, 2006). A few deposits of the district were not accessible at the time the fieldwork was conducted, and as a result few data could be collected from them (e.g. Sokunu; Figure 17). Out of the eleven deposits accessible that were visited and mapped, five deposits were defined as being of key importance for the understanding of the overall district architecture and mineralization style. These deposits highlight critical components of character of the host rocks, host rock controls on mineralization and also key structural features with different relative timing. The five deposits selected for detailed analysis were, from north to south: Sanu Tinti, Bidini, Kami, Kosise and Sintroko PB1. The Sanu Tinti, Bidini and Kosise deposits are all located near or at the contact between two of the

sedimentary formations hosting gold deposits in the district, whereas the Kami and Sintroko PB1 deposits are located in the middle of the Fatoya formation.

Seven months of fieldwork in the Sigiri district were conducted over two years, starting in April 2011. Mapping, structural data collection, and sampling in the district were accomplished using open pit and limited field exposure augmented by logging of selected drill cores. All readings are given in true north coordinates. Planar features are given in dip direction/dip format (e.g., 180/45 for an E-W plane dipping at 45° to the south). Each structural element or event is suffixed by "XS" or "XY" subscripts with "X" representing a digit related to the relative timing of the deformation event mapped, "Y" representing a particular group of structural elements, and "S" standing for Sigiri. In addition, terminology includes D_{XS} for deformation events; S_{XS} for fabrics, with S₀ being bedding; F_{XS} for folds; and V_{XS} or V_{XY} for veins. For example, V_{2S} and S_{2S} are part of the D_{2S} event.

Optical imaging was used to constrain the relative timing and kinematics of various structural elements (e.g. cleavages, vein). Petrographic work on polished thin-sections was conducted at the Centre for Exploration Targeting (CET), University of Western Australia, Perth, using a Nikon Eclipse LV100 POL. Further petrographic work was conducted by SEM at the Centre for Microscopy Characterisation and Analysis of the University of Western Australia.

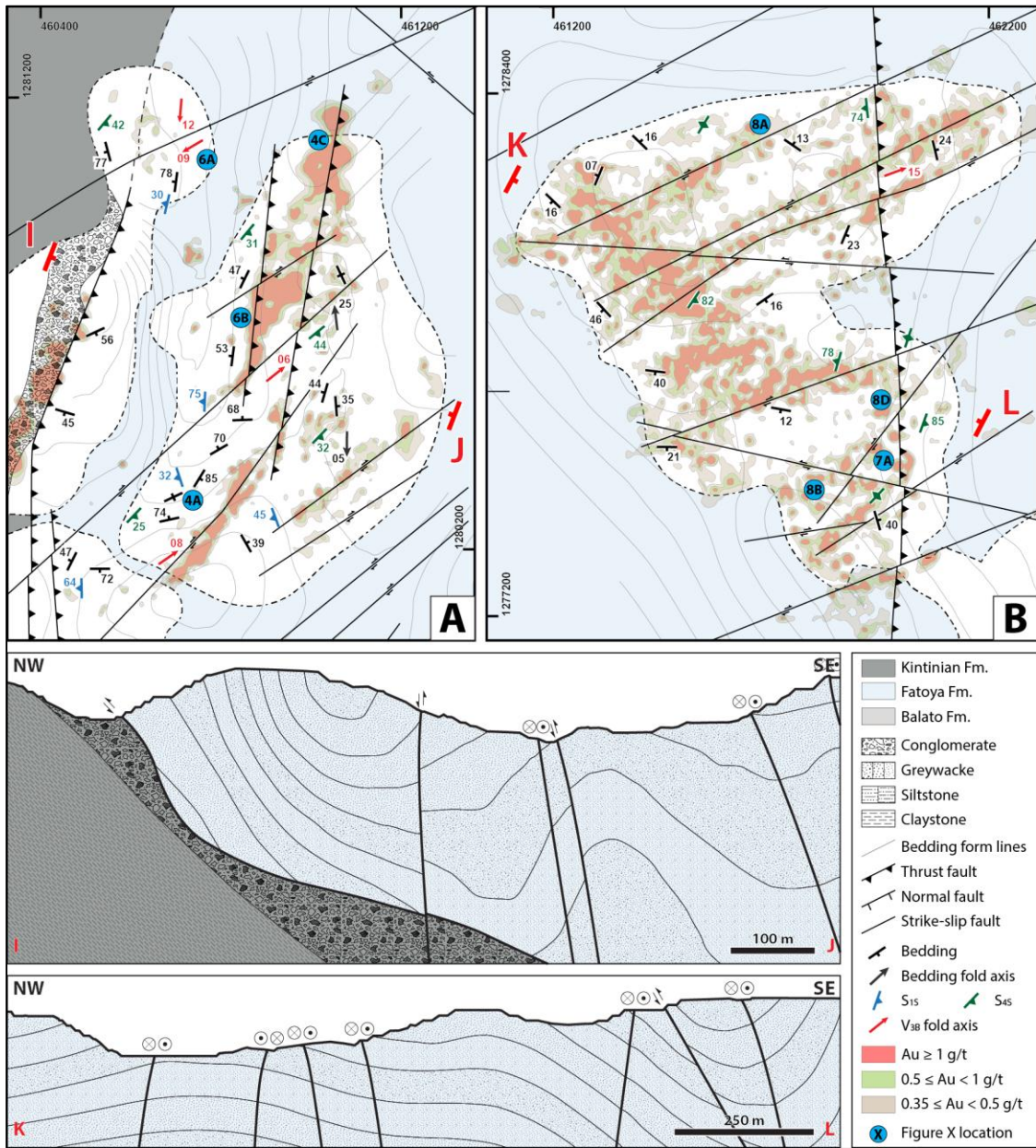
Key deposits of the Sigiri district

The following section reviews the main geological characteristics and insights into the mineralization of five key deposits from the Sigiri district: Bidini, Sanu Tinti, Kosise, Kami and Sintroko PB1 (Figure 17).

Bidini

The Bidini deposit is located in the northern part of the district (Figure 17). Bidini is hosted in the greywacke-dominated Fatoya Formation, and is adjacent to the Sanu Tinti

deposit (Figure 18A). The Fatoya Formation in the deposit has minor alternations of siltstone and shale beds.



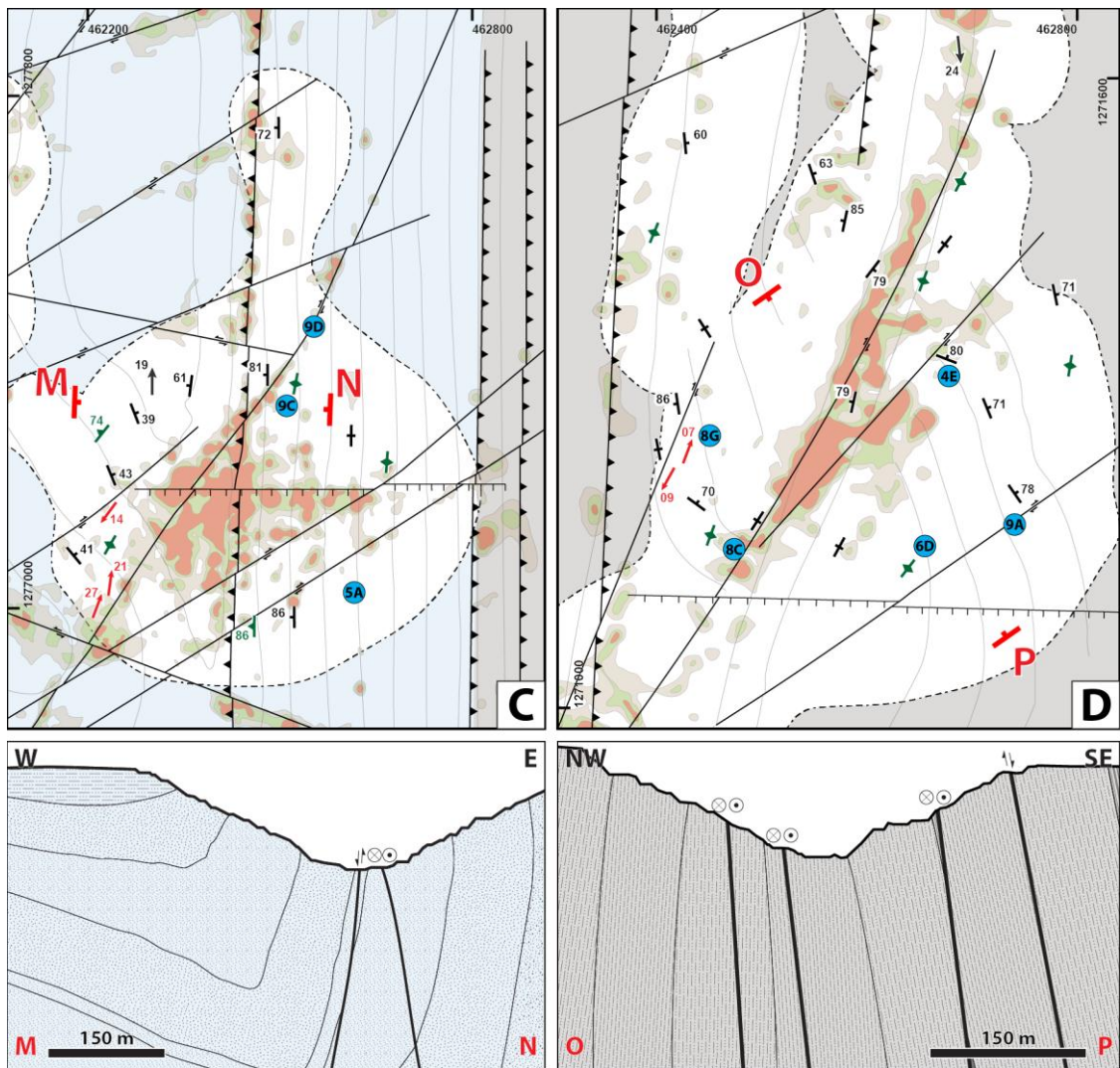


Figure 18: Detailed structural form line maps of the A) Bidini and Sanu Tinti deposits; B) Kami deposit; C) Kosise deposit, and; D) Sintroko PB1 deposit. Each map is accompanied by the deposit cross-section, denoted in red letters. Damage zones, distinct and incipient structures are all represented by a thick black line.

Discrete folds occur in the southeastern part of the Bidini deposit (Figure 19A). These gently inclined to recumbent folds are open to tight, and have a wavelength of about 15 meters and fold axes that plunge moderately to the WSW. These folds are associated with an axial planar cleavage that trends NW-SE to N-S and dips shallowly to moderately to the WSW. This moderate-dipping cleavage is the first mappable fabric in the deposit, and the folds are therefore termed F_{1S} . The discrete F_{1S} folds are refolded by a second generation of folds, termed F_{2S} . The F_{2S} folds in Bidini are not associated with any mappable axial planar foliation. The Bidini deposit itself sits on the hinge of a larger scale F_{2S} fold. This larger scale F_{2S} fold is a tight upright anticline with an estimated wavelength of about 500 meters. The axial surface of

this anticline trends NNE-SSW, and its fold axis plunges shallowly to the north and south. An asymmetric N-S trending F_{2S} syncline with a western long limb, eastern short limb and an axial surface dipping to the east, occurs in between Bidini and Sanu Tinti, giving an overall west vergence to the folding.

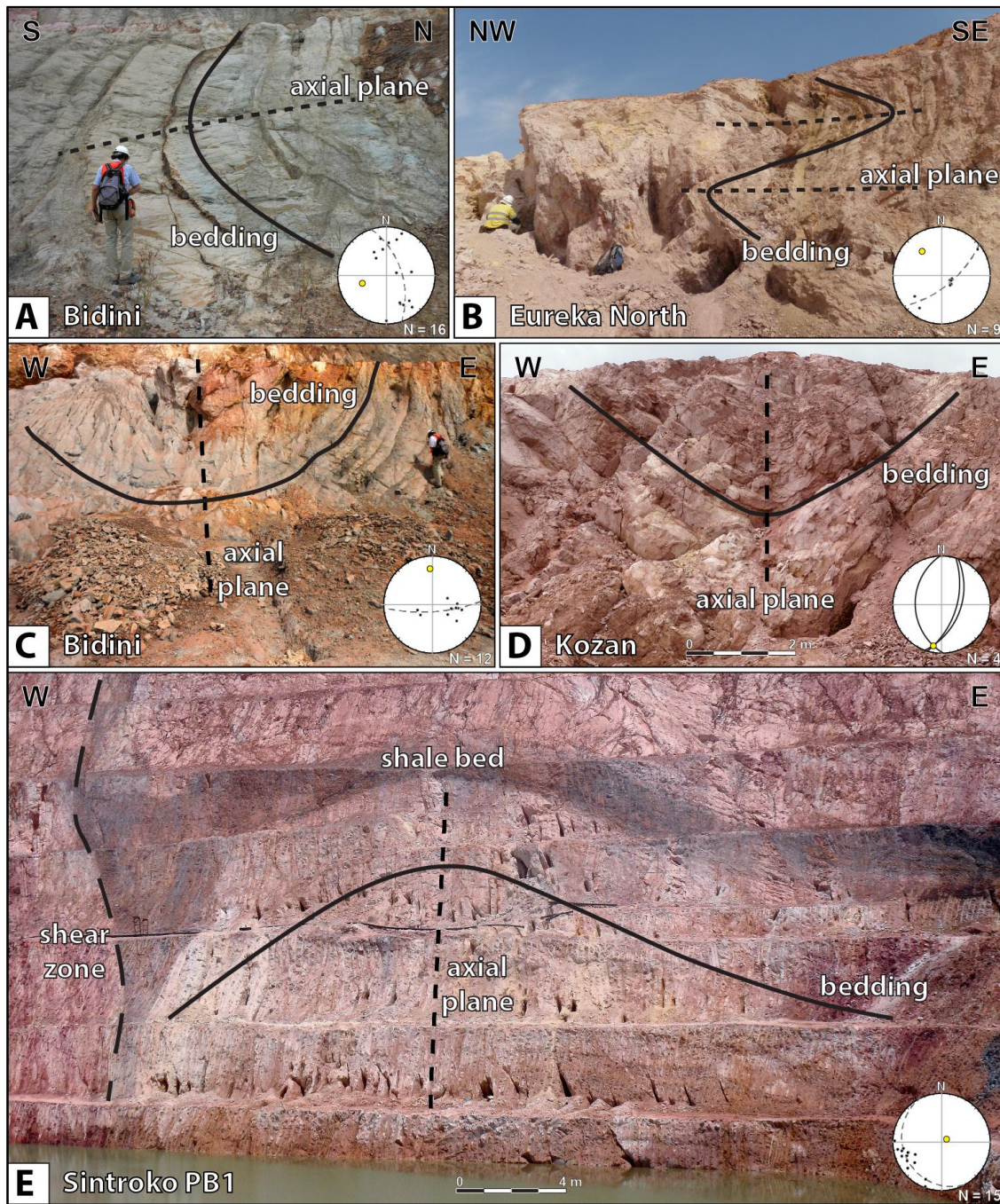


Figure 19: Photographs of folds from the Siguiri district with corresponding stereograms of structural data. On the photographs, bedding is represented by full black lines, fold axial planes by short-dashed black lines and shear zone boundaries by long-dashed black lines. In the stereograms, bedding is represented by black poles or full black great circles, constructed fold axial planes are represented by dashed black great circles and constructed fold axes are in

yellow. From top-left to bottom right: recumbent F_{1S} folds from A) Bidini (the trace of the observed axial planar S_{1S} cleavage is also represented) and B) Eureka North; C) F_{2S} fold in Bidini; D) the Kozan F_{2S} syncline, thought to be structurally adjacent to the Kosise F_{2S} syncline; E) upright F_{2S} fold with steeply plunging fold axis from Sintroko PB1. Note the consistent orientation of the veins mined by locals (vertical cavities in wall) and the rheological control on mineralization (seal cap of shales, in dark grey, with strong veining restricted to underlying sandstones).

Numerous veins can be observed to develop along bedding and F_{2S} folds in Bidini (Figure 20A). These veins, whose orientation varies across the deposit, are typically only a few millimeters to 5 centimeters thick. Multiple sub-vertical damage zones, oriented NE-SW and N-S, crosscut the F_{2S} folds and overprint the bedding parallel veins.

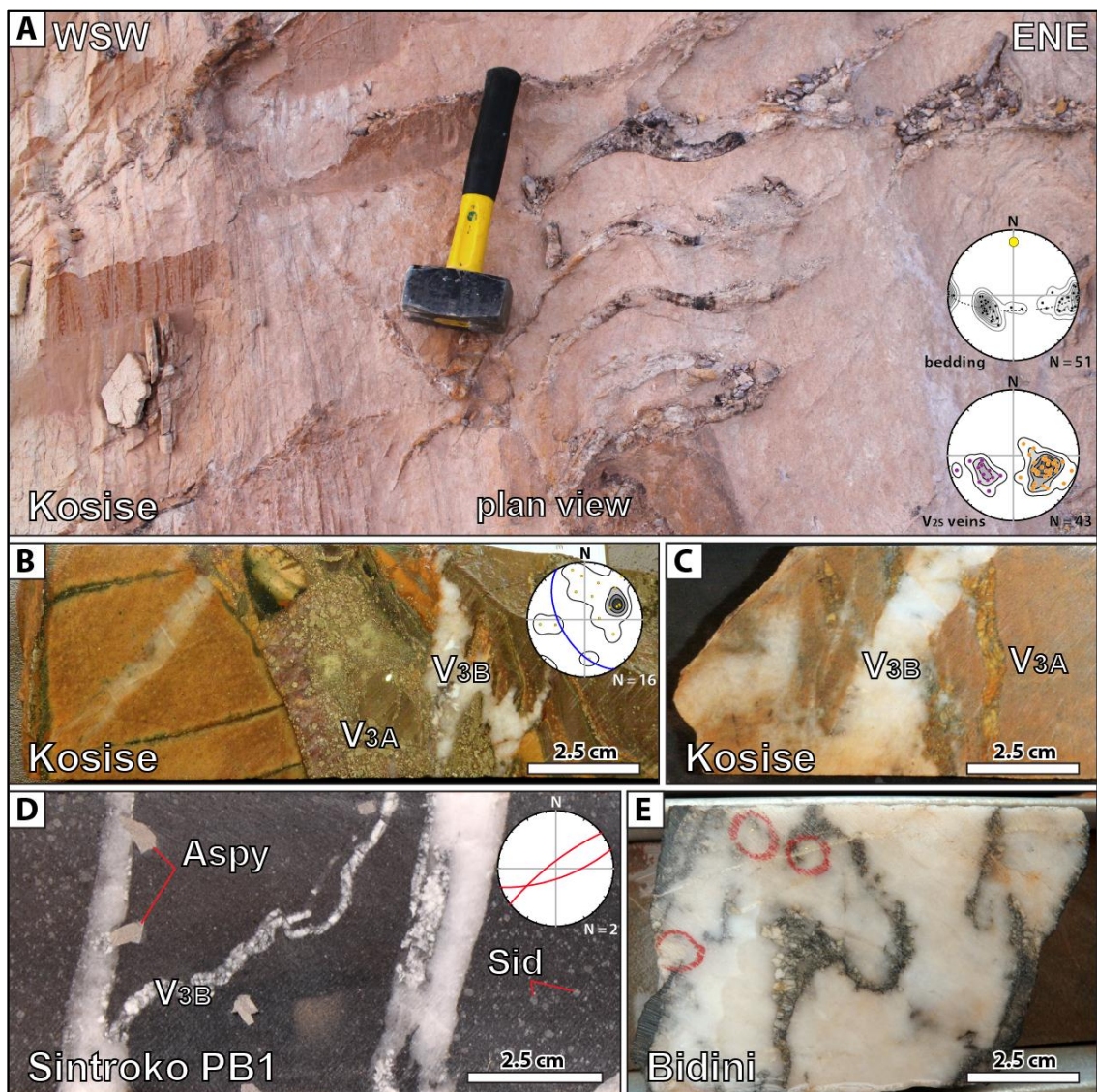


Figure 20: Photographs of the different vein generations observed in Siguiri. A) En-echelon barren quartz V_{2S} veins. The projected poles from the entire Kosise deposit of bedding, V_{2S} bedding-parallel and V_{2S} en-echelon veins, highlight that orientations and sigmoidal character of V_{2S} veins are consistent with their formation by flexural slip

along bedding during F_{2S} folding. In the equal area stereonet/Schmidt projection stereogram, bedding is represented by black poles, the constructed fold axial plane is represented by a dashed black great circle and the constructed fold axis by a large yellow disk. Bedding-parallel veins are represented by orange poles, en-echelon are in purple; B) Gold bearing ankerite-pyrite V_{3A} veins developed as a brecciated vein. In the equal area stereonet/Schmidt projection stereogram, V_{3A} poles are in yellow and a great circle was constructed in blue from their average orientations; C) Shallow V_{3B} vein cutting across multiple ankerite-pyrite V_{3A} veins; D) Steep quartz-ankerite V_{3B} mineralized veins with arsenopyrite crystal halo. The arsenopyrite typically crystallizes along the edges of the vein or in the host rock around, but rarely in the vein itself. The vein to the left displays a unitaxial geometry, characteristic of the crack-seal growth mechanism (Passchier and Trouw, 2005). Both veins are represented as red great circles in the equal angle stereonet/Wulff projection stereogram; E) Visible gold in a quartz-ankerite V_{3B} mineralized vein.

These sub-vertical structures are not defined by a discrete shear zones or fault plane but instead are represented by ten to fifteen meter wide zones of higher vein density compared to the surrounding rocks (Figure 21B). The veins developed in these incipient NE-SW and N-S damage zones can be separated into two generations. The first generation of veins displays brecciated textures and vein thickness varies from a few millimeters up to 20 centimeters (Figure 20B and 20C). The orientation of these veins could not be measured in the field. The second set of veins, oriented NE-SW and crosscutting the first generation, commonly display antitaxial textures and sheet-like geometries (Figure 20E). These veins are commonly conjugate with a bimodal vein distribution around 141/89 and 150/66 (Figure 21B). At the outcrop scale, veins following either one of these dominant orientations can also have secondary veins that result in a conjugate geometry (note examples from the Seguelen and Sintroko PB1 deposits on Figure 21C and 21D). Field observations and crosscutting relationship from drill core indicate that both these vein generations postdate the development of the bedding parallel veins.

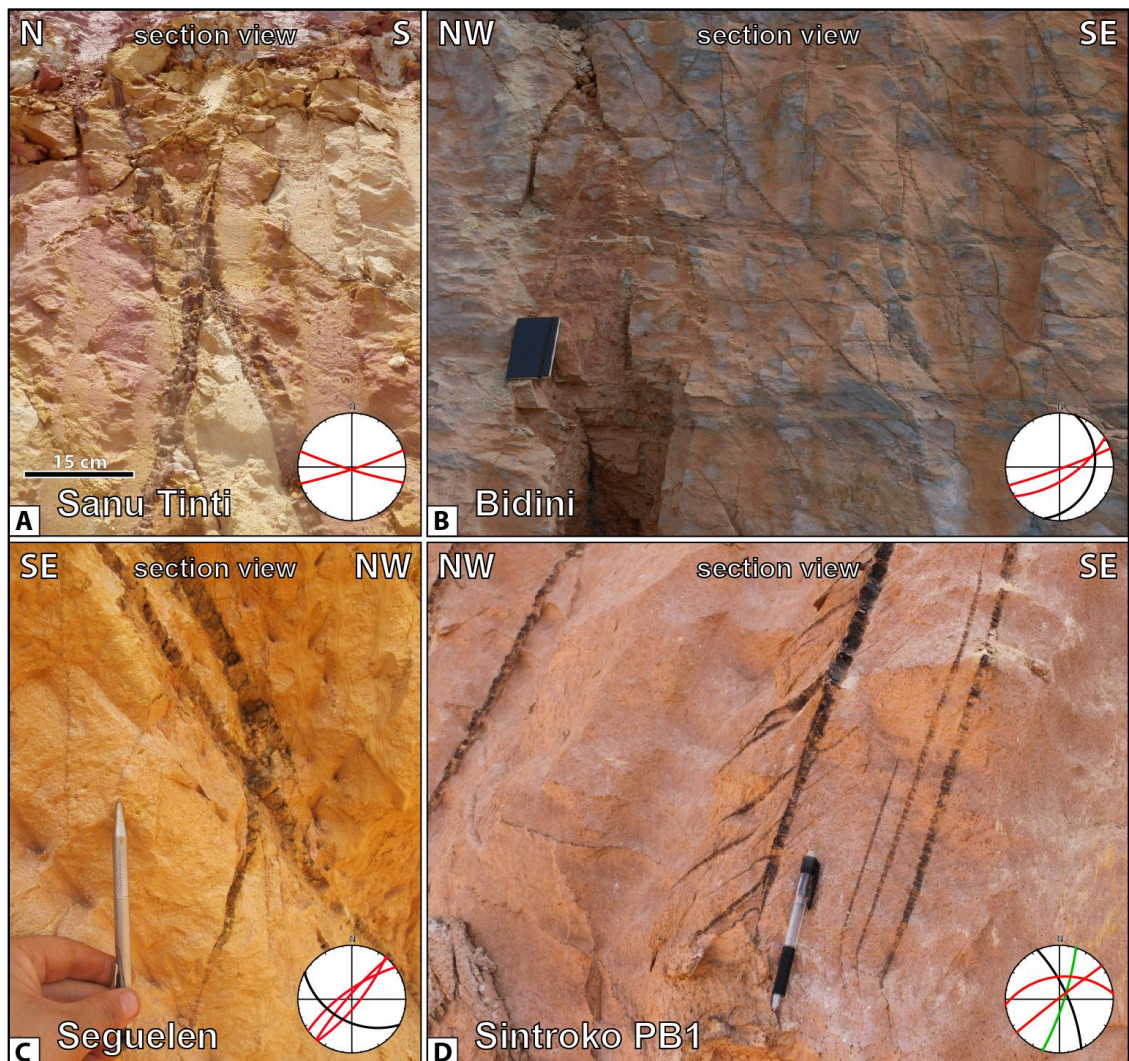


Figure 21: Photographs of conjugate V_{3B} vein sets. From top left to bottom right: A) Sanu Tinti extension deposit; B) Bidini (with sub-horizontal bedding, in black); C) Seguelen and; D) Sintroko PB1 deposit. In the equal angle stereonet/Wulff projection stereograms, bedding is represented as black great circles, V_{3B} veins are represented as red great circles, and the S_{4S} cleavage as a green great circle.

Mineralization in Bidini follows the NE-SW and N-S damage zones, and is contained in both the second and third vein generation. The first bedding-parallel vein generation dominated by quartz and minor ankerite and albite is barren. The second vein generation is composed of ankerite and pyrite (Figure 20B and 20C) and the third vein generation is composed of quartz-ankerite-arsenopyrite+/-pyrite (Figure 20D, 20E and 22).

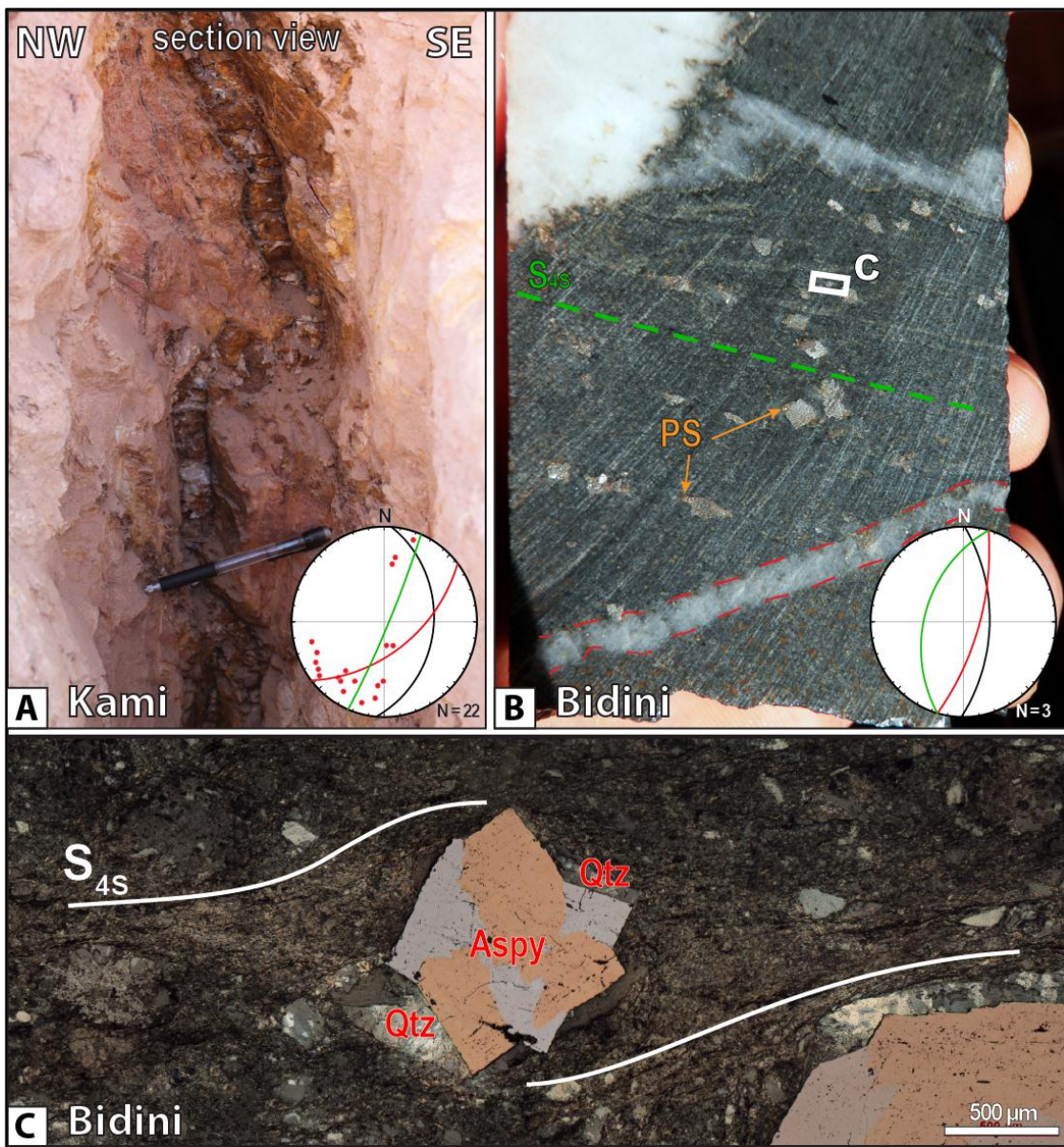


Figure 22: A) Photograph of a steep mineralized V_{3B} vein in Kami deposit overprinted by the S_{4S} cleavage. The vein (red in stereogram) and measured fold axes from other folded mined veins (red poles) are indicative of a NW-SE compression (S_{4S} cleavage in green); B) Core from Bidini showing multiple arsenopyrite crystals around a V_{3B} mineralized vein (bottom; orientation of the veins in the upper part of the photo unconstrained). The crystals display pressure shadows (PS; orange arrows) parallel to the S_{4S} cleavage (in green); C) Microphotograph from the core shown in B) of a V_{3B} twinned arsenopyrite under cross-polarized reflected light, developing pressure shadows due to S_{4S} cleavage. Aspy: arsenopyrite, Qtz: quartz. Stereograms: S_0 in black, mined veins as red great circles, mined vein fold axes as red poles and S_{4S} in green; equal angle (Wulff) projection.

Gold in the ankerite-pyrite veins is found as free gold along fractures in the sulfides or as inclusions displaying triangular textures and is associated with chalcopyrite, hematite and minor chlorite (Figure 23F). Minor arsenopyrite can also be found coeval with the fractured

pyrite. Native gold in the quartz-ankerite-arsenopyrite veins is found within the quartz or between the quartz and the ankerite rims (Figure 20E). Alteration around the ore shoots is characterized by albitisation of the host rock and carbonate alteration often characterized by the bleaching of the host rock up to a meter around individual veins (Figure 23E). A late penetrative planar fabric, termed S_{4S} , strikes to the NE and dips moderately to the SE. This late-stage S_{4S} fabric overprints all earlier structures (Figure 22B and 22C). Thin section analysis indicate this fabric is defined by sericite and it is preferentially developed in shale beds. It is also visible in greywacke beds where it is highlighted by quartz-carbonate-sericite-(pyrite) strain shadows and strain fringes around the arsenopyrite crystals associated with the steep NE-SW veins (Figure 22B and 22C).

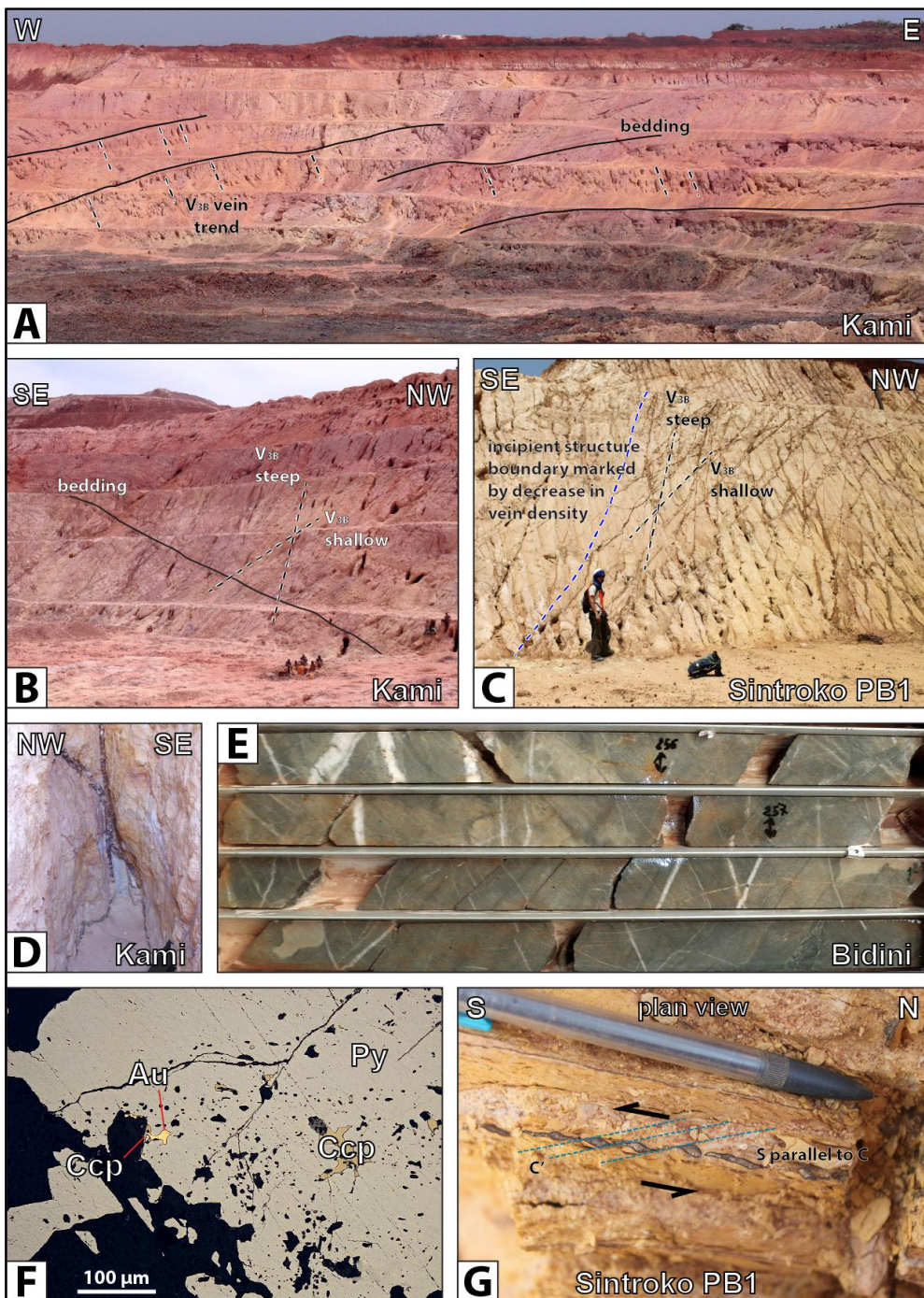


Figure 23: Photographs of various structural elements linked to mineralization. A) Domal structures in the Kami deposit. The V_{3B} veins, mined by local villagers, can be seen focused in the dome and following competent beds. Each bench is about 7 meters high. B) Conjugate vein geometry at deposit-scale. C) Minor damage zone in Sintroko PB1 displaying mutually crosscutting V_{3B} steep and shallow conjugate vein sets; D) Conjugate V_{3B} vein geometry at outcrop-scale. E) Core from the Bidini deposit displaying meter-wide carbonate alteration haloes (bleached) around V_{3B} veins; F) Microphotograph of a Sanu Tinti disseminated pyrite. Free gold is associated with chalcopyrite and displays triangular textures characteristic of infill crystallization (Taylor, 2010). G) Plan view of C/C' structures affecting the S_{4S} cleavage (highlighted by quartz; bedding parallel to S_{4S}). The kinematics indicate sinistral movement along the S_{4S} cleavage, which overprints mineralization.

Sanu Tinti

The Sanu Tinti deposit is one of the northernmost deposits (Figure 17). It sits at the contact between the greywacke-dominated Fatoya Formation to the east, and the overturned and younger Kintinian Formation to the west (Figure 18A). The Kintinian Formation in Sanu Tinti is characterized by a basal sequence of polymict, clast supported conglomerate. The remainder of the Kintinian Formation outcropping in this deposit is composed of shale and fine siltstone beds. The deposit is on the western long limb of a large scale F_{2s} N-S trending open to close syncline within the Fatoya Formation. This N-S syncline has an E-dipping axial plane that shows a fold vergence to the west, has a wavelength of about 500 meters, and extends into the Bidini deposit (Figure 19C). The axial surface of this F_{2s} syncline is upright but no planar fabric parallel to it was observed.

In the Kintinian Formation there are a few veins (~1 vol%) striking to the NE and dipping steeply to the SE that crosscut the conglomerate beds. These veins are thin (2-3 centimeters on average) but can extend over a few meters in length. In the Sanu Tinti deposit, the faulted contact between the Kintinian and the Fatoya Formations is marked by brecciated textures developed in the first few meters around the fault. The fault is oriented N-S to NNE-SSW, dips moderately to the SE and has been delineated to a depth of more than 300 meters (Figure 18A). Slickensides indicate that this contact is a thrust fault. In the Fatoya Formation, a poorly defined and spaced planar fabric trends to the NNE and moderately dips to the WNW. This fabric is overprinted by bedding parallel veins following the western long limb of the large scale F_{2s} N-S trending syncline developed in the Fatoya side of the deposit (Figure 18A).

Sub-vertical ENE-trending veins were found to cut across the large scale F_{2s} syncline. These veins often display a conjugate geometry and are a few centimeters to 15 centimeters thick, but can extend for tens of meters in length (Figure 21A). In Sanu Tinti, these conjugate veins are typically oriented in two main sets: 335/82 and 196/84. Either of these sets can have a conjugate geometry with additional secondary veins of similar orientation to the other vein set. In the northern part of the Sanu Tinti deposit, the density of these veins increases up to

20-30 vol% over 10 meters along an inferred damage zone oriented NE-SW (Figure 18A). An increase in vein density was also observed along the F_{2S} syncline hinge in the same area of the deposit. A second planar fabric, defined as S_{4S} , overprints all previously described structures. It is penetrative, oriented NE-SW in Sanu Tinti and dips gently to the SE. In the Kintinian conglomerate this S_{4S} penetrative planar fabric maintains a similar orientation but manifests as a spaced brittle fabric.

Mineralization in the Sanu Tinti deposit displays two styles. The first style is spatially associated with the footwall of the thrust fault and consists of pyrite disseminated in the Kintinian Formation conglomerate. The pyrite is often anhedral. Gold can be found free within fractures in the pyrite or as inclusions displaying triangular textures (Figure 23F), and is associated with chalcopyrite, hematite and galena. Minor tourmaline can be found associated with the pyrite. The second style consists of the sub-vertical ENE-trending veins cutting across F_{2S} folds. These veins consist of quartz, ankerite, arsenopyrite and minor disseminated pyrite. Native gold can be found within the quartz or on the margin of the quartz and ankerite (Figure 20E).

Kami and Kosise

The Kami and Kosise deposits are both hosted in the Fatoya Formation, which is dominated by meter-thick greywacke-sandstone beds fining up into, or alternating with, minor centimeter-thick beds of siltstone and shale (Figure 17). Kami sits in the centre of the Formation, whereas Kosise sits further to the east.

The Kami deposit has a structural style characterized by open F_{1S} upright folds with fold axes gently plunging to the NE or the SW and by open F_{2S} upright folds with fold axes gently plunging to the north or south. The intersection of these folds forms a broad domal structure that hosts the Kami deposit. The Kosise deposit is adjacent to Kami and is hosted on the hinge and short limb of an open N-S F_{2S} syncline which has a sub-horizontal fold axis. The axial surface of this N-S syncline is moderately inclined and indicates a fold vergence to the

west for this fold. A series of N-S faults parallels the short limb of the Kosise syncline to the east. These faults are dipping steeply to the west and are sub-parallel to the contact between the Fatoya and the Balato Formations (Figure 18B and 18C). An early cryptic sub-horizontal spaced brittle planar fabric was observed in both deposits, however its timing and significance is poorly constrained. This fabric is overprinted by a quartz-dominated vein set that develops parallel to bedding or with an en-echelon geometry along the contacts between different bedding units (Figure 20A). The bedding-parallel veins are commonly ~5 centimeters thick, and can extend for several tens of meters. The en-echelon veins are typically thinner and rarely exceed 4 centimeters in thickness. The en-echelon vein arrays can extend over 2-3 meters, but individual veins typically extend for up to 50 centimeters. This oldest vein set is not mineralized.

The veins, the open folds in Kami and the F_{2s} syncline in Kosise are crosscut by sub-vertical discrete shear zones, or by what have been defined as incipient structures. For example, a meter-wide discrete NE-SW fault zone displaying dextral kinematics is a major structural feature observed in the Kosise deposit (Figure 24C, 24D and 24E) and vein patterns along minor E-W trending fault zones in the Kami deposit indicate normal movements along these discrete structures. However, incipient structures are more common than discrete structures in the Kosise and Kami deposits, and are expressed by an abundance of veins along a 10 to 15 meters-wide damage zone of sheet-like geometry with no visible discrete zone of faulting or shearing (Figure 24B). Similar N-S, E-W, WNW-ESE and NE-SW damage zones extending along strike over a few hundred meters to more than a kilometer were recognized in the field (Figure 17, 18B and 18C). The only N-S damage zone recognized in Kosise is sub-parallel to the stratigraphy and extends to the Kozan deposit, which displays similar structural features (Figure 17 and 19D). No kinematic indicators could be observed in the WNW-ESE damage zones in Kami or Kosise.

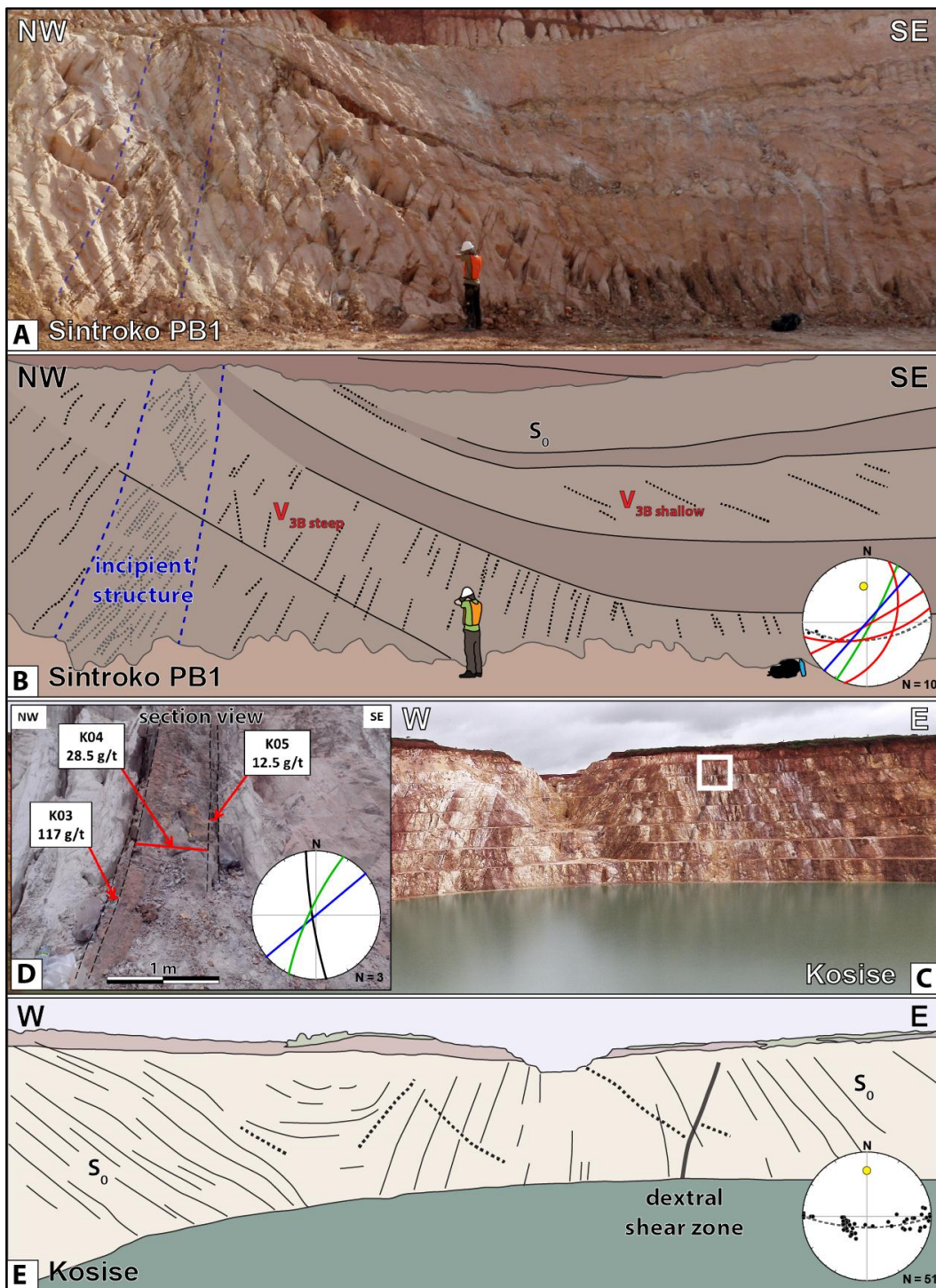


Figure 24: Photographs of some of the ore controlling structures in various deposits of the Siguiri district. These structures are enhanced due to the very deep weathering. A) and B) Incipient structure in Sintroko PB1 marked by an increase in quartz vein (V_{3B}) vein density. The mineralized veins (dotted lines in B), mined by local villagers, keep a consistent orientation and cut across the F_{2S} fold. Mineralization develops around the incipient structure, and is also controlled by the rheology of the sedimentary units. C), D) and E) NE-SW dextral shear zone. Intersections between NE-SW dextral shear zones and N-S thrust faults are typically highly mineralized, such as in Kosise (Figure 19C). Minor faults represented by dashed lines in E). Stereograms: S_0 in black, calculated F_{2S} fold axes in yellow, structures in blue, mined vein in red and S_{4S} in green; equal angle (Wulff) projection.

Gold mineralisation in the Kami and Kosise deposits is associated with veins that crosscut the oldest quartz-dominated vein sets and developed adjacent to discrete fault zones and also with veins within damage zones related to incipient structures. The vein arrays occurring adjacent to the discrete fault zones and within the damage zones, can be separated into two generations. The first generation of these veins consists of ankerite-pyrite and rare albite, and was only observed in drill core and develops in the first few meters around the damage zone linked to the discrete fault zones (Figure 20B and 20C). These veins orientation could only be constrained from drill core observation, and do not show a consistent orientation (Figure 20B). These veins are a few millimeters up to 15 centimeters thick and commonly display brecciated textures (Figure 20B). Their lateral extent is not known. Gold can be found free in pyrite fractures. These veins are associated with the bulk of the carbonate alteration observed in the Kami and Kosise deposits with millimeter-thick siderite nodules up to a meter around the vein margins. These veins are also associated with albitisation, which usually developed within the first 10 centimeters around them.

The ankerite-pyrite vein generation is crosscut by the youngest and dominant vein generation which forms the bulk of the veins associated with the damage zones in both deposits. These youngest veins consist of quartz-ankerite-arsenopyrite and rare pyrite, are from 0.5 centimeters to 10 centimeters thick, and extend over tens of meters. These quartz-ankerite-arsenopyrite veins commonly show antitaxial textures and display a bimodal orientation, defining two main sets: 150/40 and 145/70. In the field, veins from one set can be found conjugate with veins from the other, or with other secondary veins with a slightly differently orientation (Figure 23B). In the first ten to fifteen meters away from these damage zones the conjugate vein sets can also be found in domal structures along particularly competent greywacke beds (Figure 23A). The bulk of the gold found in the Kami and Kosise deposits is associated with these quartz-ankerite-arsenopyrite veins. Native gold can be found in the quartz veins and along the ankerite rims. Free gold can also be found in the arsenopyrite and along fractures associated with chalcopyrite, galena and some sphalerite. Gold grades

across some of the discrete fault zones controlling the distribution of mineralized veins can be over 100 g/t (Figure 24D). These veins develop carbonate alteration haloes up to a few tens of centimeters width mainly defined by siderite nodules.

The youngest vein generation is refolded and overprinted by a late sub-vertical fabric oriented NNE-SSW termed S_{4S} . This penetrative fabric also overprints all previous structural elements (Figure 22A). Strain shadows associated with the S_{4S} fabric commonly develop around the sulfides formed in the damage zones around the quartz-ankerite-arsenopyrite veins. These strain shadows are dominated by quartz, ankerite, chalcopyrite and rare pyrite (Figure 22). Sericite can also be found in these microstructures and typically is related to the late S_{4S} penetrative fabric. Late chloritisation can also be observed along minor sub-vertical N-S brecciated zones a few meters long.

Sintroko PB1

Sintroko PB1 is one of the southernmost deposits of the Siguiri district (Figure 17). It is hosted in the Balato formation, and is dominated by centimeter- to meter-scale alternations of shale and siltstone beds. Beds of fine to medium greywacke can also be found in Sintroko PB1 and the central area of the deposit is dominated by black shale.

The deposit sits on two open anticlines separated by an area of sheared sub-vertical NNW-SSE trending bedding in the centre of the deposit (Figure 18D). The eastern side of the deposit displays an upright open F_{2S} anticline, with a sub-vertical fold axis. The western side shows a reclined F_{2S} open anticline with a sub-vertical fold axis (Figure 19E). The wavelength of the two anticlines is estimated to be around 500 meters. Local isoclinal F_{2S} folds with an amplitude of a few meters, vertical fold axes are also commonly observed in this shale-dominated deposit. Bedding-parallel veins oriented around 310/80, and usually up to 1 centimeter thick and extending over a few meters, occur across the entire deposit. These veins and the F_{2S} folds present in Sintroko PB1 are crosscut by a major NNE-SSW shear zone in the central part of the deposit. A sub-horizontal lineation was observed along the major NNE-SSW

shear zone, but no kinematic indicators were identified. A series of sub-vertical incipient structures oriented N-S, NE-SW and E-W also crosscut the F_{2S} folds (Figure 18D). Like at Kami and Kosise these cross cutting incipient structures are not characterised by any distinctive fault plane but are rather expressed as a damage zone defined by an increase in vein density defining a planar zone 10-15 meters thick of dense veining (Figure 19E, 24A and 24B). Veining associated with the damage zones is also preferentially developed in competent beds (Figure 24A and 24B). The veins associated with the damage zones, and with the central NNE-SSW shear zones, display various orientations that can be grouped into two distinct conjugate sets. These vein sets are oriented around 172/26 and 150/70. The veins are up to 10 centimeters thick and sometimes extend over 10 meters (Figure 23C). These two vein sets display crack-seal and antitaxial textures (Figure 20D and 20E). The two vein sets commonly display conjugate relationships between themselves, and within a same set (Figure 23C). These vein sets in these deposits are commonly mined by artisanal miners. All previously described structural elements are overprinted by a sub-vertical NNE-striking penetrative fabric, S_{4S} . Kinematic indicators such as C'-type shear bands, asymmetric folding and overprinted quartz veins suggest that sinistral shearing was associated with this cleavage (Figure 23G).

Mineralization in Sintroko PB1 is associated with the veining developed in the different damage zones, and also around the central NNE-SSW shear zone. Mineralized conjugate veins consist of quartz, ankerite, arsenopyrite and rare pyrite restricted to greywacke beds. The arsenopyrite crystals are more commonly developed in the shale units typical of the shale-dominated Balato Formation. The host-rocks in the Sintroko PB1 deposit are albitised and overprinted by intense carbonate alteration associated with mineralization. Carbonate alteration is expressed by millimeter-sized siderite nodules and bleaching of the host rock (Figure 20D). Late chloritization can also be observed along heavily fractured zones of a few meters in length.

Discussion

Structural event history

The field relationships documented in the Siguiri district suggest a polyphase deformation history. All structural elements documented in the Siguiri district can be grouped in 4 sequential deformation events that have been termed D_{1S} , D_{2S} , D_{3S} , and D_{4S} . Within these events, 3 distinct folding events and 3 distinct veining events can be determined (Figure 25), allowing the relative timing and geometric controls on mineralization to be placed into the overall structural evolution of the district.

Milési et al. (1989, 1992)				Miller et al. (2013) for Mali				Steyn (2012)				This study			
Deform. events	Folds	Veins	Gold events	Deform. events	Folds	Veins	Gold events	Deform. events	Folds	Veins	Gold events	Deform. events	Folds	Veins	Gold events
D1	F1	-	-	D1	F1	-	-	D1 (diagenesis?)	F1	-	-	D_{1S}	F_{1S}	-	-
D2	F2	yes	\$	D2	F2	-	\$	D2	F2	multiple orientat.	\$	D_{2S}	F_{2S}	V_{2S}	-
D3	F3	yes	\$	D3	F3	yes	\$	D3	-	-	-	D_{3S}	-	V_{3A}	\$
D4	F4	yes	\$	D4	F4	yes	\$	D4	-	-	-	D_{4S}	F_{4S} (local)	-	?
D5	F5	yes	\$	D5	F5	yes	\$	D3	-	-	-				

Figure 25: Summary table of the deformation events and timing of the structural features recognized at Siguiri in this study with the work from Milési et al. (1989, 1992), Miller et al. (2013) and Steyn (2012).

Strain partitioning between the three stratigraphic formations recognized in the Siguiri district resulted in a heterogeneous strain distribution in the district. In the shale-dominated Balato and Kintinian Formations the strain is intense and the observed folds tend to be tight to isoclinal. By contrast, the Fatoya Formation is dominated by a greywacke-sandstone association, which displays a lower strain intensity characterized by open folds (Figure 17). As a result of this competency contrast, bedding orientations can be found to be locally quite variable (Figure 17, 26A, 26B, 26C and 26D).

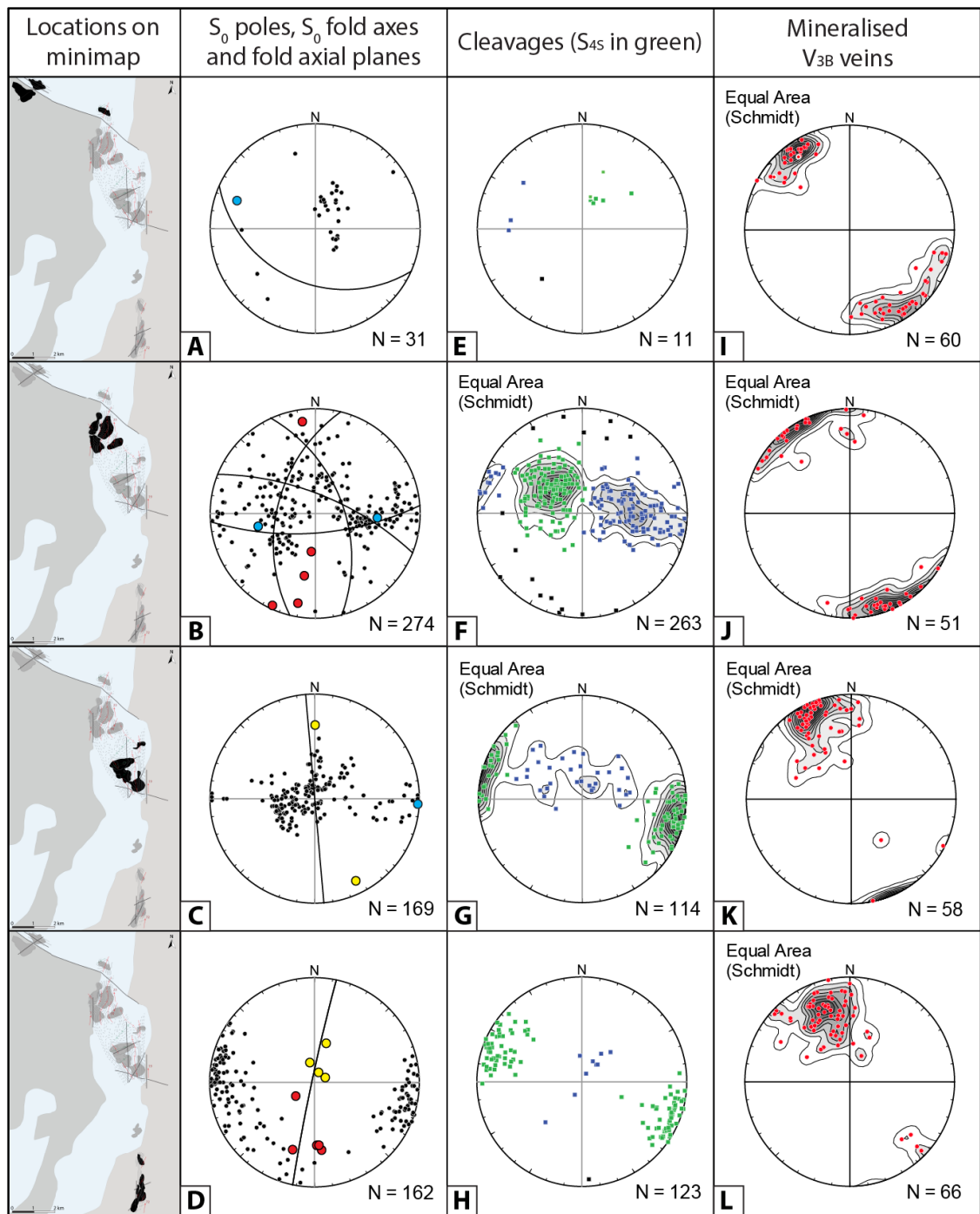


Figure 26: Stereograms of the structural data collected over the Siguiri district divided into four mine areas, from north to south (black deposit outlines on maps at left). Bedding poles in black. Measured F_{1S} fold axes in blue, measured F_{2S} fold axes in red and constructed fold axes (pole of a great circle fitting the bedding poles of an observed fold) in yellow. Measured fold axial planes represented as black great circles. Cleavages are colored according to their interpreted generation: S_{1S} in blue, late S_{4S} in green. Mineralized V_{3B} vein sets represented as red poles. Unless specified, all stereograms use equal angle (Wulff) projection.

Cryptic D_{1S}: The first deformation event D_{1S} is a ductile deformation event characterized by its cryptic F_{1S} folds, because rarely observed in the district, whose axial trace strikes E-W to NW-SE and NE-SW (Figure 17). Remnants of these folds have been observed in the northern part of the district (Bidini deposit, Figure 19A; Eureka North deposit, Figure 19B). The F_{1S} folds are commonly tight with recumbent orientation, and fold axes gently plunging to the E and WNW (axial plane and calculated fold axis on Figure 26A, 26B and 26C). In the Kami deposit, where NE-SW trending F_{1S} folds are gentle to open with wavelengths in the 100's of meters, F_{2S} N-S folds overprint the F_{1S} folds and form interpreted type 1 fold interference pattern characterized by large domes and basins (Figure 17 and 18B; Ramsay and Huber, 1987). A weakly developed cleavage (S_{1S}), shallowly to moderately dipping to the WSW is locally observed in some of the northern deposits (e.g. Bidini; Figure 26E, 26F, 26G and 26H). D_{1S} deformation is interpreted to have been linked to N-S compression, but with inconclusive outcrop exposures the understanding of this early deformation remains unclear. An alternative interpretation is that the F_{1S} folds represent syn-sedimentary slump folds (McClay, 1992), but the consistent orientation and fold axes (accounting for overprinting by subsequent events) more strongly supports a tectonic contractional setting for this folding. This first phase of deformation may be responsible for the early albitisation of the host rock across the Siguiri district.

D_{2S}: The second deformation is associated with the formation of major folds (F_{2S}) and associated D_{2S} thrust faults (e.g., at Sanu Tinti and Kosise; Figure 18A and 18C). This event is responsible for the bulk of the folding in the metasedimentary rocks and for the N-S structural grain affecting much of the Siguiri Basin. F_{2S} fold axial planes typically strike NNE-SSW to NNW-SSE, and their fold axes plunge at variable angles, and are typically steeper in the Balato Formation compared to the Fatoya Formation. The F_{2S} fold typology varies from south to north with upright horizontal isoclinal folds and upright vertical open folds in the area of the Sintroko deposit, to gentle upright to open inclined N-plunging W-verging folds near the Kosise deposit

(Figure 24E), and to open to isoclinal inclined W- to NW-verging folds near the Bidini deposit (Figure 19). The overall asymmetric fold geometry indicates a vergence to the west (Figure 17C). No axial planar cleavage (S_{2S}) was identified as being associated with this event.

A switch to a phase of brittle deformation marks the end stage of the D_{2S} event in the Siguiri district and is associated with the development of V_{2S} veining and D_{2S} brittle faults. The V_{2S} vein set is the oldest observed vein set in the Siguiri district, and it is not mineralized. The orientation of this quartz-(carbonate) set varies from 320/80 in Sintroko PB1, to 070/40, and 280/45 in the Kosise deposit. In Kosise, the former orientation displays an en-echelon geometry (Figure 20A). In the Kosise deposit, the V_{2S} vein poles typically plot along an E-W oriented girdle, consistent with the prominent F_{2S} folding event (stereogram on Figure 20A). The V_{2S} bedding parallel veins, and also the en-echelon sigmoidal vein sets, are interpreted to indicate some amount of flexural slip along bedding occurred during late-stage F_{2S} fold development (Figure 20A and 27). Based on all early and late- D_{2S} structural elements presented (Figure 17 and 18C), we interpret that D_{2S} was associated with an E-W to ESE-WNW compressional stress-field under a brittle-ductile regime.

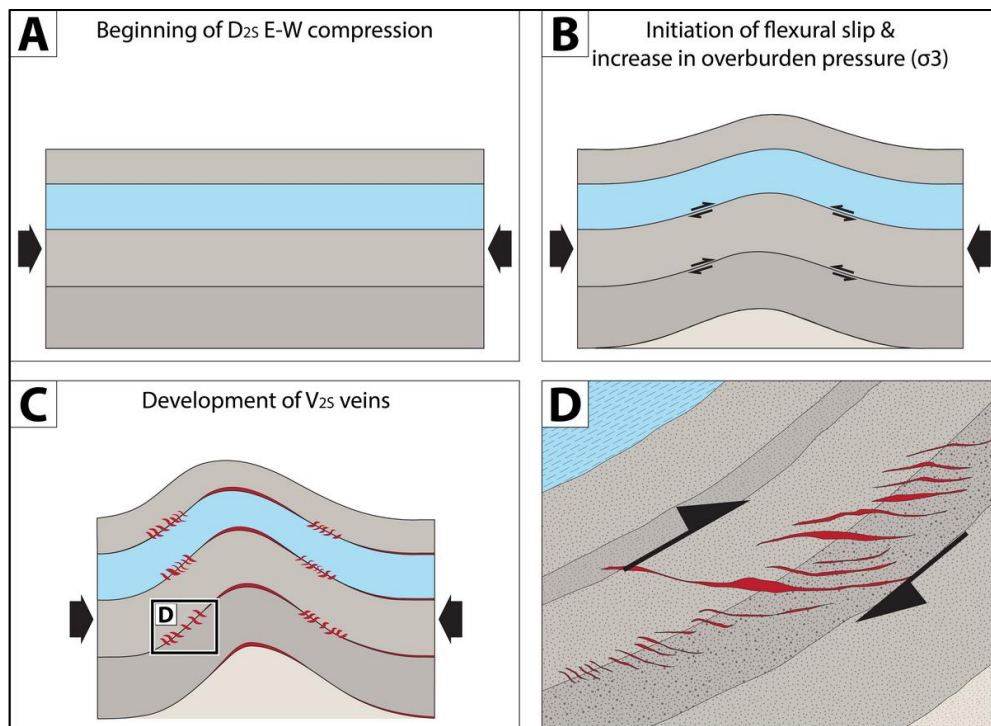


Figure 27: Schematic evolution of the early- D_{2S} compression and of the mode of formation of the bedding parallel and en-echelon V_{2S} veins associated with flexural slip.

D_{3S} : Although formally separated into a third deformation event, D_{3S} potentially marks the progressive continuation of D_{2S} . The difference is that the D_{2S} event is dominated by plastic deformation related to folding, whereas the D_{3S} event is linked to the rocks developing a network of D_{3S} faults with contrasting kinematics including thrust faults, normal faults, and strike-slip faults that extend sub-vertically to depths of more than 300 meters (constrained by drilling; Figure 18). These D_{3S} faults are typically not fully developed as discrete features, but are rather expressed as sub-vertical and poorly outlined incipient faults or planar damage zones characterized by increased density of quartz veining and associated alteration haloes that crosscut both F_{2S} folds and V_{2S} veins (Figure 24A and 24B). Establishing a relative chronology between the different D_{3S} faults was not possible in the field. These D_{3S} structures include:

- Thrust faults that are moderately dipping to sub-vertical and N-S-trending (e.g. in the Kosise deposit). In other deposits, such as in Kami, these structures are expressed as shear zones and damage zones displaying arrays of V_{3S} veins that cut across bedding.
- Local E-W trending sub-vertical normal faults, typically expressed as damage zones.
- A WNW-ESE trending fault population that dips moderately to the SSW and is axial planar to the F_{1S} folds. Such a fault, located in the northernmost part of the Siguiri district (Figure 17), was interpreted by Egal et al. (1999) to display sinistral movement.
- Sub-vertical NE-SW- to ENE-WSW-trending strike-slip brittle to brittle-ductile shear zones and damage zones exhibiting dextral movement.

Although no clear crosscutting relationships could be determined all the faults are associated with similar vein arrays, suggesting a probable coeval development. Alternatively, some of these faults may have developed earlier, such as the WNW-ESE sinistral faults that may have developed during D_{1S} or the N-S thrusts (and possibly the E-W normal faults acting as local accommodating faults) that may have developed during D_{2S} , but were all reactivated during D_{3S} . These structures may therefore represent more fundamental and deeper structures

that controlled the location of the Siguiri district within the sediments of the Siguiri Basin (dashed lines on Figure 16B).

Two vein sets were recognized along all these faults, V_{3A} and V_{3B} . The first set, V_{3A} (Figure 20B and 20C), comprises ankerite-pyrite-(albite). The orientation of this vein set is poorly constrained but varies significantly around a 240/55 mean (in the Kosise and Seguelen deposits; stereogram on Figure 20B). This orientation is sub-parallel to the WNW-ESE sinistral structures. The V_{3A} set were also observed close to NE-SW dextral shear zones in drill core and are confined within the first tens of meters from these structures. However, the full extent of this vein set remains unclear due to the highly weathered nature of these carbonate-dominated veins in the different deposits.

The second vein set associated with these faults, V_{3B} (Figure 20D), represents the bulk of veining observed in the Siguiri district and crosscuts the V_{2S} and V_{3A} vein sets. Despite substantial variations in the orientation of S_0 , the orientation of this quartz-ankerite-arsenopyrite-(pyrite) vein set remains constant throughout the Siguiri district (Figure 26I, 26J, 26K and 26L), and clearly overprints the first (F_{1S}) and second (F_{2S}) folding generations. Oriented around 170/35 (V_{3B} shallow) and 160/70 (V_{3B} steep; Figure 26I, 26J, 26K and 26L), both average vein orientations display a hybrid/conjugate geometry (McClay, 1992). These geometries are formed by conjugate V_{3B} shallow veins or conjugate V_{3B} steep veins. In addition both these geometries can be found mutually cross-cutting each other in the field (Figure 21C, 23B, 23C, 23D and 28I to 28K). These veins commonly display crack-seal textures typical of gold bearing veins in orogenic-type deposits and consistent with fault-valve pulsative behaviour (Sibson et al., 1988; Sibson et al., 1998). The steep orientation is the most prominent vein set developed in Siguiri and was also observed and mined by artisanal miners within and outside of the Siguiri district. Higher densities of these veins develop around all four orientations of discrete and incipient faults described in the previous sections and represent the main ore shoots in the district (Figure 24A, 24B and 28C and 28F). Conjugate analyses on the V_{3B} veins, together with the fault pattern geometry mapped in the pits, indicates that the stress-field

associated with D_{3S} varies from between NW-SE extension to strike-slip deformation related to NW-SE extension and NE-SW compression, which is different to the earlier D_{2S} E-W to ESE-WNW compression.

D_{4S} : The third and last fold generation recorded in the district (F_{4S} ; Figure 22A) is oriented ENE-WSW to NE-SW. At the outcrop to deposit-scale the F_{4S} folds crenulate the F_{2S} folds and fold the V_{3S} veins (Figure 22A, 26A, 26B, 26C and 26D). A penetrative planar fabric (S_{4S}) is axial planar to these local F_{4S} folds. The S_{4S} fabric is a sericite-bearing cleavage that transects the F_{2S} fold hinges in many areas, such as in the Kosise deposit (Figure 17), and develops strain shadows around the arsenopyrite crystals in the selvage of V_{3B} veins (Figure 22B and 22C). Overall, D_{4S} is interpreted to have been associated with a NW-SE compression. The domes and basins most notably developed in the Kami deposit, could therefore have developed by overprinting of the F_{2S} N-S folds by the D_{4S} NW-SE compression. The V_{3B} mineralized veins located in these domes suggest that these domes developed pre- to syn- D_{3S} veining and thus cannot have formed by F_{2S}/F_{4S} interference. However, D_{4S} may have amplified the domes and basins.

The S_{4S} dip angle and dip direction varies across the Siguiri district, from sub-vertical and ESE- to WNW-dipping in the south, to shallowly SE-dipping in the north. Variations in S_{4S} dip angle and dip direction in the northern part of the district are interpreted to be related to the pre-existing faults and the rotation of cleavage trajectories around these structures, a mechanism described by Dewey et al. (1998).

The deformation events and structural features identified in the Siguiri district can be correlated with the ones described by Milési et al. (1989, 1992), Miller et al. (2013) and Steyn (2012). This correlation is summarized in Figure 25 and indicates that D_{1S} correlates with the D1 N-S compressional event recognized by Milési et al. (1989, 1992), Miller et al. (2013) and possibly Steyn (2012). Milési et al. (1989) constrained the timing of this deformation event

between ca. 2100 and 2090 Ma and related it to the thrusting of the Paleoproterozoic Baoulé-Mossi domain onto the Archean Kenema-Man domain. No gold mineralization was found to be associated with this first deformation event by these authors.

The folds developed during D_{2S} and the D_{3S} ductile-brittle structures correlate with the second Eburnean tectono-metamorphic phase defined by Milési et al. (1989) and Steyn (2012) as D2, and dated between 2091±33 and 2074±7 Ma in southern Mali (Liégeois et al., 1991). By comparison, Miller et al. (2013) recognizes 2 different deformation events, D2 and D3, both E-W to ENE-WSW compressional events, with D3 developing mineralized veins. The interpretations proposed by these last authors therefore best matches the one proposed in the present study.

The last phase of deformation recognized in the present paper, D_{4S}, was recognized as D3 by Milési et al. (1989) and interpreted to occur around ca. 2075 Ma. Miller et al. (2013) also recognized this event, defined as D4, a NW-SE compression. Regionally and in many other areas of the Craton (Ashanti, Prestea, Kalana; Milési et al. 1992), this deformation event is typically associated with the main phase of gold mineralization. However, this event does not appear to be mineralized in the Siguiri district.

Finally, Steyn (2012) recognized a last deformation event, termed D3, associated with an E-W extension and which was not found to be mineralized in gold. This deformation event was not recognized by the present study, Milési et al. (1989, 1992) or Miller et al. (2013) but may correspond to late post-orogenic collapse.

Mineralization

Observations from the five key deposits highlight the relative homogeneity of the gold mineralization style in the Siguiri district (Figure 23 and 28). Gold mineralization is either disseminated in style or vein-hosted. Both styles of mineralization exhibit carbonate alteration mainly developing millimeter-scale siderite nodules in shale-rich beds, bleaching in greywacke beds and further albitisation of the already albitised host rock (Figure 28K).

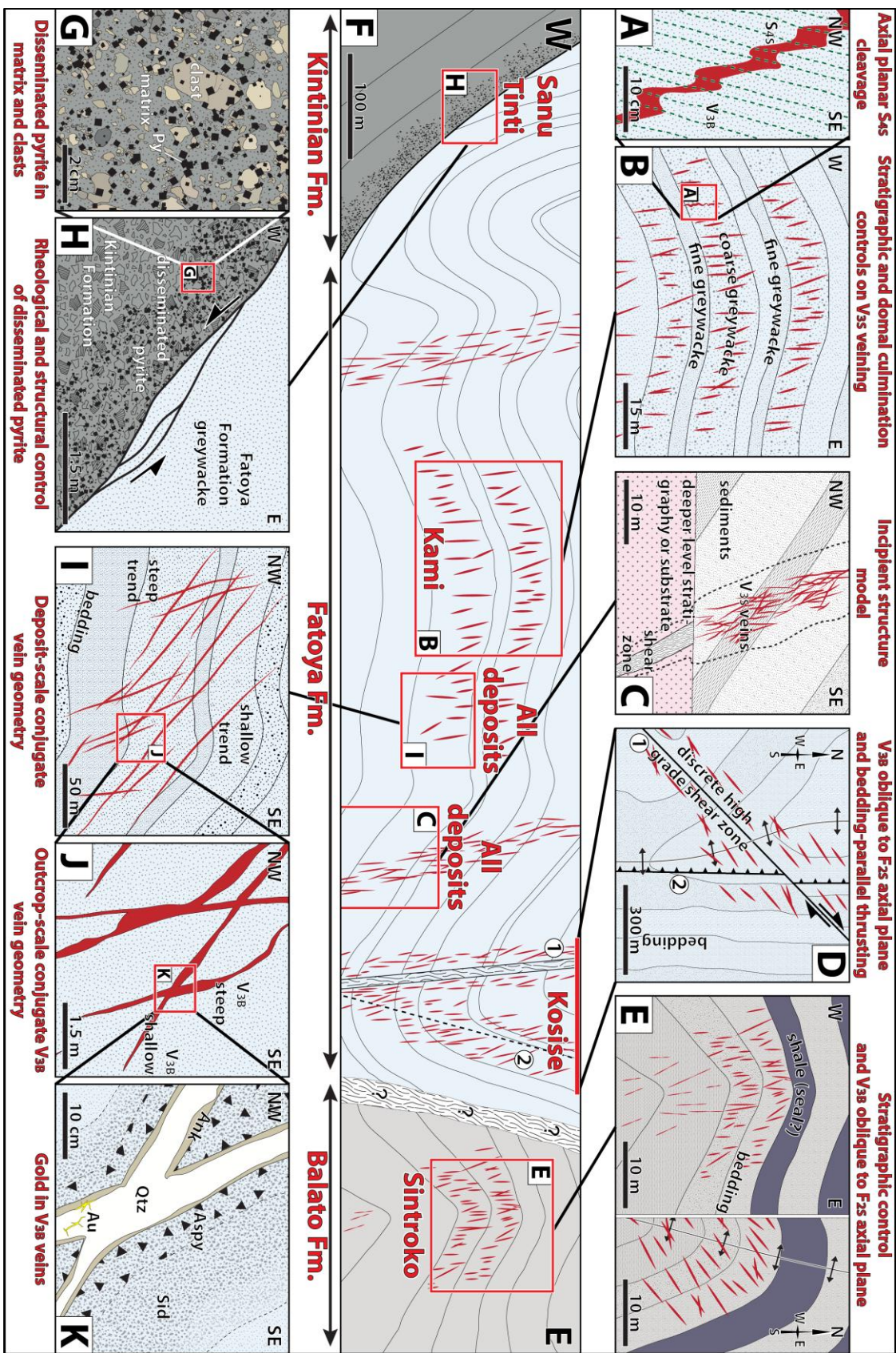


Figure 28: Summary figure of the different controls on D_{3S} mineralization found in the orogenic gold Siquiri district.

The disseminated mineralization, specific to the Sanu Tinti deposit (Sanu Tinti style of gold mineralization; Figure 28F to 28H), is focused in porous conglomeratic beds and characterized by corroded and fractured pyrite with gold, chalcopyrite, galena fracture infills. The timing of the Sanu Tinti style of mineralization is constrained between the formation of the overprinting S_{4S} cleavage and the timing of the thrust fault along which the disseminated pyrite has developed (this fault is reactivated in early- D_{3S} , but most likely have formed during D_{2S}).

The vein hosted gold mineralization texture (Kosise style of mineralization) forms the bulk of the gold endowment in the Siguiri district, and contrasts with the disseminated style observed in Sanu Tinti (Figure 28A to 28F and 28I to 28K). This style of mineralization is associated with the V_{3A} and V_{3B} vein sets. The V_{3A} veins typically contain abundant free gold in pyrite fractures. These veins are associated with localized carbonate alteration of the host rock, developing millimeter-sized siderite nodules within the first few centimeters to meters around them. Albite can sometimes be found in these veins but this set is usually cross-cutting the already albitised host-rock. The V_{3B} veins are filled with quartz-ankerite with arsenopyrite, pyrite and minor millimetric siderite nodules along the selvages (Figure 28K). These veins can infrequently be found associated with minor albite, but are overall cross-cutting the albitised host-rock. Native gold occurs in the quartz (Figure 20E) or at the contact between quartz and ankerite. Currently, most gold produced at Siguiri is associated with the V_{3B} vein set.

There is a first-order structural control on both the disseminated and vein hosted gold mineralization in the Siguiri district, in that both occur within the first ten to twenty meters of the four groups of faults mapped in this study (Figure 28C, 28D and 28F). These structures, which cut across F_{2S} folds (Figure 28D and 28E), are expressed differently across the Siguiri district. Most of these are incipient faults, and expressed as damage zones around incipient structures such as in Kosise (Figure 28D), delineated by zones of dense veining (Figure 28C and 28F). These damage zones are cryptic and therefore difficult to recognize on the field and in geophysics but based on their regular orientation, could be linked to fundamental deeper

structures (Figure 28C). However, some are represented by discrete shear zones, in some cases via bedding-parallel thrusting (Figure 28D and 28F) or as distinct cross-cutting faults (Figure 28H).

Antiformal structures and competency contrasts have a second-order control on gold mineralization in the Siguiri district. High vein densities are commonly focused in antiformal closures (such as in the Kami and Sintroko deposit (Figure 19E, 23A, 28B, 28F). We infer fluid flow was focused into antiformal fold hinges, with possible shale rich units acting as local seals to fluid flow, such as in Sintroko PB1 (Figure 19E, 28E). Whilst the V_{3B} veins have the appearance in section of occurring along the F_{2S} axial plane, they are actually oblique to this trend and cross cut the F_{2S} axial planes (Figure 28E).

As initially suggested by Steyn (2011), competency contrasts also play an important role in the focusing of mineralizing fluids and on the location of the ore shoots through strain partitioning. At the scale of the Siguiri district the more competent Fatoya Formation hosts most of the deposits and this reflects the fact this unit has a rheology that preferentially fractures rather than forming a penetrative cleavage. At a deposit scale, veining develops more intensely in competent greywacke beds (Figure 19E, 23A, 24A, 24B, 28E and 28F). Competency contrast is also thought to have played an important role in the Sanu Tinti deposit where mineralized sulfides are found disseminated in the porous conglomerate layers of the Kintinian Formation rather than in the less permeable greywacke and shale beds of the Fatoya Formation (Figure 28F to 28H). Compared to the general characteristics described by Dube and Gosselin (2007), the styles, controls, and late timing of mineralization (syn- D_{3S}) with respect to the main compressional event (D_{2S}), is consistent with an orogenic gold style of mineralization in the Siguiri district.

Stress-field evolution during D_{2S} and early-D_{3S}

Based on the structural elements observed, and their relative timing, a stress-field reconstruction was undertaken in the Siguiri district for the syn-D_{2S} ductile and early- to late-D_{3S} brittle part of the deformation history. Paleo-stress reconstruction for the syn-D_{2S} ductile part of the deformation history, was based on the geometry of the F_{2S} folds and the orientations of their axial planes. The reconstruction of the paleo-stress orientations for the D_{3S} brittle part of the deformation history was based on fault and V_{3B} conjugate vein orientations assuming that locally, the Andersonian fault and Mohr-Coulomb failure models prevailed at the time of faulting and that all V_{3B} conjugate veins were not following pre-existing structures. The orientation of σ1 was reconstructed as bisecting the acute angle between two conjugate veins, while σ2 lays at their intersection and σ3 bisects the obtuse angle the conjugate makes (Anderson, 1951; McClay, 1992). This analysis was only based on V_{3B} conjugate sets across the whole district since data from the V_{3A} vein set were insufficient.

The D_{2S} E-W compressional event, highlighted by the N-S trending F_{2S} fold axial planes, indicates it was related to a horizontal main stress axis (σ1) and a vertical σ3, or overburden pressure (Figure 29A). This stress-field is compatible with the mapped N-S thrust faults, and with the E-W normal faults. In this model, D_{2S} E-W compression forms F_{2S} folds with N-S trending axial planes and N-S thrust faults that may have collectively developed local N-S trending extension, accommodated by E-W normal faults. However, the later strike-slip structures that transect the F_{2S} folds and also control V_{3S} veining, such as the NE-SW dextral shear zone in Kosise, require σ3 to have been horizontal. We interpret that from D_{2S} to D_{3S} there was a switch in the orientation of σ3 from vertical to low angle. This change is thought to be responsible for the formation of the dextral NE-SW shear zones, sinistral WNW-ESE faults as well as the E-W normal faults. The V_{3S} veins are interpreted to be part of this event. Two alternate models could also be proposed: 1) this stress-switch between D_{2S} and D_{3S} may have occurred within a single deformation event or; 2) the strike-slip faults may have developed in a separate deformation event, post-dating D_{2S} E-W compression but predating the development

of V_{3B} veins. In the first alternate model, stress-switches are considered to be the progressive continuation of D_{2S} E-W compression whereas in the second alternate model, switches in the main stress axis orientations may have been separated in time.

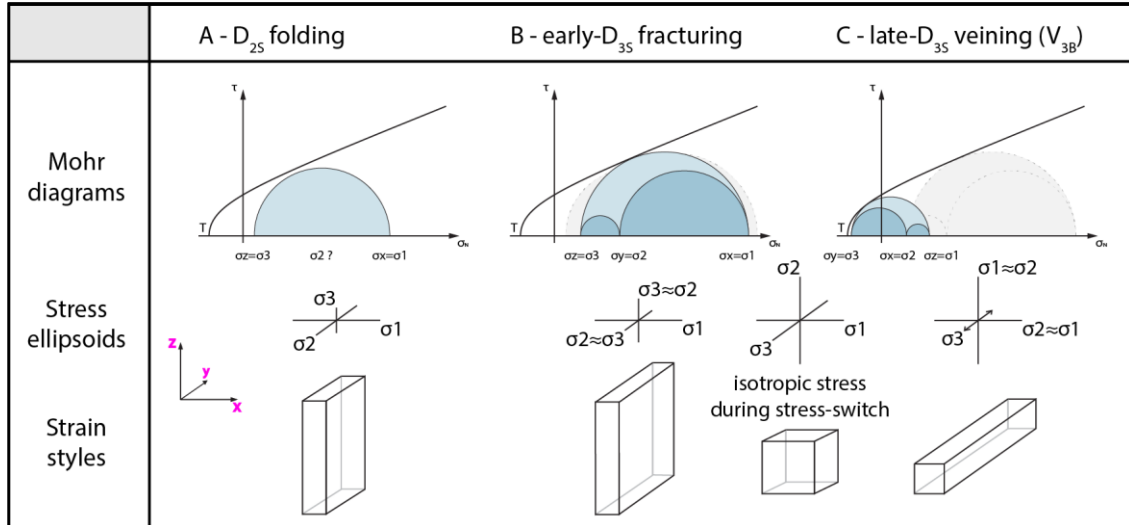


Figure 29: Simplified stress-strain representation of the evolution of D_{2S} deformation from A) early- D_{2S} compression and folding to; B) late- D_{2S} transpression and fracturing and; C) syn- V_{3B} mineralized veining. Relative scale bars.

Transpressional model for the Siguiri District

Transpression is the result of coeval compression and shearing movements that constitutes a fault-bounded zone of deformation and is also referred to as wrench/transcurrent tectonics (Sanderson and Marchini, 1984). Transpression is commonly associated with oblique tectonic plate convergence and typically accommodates fault movements on the same fault or series of reverse dextral or sinistral faults, and form “flower structures” (Figure 30A; Dewey et al., 1998; Fossen and Tikoff, 1998). In the Siguiri district, such structures were not observed. Instead, strike-slip and dip-slip movements were accommodated along the four different orientations of faults observed throughout the district.

Field data from the Siguiri district indicate that dip-slip movements (or pure shear component) were accommodated by the N-S thrust faults, these structures dominantly border the low-strain central part of the Siguiri district (Fatoya formation). Strike-slip movements (or simple shear component) were accommodated by the NE-SW dextral shear zones and the

WNW-ESE sinistral shear-zones. The E-W normal faults have a geometry consistent with having accommodated localized N-S extension (Figure 30C) and also acting as relay normal faults in between the strike-slip structures. Based on the fault configurations, and their coeval movements, we interpret that strain decoupling was a mechanism responsible for the accommodation of the strike-slip and dip-slip components on separate, but coeval structures. This type of geometry is characteristic of decoupled transpression (Figure 30B and 30C).

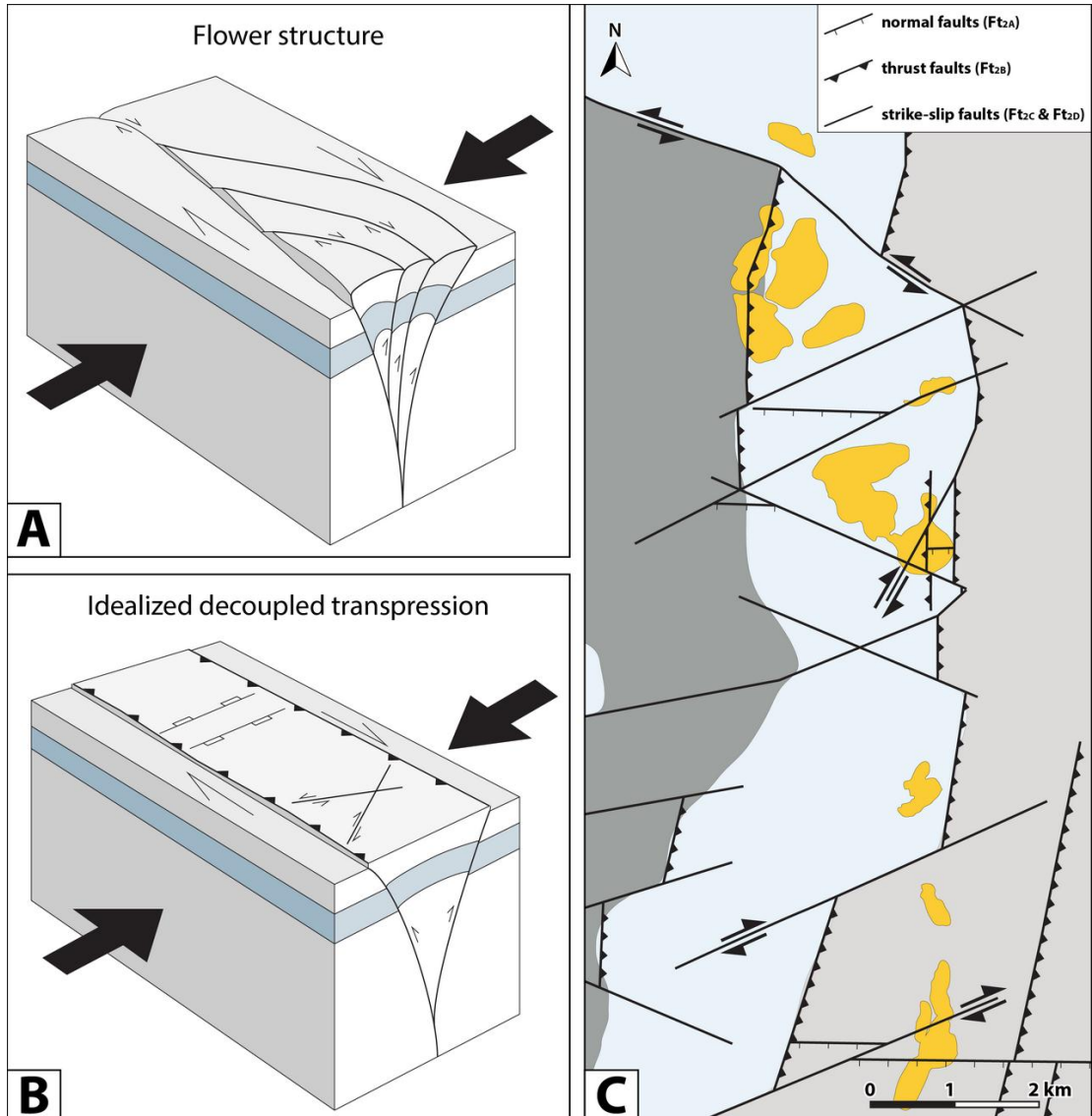


Figure 30: Idealized block models of different types of transpression (modified from <http://maps.unomaha.edu/>) and faults relationships during transpression. A) classic flower structure (Sanderson and Marchini, 1984) showing a coupling between structures accommodating pure and simple shear; B) Bloc model of an idealized decoupled transpression. Pure and simple shear are accommodated along distinct thrust faults and strike-slip faults, respectively; C) Simplified map view of the decoupled early-D_{3S} transpression observed in the Siguiri district. Formation and deposit colors as in Figure 17.

The change from syn-D_{2S} compression ($\sigma_1 > \sigma_2 > \sigma_3$; Figure 29A) to early-D_{3S} transpression (Figure 29B) may be linked to a progressive increase in the overburden pressure (σ_3), or an increase in the amount of NW-SE extension due to changes in far field stresses. Either of these processes are interpreted to have caused a stress switch that rendered σ_3 approximately equal to σ_2 , eventually leading to a change in the σ_3 orientation (Figure 29B). This allowed the formation (and reactivation) of the four different fault orientations.

Localized stress switches associated with late-D_{3S} mineralized veining

In addition to the district-scale stress-switch from D_{2S} compressional to early-D_{3S} transpressional deformation, there is evidence for more localized stress-switches in the Siguiri district. These have been inferred based on the analysis of individual V_{3B} conjugate vein sets that have mainly developed along the faults observed throughout the district. The V_{3B} conjugate vein sets were found to be mutually cross-cutting each other in the field (Figure 21C, 23C, 28C, 28F, 28I and 28J). For this structural analysis stereograms of the paleo-orientation of σ_1 , σ_2 and σ_3 were constructed for each measured conjugate vein set (Figure 31).

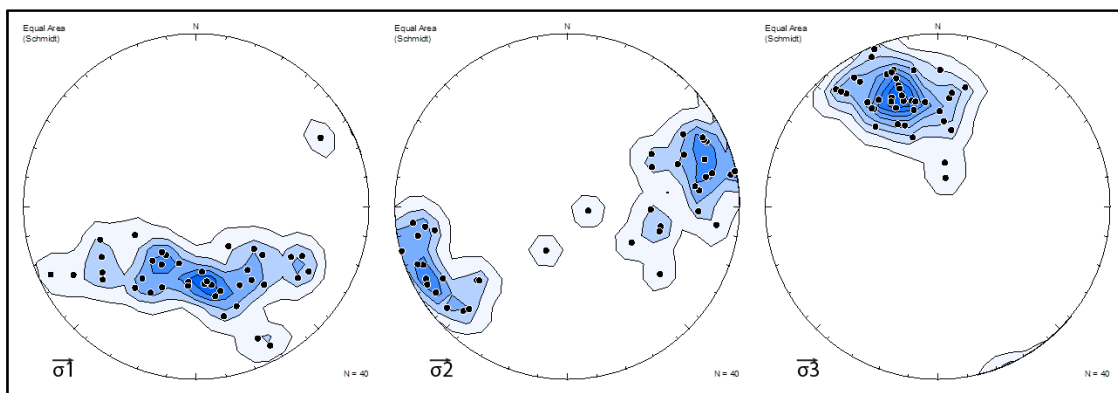


Figure 31: Stereograms of the calculated orientation of the principal stress axes during the late-D_{3S} transtension based on conjugate mineralized V_{3B} veins. Respectively from left to right: σ_1 , σ_2 and σ_3 orientation. Sigma 1 and σ_2 orientations vary and plot on the same girdle whereas σ_3 orientation remains constant.

No spatial gradient was observed in the main stress orientations from north to south or east to west throughout the Siguiri district. The main feature identified was that, at the time of veining, σ_3 remained consistently sub-horizontal and oriented to the NNW. However, σ_1

and σ_2 plot along the same WSW-ENE girdle, with a sub-vertical and a sub-horizontal density maximum, respectively. This unusual feature indicates that the V_{3B} conjugate vein sets were associated with varying orientations of σ_1 and σ_2 : from a sub-vertical σ_1 and sub-horizontal σ_2 , to a sub-horizontal σ_1 and vertical σ_2 . The first stress-field configuration is characteristic of extension whereas the second configuration is characteristic of strike-slip deformation. The simplest explanation for this relationship is that at the time of V_{3B} veining, σ_1 and σ_2 were of similar magnitude (e.g. a high stress-shape ratio; Figure 29C). In this syn- V_{3B} high stress-shape ratio environment, σ_1 and σ_2 were similar in magnitude and could easily change their orientation along the same WSW-ENE girdle. This occurred while the orientation of σ_3 remained consistently sub-horizontal and oriented to the NNW. Such a stress-field configuration is indicative of transtensional deformation during V_{3B} veining (Figure 29C). The change in stress-shape ratio from early- D_{3S} transpression where the coeval movement of dip-slip and strike-slip faults indicate that $\sigma_2 \approx \sigma_3$ (low stress-shape ratio; Miller and Wilson, 2004; Figure 29B) to syn- V_{3B} (late- D_{3S}) gold mineralization (with $\sigma_1 \approx \sigma_2$; Figure 29C) is interpreted to have resulted from the joint reduction of the maximum stress (σ_1) and further increase in overburden (σ_3 switches to σ_2). This is interpreted to have occurred at an early stage of the D_{3S} transpressional event while all fault orientations were active as fluid conduits facilitating the upward migration of mineralizing fluids (Figure 29B and 29C).

Stress-switches, precursors or triggers to mineralization

The timing of gold mineralization during the waning stages of the progressive D_{2S}/D_{3S} deformation is interpreted to have been associated with the transtensional regime during mineralization. This reflects the greater ease for overpressured fluids, to open fault-fracture meshes during transient extensional/transtensional events amidst a protracted and longer compressional/transpressional cycle (Sibson, 2013). These transient events of stress-switch were interpreted in the Siguiri district to be linked to the reduction of the deviatoric stress tensor and require a major reduction of differential stress (early- D_{3S} and syn- V_{3B} /late- D_{3S}

stress-witches). Mineralizing fluids became mobile through this process, permitting fault reactivation, hydraulic fracturing and fault-valve behavior responsible for gold mineralization. Another possibility is that with near-isotropic stress field, active fluid pathways and permeability creation ceases, and allows buildup of high fluid pressure, triggering pulses of mineralization in vertical "exit conduits" (e.g. McCuaig and Hronsky, 2014; Miller et al., 1994). It is thus proposed that "late-orogenic" declines of both the differential stress and deviatoric stress tensor are required precursors for the initiation of mineralizing stress-switches and the development of orogenic gold mineralization.

The transient stress-switch phenomena may be envisaged as a non-physical barrier to fluid flow during a prolonged phase of deformation. Prior to the switch, fluids are stored under high pressure in the rock mass and fluid mobility and veining are minor. When the switch occurs, a stress threshold is overcome allowing the barrier to be breached and fluids to flow into an organized vein network.

Geodynamic interpretation and drivers of stress-switches

Drivers of the different stress-switches observed in the Siguiri district may have a local cause, including: 1) continuous local overburden build up; 2) fault irregularities; 3) earthquake focal behaviour dynamics, or 4) a regional scale mechanism, such as plate convergence rate drop (Upton and Craw, 2013; Goldfarb et al., 2001; Beroza and Zoback, 1993). However, stress-switches have been documented in many other orogenic gold systems around the world, including Archean examples (Bouiller and Robert, 1992; Holyland and Ojala, 1997; Nguyen et al., 1998; Goldfarb et al., 2001; McCuaig and Hronsky, 2014; e.g. in the Yilgarn: the Waroonga and New-Holland-Genesis deposits, Thébaud et al., 2013). In the Birimian of West Africa, stress-switches have been recognised as one of the crucial triggers for mineralization in several gold deposits (Ashanti in Ghana, Sadiola, Loulo and possibly Morila in Mali, Allibone et al., 2002a; Masurel et al., this volume; Lawrence et al., 2013a; McFarlane et al., 2011). Mineralization in all these deposits relates to a similar transient moment in the Eburnean

orogenesis, somewhere around 2070-2080 Ma (Lawrence et al., 2013b), referred to as the “late-orogenic” phase by Milési et al. (1992). This timing suggests that the stress-switches responsible for gold mineralization in the Siguiri district, occurring between the early-D_{3S} transpression and the syn-V_{3B} (late-D_{3S}) transtension, have been caused by a regional mechanism. Such a regional mechanism may have been driven either by far-field stress variations or body forces. Variations in the regional far-field stress, as documented in Allibone et al. (2002b), Blewett et al. (2010), Goldfarb et al. (1991) and Upton and Craw (2013), arise from a transient alteration of an ongoing geodynamic process, such as the modification of the collision rate, an overall change in plate motion (Fig. 9 from Goldfarb et al., 2005), or the sudden rise of magma from a hot spot (Goldfarb et al., 2001; Idnurm, 2000), while variations in body forces are commonly linked to readjustments of topographic highs or delamination (Rey and Houseman, 2006).

Based on the regional extent of the stress-switches identified in Siguiri and throughout the rest of the West African Craton, we propose that the dominant stress drivers affecting the district evolved from a far field stress dominated to a body forces dominated environment. In a far field stress dominated environment, such as during an accretion, the local stress-field is controlled by the regional stress-field orientation, such as the plate boundary motions. In a body forces dominated environment, such as during late delamination or readjustment of topographic highs, the local stress-field is controlled by the local variations in stress-field orientation, such as the location of delaminated lithosphere or of topographic highs. The progressive evolution from a far field stress dominated to a body forces dominated environment, whose local expression in the Siguiri district ranges from the early increase in overburden pressure to the late syn-gold transtensional deformation, is responsible for the reduction of the deviatoric component of the stress tensor (Engelder, 1994).

Conclusion

The clastic sediment-hosted orogenic gold deposits of Siguiri, in northeast Guinea, are primarily hosted in the greywacke of the Fatoya Formation and to lesser extents in the turbidites of adjacent Balato and Kintinian Formations. The district has been the site of a protracted and polyphase deformation divided into four local deformation stages (D_{1S} to D_{4S}), all of which are attributed to Eburnean orogenesis. D_{1S} was a cryptic N-S compressional event. The main deformation event D_{2S} , was an E-W to ENE-WSW directed compressional event responsible for the bulk of the deformation affecting the Siguiri Basin metasediments. D_{3S} represents a progressive evolution of D_{2S} compression into an E-W transpressional event, evolving into a transient period of NNW-SSE transtension. This latter episode of deformation is associated with the bulk of veining observed in the Siguiri district and is also the main stage of mineralization. The last deformation event, D_{4S} , was a NE-SW compressional event which created a penetrative cleavage in the entire rock mass and is post the main stage of mineralization at Siguiri.

The orogenic gold mineralization in the Siguiri district is associated with two principal vein types: 1) early gold-rich pyrite and ankerite brecciated veins proximal to NW-SE structures and 2) crosscutting quartz-carbonate-arsenopyrite conjugate veins. The second, and most common vein type, is preferentially developed along four orientations of discrete faults or incipient structures: N-S to NNE-SSW thrusts, NE-SW to ENE-WSW dextral shear zones, E-W normal faults and WNW-ESE sinistral shear zones. These structures may represent the local expression of more fundamental and deeper structures that control the location of the Siguiri district within the Siguiri Basin.

Based on finite strain and conjugate vein analysis, the veining and gold mineralization are interpreted to have culminated late during the D_{3S} progressive deformation event, as the local stress-field was switching in response to the waning of the regional maximum stress. The stress-switches documented in this study have been widely recognized to happen at 2070-2080 Ma across the whole West African Craton and are not restricted to the study area.

The regional stress-switches documented in this paper are interpreted to be related to the lowering of both the deviatoric stress and of the differential stress and are viewed as a precursor or trigger for rapid fluid flow and orogenic gold mineralization.

Acknowledgements

This project is funded by AngloGold Ashanti Limited. Eddie Connell, Shawn Kitt, Katharina Wulff, Craig Duvel and all brownfield geologists are acknowledged for providing site access, support, inspiring discussions and some good laughs. Prof. Julien Bourget (University of Western Australia) is also acknowledged for his help regarding sedimentology. John Miller and T. Campbell McCuaig acknowledge receipt of ARC Large Linkage Grant LP110100667. The authors also acknowledge the facilities, and the scientific and technical assistance of the Australian Microscopy and Microanalysis Research Facility at the Centre for Microscopy, Characterisation and Analysis, The University of Western Australia, a facility funded by the University, State and Commonwealth Governments. Finally, thanks to Marc Bardoux, Richard Goldfarb and the third anonymous person who reviewed this paper.

References

- Abouchami, W., Boher, M., Michard, A., and Albarede, F., 1990, A Major 2.1 Ga Event of Mafic Magmatism in West Africa - an Early Stage of Crustal Accretion: Journal of Geophysical Research-Solid Earth and Planets, v. 95, p. 17605-17629.
- Allibone, A. H., McCuaig, T. C., Harris, D., Etheridge, M., Munroe, S., Byrne, D., Amanor, J., and Gyapong, W., 2002a, Structural Controls on Gold Mineralization at the Ashanti Gold Deposit, Obuasi, Ghana, 9, p. 65-93.
- Allibone, A. H., Teasdale, J., Cameron, G., Etheridge, M., Uttley, P., Soboh, A., Appiah-Kubi, J., Adanu, A., Arthur, R., and Mamphey, J., 2002b, Timing and structural controls on gold mineralization at the Bogoso gold mine, Ghana, West Africa: Economic Geology, v. 97, p. 949-969.

Anderson, E. M., 1951, The Dynamics of Faulting and Dyke Formations, Oliver and Boyd.

AngloGold Ashanti Ltd., 2013, Mineral resource and ore reserve report: Available from:

<www.agareports.com/13/download/AGA-RR13.pdf>. [12/05/2015]

AngloGold Ashanti Ltd., n.d., Reports: Available from:

<<http://www.anglogoldashanti.com/en/Media/Pages/reports.aspx>>. [15/05/2015]

Begg, G. C., Griffin, W. L., Natapov, L. M., O'Reilly, S. Y., Grand, S. P., O'Neill, C. J., Hronsky, J. M.

A., Djomani, Y. P., Swain, C. J., Deen, T., and Bowden, P., 2009, The lithospheric architecture of Africa: Seismic tomography, mantle petrology, and tectonic evolution: *Geosphere*, v. 5, p. 23-50.

Beroza, G. C., and Zoback, M. D., 1993, Mechanism diversity of the Loma Prieta aftershocks and the mechanics of mainshock-aftershock interaction: *Science*, v. 259, p. 210-213.

Blewett, R., Czarnota, K., and Henson, P., 2010, Structural-event framework for the eastern Yilgarn Craton, Western Australia, and its implications for orogenic gold: *Precambrian Research*, v. 183, p. 203-229.

Davis, J., Miller, J., Thébaud, N., McCuaig, C., Begg, G., Jessel, M., Hein, K., Baratoux, L., 2015, Craton-scale lithostratigraphic correlation as an insight for the geodynamic evolution of the South West African Craton: *Proceedings of the 50th SGA conference*.

Dewey, J., Holdsworth, R., and Strachan, R., 1998, Transpression and transtension zones: Geological Society, London, Special Publications, v. 135, p. 1-14.

Dube, B., and Gosselin, P., 2007, Greenstone-hosted quartz-carbonate vein deposits: *Mineral Deposits of Canada: A Synthesis of Major Deposit-Types, District Metallogeny, the Evolution of Geological Provinces, and Exploration Methods*: Geological Association of Canada, Mineral Deposits Division, Special Publication, v. 5, p. 49-73.

Egal, E., Lahondère, D., Costea, A. C., Diabate, B., Diallo, A., Diallo, A. B., Diallo, S., Gaye, F., Iliescu, D., and Minthe, D., 1999, Carte géologique de la Guinée à 1/200 000; Feuille Sigiri, BRGM.

Egal, E., Thiéblemont, D., Lahondère, D., Guerrot, C., Costea, C. A., Iliescu, D., Delor, C., Goujou, J., Lafon, J., Tegyey, M., Diaby, S., and Kolie, P., 2002, Late Eburnean granitization and tectonics along the western and northwestern margin of the Archean Kénéma-Man domain (Guinea, West African Craton): *Precambrian Research*, v. 117, p. 57-84.

Engelder, T., 1994, Deviatoric stressitis: a virus infecting the Earth science community: *Eos, Transactions American Geophysical Union*, v. 75, p. 209-212.

Feybesse, J.-L., and Milési, J.-P., 1994, The Archean/Proterozoic contact zone in West Africa: a mountain belt of décollement thrusting and folding on a continental margin related to 2.1 Ga convergence of Archean cratons?: *Precambrian Research*, v. 69, p. 199-227.

Feybesse, J., Bangoura, A., Billa, M., Costea, A., Diabaté, B., Diaby, S., Diallo, A., Diallo, S., Diallo, A., and Egal, E., 1999, Notice explicative de la Carte géologique de la Guinée à 1/200 000, Feuille no. 19, Kankan: BRGM, DNRGH, Ministère des Mines, de la Géologie et de l'Environnement, Conakry, Guinée, 27p.

Fougerouse, D., Micklethwaite, S., Ulrich, S., Miller, J., Godel, B., Adams, D. T. and McCuaig, T. C., this volume, Evidence for Two Stages of Mineralization in West Africa's Largest Gold Deposit: Obuasi, Ghana: *Economic Geology*

Fossen, H., and Tikoff, B., 1998, Extended models of transpression and transtension, and application to tectonic settings: *Geological Society, London, Special Publications*, v. 135, p. 15-33.

Goldfarb, R. J., Newberry, R. J., Pickthorn, W. J., and Gent, C. A., 1991, Oxygen, hydrogen, and sulfur isotope studies in the Juneau gold belt, southeastern Alaska; constraints on the origin of hydrothermal fluids: *Economic Geology*, v. 86, p. 66-80.

Goldfarb, R., Groves, D., and Gardoll, S., 2001, Orogenic gold and geologic time: a global synthesis: *Ore geology reviews*, v. 18, p. 1-75.

Goldfarb, R. J., Baker, T., Dube, B., Groves, D. I., Hart, C. J., and Gosselin, P., 2005, Distribution, character, and genesis of gold deposits in metamorphic terranes: *Economic Geology* 100th Anniversary Volume, p. 407-450.

Groves, D., 1993, The crustal continuum model for late-Archaean lode-gold deposits of the Yilgarn Block, Western Australia: Mineralium Deposita, v. 28, p. 366-374.

Groves, D. I., Goldfarb, R. J., Knox-Robinson, C. M., Ojala, J., Gardoll, S., Yun, G. Y., and Holyland, P., 2000, Late-kinematic timing of orogenic gold deposits and significance for computer-based exploration techniques with emphasis on the Yilgarn Block, Western Australia: Ore Geology Reviews, v. 17, p. 1-38.

Holyland, P., and Ojala, V., 1997, Computer-aided structural targeting in mineral exploration: Two-and three-dimensional stress mapping: Australian Journal of Earth Sciences, v. 44, p. 421-432.

Idnurm, M., 2000, Towards a high resolution Late Palaeoproterozoic–earliest Mesoproterozoic apparent polar wander path for northern Australia: Australian Journal of Earth Sciences, v. 47, p. 405-429.

Kerrich, R., Goldfarb, R. J., and Richards, J. P., 2005, Metallogenic provinces in an evolving geodynamic framework: Economic geology, v. 100, p. 1097-1136.

Lahondère, D., Thiéblemont, D., Tegyey, M., Guerrot, C., and Diabate, B., 2002, First evidence of early Birimian (2.21 Ga) volcanic activity in Upper Guinea: the volcanics and associated rocks of the Niani suite: Journal of African Earth Sciences, v. 35, p. 417–431.

Lawrence, D. M., Treloar, P. J., Rankin, A. H., Harbidge, P., and Holliday, J., 2013a, The geology and mineralogy of the Loulo Mining District, Mali, West Africa: evidence for two distinct styles of orogenic gold mineralization: Economic Geology, v. 108, p. 199-227.

Lawrence, D. M., Treloar, P. J., Rankin, A. H., Boyce, A., and Harbidge, P., 2013b, A fluid inclusion and stable isotope study at the Loulo mining district, Mali, West Africa: Implications for multifluid sources in the generation of orogenic gold deposits: Economic Geology, v. 108, p. 229-257.

Liégeois, J.-P., Claessens, W., Camara, D., and Klerkx, J., 1991, Short-lived Eburnian orogeny in southern Mali. Geology, tectonics, U-Pb and Rb-Sr geochronology: Precambrian Research, v. 50, p. 111-136.

Masurel, Q., Thébaud, N., Miller, J., Ulrich, S., Hein, K.A.A., Cameron, G., Béziat, D. and

Bruguier, O., this volume, Sadiola Hill: a world-class gold deposit in Mali, West Africa:

Economic Geology.

McClay, K. R., 1992, The mapping of geological structures, John Wiley and Sons.

McCuaig, T. C., and Hronsky, J. M. A., 2014, The Mineral System Concept: The Key to Exploration Targeting: in: Kelley, K.D., and Golden, H. (eds), SEG 2014: Building Exploration Capability for the 21st Century: Society of Economic Geologists Special Publication 18, p. 153-175.

McFarlane, C. R. M., Mavrogenes, J., Lentz, D., King, K., Allibone, A., and Holcombe, R., 2011, Geology and Intrusion-Related Affinity of the Morila Gold Mine, Southeast Mali: Economic Geology, v. 106, p. 727-750.

Micklethwaite, S., Sheldon, H. A., and Baker, T., 2010, Active fault and shear processes and their implications for mineral deposit formation and discovery: Journal of Structural Geology, v. 32, p. 151-165.

Milési, J. P., Feybesse, J. L., Ledru, P., Dommange, A., Ouedraogo, M. F., Marcoux, E., Prost, A., Vinchon, C., Sylvain, J. P., Johan, V., Teguey, M., Calvez, J. Y., and Lagny, P., 1989, Les minéralisations aurifères de l'Afrique de l'Ouest. Leurs relations avec l'évolution lithostructurale au Protérozoïque inférieur: Chronique de la recherche minière, v. 497, p. 3-98.

Milési, J.-P., Ledru, P., Feybesse, J.-L., Dommange, A., and Marcoux, E., 1992, Early Proterozoic ore deposits and tectonics of the Birimian orogenic belt, West Africa: Precambrian Research, v. 58, p. 305-344.

Miller, J. M., Davis, J., Baratoux, L., McCuaig, T. C., Metelka, V. and Jessel, M., 2013, Evolution of gold systems in Guinea, southern Mali and western Burkina Faso: AMIRA International Ltd P934A - West African Exploration Initiative - Stage 2 Final report, Appendix D1, confidential

Miller, J. M., and Wilson, C. J., 2004, Stress controls on intrusion-related gold lodes: Wonga gold mine, Stawell, Western Lachlan Fold Belt, southeastern Australia: Economic Geology, v. 99, p. 941-963.

Miller, L. D., Goldfarb, R. J., Gehrels, G. E., and Snee, L. W., 1994, Genetic links among fluid cycling, vein formation, regional deformation, and plutonism in the Juneau gold belt, southeastern Alaska: Geology, v. 22, p. 203-206.

Mulder, T., and Alexander, J., 2001, The physical character of subaqueous sedimentary density flows and their deposits: Sedimentology, v. 48, p. 269-299.

Nguyen, P. T., Harris, L. B., Powell, C. M., and Cox, S. F., 1998, Fault-valve behaviour in optimally oriented shear zones: an example at the Revenge gold mine, Kambalda, Western Australia: Journal of Structural Geology, v. 20, p. 1625-1640.

Paranhos, C. J., 2008, Siguiri gold mine - State of knowledge of the main geological controls of gold mineralization, unpublished.

Parra-Avila, L. A., 2015, 4D Evolution of the Paleoproterozoic Baoulé-Mossi Domain of the West African Craton: PhD thesis, University of Western Australia

Parra-Avila, L. A., Belousova, E., Fiorentini, M. L., Baratoux, L., Davis, J., Miller, J., and McCuaig, T. C., in press, Crustal Evolution of the Paleoproterozoic Birimian terranes of the Baoulé-Mossi domain, southern West African Craton: U-Pb and Hf-isotope studies of detrital zircons: Precambrian Research.

Passchier, C. W., and Trouw, R. A. J., 2005, Microtectonics, Springer, 366 p.

Ramsay, J. G., and Huber, M. I., 1987, The techniques of modern structural geology: Vol.2: Folds and fractures: London, Academic Press.

Rey, P. F., and Houseman, G., 2006, Lithospheric scale gravitational flow: the impact of body forces on orogenic processes from Archaean to Phanerozoic: Geological Society, London, Special Publications, v. 253, p. 153-167.

Sanderson, D. J., and Marchini, W., 1984, Transpression: Journal of Structural Geology, v. 6, p. 449-458.

Schodde, R., and Hronsky, J., 2006, The role of world-class mines in wealth creation: Special

publication-society of economic geologists, v. 12, p. 71.

Sibson, R. H., 1987, Earthquake rupturing as a mineralizing agent in hydrothermal systems:

Geology, v. 15, p. 701-704.

Sibson, R. H., 1992, Fault-valve behavior and the hydrostatic-lithostatic fluid pressure

interface: Earth-Science Reviews, v. 32, p. 141-144.

Sibson, R. H., 2013, Stress switching in subduction forearcs: Implications for overpressure

containment and strength cycling on megathrusts: Tectonophysics, v. 600, p. 142-152.

Sibson, R. H., and Scott, J., 1998, Stress/fault controls on the containment and release of

overpressured fluids: Example from gold-quartz vein systems in Juneau, Alaska;

Victoria, Australia and Otago, New Zealand: Ore Geology Reviews, v. 13, p. 293-306.

Sibson, R. H., Robert, F., and Poulsen, K. H., 1988, High-angle reverse faults, fluid-pressure

cycling, and mesothermal gold-quartz deposits: Geology, v. 16, p. 551-555.

Steyn, J. G., 2012, Structural geology and controls of gold mineralization in the Sigiri Mine,

Guinea, West Africa: MSc thesis, Stellenbosch University.

Taylor, R., 2010, Ore textures: recognition and interpretation, Springer Science & Business

Media.

Thébaud, N., Miller, J., McCuaig, C., Fisher, L. and Sonntag, I., 2013, The orogenic and not so

oreogenic gold deposits of the Agnew Gold Camp (Yilgarn Craton, Western Australia), v.

3, p. 1201-1204, In proceeding of: SGA- 12th biennial meeting

Thiéblemont, D., Goujou, J. C., Egal, E., Cocherie, A., Delor, C., Lafon, J. M., and Fanning, C. M.,

2004, Archean evolution of the Leo Rise and its Eburnean reworking: Journal of African

Earth Sciences, v. 39, p. 97-104.

Upton, P., and Craw, D., 2013, Extension and gold mineralization in the hanging walls of active

convergent continental shear zones: Journal of Structural Geology.

Villeneuve, M., and Cornée, J., 1994, Structure, evolution and palaeogeography of the West African craton and bordering belts during the Neoproterozoic: Precambrian Research, v. 69, p. 307-326.

Watts, M., 2010, An introduction to the geology of Siguiri gold mine and the economic potential of the fresh rock in block 1, unpublished.

CHAPTER 4: PAPER THREE

MINERALISATION FOOTPRINTS AND REGIONAL TIMING

OF THE SIGUIRI OROGENIC GOLD DISTRICT (GUINEA,

WEST AFRICA)

The following paper focuses on deposit to microscopic scale observations and presents the petrographic and geochemical characteristics of the Siguiri district and of its gold mineralisation.

This study is based on field observations, drill core logging, petrography, geochemistry and in situ analyses by LA-ICP-MS of sulphide minerals acquired in three key deposits of the Siguiri district. For each deposit, a log, a cross-section and numerous polished thin-sections are presented.

Based on this work, gold mineralisation characteristics were found to be consistent across the different deposits making the Siguiri district. Gold mineralisation in the district was found to be polyphase and to have occurred mainly during D_{3S}, but was interpreted to have also occurred during D_{4S} deformation. The timing of gold mineralisation in the Siguiri district is also constrained in this study and compared with gold mineralisation events from other orogenic gold deposits of the West African Craton. This comparison indicates that gold mineralisation in the Siguiri district is coeval with gold events in numerous other orogenic gold deposits from the West African Craton but that a latter timing of gold mineralisation can also be recognized across the Craton. This study hence suggests that latter gold mineralisation than that recognized in the Siguiri district could be found elsewhere in the Siguiri Basin.

This chapter will be submitted to Mineralium Deposita and is hence formatted accordingly. It was revised a number of times by all co-authors.

Mineralisation footprints and regional timing of the Siguiri orogenic gold district (Guinea, West Africa)

Erwann Lebrun¹, Nicolas Thébaud¹, John Miller¹, Malcolm Roberts², Noreen Evans³

¹: Centre for Exploration Targeting and ARC Centre of Excellence for Core to Crust Fluid Systems, School of Earth and Environment, Robert Street Building, M006, The University of Western Australia, 35 Stirling Highway, Crawley, WA, 6009, Australia

²: Centre for Microscopy, Characterisation and Analysis, M010, The University of Western Australia, 35 Stirling Highway, Crawley, WA 6009, Australia

³: John de Laeter Centre for Isotope Research, TIGeR, Department of Applied Geology, Curtin University, Perth, WA 6845, Australia

Abstract:

Siguiri is a world-class orogenic gold district hosted in the weakly metamorphosed Upper Birimian to Lower Tarkwa Group sediments of the Siguiri Basin (Guinea). The district is characterized by a protracted deformation history associated with four main deformation events: D_{1S} is a N-S compression; D_{2S} is an E-W compression progressively evolving into an early-D_{3S} transpression and then into a late-D_{3S} NNW-SSE transtension, and D_{4S} is a NE-SW compression. Field observations, petrography and chemical analyses applied to three key deposits of the Siguiri district (Bidini, Sintroko PB1 and Kosise) suggest that the hydrothermal activity in the district is polyphase and can be subdivided into four distinct hydrothermal events. The first hydrothermal event is associated with the development of barren bedding-parallel and en-echelon V_{2S} quartz-dominated-(pyrite) veins. The second hydrothermal event is characterised by the development of V_{3A} pyrite-ankerite veins late during D_{3S}. Laser ablation data show that this vein set contains an anomalous gold content of up to 43.3 ppm locked in its pyrite crystal lattice. The third and most

prominently developed hydrothermal event, is also the second and principal gold mineralisation event to develop late during D_{3S} deformation. It is associated with two distinct mineralisation textures. The first texture is best exposed in the Kosise deposit and is characterised by gold bearing quartz-ankerite-arsenopyrite conjugate V_{3B} veins. Although the bulk of the gold is hosted native in V_{3B} veins, LA-ICP-MS analyses show that gold can also be found locked into the arsenopyrite crystal lattice (up to 55.5 ppm). The second mineralisation texture is best expressed in the Sanu Tinti deposit and consists of disseminated barren pyrite hosted in a polymict conglomerate.

The second and third hydrothermal events are both structurally controlled by a series of early-D_{3S} N-S, NE-SW, WNW-ESE and E-W sub-vertical incipient structures expressed as damage zones of higher V_{3S} vein density. A composite geochemical cross-section across damage zones from the Kosise deposit, indicates that gold mineralisation in the Siguiri district is associated with enrichments in Ag, Au, As, Bi, Co, Mo, Sb, Se, S, Te and W. Geochemical variations associated with the ore shoots in the Siguiri district are consistent with petrographic observations and highlight an albite-carbonate-sulphide-sericite alteration system.

The fourth and last hydrothermal event is associated with the development of a late penetrative S_{4S} cleavage during D_{4S} deformation. This late deformation event overprints all pre-existing hydrothermal events and is associated with the deposition of free gold, chalcopyrite and galena along fractures in V_{3A} pyrite and V_{3B} pyrite and arsenopyrite.

Mineral and geochemical footprint and timing of the gold events in the Siguiri district, when compared with other deposits of the West African Craton, highlight the synchronicity of gold mineralisation in Siguiri (syn-D_{3S} and syn-D_{4S} events) with other events of gold mineralisation in this part of the Craton, such as the early Au-Sb-Bi-(Te-W) mineralisation at the Morila deposit in Southeast Mali. Results support the idea that late Eburnean-age gold mineralisation in the Siguiri district and in the West African Craton as a whole, is polyphase and that economic post-D_{4S} gold mineralisation could be found in the Siguiri Basin.

Keywords: West Africa, Siguiri, orogenic gold, laser ablation, geochemistry, timing, polyphase, targeting

Introduction

Orogenic gold deposits typically encompass a wide variety of host rocks, metamorphic facies, mineral assemblages and textures, with variations sometimes observed within a single deposit (Goldfarb et al., 2005; Robert et al., 2005; Groves et al., 2003). Finding the footprint of orogenic gold mineralisation therefore represents a great challenge for explorers (e.g. Groves et al., 2000; Neumayr et al., 2008). However, as the geochemical and petrological footprints of orogenic gold deposits are more extensive than the ore zone itself (Eilu and Mikucki, 1998; Kishida and Kerrich, 1987), characterisation of mineral alteration assemblages at the deposit scale provides the exploration geologist with useful vectoring tools for targeting (Eilu and Groves, 2001; Eilu et al., 1999). With the development in recent years of laser ablation inductively coupled plasma mass spectrometry (LA-ICP-MS) techniques and associated low detection limits, studies on the characterization and quantification of trace elements in sulphides associated with orogenic gold deposits have become more common (Large et al., 2011; Large et al., 2012; Pitcairn et al., 2006). These studies typically focus on the use of LA-ICP-MS data acquired on sulphides to resolve the controversial source of mineralising fluids (Groves et al., 2003; Tomkins, 2013, Large et al., 2011). However, trace element signatures of sulphides can also be used to distinguish between different sulphide generations associated with multiple hydrothermal events (Zhao et al., 2011).

The wide diversity of gold mineralisation types recorded in the West African Craton such as intrusion related gold (McFarlane et al., 2011), orogenic gold (Lawrence et al., 2013a; Fougerouse et al., in press; Allibone et al., 2002; Oberthür et al., 1998), paleoplacers (Hirdes and Nunoo, 1994; Davis et al., 1994), Cu-Au porphyry (Béziat et al., 2013), renders essential the detailed petrographic and geochemical characterisation of a deposit to resolve its nature (or footprint). In turn, this footprint can become a backbone for exploration strategies.

This study focuses on characterisation of the mineral assemblages and mineralisation in three key deposits of the world-class orogenic gold Siguiri district (Guinea, West Africa) and its geochemical and petrological footprints. The Siguiri district is the only large (> 50 t Au)

orogenic gold deposit found in the Siguiri Basin, one of the largest sedimentary basins of the West African Craton. Therefore, the Siguiri district provides a unique opportunity to characterise the alteration haloes associated with gold mineralisation found in the Basin. Laser ablation data are used to constrain the relative timing of the different generations of pyrite observed, allowing the creation of a district-scale paragenetic sequence, which serves to highlight the polyphase nature of gold mineralisation in the Siguiri district. Comparison between the timing of the main gold mineralisation event in the district with events from other orogenic gold systems of the West African Craton can elucidate the temporal patterns of mineralisation on the regional scale, with implications for prospectivity.

Geological context

The Siguiri district is located in the north-western part of the Baoulé-Mossi domain, in the West African Craton (Lebrun et al., *in review* 2015a; Chapter 3; Lebrun et al., *in review* 2015b; Chapter 2). The district sits in the sedimentary Basin of Siguiri, Guinea (Figure 32). Mineralisation is hosted by three sedimentary formations, all metamorphosed to sub-greenschist facies. To the east, the Balato Formation is dominated by fine-grained pelitic sediments, such as shale and siltstone. It is overlain by the Fatoya Formation, which spreads in the centre of the district and dominated by coarser sediments, mainly greywacke and sandstone beds. The Kintinian Formation, to the west, overlies the Fatoya and is characterised by very fine shale with abundant centimetric interbeds of limestone and at least two decametric to hectometric interbeds of conglomerate. The three Formations have been dated at ca. 2115 Ma (Upper Birimian) and the Kintinian Formation is interpreted to be part of the Lower Tarkwa Group (Lebrun et al., *in review* 2015b; Chapter 2).

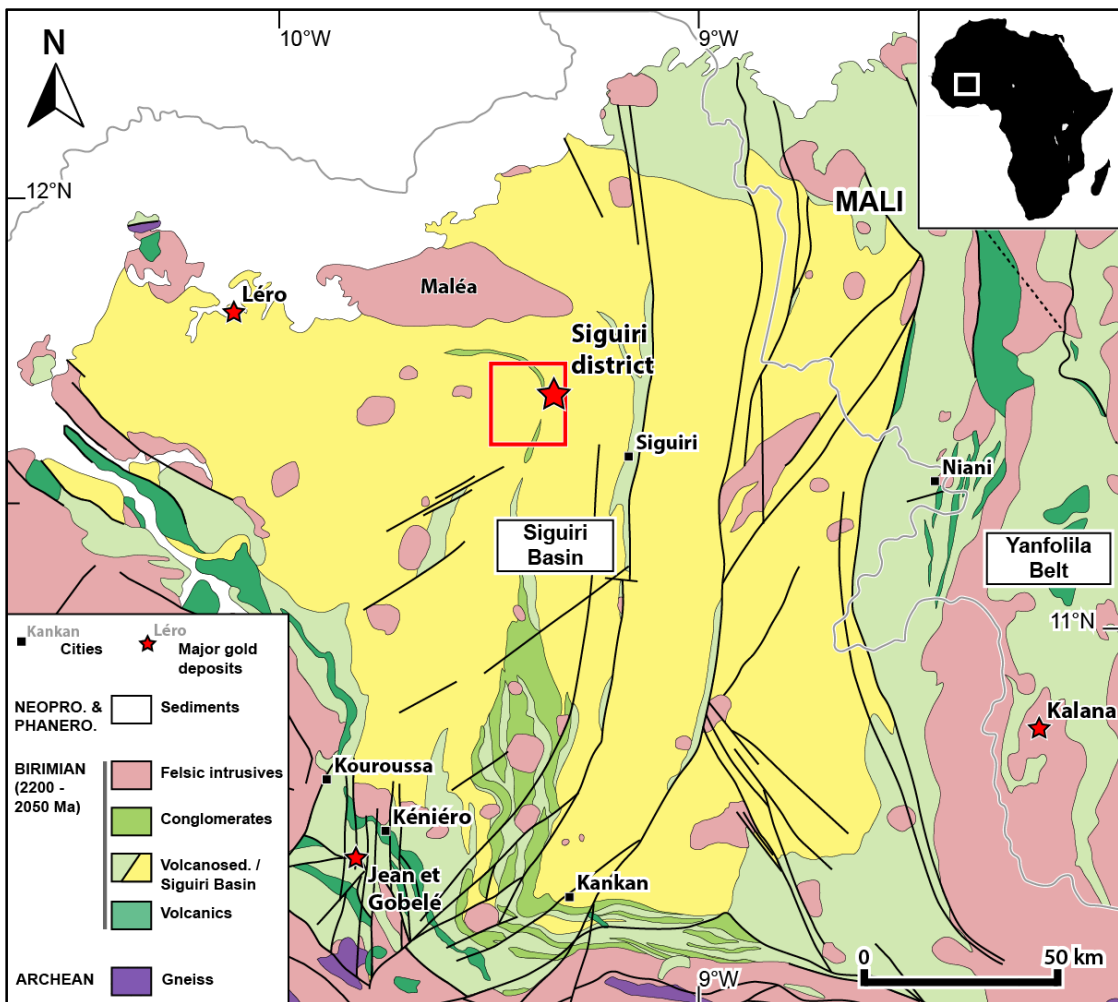


Figure 32: Geological map of the Siguiri Basin. Location of the Siguiri district map in red. After Miller et al., 2013, Milési et al. (1989) and Lebrun et al., (in review 2015b); Chapter 2.

Four deformation events have been recognised in the Siguiri district (Lebrun et al., in review 2015a; Chapter 3). The first event, D_{1S} , is characterised by E-W folds and a discreet shallow dipping axial planar S_{1S} cleavage. It was interpreted as the product of N-S compression. The second event, D_{2S} , is responsible for the bulk of the deformation and for the structural grain observed in the Siguiri Basin. The F_{2S} folds crenulate F_{1S} folds at a district scale and develop type 1 fold interference patterns at a deposit scale (Ramsay and Huber, 1987). The D_{2S} event is associated with W-verging folds, the axial plane of which varies from NNE-SSW to NNW-SSE in orientation. The plunge of the F_{2S} fold axes varies from sub-vertical in the Balato Formation, to almost sub-horizontal in the Fatoya Formation. No axial planar S_{2S} cleavage was found to be associated with this event. This second deformation event was interpreted as

having been associated with an E-W to ENE-WSW compression associated with N-S thrust faults and E-W normal faults. This deformation event progressively evolved to an early-D_{3S} transpression, characterized by the reactivation of the N-S and E-W faults, and the development of NE-SW dextral and WNW-ESE sinistral shear zones (Figure 33). In the Siguiri district, these structures are typically expressed as sub-vertical incipient structures, represented by discreet damage zones associated with a ten-fifteen meters wide halo of increased vein density, developed during the late-D_{3S} NNW-SSE transtensional event (Lebrun et al., in review 2015a; Chapter 3). All structural elements in the Siguiri district were overprinted during the youngest deformation event, D_{4S}, which is characterized by local F_{4S} folds with sub-horizontal NE-SW trending fold axes, affecting late-D_{3S} structures. The D_{4S} event is associated with a penetrative sub-vertical NNE-SSW S_{4S} cleavage, axial planar to the F_{4S} folds at the outcrop scale. This last deformation event was interpreted as having been associated with NW-SE compression (Lebrun et al., in review 2015a; Chapter 3). The S_{4S} cleavage parallels the sub-solidus fabric observed in the pre- to syn-tectonic Maléa monzogranite, which intrudes the Siguiri Basin sediments to the north of the district (Figure 32; Lebrun et al., in review 2015b; Chapter 2).

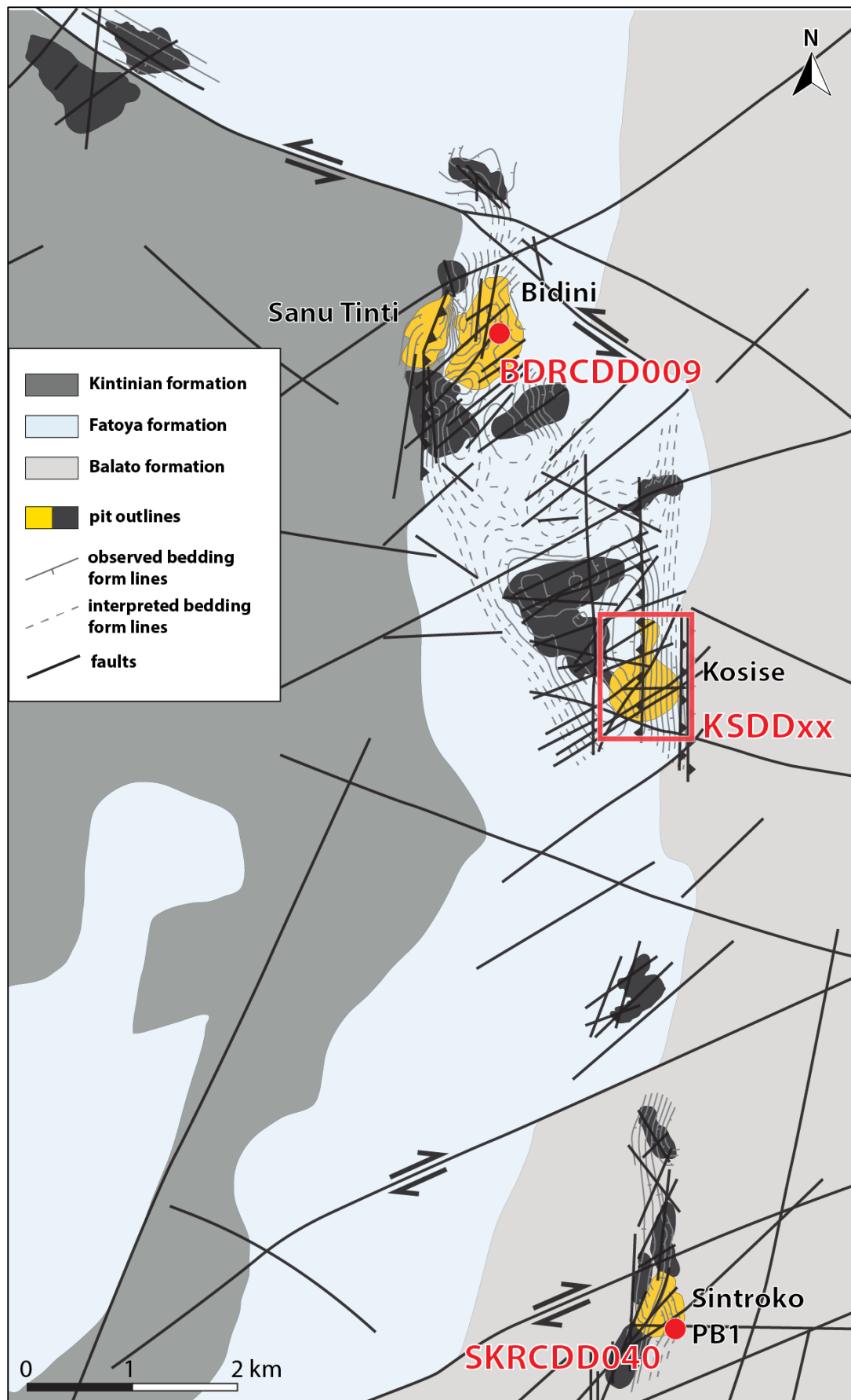


Figure 33: Form line map of the Siguiri gold district and its different deposits. Locations of the logged drill holes and areas of interest highlighted in red. After Lebrun et al., (in review 2015a); Chapter 3.

Hydrothermal activity in the Siguiri district is mainly characterised by veining developed during D_{2S} E-W compression and late-D_{3S} NNW-SSE transtension. Veining developed during D_{2S} is expressed as bedding parallel and en-echelon V_{2S} vein arrays (Figure 34) interpreted to have developed by flexural slip along bedding during F_{2S} folding (Lebrun et al., in review 2015a; Chapter 3). The V_{2S} veins are crosscut by the V_{3S} veins developed late during D_{3S} transtension along the early-D_{3S} faults. Based on drill core observations, two different vein sets were identified: V_{3A} and V_{3B} (Figure 34). The V_{3A} vein set commonly has brecciated textures and varies significantly in orientation across the district (Figure 34C). The second vein set, V_{3B}, crosscut both V_{2S} and V_{3A} sets but is overprinted by S_{4S}. The V_{3B} vein set displays conjugate geometries, with individual veins dipping steeply or moderately to the SE. This vein set represents the main source of gold mined in the Siguiri district.

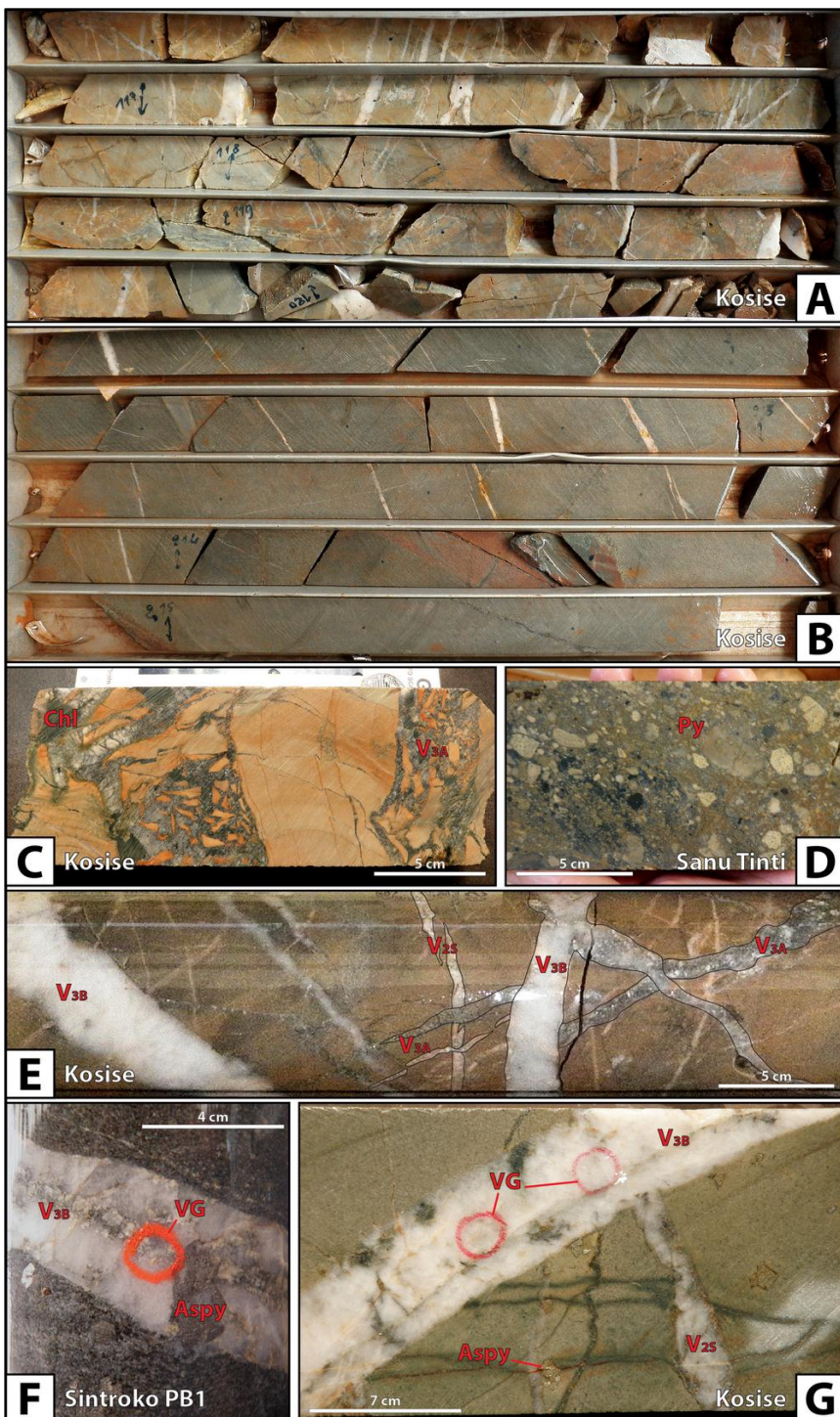


Figure 34: Photographs of A) veining and alteration associated with a high grade zone in the Kosise deposit (hole KSDD024); B) example of an unaltered and unmineralised zone from the Kosise deposit (hole KSDD024, sample O); C) example of V_{3A} carbonate-pyrite breccia veins. Only minor pyrite was found in this sample but abundant chlorite was found instead; D) Sanu Tinti style of mineralisation showing disseminated pyrite in a conglomerate interbed (hole BDRCDD009); E) drill core from Kosise showing the crosscutting relationship between V_{2S}, V_{3A} and V_{3B} vein sets; F) native gold found in the centre of an antitaxial V_{3B} quartz-ankerite-arsenopyrite vein; G) native gold in an antitaxial V_{3B} quartz-ankerite-arsenopyrite vein overprinting a V_{2S} quartz-(carbonate) vein. Chlorite is partially replacing the Fe-carbonates. VG: visible gold.

Methodology

Field approach and sampling

Field approach

Structural elements and controls on gold mineralisation in the Siguiri district are very consistent from one deposit to the next (Lebrun et al., in review 2015a; Chapter 3). For this reason, key deposits were selected based on the formation and host rocks, the understanding of the deposit structural framework, and the accessibility to fresh outcrops and core intersects. Three deposits were identified as representative of the Siguiri district mineralisation: the Bidini, Kosise and Sintroko PB1 deposits (Figure 33).

General sampling

Sampling was designed to: 1) constrain the paragenesis of the district; 2) characterise the geochemical halo associated with a representative mineralised shear zone; 3) compare the geochemical changes between formations and host rocks, and; 4) compare the sulphide major and trace elements and gold content of each vein generation and hydrothermal events. A total of 37 representative fresh rock samples were collected. Due to the weathering profile reaching depths over 200 m, drill core logging was conducted and used to guide sampling. Samples were collected from drill-core and the sample-size was kept consistent to a quarter core of 50 cm long (~1 kg) for most samples and about 2 to 3 kg for conglomerate samples. Seven samples were collected in the Bidini deposit from hole BDRCDD009 (Figure 35A), which starts in the Fatoya Formation and ends in the Kintinian Formation. Five of these samples were collected from the conglomerate interbeds (samples BD2, BD3 and BD5 to BD7; Table 3 in Electronic Appendices) while the last two samples were of greywacke and shale beds from the Kintinian Formation (samples BD1 and BD4; Table 3 in Electronic Appendices; Figure 36). Eighteen samples were collected along holes KSDD018, KSDD020, KSDD022 and KSDD024 from the Kosise deposit (samples A to R; Table 3 in Electronic Appendices; Figure 35B). All of these drill-holes intersect the Fatoya Formation only. Sampling was focused on the greywacke beds,

which are the dominant lithology in the Fatoya Formation. Six extra samples of Fatoya greywacke were collected from the Kami deposit (hole KMRCDD293). Six samples were also collected from hole SKRCDD040 in the Sintroko PB1 deposit (Figure 35C). This hole intersects the Balato Formation only. Sampling was focused on both shale and fine greywacke beds within and ~75 m away from the main ore zone (samples SK1 to SK6; Table 3 in Electronic Appendices).

Geochemical sampling

Geochemical sampling was conducted in the Bidini, Kosise and Sintroko PB1 deposits. Sampling was designed to obtain the baseline geochemistry of each sedimentary Formation. In order to characterise the geochemical variations associated with early-D_{3S} mineralised faults, samples were collected along a NW-SE composite section, across a discrete NE-SW dextral shear zone in the Kosise deposit and across a NE-SW shear zone and a bedding-parallel N-S reverse fault (Figure 35B). The Kosise deposit was chosen because it is hosted in the Fatoya formation, host to most of the deposits (Figure 33), and because its structural framework is relatively simple and well constrained. Sample spacing was modified according to the shear-zone proximity, grade distribution and apparent alteration. Sampling at intervals of about 10 metres was used in the distal part of the section while shorter intervals of a few metres were used around proximal alteration zones. Veins were trimmed off from all samples to avoid nugget effects. The veins were retained and used to make polished thin-sections, for subsequent LA-ICP-MS analyses on their associated sulphides.

Analytical work and data processing

Petrography and mineral chemistry

The paragenetic sequence was characterised mainly through the use of optical and electron microscopy. Optical microscopy was conducted on a Nikon Eclipse LV100 POL at the Centre for Exploration Targeting (CET) at the University of Western Australia (UWA). Electron

microscopy and semi-quantitative analyses complemented the optical microscopy work. They were conducted at the Centre for Microscopy, Characterisation and Analysis (CMCA) at UWA, on a Tescan Vega3 XM SEM equipped with an Oxford instrument X-ACT energy dispersive detector (EDS). Operating conditions for the SEM-EDS included an accelerating voltage of 15–20 kV, a working distance of 15 mm, a beam current of 1.5 nA and a detector process time of 4 s.

Electron Probe Micro-Analysis (EPMA) was used to determine the Fe and As content in the different generations of sulphides. Iron concentrations were later used as internal standards for laser ablation data processing. Analyses were carried out on a JEOL 8530F Hyperprobe, at the CMCA. Operating were 40 degrees take-off angle with a beam energy of 20 keV, beam current of 80 nA, and the beam was fully focussed. The elements were acquired using analyzing crystals LiF for Fe $\text{k}\alpha$, Co $\text{k}\alpha$, Ni $\text{k}\alpha$, Au $\text{l}\alpha$, Sb $\text{l}\alpha$, Ti $\text{k}\alpha$ and Te $\text{l}\alpha$, PETJ for S $\text{k}\alpha$, and TAP for As $\text{l}\alpha$. The standards used for instrument calibration were a series of proprietary sulphides, oxides and metals. The counting time was 20 seconds for Fe $\text{k}\alpha$, S $\text{k}\alpha$, 60 seconds for As $\text{l}\alpha$, Co $\text{k}\alpha$, Ni $\text{k}\alpha$, Ti $\text{k}\alpha$, Sb $\text{l}\alpha$, Te $\text{l}\alpha$, and 100 seconds for Au $\text{l}\alpha$. Mean atomic number background intensity and on-peak interference corrections were applied throughout (Donovan and Tingle, 1996; Donovan et al., 1993). Detection limits ranged from 40 ppm for Ti, 70 ppm for S, 90 ppm for Ni, 150 ppm for As and 360 ppm for Au $\text{l}\alpha$. The matrix correction method was ZAF utilising the algorithm of Armstrong/Love Scott (Armstrong, 1988).

X-Ray Diffraction (XRD) was used to characterise the modal composition and its variations of the geochemical samples collected in the Kosise deposit. Analyses were conducted on a Panalytical Empyrean multi-purpose research XRD spectrometer at the CMCA, UWA. Spectra were processed with the HighScore Plus software and the final weighted R profile values were all between 5.89 and 11.4 with an average of 8.7.

LA-ICP-MS was conducted on all generations of pyrite and arsenopyrite found in the district ($\text{V}_{2\text{S}}$, $\text{V}_{3\text{A}}$, $\text{V}_{3\text{B}}$ and syn- $\text{D}_{4\text{S}}$), as well as on unconstrained disseminated pyrite hosted in the conglomerate of the Bidini deposit (Table 4 in Electronic Appendices). Samples of pyrite

from V_{2S}, V_{3A}, V_{3B} veins and syn-D_{4S} all came from the Fatoya and Kintinian Formations (Kosise and Bidini deposits). Small amounts of pyrite were found in the Balato Formation (Sintroko PB1 deposit) and could not be linked to any of the four generations. Samples of arsenopyrite came from the Balato and Fatoya Formations (Sintroko PB1 and Bidini deposits). Samples were separated according to the nature of their host rock (either greywacke, shale or conglomerate; Table 5 in Electronic Appendices). Laser ablation was used to provide the missing links between the different textures of the hydrothermal mineral assemblages observed in the Siguiri district. In particular, laser ablation and EPMA data allowed the comparison of the major and trace element signatures from the multiple pyrite generations from Kosise and Sintroko PB1 and the pyrite found in the Bidini conglomerate. Analysis of sulfides in thin-section was determined utilizing a Resonetics RESOlution M-50A-LR incorporating a Compex 102 excimer laser, coupled to an Agilent 7700s quadrupole ICP-MS at the GeoHistory Facility, John de Laeter Centre, Curtin University. Following a 20s period of background analysis, samples were spot ablated for 60 s at a 7Hz repetition rate, using a 75 µm beam and laser energy of 2.5 J cm⁻². The sample cell was flushed with ultrahigh purity He (0.68 L min⁻¹) and N₂ (2.8 mL min⁻¹) and high purity Ar was employed as the plasma carrier gas. International glass standard GSD-1G was used as the primary reference material, to calculate elemental concentrations (using ⁵⁷Fe determined by EPMA as the internal standard element) and to correct for instrument drift on all elements except Au. Certified sulfide standard Laflamme Po726 (synthetic pyrrhotite doped with platinum group elements and Au) was utilized as the primary standard for Au and S calculation. Standard blocks, included secondary standards treated as unknowns, were run every 10 unknowns. The mass spectra were reduced using Iolite (Paton et al, 2011 and references therein). Data were collected on a total of 21 elements; (¹⁰⁷Ag, ⁷⁵As, ¹⁹⁷Au, ¹³⁷Ba, ²⁰⁹Bi, ⁵⁹Co, ⁵²Cr, ⁶³Cu, ⁵⁵Mn, ⁹⁵Mo, ⁶⁰Ni, ²⁰⁸Pb, ¹²¹Sb, ⁷⁷Se, ²⁸Si, ¹¹⁸Sn, ⁴⁷Ti, ²⁰⁵Tl, ⁵¹V, ⁶⁶Zn and ⁹⁰Zr). Precision, as determined on secondary standards ranged from <1% to 4% (Table 4 and 5 in Electronic Appendices).

Whole-rock major and trace element geochemical analyses

Whole-rock major and trace element compositions were measured on each sample collected from Bidini, Kosise and Sintroko PB1. The aim was to identify 1) the different geochemical variations associated with mineralisation between the three sedimentary formations hosting the Siguiri district, and; 2) the main geochemical differences between these formations.

Geochemical analyses (Table 3 in Electronic Appendices) were carried out by Intertek Genalysis Laboratories in Perth, using a combination of analytical techniques detailed in Table 6 in Electronic Appendices. The Geological Survey of Western Australia (GSWA) Bunbury basalt and Kerba granite standards were included to monitor instrument precision. Data precision for both standards was typically within 3% for major elements and 10% for trace elements. Detection limits for each element are provided in Table 6 in Electronic Appendices. XRF analyses, reported as oxides by Intertek Genalysis Laboratories, were converted in Microsoft Excel into elemental weight percent.

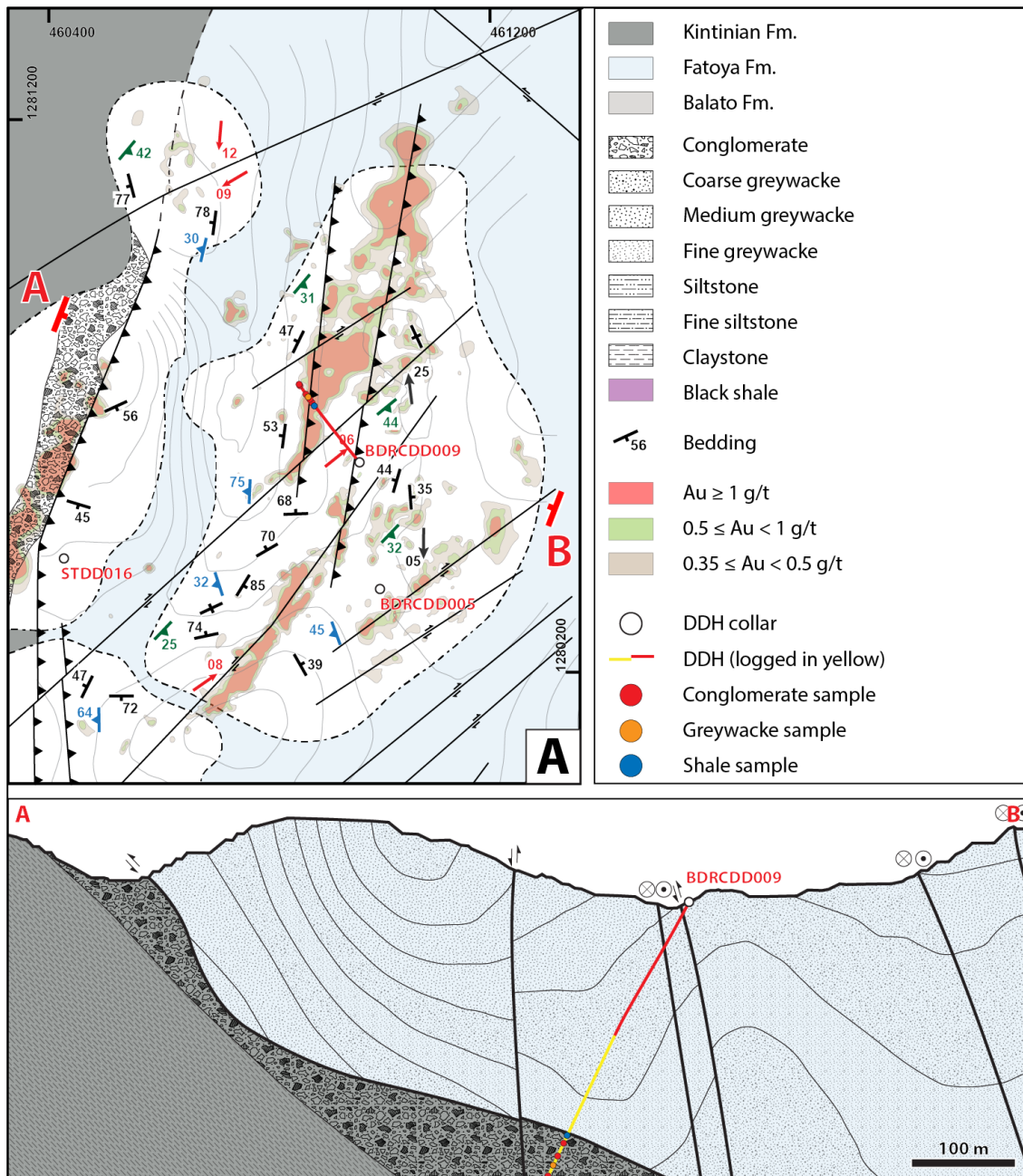
Data were separated according to formation, host rock types and least altered samples for each formation and host rock type were chosen. Normalisation was conducted using least altered samples of the same rock type. These least altered samples (Table 3 in Electronic Appendices) were selected based on their distance from mineralised shear zones, visible signs of alteration in hand-specimens (e.g. veining, bleaching), the amount of alteration minerals in thin-section, and gold grades. Sample BD3 was used to normalise the Kintinian conglomerate samples, sample F was used for the Fatoya Formation shale samples, sample O for the Fatoya Formation greywacke samples, sample SK6 for the Balato shale samples and sample SK4 for the Balato greywacke samples. Since no least altered shale and greywacke could be sampled directly in the Kintinian Formation, Kintinian samples BD1 and BD4 were normalised to a sample of shale and greywacke representative of the Siguiri district. The Fatoya samples F and O were therefore chosen for the normalisation of BD1 and BD4, respectively. Geochemical data were plotted using ioGAS.

Results

Bidini

Lithostratigraphy and structure

The Bidini deposit is located in the northern part of the district (Figure 33). It is hosted by the greywacke-dominated Fatoya Formation and is located east of the contact with the Kintinian Formation (Figure 35A).



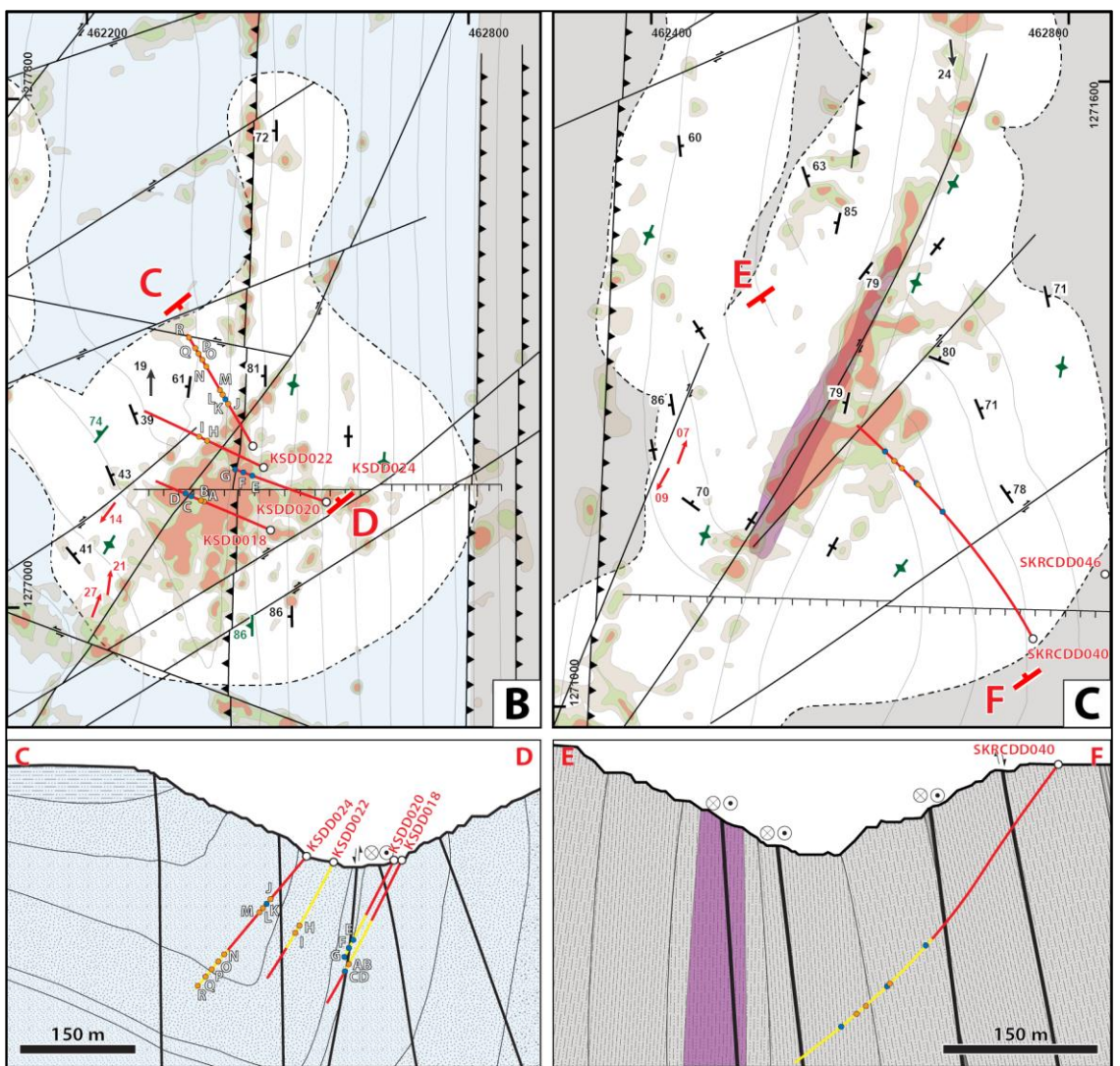


Figure 35: Simplified structural maps and cross-sections of key deposits from the Siguiri district (location map on Figure 33). A) Sanu Tinti and Bidini; B) Kosise, and; C) Sintroko PB1. Locations of the drill holes and collected samples highlighted.

Fatoya Formation sediments in the Bidini deposit display various sedimentary features that can be used as way-up indicators, such as: cross-bedding, rip-up clasts and ripple marks. Metre-thick beds of medium grained greywacke and sandstone dominate, however fine alternations of siltstone and shale can also be occasionally found, as well as some black shale layers. In this deposit, the Fatoya Formation is overlying up to 100 m of conglomerate interbeds, intersected in core BDRCDD009 (Figure 35A and 36).

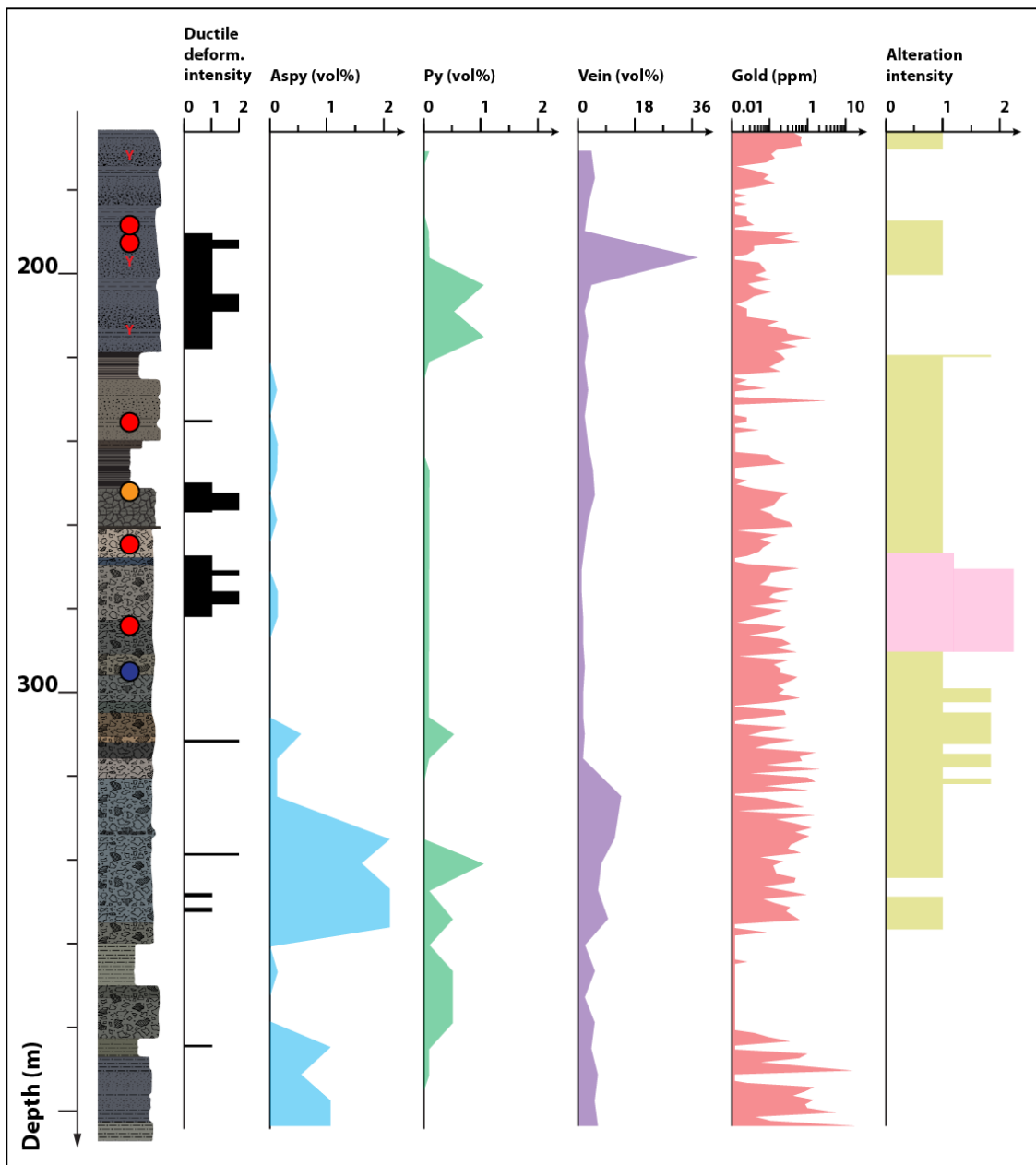


Figure 36: Log of hole BDRCDD009 (location map on Figure 34). The log has been overturned to account for the stratigraphy, the Kintinian formation being younger than the Fatoya formation (Lebrun et al., *in review* 2015b; Chapter 2). The alteration intensity section displays carbonate alteration in light brown and albitisation in light pink. Way-up indicators in red are based on graded bedding ripple marks and rip-up clasts. Position of the collected samples reported as coloured disks (conglomerate samples in red, shale in blue and greywacke in orange).

These conglomerates are part of the younger Kintinian Formation and outcrop in the Sanu Tinti deposit (Figure 33). They are separated from the Fatoya Formation sediments by a moderately dipping NNE-striking reverse fault (Figure 37F). The conglomerate interbeds are

polymict, clast supported and interpreted to be the product of repeated subaqueous debris flow events (Figure 37E; Lebrun et al., in review 2015b; Chapter 2).

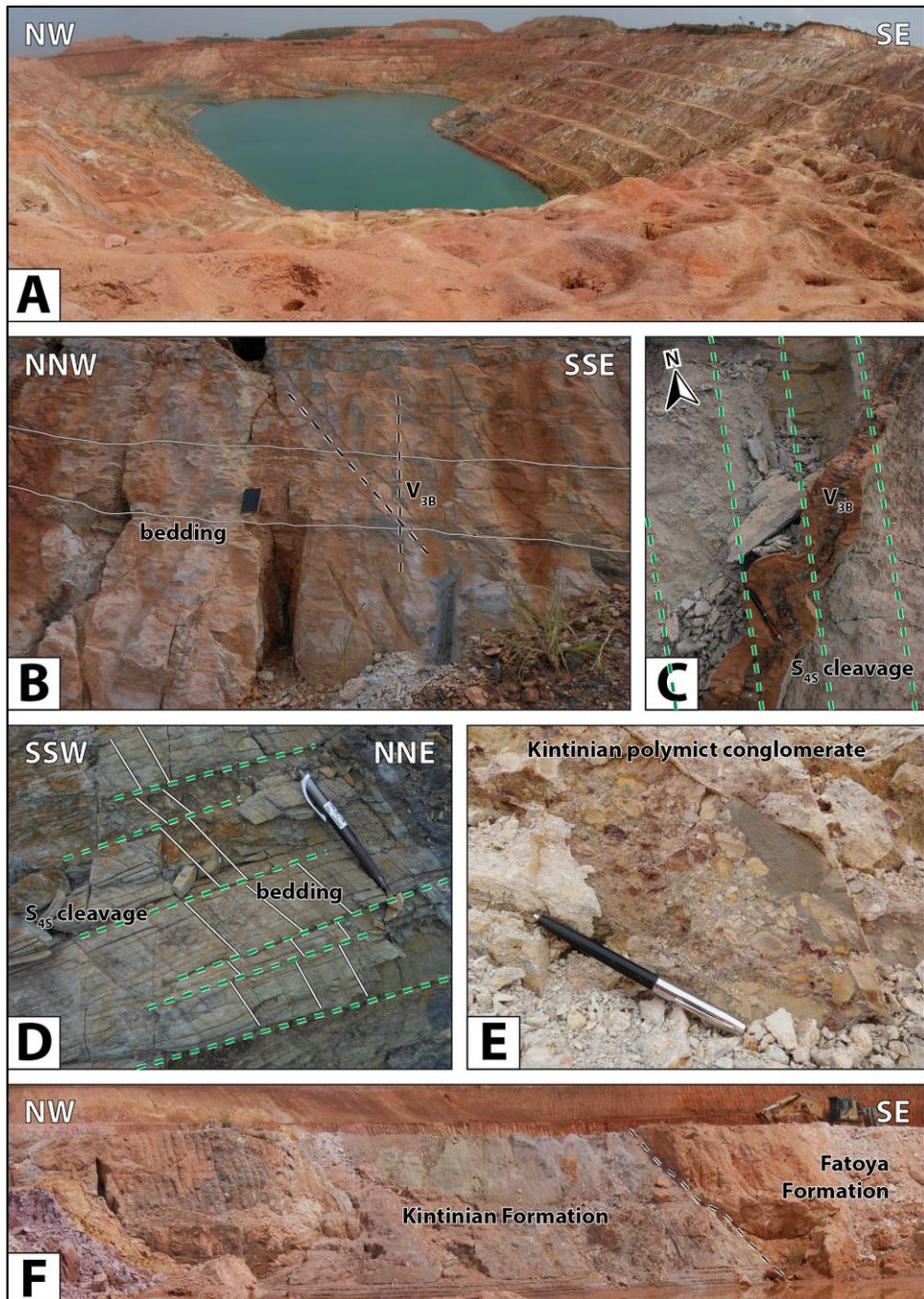


Figure 37: Photographs of the main structural elements from the Bidini and Sanu Tinti deposits. A) Overview of the Bidini deposit. In the foreground, 5 to 20 m-deep holes dug by local villagers are used to reach V_{3B} veins in one of the high grade zones along which the deposit sits. A second high grade zone is visible on the right (just below the (SE) symbol). B) Conjugate relationships between V_{3B} veins. C) Folded V_{3B} vein and axial planar S_{4S} cleavage. D) Pyrite developed along the S_{4S} cleavage. E) Close-up photograph of the polymict conglomerate from the Kintinian Formation found below the Bidini deposit and in the Sanu Tinti deposit. F) Structural contact (fault) between the Kintinian and Fatoya Formations in the Sanu Tinti deposit.

In the Bidini deposit, bedding strikes N-NE on average with multiple small-scale open F_{2S} folds. The deposit sits on the hinge of a refolded F_{2S} anticline the fold axes of which dip shallowly to the north and south (Figure 33 and 35A). The F_{2S} folds are crosscut by multiple early- D_{3S} sub-vertical incipient structures oriented NE-SW and N-S (Figure 37A). These incipient structures are mainly developed in the centre of the deposit and are expressed as discreet damage zones associated with areas about ten metres wide where the density of mineralised V_{3B} veins increases (Figure 37B; Lebrun et al., in review 2015a; Chapter 3). These damage zones can extend up to 300 metres in depth (Figure 35A). Veining in Bidini is dominated by the V_{3B} vein set (Figure 37B and 37C) and some V_{3A} veins. In drill core, V_{3A} veins often have brecciated textures and range from a few mm up to 20 cm. In comparison, individual V_{3B} veins typically have antitaxial textures (Passchier and Trouw, 2005) and are only a few cm to 15 cm thick but can extend for up to tens of metres. Supergene alteration has formed a centimetre wide halo of iron oxides around the V_{3B} veins, preserving them from further weathering (Figure 37C).

Mineral assemblages and mineralisation

Hydrothermal mineral assemblages in the Bidini deposit occurs as two styles of mineralisation dependant on whether these assemblages are hosted by the greywacke or shale beds of the Fatoya Formation or in the conglomerate of the Kintinian Formation. In the Fatoya Formation, hydrothermal activity has formed veins whereas in the Kintinian Formation, hydrothermal alteration is disseminated throughout the matrix and clasts of the conglomerate (Figure 34D).

In the Fatoya Formation, mineralisation is controlled by early- D_{3S} N-W and NE-SW damage zones, around which V_{3S} veining develops. Both the V_{3A} and the V_{3B} vein sets were found in Bidini. The V_{3A} carbonate-pyrite veins show coeval growth of pyrite and minor arsenopyrite. These veins are often found associated with a halo of siderite nodules overprinting metamorphic sericite. Minor albite can also be found in this vein set. Free gold occurs along fractures in V_{3A} pyrite and is associated with chalcopyrite and galena. The V_{3B}

veins typically have rims of ankerite and a core of quartz, and are associated with sulphides. These sulphides are typically located along the selvages or disseminated as haloes of up to a meter thick around the veins, where arsenopyrite is dominant. However, a halo of pyrite can be found instead of, or accompanying, the arsenopyrite crystals. Pyrite associated with V_{3B} veins can sometimes be found pseudomorphosing the siderite nodules in the albited host rock (Figure 38A). Free gold can be found in the quartz or at the contact between the carbonates and the quartz. In drill core, each vein is associated typically with carbonate alteration of up to a few metres and expressed as bleaching and/or by millimetre-sized siderite nodules. The mineralised damage zones, highlighted by the V_{3B} veins, form widespread carbonate alteration haloes of up to a hundred metres (e.g. BDRC009; Figure 36). Native gold is found in the quartz or at the contact between quartz and ankerite in the V_{3B} veins. Free gold can also be found in V_{3B} arsenopyrite fractures, in association with chalcopyrite and galena (Figure 38B). The V_{3B} veins are overprinted and folded by the S_{4S} cleavage (Figure 37C), which commonly develops strain shadows of pyrite, chalcopyrite, quartz and carbonate around the V_{3B} arsenopyrite. Pyrite and chalcopyrite can also be found along the S_{4S} penetrative cleavage (Figure 37D).

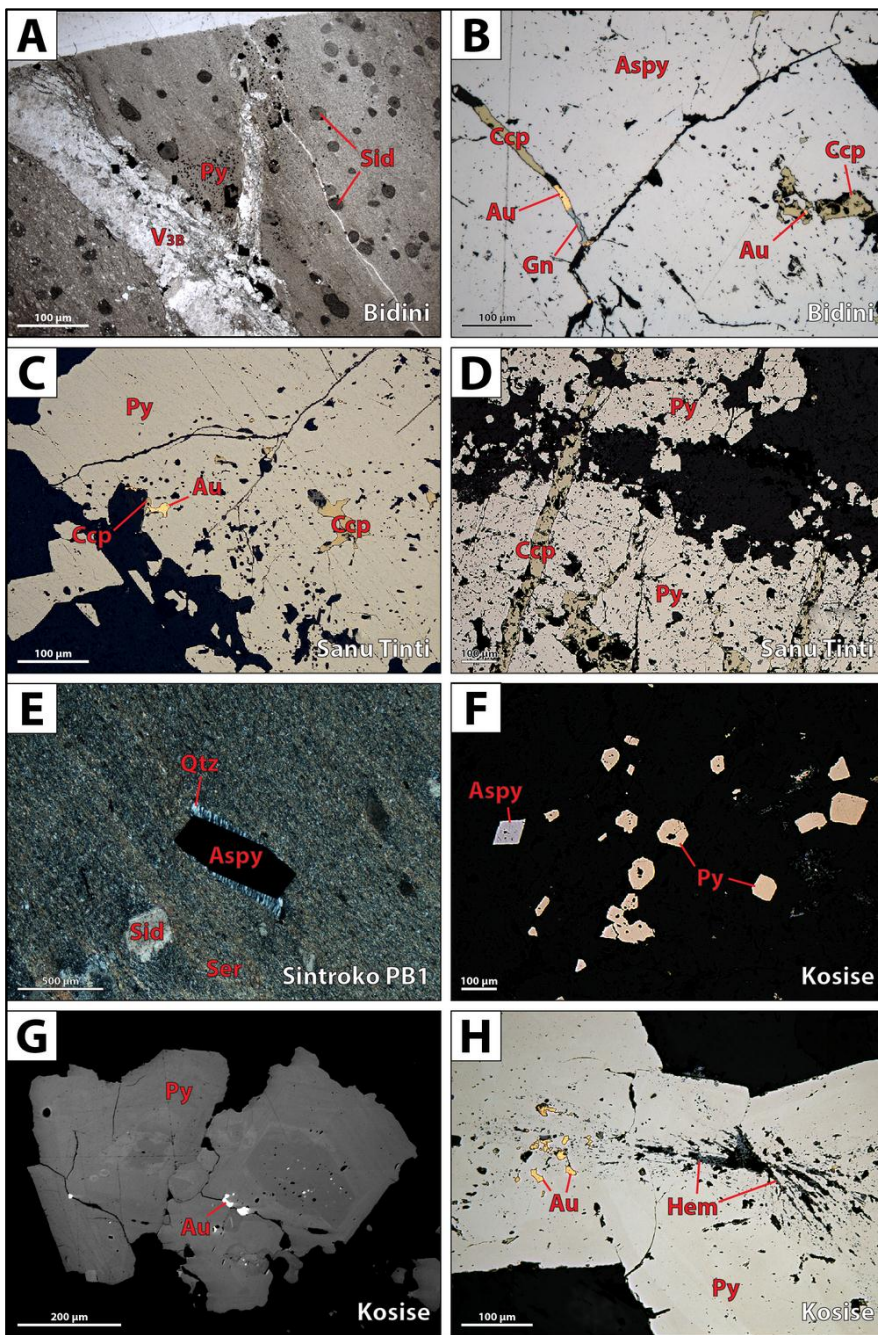


Figure 38: Microphotographs of A) siderite nodules being pseudomorphosed by V_{3B} pyrite; B) A V_{3B} arsenopyrite fractured and showing gold-chalcopyrite-(galena) infills; C) Sanu Tinti style V_{3B} pyrite fractured and showing gold-chalcopyrite infills; D) Sanu Tinti style V_{3B} pyrite overprinted by chalcopyrite veinlets; E) V_{3B} arsenopyrite showing quartz strain fringes associated with the development of the S_{4S} penetrative cleavage. This cleavage is also responsible for the preferential orientation of the sericite and the strain shadows developing around the siderite nodules; F) Coeval V_{3A} pyrite and arsenopyrite crystals; G) backscattered electron image of V_{3A} pyrite displaying As-rich and As-poor growth rings and being crosscut by gold infilled fractures; H) hematite inclusions in V_{3A} pyrite associated with gold. Hematite laths seem to follow the pyrite crystal lattice while gold display triangular textures typical of open space infill (Taylor, 2010). Aspy: arsenopyrite, Au: gold, Ccp: chalcopyrite, Gn: galena, Hem: hematite, Py: pyrite, Qtz: quartz, Ser: sericite, Sid: siderite.

Hydrothermal mineral assemblages in the underlying Kintinian conglomerate have very distinct textures. The gold-bearing mineral assemblage is dominated by disseminated sulphides, largely pyrite, developed along the NNE-striking hangingwall of the conglomerate and exhibits little to no V₃B veining (Figure 34D). Minor tourmaline, chalcopyrite and gold were found associated with the disseminated pyrite. Free gold was commonly found as inclusions or within fractures in the pyrite and associated with chalcopyrite (Figure 38C). Gold bearing pyrites are crosscut or have strain shadows of chalcopyrite, hematite and chlorite (Figure 38D). The hematite-chlorite association was also found with magnetite (pseudomorphosed by pyrrhotite) and titanite (also pseudomorphosed by pyrrhotite). High-grade mineralisation zones are associated with pyritisation, carbonate alteration and intense albitisation.

Sintroko PB1

Lithostratigraphy and structure

Sintroko PB1 is one of the southernmost deposits of the Siguiri district and is hosted by the Balato Formation (Figure 33). Rocks at Sintroko PB1 consist of centimetre- to decimetre-thick beds of shale-siltstone interlayered with medium to fine-grained greywacke and sandstone beds. A distinctive 10 to 20 m thick black shale layer runs through the centre of the deposit (Figure 35C and 39A).

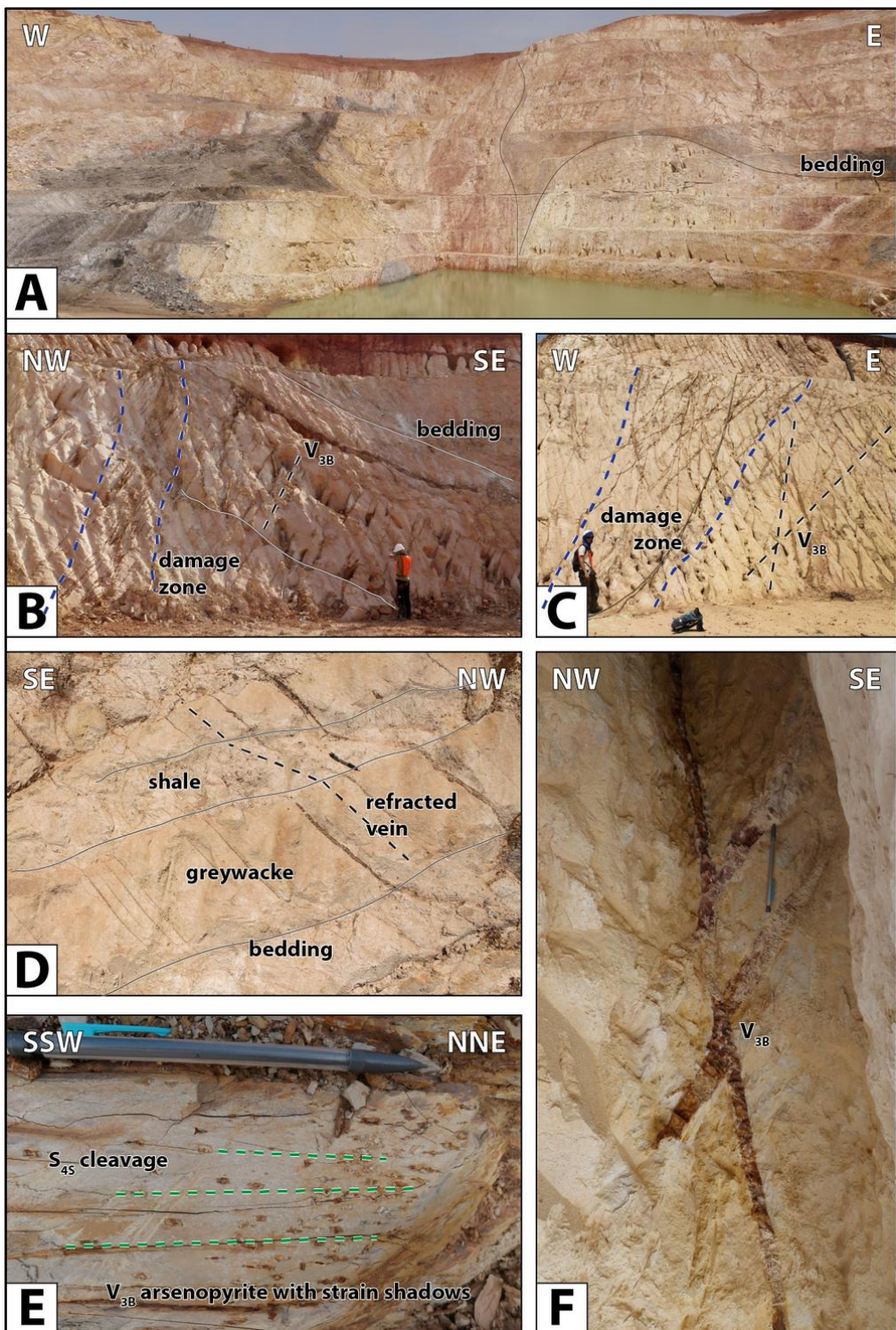


Figure 39: Photographs of the main structural elements found in the Sintroko PB1 deposit. A) Overview of the deposit. The main ore shoot found in this deposit follows the black shale layer (left) and crosscut the F_{25} sub-vertical fold found on the eastern side of the deposit (right). B) Photograph of an ore shoot, expressed as a sub-vertical damage zone associated with dense V_{3S} veining. C) Another example of a high grade damage zone and of the large scale conjugate geometry displayed by the V_{3B} veins. D) Refraction of V_{3B} vein orientations between beds of greywacke and shale. E) Strain shadows around arsenopyrite crystals developed around a V_{3B} vein (crumbled down on the right) by the S_{45} cleavage. F) Conjugate relationship of the V_{3B} veins at the outcrop scale.

Bedding is sub-vertical in this deposit. In the central black shale area, bedding is oriented NNW-SSE while the eastern and western sides of the deposit show open F_{2S} folding with sub-vertical fold axes. Isoclinal F_{2S} folds with vertical fold axes are also commonly observed (Lebrun et al., in review 2015a; Chapter 3). The F_{2S} folds are associated with bedding-parallel V_{2S} veins typically ~5 cm thick and locally up to tens of centimetres thick. These veins can extend over several tens of metres along bedding. En-echelon V_{2S} veins in Sintroko PB1 are commonly thinner than the bedding-parallel variation in V_{2S} , and rarely exceed 4 cm in thickness. In cross-section, en-echelon vein arrays extend over 2-3 m, but individual veins typically extend for a maximum of 50 cm only. The F_{2S} folds and associated V_{2S} veins are crosscut by an early- D_{3S} NE-striking sub-vertical shear zone sub-parallel to the central black shale unit (Figure 35C). This shear zone, the most visible structural element in the deposit, is accompanied by two other sub-vertical NE-SW damage zones that cut across bedding. These damage zones exhibit an increased density of veins (Figure 39B, 39C). The veins associated with these incipient structures are dominated by the V_{3B} vein set and no V_{3A} veins were observed in Sintroko PB1. The V_{3B} vein set commonly has conjugate geometries characterised by NE-SW striking veins dipping either moderately to the SE or steeply to the SE or the NW (Figure 39F).

Mineral assemblages and mineralisation

The hydrothermal mineral assemblages in Sintroko PB1 are hosted in the veins developed in and around the NE-SW shear zone sub-parallel to the central black shale layer (Figure 35C) and NE-SW damage zones. Veining becomes more prominent in more competent units such as greywacke and is refracted in shale beds (Figure 39D). The mineralogy of V_{2S} veins consists of quartz and minor ankerite. Free gold is hosted within V_{3B} quartz-ankerite-sulphide vein and located in the quartz core of the veins or at the contact between the quartz and the ankerite rims. Arsenopyrite, developed in and around the V_{3B} veins (Figure 39E) is the main sulphide phase in shale beds whereas pyrite becomes more common in greywacke and

sandstone beds. In drill core, high-grade mineralised zones are typically associated with a carbonate alteration halo extending up to a couple tens of metres across (e.g. SKRCDD040; Figure 40). Sericite is developed mainly along the S_{4S} cleavage and pyrrhotite, chalcopyrite and quartz can be found in the strain shadows around V_{3B} arsenopyrite (Figure 38E and 39E).

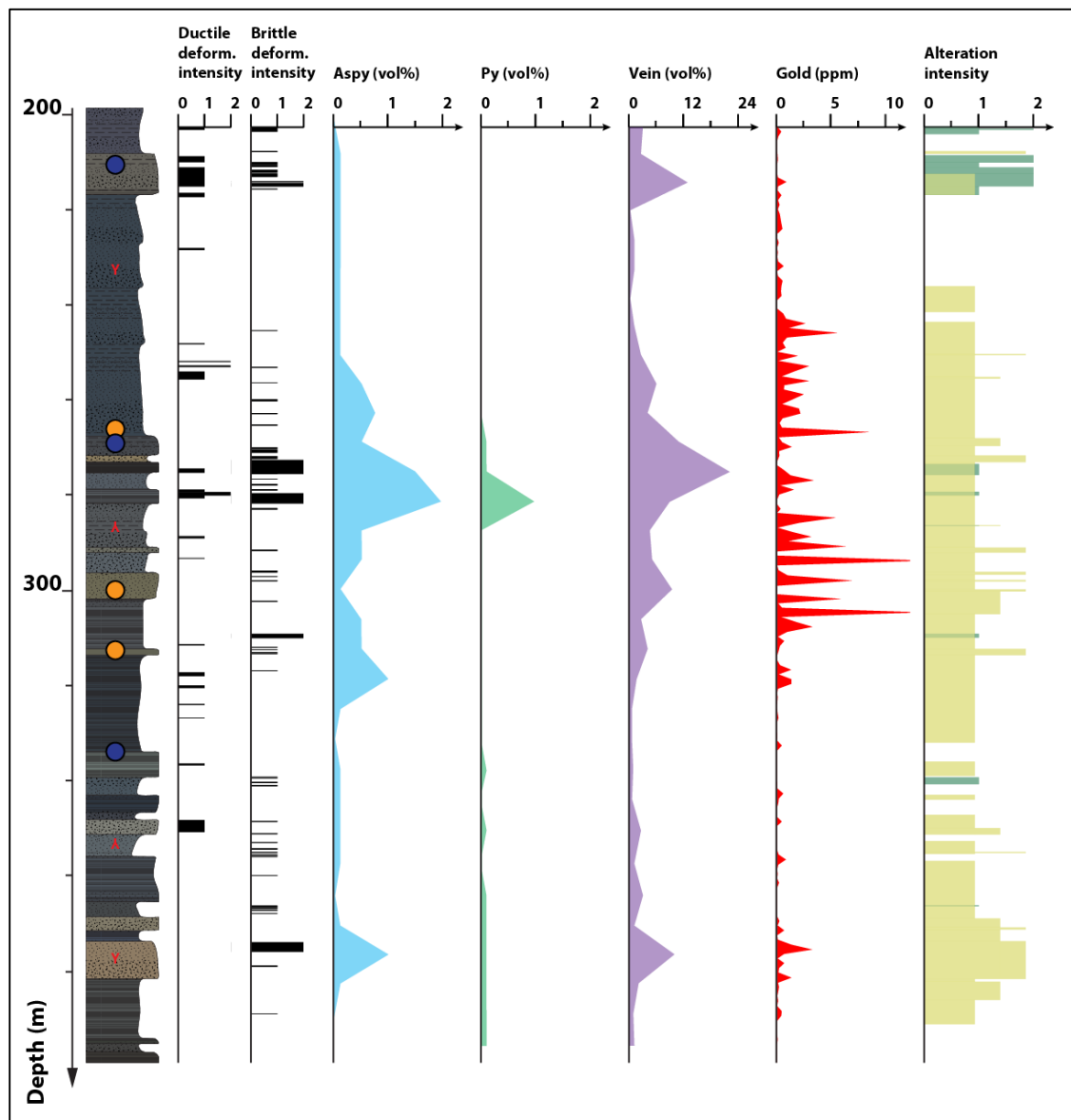


Figure 40: Log of hole SKRCDD040 (location map on Figure 39). This log highlights the strong link between brittle deformation, veining, sulphidation and carbonate alteration with gold. The alteration intensity section displays carbonate alteration in light brown and overprinting chloritisation in green. Way-up indicators in red are based on graded bedding ripple marks and rip-up clasts. Position of the collected samples reported as coloured disks (shale samples in blue, greywacke in orange).

Kosise

Lithostratigraphy and structure Kosise

The Kosise deposit is hosted by the Fatoya Formation and is located to the west of the contact with the Balato Formation (Figure 33). Sedimentary beds in Kosise are typically a metre thick and commonly display sedimentary features, such as graded bedding, ripple marks, rip-up clasts as well as loading and cross-bedding structures. These sedimentary features were used as way-up indicators and show that the Fatoya Formation in this deposit is normally graded. Kosise lithostratigraphy is dominated by beds of medium to coarse-grained greywacke and some beds of sandstone can also be found in the north of the deposit. Rare alternations of thin siltstone and shale beds can also be found.

Kosise is located in a F_{2S} syncline oriented N-S with a sub-horizontal fold axis (Figure 35B). This fold is open, has a vergence to the west (Figure 41A) and has bedding-parallel and en-echelon V_{2S} veins along both limbs. A number of early- D_{3S} sub-vertical structures crosscut the F_{2S} syncline, including: NE-SW dextral shear zones, a N-S thrust fault developed along the steep limb of the fold, and an E-W normal fault (Figure 41C; Lebrun et al., in review 2015a; Chapter 3). Most of the early- D_{3S} structures present in this deposit are damage zones and incipient faults, highlighted only by the increase in vein density developed late- D_{3S} in the first ten-fifteen metres around them (Figure 41B). The two different V_{3S} vein sets (V_{3A} and V_{3B}) were observed around the damage zones, both in the field and drill core. The V_{3A} vein set develops in the first few metres of the damage zones whereas the V_{3B} vein set commonly displays a dense lateral extension of up to fifteen metres. In the Kosise deposit, the orientation of V_{3A} veins is extremely variable with individual veins showing brecciated textures. In contrast, V_{3B} veins are conjugate and oriented around 150/40 and 145/70, with common antitaxial textures (Figure 34G).

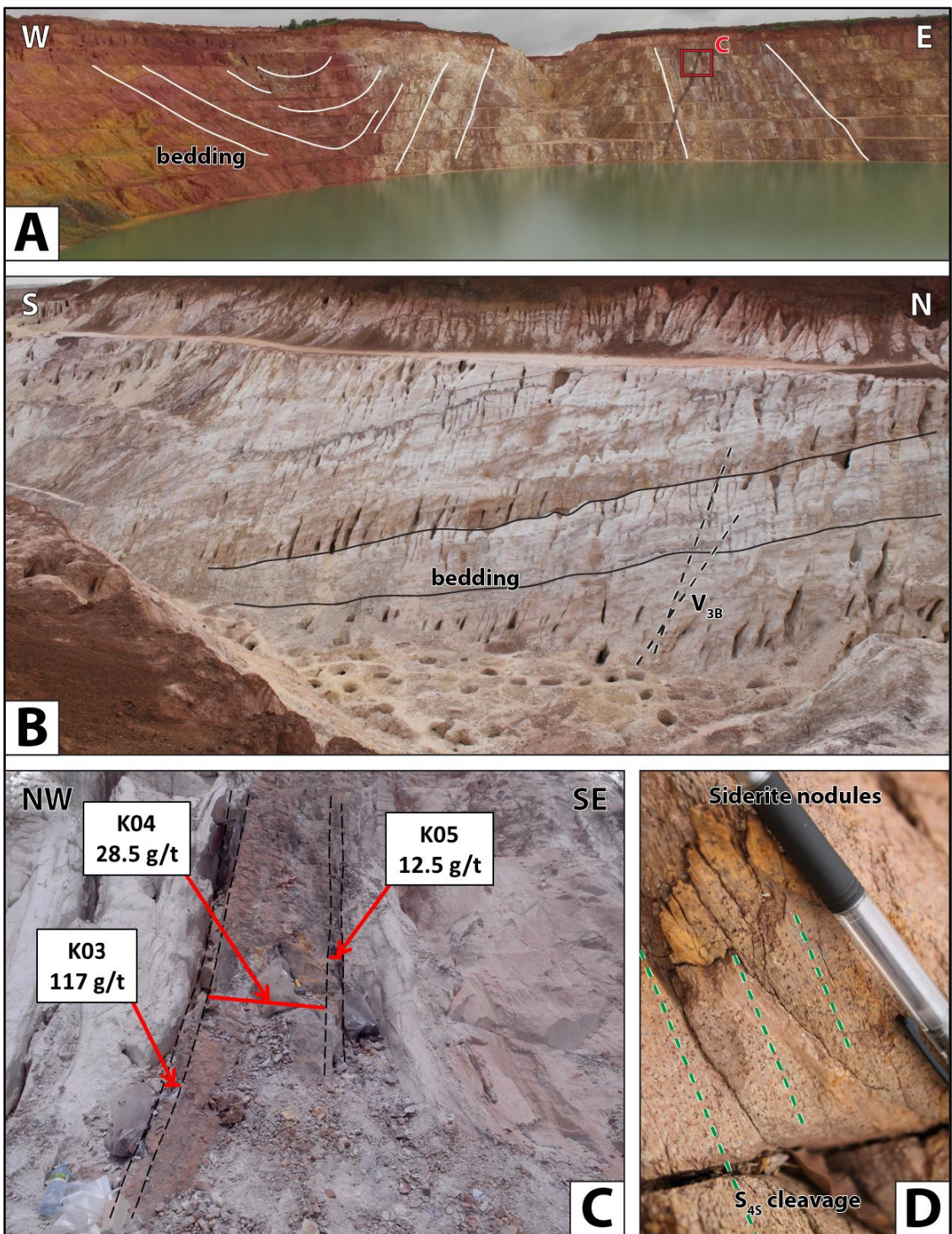


Figure 41: Photographs of the main structural elements found in the Sintroko PB1 deposit. A) Overview of the deposit. The northern part of the deposit (centre) hosts a bedding parallel thrust fault that develop intense V_{3S} veining (B). B) Veining developed in the northern part of the deposit. The V_{3B} veins are stratigraphically controlled and mainly hosted in the greywacke and sandstone beds. C) Close-up photograph of one of the rare discrete structures controlling gold grades in the Siguiri district, a dextral NE-SW shear zone. Gold grades across this shear zone are over 100 g/t Au. D) Siderite nodules developed around the ore shoots. The sub-vertical S_{4S} cleavage overprints these nodules.

Mineral assemblages and mineralisation

The XRD analyses on the Kosise samples show that the greywacke host rock is comprised of >40 vol% albite, 7 vol% carbonate, >5 vol% chamosite (chlorite family), 15 vol% white micas and 27 vol% quartz. In the shale beds chamosite and white mica increase to 8 vol% and 28 vol%, respectively and quartz decreases to 17 vol%. These abundances vary by only a few percent across the ore shoots (Table 3 in Electronic Appendices). The V_{2S} en-echelon veins crosscut the already albitised and sericitised host rock. In Kosise, these veins are dominated by quartz with rare ankerite and albite. No free gold was observed in V_{2S} pyrite. The rest of the hydrothermal mineral assemblages in the Kosise deposit are controlled by the N-S, NE-SW and E-W structures. The deposit sits at their intersection (Figure 35B) and gold grade within some of the shears can be greater than 100 g.t⁻¹ (Figure 41C). Similar to Sintroko PB1, vein distribution is also partly controlled by the host rock rheology, with veining becoming more important in more competent units (Figure 41B). Local miners primarily excavate the V_{3B} veins and ignore the V_{2S} and V_{3A} vein sets. However, petrography confirms that both V_{3A} and V_{3B} vein sets are mineralised in gold. Carbonate-pyrite V_{3A} veins show the early to coeval growth of minor arsenopyrite along with pyrite (Figure 38F) and SEM imaging coupled with qualitative EDS on V_{3A} pyrites shows As zoning (Figure 38G). Gold in the V_{3A} pyrites is located in fractures or as inclusions with triangular textures, characteristic of infill (Taylor, 2010). Gold is associated with chalcopyrite and hematite (Figure 38H). As in all other deposits, sulphides associated with V_{3B} veins change according to the host lithology with arsenopyrite dominating in shale beds and pyrite modal percentages increasing in greywacke and sandstone beds. Alteration around the ore shoots is characterised by carbonate alteration haloes associated with bleaching and millimetre-sized siderite nodules (Figure 41D).

Whole-rock multi-element geochemistry

Baseline geochemistry

Comparison of the baseline geochemistry for the least altered samples of all three rock types (conglomerate, shale and greywacke) from each three formations hosting the Siguiri district indicates that most elements have similar concentrations in all rock types of all three formations (Table 3 in Electronic Appendices). However, when data from the Kintinian, Fatoya and Balato Formations are normalised to a sample representative of the dominant lithology found in the Siguiri district (least altered greywacke from Kosise in the Fatoya Formation), variations in a suite of elements can be observed (Figure 42A). The baseline geochemical variations between the three formations are also observed when comparing the geochemistry of all collected samples (least altered and altered; Figure 43).

In particular, baseline geochemistry of the Kintinian Formation is associated with increased concentrations of Ca, F, Li, Mg, Ni, Sc, Sn, Sr, U, V (+ minor increases in Ga and W) and decreased concentrations of As, Cu, Pr, Si and Zr when compared to the Fatoya and Balato Formations (Figure 43; Table 3 in Electronic Appendices). Baseline geochemistry of the Balato Formation, when compared to those for the Kintinian and Fatoya Formations, is associated with a marked increase in Ba, minor increases in concentration of Bi, Cu, Hf, Pr, Sr, Th, Zn, Zr and a minor decrease in Ge (Figure 43; Table 3 in Electronic Appendices). These variations shows that the Balato Formation differs geochemically mainly from the Kintinian Formation (Figure 42A and 43). The baseline geochemistry of the Fatoya Formation is associated with increased concentration in Si whereas minor decreases in Ca, Mg, Sn and Sr can be observed when compared to the Kintinian and Balato Formations (Figure 43; Table 3 in Electronic Appendices).

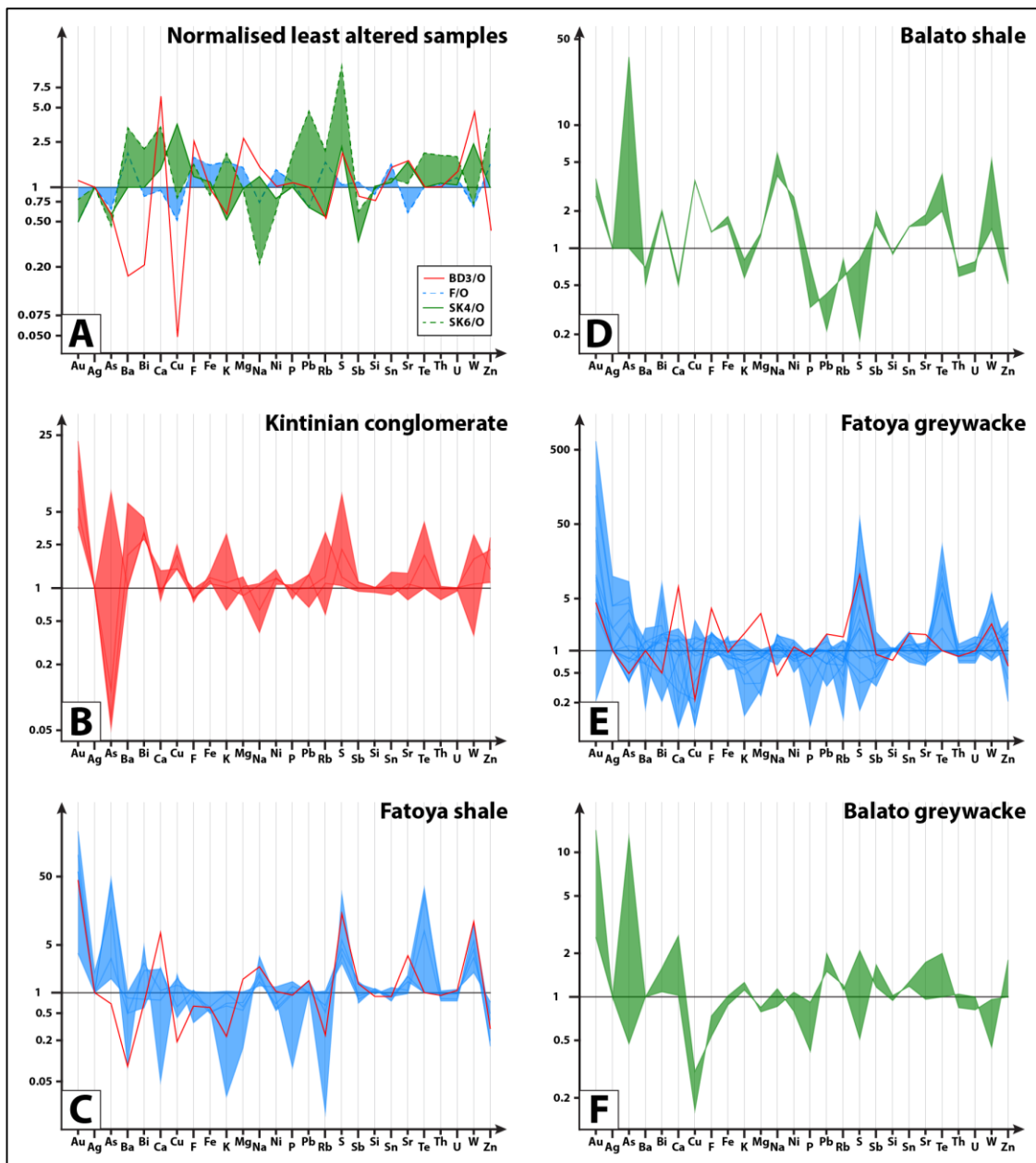


Figure 42: Geochemical spider-diagrams of the A) least altered samples collected in the Siguiri district and normalised to least altered Fatoya greywacke sample (sample O, collected in the Kosise deposit), representative of the lithologies hosting the bulk of the mineralisation in Siguiri. Kintinian conglomerate in red, Fatoya samples in blue, Balato samples in green, shale samples as dashed lines, greywacke samples as solid lines; B) Kintinian conglomerate samples normalised to the least altered sample; C) Fatoya shale samples and Kintinian shale sample normalised to the least altered Fatoya shale sample; D) Balato shale samples normalised to the least altered sample; E) Fatoya greywacke samples and Kintinian greywacke sample normalised to the least altered Fatoya shale sample, and; F) Balato greywacke samples normalised to the least altered sample.

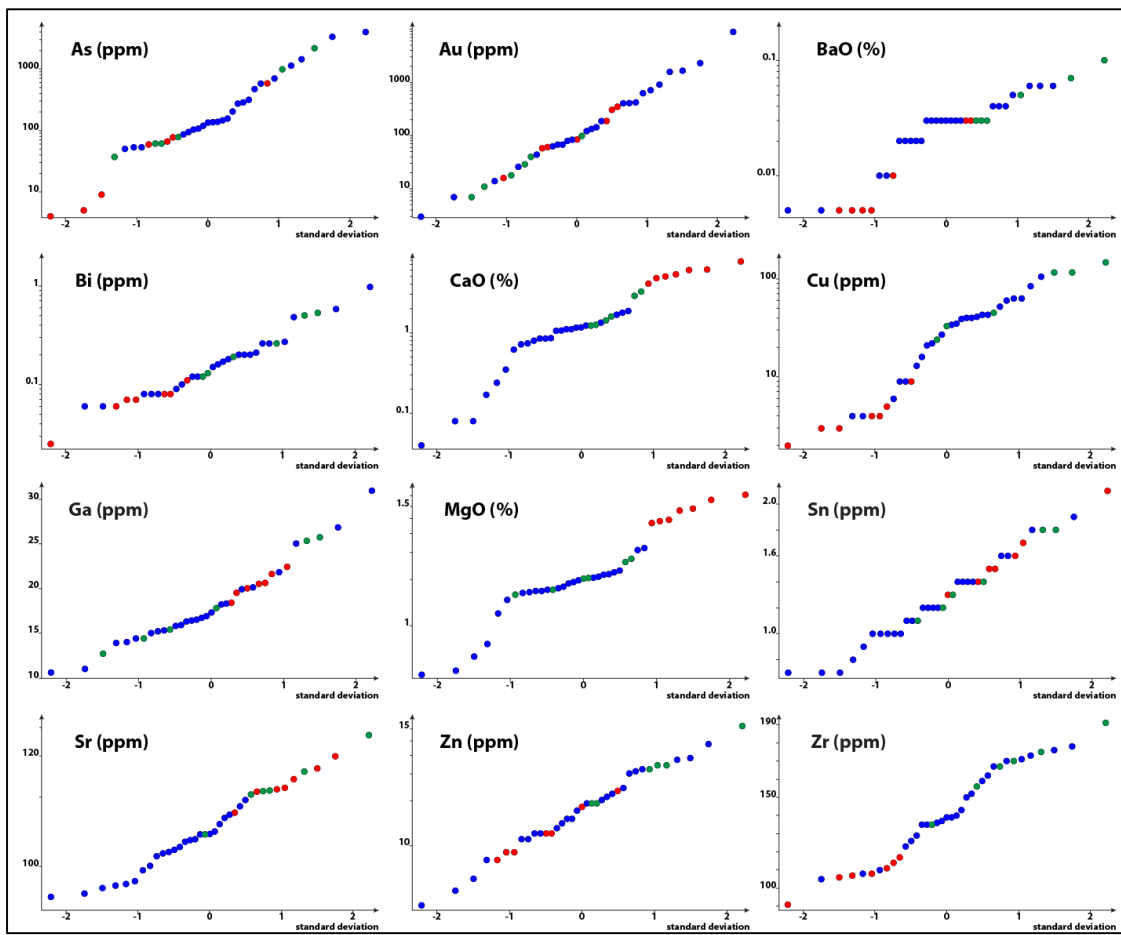


Figure 43: Normal probability plots of the whole-rock geochemical samples from the Balato (in green), Fatoya (in blue) and Kintinian Formations (in red). The values plotted along the X axis are in units of standard deviation (mean = 0 and a standard deviation = 1). Normal probability plots are used to verify if a dataset displays a normal distribution (straight line) and/or if multiple populations can be separated.

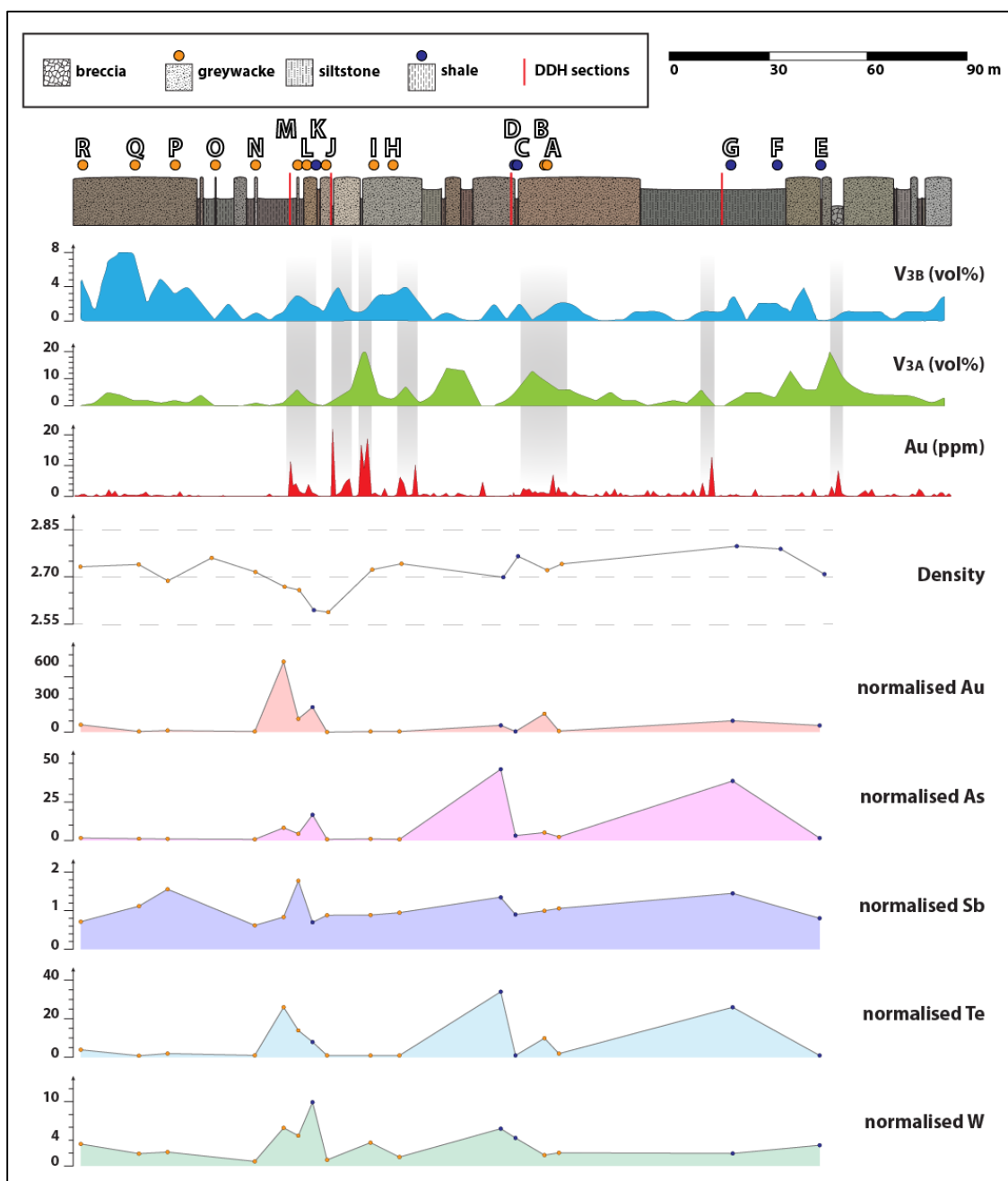
Alteration

Comparison between least altered samples and mineralized samples of each rock types and in each formation allow for the characterization of the suite of elements enriched or depleted towards the ore zones. In the Kintinian conglomerate (Figure 42B), mineralisation is associated with major increases in Au, Ba, Bi, Cu, K, Rb, S, Te, W, Zn, minor increases in F, Fe, Mg, Ni, Sn and minor decreases in As and Na compared to the least altered conglomerate sample (Table 3 in Electronic Appendices). Geochemical variations linked to mineralisation in the Fatoya shale beds are associated with major increases in Au, As, Bi, Na, S, Te, W, minor increases in Ag, Cu, Sr and decreases in Ba, K, P, Rb, Zn (Figure 42C). Geochemical variations

linked to mineralisation in the Kintinian Formation shale beds are associated with major increases in Au, Ca, Na, S, Sr, W, minor increases in Mg, Pb, Sb and decreases in Ba, Cu, K, Rb and Zn compared to the least altered shale sample from the Fatoya Formation (Figure 42C). Geochemical variations linked to mineralisation in the Balato Formation shale beds are associated with major increases in Au, As, Bi, Cu, F, Fe, Na, Ni, Sb, Sn, Sr, Te, W, minor increases in Mg and decreases in Ba, Ca, K, P, Pb, Rb, S, Th, U and Zn compared to the least altered shale sample from this formation (Figure 42D). Comparison of the geochemical variations between the altered greywacke from the Fatoya Formation and the least altered greywacke from the same formation indicates major enrichments in Au, Ag, As, Bi, S, Te, W and depletions in Ba, Ca, Cu, K, Mg associated with mineralisation (Figure 42E). Geochemical alteration in the Kintinian Formation greywacke is characterised by enrichments in Au, Ca, F, Mg, Pb, S, Sn, Sr, W and depletions in As, Bi, Cu and Na (Figure 42F). Comparison of the geochemical variations between the altered greywacke from the Balato Formation and the least altered greywacke from the same formation indicates major enrichments in Au, As, Bi, Ca, Pb, S, Sb, Sr, Te, Zn, minor enrichments in K, Rb, Sn and depletions in Cu, F, P and W associated with mineralisation (Figure 42F).

In addition, high-grade zones in Kosise (some over 100 g.t⁻¹ Au; Lebrun et al., in review 2015a; Chapter 3) are associated with a geochemical alteration halo at least 15 metres wide, characterized by an increase towards the ore shoots in: Ag, Au, As, Bi, Co, Mo, Sb, Se, S, Te and W (Figure 44 and Table 3 in Electronic Appendices). In detail, Au increases from 3 to 8931 ppm, As increases from 50 to 3996 ppm, Bi increases from 0.06 (just above detection limit; = 0.05 ppm) to 0.97 ppm, Mo increases from 0.3 to 2.3 ppm, Sb increases from 0.6 to 3.2 ppm, S increases from 0.06 to 4.47 ppm, and W increases from 3.5 to 34.9 ppm. Within the same alteration halo around the ore shoot, Ca, Cs, F, Ga, Hf, Li, Mg, P and V decrease (Figure 44 and data in Table 3 in Electronic Appendices). In particular, Mg decreases from 0.29 to 1.92 wt%, P decreases from 0.005 to 0.087 wt%, and V decreases from 17 to 159 ppm. Concentrations of Ca display a peculiar behaviour, increasing a few tens of metres away from the main ore shoot.

Silicon in the host rock does not show significant variation, due to the removal of all veins from the analysed samples. Saturation indices (molar ratios) for muscovite ($3K/Al$) and albite (Na/Al ; Kishida and Kerrich, 1987) vary from 0.07 to 0.66 and from 0.26 to 0.84 respectively, and clearly show a respective increase and decrease towards the ore shoots (Figure 44).



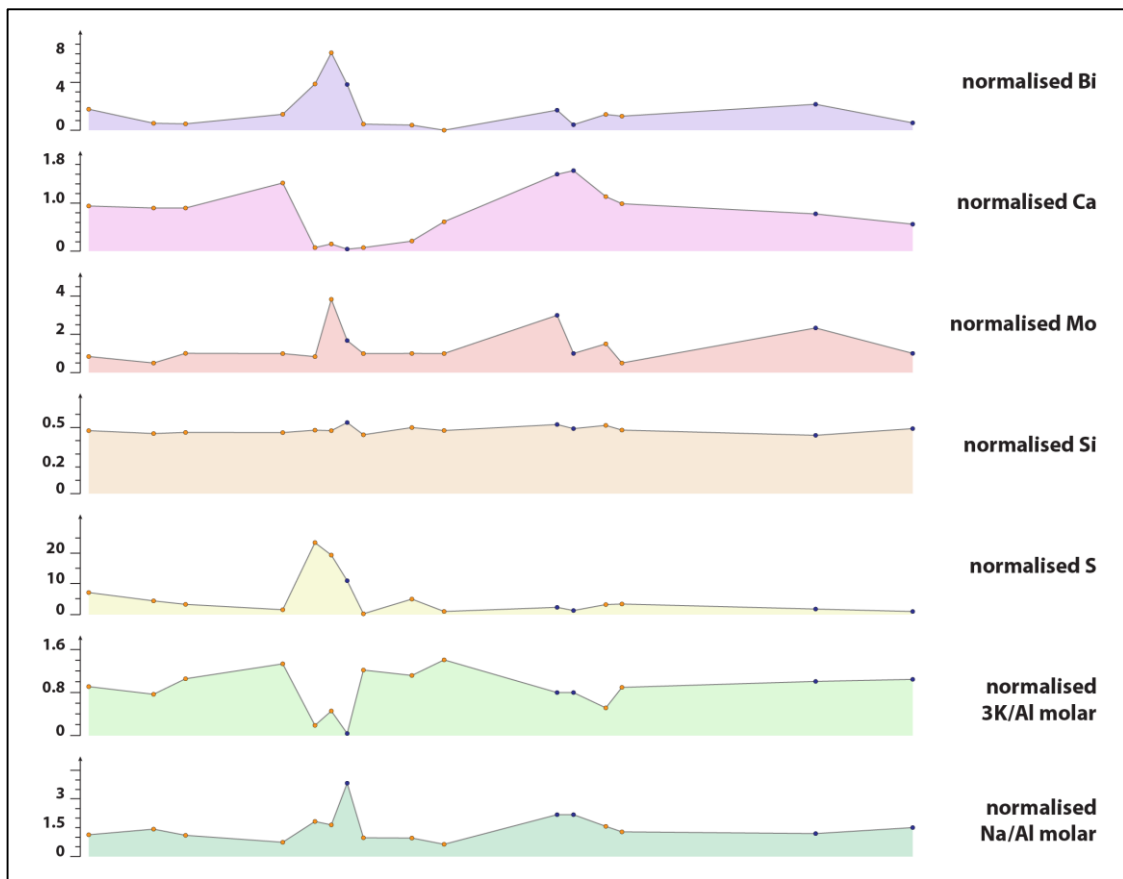


Figure 44: Composite log and geochemical cross-section from the Kosise deposit. Two mineralised zones were identified (around samples J, K, L, M and samples A, B, C, D) and are in close proximity to shear zones and a thrust fault (Figure 42 and 43). The main mineralised zone (samples J, K, L, M) is associated with typical orogenic gold enrichments in Au-As-Sb-Te and W. Each geochemical sample was normalised to the corresponding greywacke or shale least altered sample (O and F, respectively). The composite geochemical cross-sections also show enrichments in Bi, Mo and S around the main mineralised zone (samples J, K, L, M). Ca increases away from the main mineralised zone and is interpreted to represent the reaction front. The fact that Si does not show any variation across the ore shoots is attributed to the removal of the veins in each sample (host rock characterization only). Molar and normalised 3K/Al and Na/Al saturation indices (Kishida and Kerrich, 1987) both highlight both mineralised zones. Each geochemical sample was normalised to the corresponding greywacke or shale least altered sample (O and F, respectively).

LA-ICP-MS and EPMA

Pyrite

Pyrite associated with the V_{2S}, V_{3A} and V_{3B} vein sets, with the S_{4S} cleavage (syn-D_{4S}) and disseminated pyrite hosted in the Kintinian conglomerate were analysed by LA-ICP-MS. Major

and trace element signatures of the V_{2S}, V_{3A}, V_{3B} and D_{4S} pyrite vary in the Ag-As-Au-Cu-Sb-Se-Zr geochemical space (Figure 45F, 45G, 45H and 45J). Major and trace element signatures of pyrite associated with V_{2S} and V_{3A} veins cluster in the high Ag-As-Au-Sb – low Cu-S-Se-Zr part of this geochemical space whereas V_{3B} pyrite, Sanu Tinti conglomerate pyrite and syn-D_{4S} pyrite major and trace element contents cluster in the in the low Ag-As-Au-Sb – high Cu-S-Se-Zr part of this space. This clustering, first noticed when plotting pyrite data from greywacke beds from the Fatoya Formation only, was also observed when considering pyrite hosted in all formations, host rocks and deposits (Figure 45).

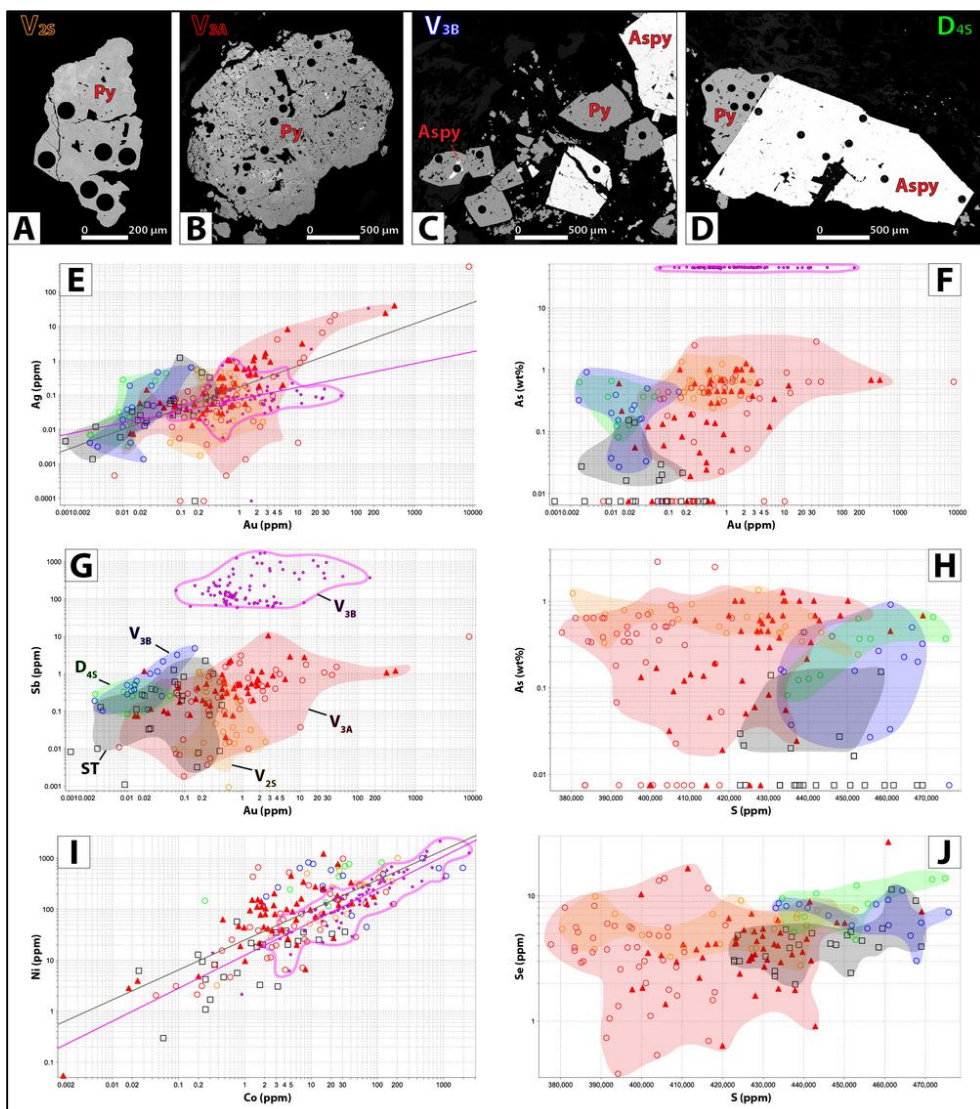


Figure 45: LA-ICP-MS and EPMA data from the different generations of pyrite and arsenopyrite observed in the Siguiri district. V_{2S} pyrite (A) is represented in orange. V_{3A} pyrite (B) is represented in red. V_{3B} pyrite is represented in blue and V_{3B} arsenopyrite in pink (C). D_{4S} pyrite is represented in green (D) and finally, Sanu Tinti style disseminated pyrite is represented in black. Regression lines are in black for pyrite and pink for arsenopyrite in E) and I).

Comparison between the major and trace element signatures of pyrite from the Fatoya and Kintinian Formations show variations in Co, ranging from below detection limit up to 1962.3 ppm in the Fatoya Formation, and from below detection limit to 32.6 ppm in the Kintinian Formation. Values for Ni range from below detection limit to 1248 ppm in the Fatoya Formation, and from below detection limit to 57 ppm in the Kintinian Formation. Values for Cu range from below detection limit to 3688 ppm in the Fatoya Formation, to 2 ppm and 4393 ppm in the Kintinian Formation. In addition, laser ablation data shows that V_{3A} pyrite hosted in greywacke from the Kosise deposit (Fatoya Formation; Figure 45A) has gold grades up to 43.3 ppm, while the other pyrite generations do not reach grades higher than 3 ppm (the three higher values reported on Figure 45E were obtained from gold inclusions). In summary, pyrite from the Fatoya Formation is associated with increased concentrations in As, Au, Co, Ni (and minor Bi, Mn), and a depletion in Cr, Cu, S, Si, Sn, Zr when compared to the major and trace element signatures of pyrite hosted in the Kintinian Formation (Table 5 in Electronic Appendices). Moreover, the crystal lattice of the different generation of pyrite shares similar Ag/Au and Ni/Co ratios, around 7.5 and 2.81 respectively (Figure 45E and 45I).

Arsenopyrite

Arsenopyrite was found associated only with V_{3B} veins. Aside from their differences in major element concentrations, arsenopyrite and all generations of pyrite can also be distinguished when comparing their respective trace element signatures in Bi, Mo, Pb, Sb, Se (and to some extent Co, Cr and Ni). Compared to all generations of pyrite, V_{3B} arsenopyrite is enriched in all these elements (Figure 45F, 45G, 45H and 45J and Table 5 in Electronic Appendices).

Concentrations of As (obtained by EPMA) and Sb vary with Au grades in the Balato and Fatoya samples, increasing from ~43.2 wt% to ~46.2 wt% As and from ~125 ppm to ~1600 ppm Sb respectively. Also, V_{3B} arsenopyrite lattice contains significant gold concentrations of up to 55.5 ppm (higher values reported on Figure 45E were obtained on a gold inclusion). The crystal

lattice of the V_{3B} arsenopyrite have similar Ag/Au and Ni/Co ratios to all pyrite generations, around 7.5 and 2.81 respectively (Figure 45E and 45I). In summary, while no arsenopyrite was found in the Kintinian Formation, arsenopyrite from the Balato Formation shows enrichment in Ag, Co, Cr, Cu, Sb, Ti (and minor Mn) and depletion in As when compared to the arsenopyrite hosted in the Fatoya Formation (Table 5 in Electronic Appendices).

Discussion

Polyphase hydrothermal activity and gold mineralisation

Field observations of vein cross-cutting relationships, core logging and petrographic descriptions from Bidini, Sintroko PB1 and Kosise, permit the construction of local paragenetic sequences for each individual deposit studied. When compared to one another, the local paragenetic sequences are homogeneous across the Siguiri district and are characterised by four distinct hydrothermal events. These events were correlated in the district-scale paragenetic sequence (Figure 46) summarized below. Together, the laser ablation data (Figure 45) and the general paragenetic sequence of the district, reflects the polyphase character of gold mineralisation in Siguiri and three distinct gold mineralisation events were identified.

	sedim. & metam.	D_{2s} V_{2s}	D_{3s} V_{3A}	D_{3s} V_{3B}	D_{4s}
Quartz		→	→	→	→
Albite		→	→	→	→
Zircon			→	→	
Carbonate		→	→	→	→
Biotite			→	→	→
Chlorite			→	→	→
Sericite	→	→	→	→	→
Titanite				→	→
Tourmaline				→	→
Monazite				→	→
<hr/>					
Arsenopyrite			→	→	→
Pyrite		---	→	→	→
Chalcopyrite			→	→	→
Sphalerite			→	→	→
Hematite		---	→	→	→
Ilmenite			→	→	→
Pyrrhotite			→	→	→
Marcasite			→	→	→
Rutile		→			→
Galena					→
Magnetite					→
<hr/>					
Gold			→	→	→

Figure 46: Paragenetic sequence for the Siguiri district.

The mineralogy of the host-rock in the Siguiri district is dominated by plagioclase, quartz and shows moderate to intense sericitisation and albitisation. Minor biotite and chlorite, possibly detrital, were also found in the host rock mineral assemblage as well as numerous detrital zircons (dated by U-Pb SHRIMP geochronology; Lebrun et al., in review 2015b; Chapter 2).

The first hydrothermal event occurs during D_{2s} E-W compression and is characterised by the development of the bedding-parallel and en-echelon V_{2s} quartz-(ankerite) veins. The V_{2s} veins developed in response to flexural slip during F_{2s} folding (Lebrun et al., in review 2015a; Chapter 3) are associated with minor albite, sericite, pyrite and traces of rutile. These veins do not present significative gold mineralisation and show little development of alteration around their margins.

The second hydrothermal event, occurs late during D_{3S} NNW-SSE transtension and is represented by the V_{3A} ankerite-pyrite-(albite) brecciated veins that crosscut the V_{2S} veins. The V_{3A} veins represent the most proximal expression of V_{3S} veining developed along the early-D_{3S} N-S, NE-SW, WNW-ESE and E-W damage zones. The V_{3A} veins have developed in the core of the sub-vertical structures controlling gold mineralisation. V_{3A} veins are associated with minor sericite, quartz, chlorite, rare monazite and arsenopyrite, pyrrhotite and late chalcopyrite and sphalerite. V_{3A} veins are also characterized by a halo of carbonate alteration and pyritisation. Carbonate alteration is expressed as millimetre-sized siderite nodules and bleaching of the host-rock. The V_{3A} vein set also represents the first episode of gold mineralisation recognized in the Siguiri district. Gold was found locked in the V_{3A} pyrite crystal lattice (up to 43.3 ppm Au; Figure 45; Table 5 in Electronic Appendices).

The third hydrothermal event also occurred late during D_{3S}, and developed along the ten to fifteen metre-thick sub-vertical damage zones formed early during D_{3S} deformation. This event is mainly characterised by intense V_{3B} quartz-ankerite-arsenopyrite veining and is ubiquitous in the Siguiri district. The conjugate V_{3B} veins moderately to steeply dip to the SE and are associated with minor albite and pyrite. This vein-hosted mineralisation is also characterized by minor sericitisation and carbonate alteration mainly expressed as millimetre-sized siderite nodules. The third hydrothermal event is also represented by a distinct texture, only observed in the Bidini and Sanu Tinti deposits. The mineralisation texture found in the Kintinian polymict conglomerate is represented by disseminated pyrite, accompanied by tourmaline, rare monazite and traces of late chalcopyrite, sphalerite, hematite and ilmenite. Minor sericitisation and carbonate alteration is also associated with this mineralisation texture. This disseminated mineralisation shows some degree of structural control (Kintinian-Fatoya N-S thrust contact) but is mainly stratigraphically controlled by the Kintinian conglomerate. Comparison of major and trace element signatures by LA-ICP-MS and EPMA between the disseminated pyrite and the other generations of pyrite associated with D_{2S}, D_{3S} and D_{4S} deformation indicates that the Sanu Tinti disseminated pyrite presents geochemical

affinities with D_{3S} and D_{4S} pyrite associated with the V_{3B} veins and the S_{4S} cleavage, respectively (Figure 45). Since petrographic observations indicate that the Sanu Tinti disseminated pyrite is overprinted by the S_{4S} cleavage, we propose that both V_{3B} and Sanu Tinti disseminated pyrite formed coevally late during D_{3S}. Both mineralisation textures developed along the early-D_{3S} N-S thrust at the contact between the Kintinian and the Fatoya Formation. The change in mineralisation texture from the Fatoya to the Kintinian Formation is common in orogenic gold deposits (Dubé and Gosselin, 2007; Bierlein and Maher, 2001; Groves, 1993) and interpreted to be linked to the higher porosity and lower competency of the Kintinian conglomerate compared to the sediments of the Fatoya Formation. The second and main episode of gold mineralisation identified in Siguiri was found to be associated with both mineralisation textures. In the V_{3B} vein-hosted mineralisation, gold was found in the veins and in the lattice of the arsenopyrite crystals (up to 55.5 ppm Au; Figure 45; Table 5 in Electronic Appendices). In the disseminated pyrite, gold was found free along fractures associated with chalcopyrite, hematite and galena. The crystal lattice of the disseminated pyrite was however found to be barren (~3 ppm Au maximum; Figure 45; Table 5 in Electronic Appendices).

The last hydrothermal event is a late overprint, which developed during D_{4S} NW-SE compression and formed the S_{4S} cleavage. This cleavage is characterised by strain shadows of sericite, quartz, ankerite and albite around V_{3B} arsenopyrite crystals. Chlorite, hematite, pyrite, chalcopyrite, pyrrhotite, sphalerite, magnetite can also be found in these strain shadows or in veinlets overprinting the syn-V_{3B} disseminated pyrite in the Kintinian conglomerate. Even though no significant gold was found locked in syn-D_{4S} pyrite (~3 ppm Au maximum), free gold has been described in both Bidini and Kosise deposits infilling fractures or strain shadow of early mineralised V_{3B} pyrite and arsenopyrite with chalcopyrite, hematite and galena. Two alternative models can be proposed to explain this infill. In the first model, a new gold input may be related to the late syn-D_{4S} hydrothermal event. In the second alternative model, gold may have been remobilised during D_{4S}, relocating the invisible gold locked in the V_{3A} and V_{3B} pyrite and arsenopyrite crystal lattice into fractures and pressure shadow. Such behaviour has

been described by a number of authors in recent years (Cook et al., 2013; Large et al., 2011; Wilkinson et al., 1999). The present dataset do not allow to conclude in regards to D_{4S} gold occurrence and further work would be required to assess whether gold remobilisation occurred or not.

Geochemical footprint of the ore shoots

The alteration associated with the superimposition of all four hydrothermal events was geochemically characterised across the Siguiri district (Figure 42, 43 and 44). In the different deposits and in the representative Kosise deposit in particular, the geochemical variations associated with this style of mineralisation are characterised by enrichments in Ag, Au, As, Bi, S, Sb, Te and W within the first fifteen meters around the ore shoots at minimum (Figure 44). These enrichments relative to the geochemical baseline of the hosting formation, are characteristic of hypozonal to mesozonal orogenic gold deposits (Groves et al., 1998; Eilu et al., 1999; Groves et al., 2003) and are accompanied, in Siguiri, by additional increases in Co, Mo, Na/Al (molar), Se and decreases in Ca, Cs, F, Ga, Hf, 3K/Al (molar), Li, Mg, P and V across the main ore shoot. These variations can be directly related to the hydrothermal mineral assemblage associated with the V_{3A} and V_{3B} gold mineralisation event. In detail, Co is found as a trace element in pyrite and arsenopyrite. The increase in S is related to sulphidation, and the peculiar behaviour of Ca along the transect is interpreted to mark the carbonate reaction front. The molar ratio 3K/Al and Na/Al can be linked to albitisation (Eilu and Groves, 2001) developed around the veins. Decrease in V can also be related to a decrease in micas towards the ore shoot (Bateman and Hagemann, 2004). The absence of silica variation across the ore zones is interpreted as linked to the removal of all veins from the analysed samples. Together, these geochemical indicators and their variations can assist exploration by highlighting hydrothermal alteration trends and define vectors to mineralisation, altogether increasing the size of the targets (Christie and Brathwaite, 2003).

Mineralising fluids

If we consider that sulphide major and trace element signatures reflect the composition of the mineralising fluid responsible for the formation of these sulphides (Pitcairn et al., 2006), then the compositional clustering between V_{2S} and V_{3A} pyrite, on one side, V_{3B} and syn-D_{4S} pyrite on the other side, suggests that at least two distinct mineralising fluids can be distinguished in the Siguiri district. Two hypotheses can be formulated on the possible origins of the compositional variations between these two fluids.

The first hypothesis involves a unique source fluid (Salier et al., 2005) and the effect of physico-chemical processes, to trigger compositional changes and the formation of two distinct mineralising fluids between the V_{3A} and the syn-V_{3B} hydrothermal events. Such changes are typically caused by changes in the fluid-rock or fluid-fluid interactions, such as the modification of the fluid pathway (Voicu et al., 2000) or fluid mixing (Boiron et al., 2003; Ridley and Diamond, 2000). The second hypothesis that can be proposed involves two different source fluids, pumped through the Siguiri district at different time during its hydrothermal evolution. The first fluid was responsible for the deposition of V_{2S} and V_{3A} vein-hosted mineralisation whereas the second fluid deposited syn-V_{3B} and syn-D_{4S} mineralisation. Change from the first fluid to the second may have been caused by a change of source reservoir or by a change in the fluid source chemistry. In this hypothesis, fluid-rock and fluid-fluid interactions (Heinrich, 2007) only play a minor role on the final composition of the two fluids. Further work beyond the scope of this study (e.g. fluid inclusion, stable isotope studies, seismic profiles) would be required to potentially characterise the source(s) of these fluids (Ho et al., 1992; Ridley et al., 2000; Tomkins, 2013).

However, based on field observations of arsenopyrite versus pyrite crystallisation in shale versus greywacke beds and the differences of the geochemical baseline between the Kintinian, Fatoya and Balato Formations (As contents over 5 times lower in the Kintinian Formation compared to the Fatoya and Balato Formations), we suggest that As controls the crystallisation of arsenopyrite over pyrite and is mainly provided by the host rock. This result is

supported by other studies (Pitcairn et al., 2006; Price and Pichler, 2006). Variations in As content also have a direct impact on the unit cell parameters of the pyrite crystal lattice (a, b, c distances between atoms and α , β , γ angles between a, b and c) which affects the capacity of this mineral to contain gold (Large et al., 2011; Savage et al., 2000). This conclusion is highlighted by the covariance in the LA-ICP-MS and EPMA datasets of Au and As in V_{3A} pyrite: more Au is incorporated into the pyrite crystal lattice along with the increase in As (Figure 45F). The low As content of the Kintinian Formation is thus interpreted to be responsible for the low Au content of the syn-V_{3B} pyrite disseminated in the Kintinian conglomerate below the Bidini deposit and outcropping in the Sanu Tinti deposit.

Comparison with other West African orogenic gold deposits

The Siguiri mineralisation footprint has many similarities with other West African orogenic gold deposits. In particular, mineralisation at the Massawa deposit in Eastern Senegal (Treloar et al., 2014) is structurally controlled and hosted along sub-vertical NE-trending shear zones similar to the Kosise deposit. Mineralisation consists of disseminated arsenopyrite/pyrite similar to that found in the Bidini-Sanu Tinti conglomerate and is associated with carbonate-sericite alteration. This first mineralisation event in Massawa is overprinted by late Au-Sb-Te veining absent from in Siguiri. This overprint is associated with coarse visible gold. Mineralisation at the Sadiola Hill deposit in Western Mali (Masurel et al., in press 2015) is structurally controlled and hosted along sub-vertical N-S and NNE-trending shear zones. Au-As-Sb mineralisation is mainly associated with disseminated sulphides but can also be found associated with sulphide veinlets and quartz-carbonate-sulphides-(biotite-tourmaline) veins. Potassic alteration dominates at the Sadiola Hill deposit and is associated with carbonate alteration. Mineralisation at the Yalea deposit in Western Mali (Lawrence et al., 2013a) is structurally controlled and hosted along sub-vertical N-S and NNE-trending shear zones. Mineralisation is comprised of quartz-ankerite-sulphide veins, similar to the Kosise style of mineralisation, and is also associated with chlorite-carbonate-sericite-quartz-albite alteration.

Early Au-Sb-Bi-(Te-W) mineralisation at the Morila deposit in Southeast Mali (McFarlane et al., 2011) is categorised as intrusion-related but is overprinted by As-Au-Ag orogenic style mineralisation. This late overprint is hosted along a NNE-trending shear zone. Mineralisation is characterised by disseminated arsenopyrite containing polygonal gold blebs and is associated with albitisation and the development of titanite. Mineralisation in the Obuasi gold mine in Ghana (Fougerouse et al., 2015) is similar to that in the Siguiri district. Mineralisation in Obuasi is structurally controlled and displays two distinct textures: disseminated gold-bearing sulphides (predominantly arsenopyrite in shale) and quartz-carbonate veins associated with native gold. Obuasi mineralisation is also associated with chlorite-quartz and carbonate alteration (e.g. ankerite, siderite nodules; Fougerouse et al., 2015). Other examples of similar mineralisation footprint in West Africa include Wassa/Benso, Damang (Parra-Avila et al., in review 2015; Pigois et al., 2003).

The structural framework and geochronology of the Kédougou-Kénieba Inlier (KKI), Guinea, Mali, Ghana, and other West African references (Milési et al., 1989; Milési et al., 1992) show that gold mineralisation in West Africa between ca. 2110-2060 Ma, occurred during two main events (Figure 47). Both gold mineralisation events are chronologically associated with two distinct suites of intrusive rocks previously distinguished by Hirdes and Davis (2002).

The first gold mineralisation event occurs between ca. 2102-2085 Ma and is coeval with a first episode of magmatism characterised by the emplacement of granodiorite and felsic flows in the KKI and quartz-diorite in the Morila deposit (McFarlane et al., 2011; Parra-Avila, 2015; Figure 47). This first magmatic event was interpreted as associated with the syn-D_{3Lo} gold-tourmaline event in Loulo (KKI) and with the syn-D_{2M} intrusion related gold mineralisation in Morila and early gold mineralisation at Obuasi (Fougerouse et al., 2015; Lawrence et al., 2013a; Lawrence et al., 2013b; McFarlane et al., 2011).

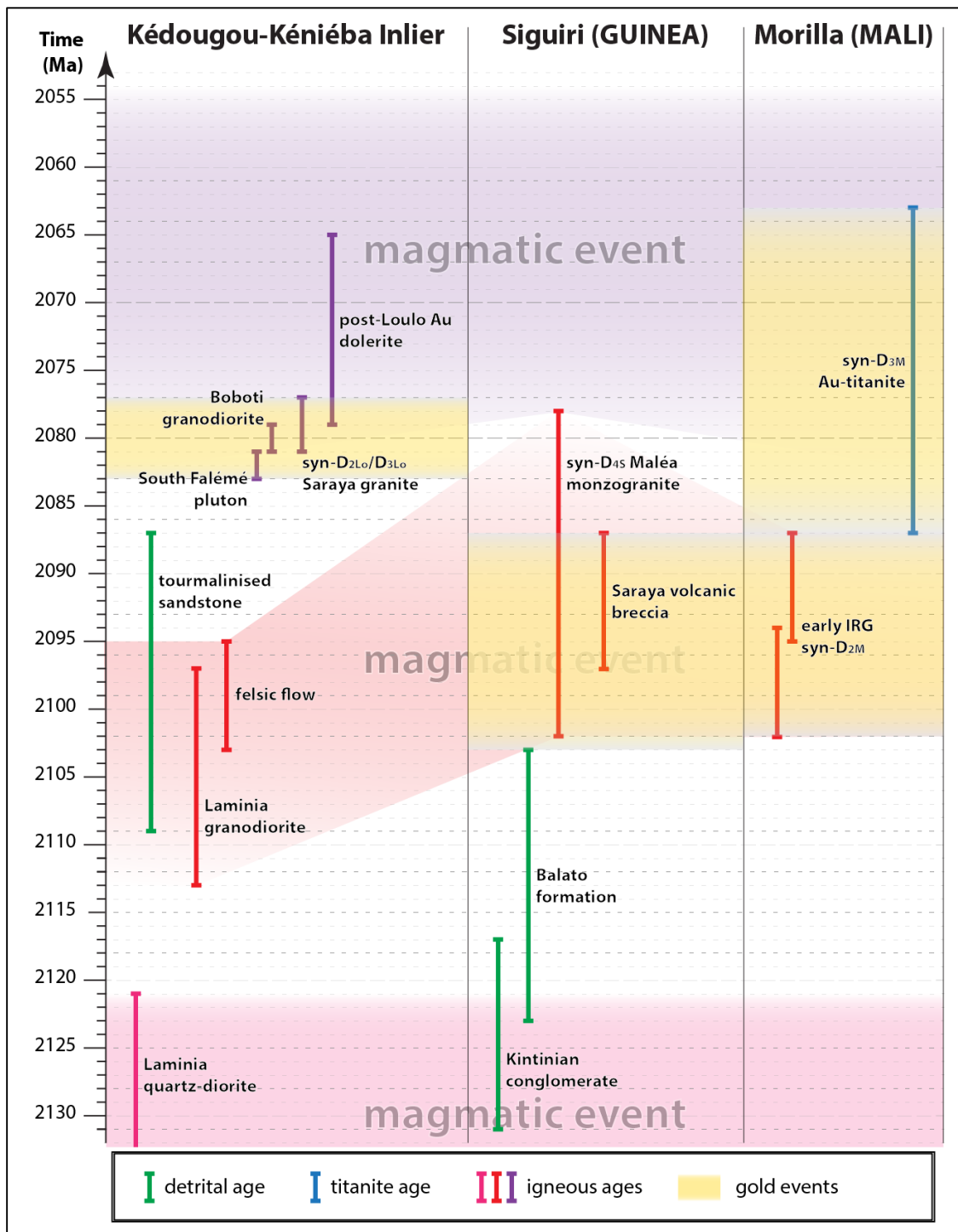


Figure 47: Synthetic time chart comparison of some key late Eburnean gold mineralisation events and their timing.

From Dia et al. (1997), Fougerouse et al. (2015), Hirdes and Davis (2002), Lawrence et al. (2013a), Lawrence et al. (2013b), Lebrun et al. (in review 2015a); Chapter 3, Lebrun et al. (in review 2015b); Chapter 2, Masurel et al. (in press), McFarlane et al. (2011), Miller et al. (in review 2015), Parra-Avila (2015), Parra-Avila et al., (in review 2015).

The second gold mineralisation event was coeval with a younger episode of magmatism responsible for the emplacement of the Saraya granite, Falémé calc-alkaline pluton, Boboti granodiorite and Loulo dolerite in the KKI (Lawrence et al., 2013a; Hirdes and

Davis, 2002; Masurel et al., in press 2015; Figure 47). This younger episode of magmatism, dated between ca. 2085-2054 Ma, is coeval with the second episode of gold mineralisation, recognized in the deposits of Loulo in the KKI, Morila in Mali, as well as Damang and Obuasi in Ghana (Fougerouse et al., 2015; Hirdes and Davis, 2002; McFarlane et al., 2011).

In comparison, the Siguiri district syn-D_{3S} orogenic gold mineralisation (V_{3A} and V_{3B} veining) was overprinted by a latter phase of gold mineralisation or remobilisation, syn-D_{4S}. The D_{4S} deformation was responsible for the development of the NNE-SSW S_{4S} cleavage, sub-parallel to the sub-solidus fabric observed in the Malea monzogranite, outcropping to the north of the district (Figure 32) and emplaced along with the Saraya volcanic breccia during the first episode of magmatism discussed above (Figure 47). Based on the orientation of the S_{4S} cleavage and sub-solidus fabric in the Malea monzogranite, we interpret the emplacement of this intrusive and of the Saraya volcanic breccia as coeval with the formation of the S_{4S} cleavage recognized in the Siguiri district. Thus, it is proposed that the gold events in Siguiri (syn-D_{3S} and syn-D_{4S}) occurred during the ca. 2102-2085 Ma episode of gold mineralisation recognized across the West African Craton. These conclusions have a direct impact on orogenic gold exploration since these suggest that younger economic gold mineralisation coeval with the second episode of magmatism at ca. 2085-2054 Ma, such as the late gold overprint in Morila, could be found in the Siguiri Basin.

Conclusion

The Siguiri district, hosted in the weakly metamorphosed sediments of the Siguiri Basin (Guinea) is characterized by a polyphase hydrothermal history and two textures of the hydrothermal mineral assemblages. The dominant texture, or Kosise style, displays vein haloes structurally controlled by early-D_{3S} N-S, NE-SW, WNW-ESE and E-W damage zones. In comparison, the other texture, or Sanu Tinti style, is only found in the conglomerate interbeds of the Kintinian Formation. The hydrothermal mineral assemblage associated with this style is

disseminated and dominated by pyrite. A discreet structural control can be observed along a N-S thrust fault marking the contact with the Fatoya Formation.

Both styles are associated with gold. The first episode of gold mineralisation is related to the development of the Kosise style V_{3A} pyrite-ankerite veins in which gold can be found locked in the pyrite crystal lattice (Au values up to 43.3 ppm). The second episode of gold mineralisation is associated with the Kosise style V_{3B} quartz-ankerite-arsenopyrite conjugate veins and with the Sanu Tinti style syn-V_{3B} disseminated pyrite. Native gold can be found in the V_{3B} veins and invisible gold (up to 55.5 ppm) can be found locked in the arsenopyrite crystal lattice. Both these gold episodes are overprinted by a late penetrative NNE-SSW S_{4S} cleavage associated with free gold-chalcopyrite-galena infilling V_{3A} pyrite and V_{3B} pyrite and arsenopyrite fractures.

Geochemistry conducted in different deposits and a composite geochemical cross-section across ore shoots reveals that gold mineralisation in the Sigiri district is associated with host rock enrichments in: Ag, Au, As, Bi, Sb, Te and W, typical of mesozonal to hypozonal orogenic gold deposits. These enrichments are also accompanied by additional increases in Co, Mo, Na/Al (molar), Se and S and decreases in Ca, Cs, F, Ga, Hf, 3K/Al (molar), Li, Mg, P and V across the main ore shoot. These chemical changes can be linked to the paragenetic sequence, are indicative of an albite-carbonate-sulphide-sericite alteration associated with the ore shoots and may increase the size of the targets for exploration.

Comparison of the syn-D_{3S} and syn-D_{4S} gold mineralisation timing at the Sigiri district with other orogenic gold deposits from West Africa indicates that these gold mineralisation events are coeval with other gold events recognized Craton-wide at ca. 2102-2085 Ma. The overprinting gold mineralisation event recognized Craton-wide at ca. 2085-2054 Ma is not represented in the Sigiri district but represents the main source of gold in other deposits of the West African Craton (e.g. Morila, Loulo, Sadiola). This study support the idea that gold mineralisation in Sigiri and in West Africa is polyphase and that careful consideration of the Sigiri district mineralisation timings could lead to future gold discovery in the Sigiri Basin.

Acknowledgements

This project was funded by AngloGold Ashanti Limited. Eddie Connell, Shawn Kitt, Katharina Wulff and Craig Duvel are acknowledged for providing site access, support and inspiring discussions. Dr Robert Hart is also thanked for the explanations on how to process XRD data. The authors also acknowledge the facilities, and the scientific and technical assistance of the Australian Microscopy & Microanalysis Research Facility at the Centre for Microscopy, Characterisation & Analysis, the John de Laeter Centre for Isotope Research, The University of Western Australia and Curtin University. Finally, thanks to everyone I could not mention here above.

References

- Allibone, A. H., McCuaig, T. C., Harris, D., Etheridge, M., Munroe, S., Byrne, D., Amanor, J., and Gyapong, W., 2002, Structural Controls on Gold Mineralization at the Ashanti Gold Deposit, Obuasi, Ghana, 9, p. 65-93.
- Armstrong, J. T., 1988, Quantitative analysis of silicates and oxide minerals: Comparison of Monte-Carlo, ZAF and Phi-Rho-Z procedures: Microbeam Analysis, p. 239-246.
- Bateman, R., and Hagemann, S., 2004, Gold mineralisation throughout about 45 Ma of Archaean orogenesis: protracted flux of gold in the Golden Mile, Yilgarn craton, Western Australia: Mineralium Deposita, v. 39, p. 536-559.
- Béziat, D., Naré, G., Matuszak, M., Le Mignot, E., Salvi, S., Fougerouse, D., Siebenaller, L., André-Mayer, A.S., Naba, S. and Franceschi, G, 2013, Etude pétrologique des roches magmatiques associées aux mineralisations Cu-Au du prospect de Gongondy, District de Gaoua, Burkina Faso: AMIRA International Ltd P934A - West African Exploration Initiative - Stage 2 Final report, Appendix E1, p. 446-536, confidential.
- Bierlein, F. P., and Maher, S., 2001, Orogenic disseminated gold in phanerozoic fold belts—examples from Victoria, Australia and elsewhere: Ore Geology Reviews, v. 18, p. 113-148.

Boiron, M.-C., Cathelineau, M., Banks, D. A., Fourcade, S., and Vallance, J., 2003, Mixing of metamorphic and surficial fluids during the uplift of the Hercynian upper crust: consequences for gold deposition: *Chemical Geology*, v. 194, p. 119-141.

Christie, A. B., and Brathwaite, R. L., 2003, Hydrothermal alteration in metasedimentary rock-hosted orogenic gold deposits, Reefton goldfield, South Island, New Zealand: *Mineralium deposita*, v. 38, p. 87-107.

Cook, N. J., Ciobanu, C. L., Meria, D., Silcock, D., and Wade, B., 2013, Arsenopyrite-pyrite association in an orogenic gold ore: tracing mineralization history from textures and trace elements: *Economic Geology*, v. 108, p. 1273-1283.

Craig, J. R., and Vaughan, D. L., 1994, *Ore microscopy & ore petrography – 2nd edition*, John Wiley & Sons, 448 p.

Davis, D., Hirdes, W., Schaltegger, U., and Nunoo, E., 1994, U-Pb age constraints on deposition and provenance of Birimian and gold-bearing Tarkwaian sediments in Ghana, West Africa: *Precambrian Research*, v. 67, p. 89-107.

Dia, A., Van Schmus, W., and Kröner, A., 1997, Isotopic constraints on the age and formation of a Palaeoproterozoic volcanic arc complex in the Kedougou Inlier, eastern Senegal, West Africa: *Journal of African Earth Sciences*, v. 24, p. 197-213.

Donovan, J. J., Snyder, D. A. and Rivers, M. L., 1993, An Improved Interference Correction for Trace Element Analysis: *Microbeam Analysis*, v. 2, p. 23-28.

Donovan, J. J. and Tingle, T. N., 1996, An Improved Mean Atomic Number Correction for Quantitative Microanalysis: *Journal of Microscopy*, v. 2, 1, p. 1-7.

Dubé, B., and Gosselin, P., 2007, Greenstone-hosted quartz-carbonate vein deposits: *Mineral Deposits of Canada: A Synthesis of Major Deposit-Types, District Metallogeny, the Evolution of Geological Provinces, and Exploration Methods*: Geological Association of Canada, Mineral Deposits Division, Special Publication, v. 5, p. 49-73.

- Eilu, P., and Groves, D., 2001, Primary alteration and geochemical dispersion haloes of Archaean orogenic gold deposits in the Yilgarn Craton: the pre-weathering scenario: *Geochemistry: Exploration, Environment, Analysis*, v. 1, p. 183-200.
- Eilu, P., and Mikucki, E. J., 1998, Alteration and primary geochemical dispersion associated with the Bulletin lode-gold deposit, Wiluna, Western Australia: *Journal of Geochemical Exploration*, v. 63, p. 73-103.
- Eilu, P. S., Mathison, C. I., Groves, D. I., and Allardyce, W. J., 1999, Atlas of alteration assemblages, styles and zoning in orogenic lode-gold deposits in a variety of host rock and metamorphic settings, Geology and Geophysics Department (Centre for Strategic Mineral Deposits) & UWA Extension, The University of Western Australia, Publication 30, 50 p.
- Fougerouse, D., Micklethwaite, S., Halfpenny, A., Kilburn, M. and Ulrich, S., 2015, Gold remobilisation from Arsenopyrite: Crystal-plasticity and dissolution-reprecipitation reactions: Proceeding of the SGA conference 2015
- Fougerouse, D., Micklethwaite, S., Ulrich, S., Miller, J., Godel, B., Adams, D. T. and McCuaig, T. C., in press, Evidence for Two Stages of Mineralization in West Africa's Largest Gold Deposit: Obuasi, Ghana: *Economic Geology*
- Goldfarb, R. J., Baker, T., Dube, B., Groves, D. I., Hart, C. J., and Gosselin, P., 2005, Distribution, character, and genesis of gold deposits in metamorphic terranes: *Economic Geology* 100th Anniversary Volume, p. 407-450.
- Groves, D., 1993, The crustal continuum model for late-Archaean lode-gold deposits of the Yilgarn Block, Western Australia: *Mineralium Deposita*, v. 28, p. 366-374.
- Groves, D. I., Goldfarb, R. J., Gebre-Mariam, M., Hagemann, S., and Robert, F., 1998, Orogenic gold deposits: a proposed classification in the context of their crustal distribution and relationship to other gold deposit types: *Ore geology reviews*, v. 13, p. 7-27.
- Groves, D. I., Goldfarb, R. J., Knox-Robinson, C. M., Ojala, J., Gardoll, S., Yun, G. Y., and Holyland, P., 2000, Late-kinematic timing of orogenic gold deposits and significance for

computer-based exploration techniques with emphasis on the Yilgarn Block, Western Australia: *Ore Geology Reviews*, v. 17, p. 1-38.

Groves, D. I., Goldfarb, R. J., Robert, F., and Hart, C. J., 2003, Gold deposits in metamorphic belts: overview of current understanding, outstanding problems, future research, and exploration significance: *Economic Geology*, v. 98, p. 1-29.

Heinrich, C. A., 2007, Fluid-fluid interactions in magmatic-hydrothermal ore formation: *Reviews in Mineralogy and Geochemistry*, v. 65, p. 363-387.

Hirdes, W., and Davis, D., 2002, U-Pb geochronology of paleoproterozoic rocks in the southern part of the Kedougou-Kenieba Inlier, Senegal, West Africa: evidence for diachronous accretionary development of the Eburnean province: *Precambrian Research*, v. 118, p. 83-99.

Hirdes, W., and Nunoo, B., 1994, The Proterozoic paleoplacers at Tarkwa gold mine, SW Ghana; sedimentology, mineralogy, and precise age dating of the Main Reef and West Reef, and bearing of the investigations on source area aspects: *Geologisches Jahrbuch D*, v. 100, p. 247-311.

Ho, S., Groves, D., McNaughton, N., and Mikucki, E., 1992, The source of ore fluids and solutes in Archaean lode-gold deposits of Western Australia: *Journal of Volcanology and Geothermal Research*, v. 50, p. 173-196.

Kishida, A., and Kerrich, R., 1987, Hydrothermal alteration zoning and gold concentration at the Kerr-Addison Archean lode gold deposit, Kirkland Lake, Ontario: *Economic Geology*, v. 82, p. 649-690.

Large, R. R., Bull, S. W., and Maslennikov, V. V., 2011, A carbonaceous sedimentary source-rock model for Carlin-type and orogenic gold deposits: *Economic Geology*, v. 106, p. 331-358.

Large, R., Thomas, H., Craw, D., Henne, A., and Henderson, S., 2012, Diagenetic pyrite as a source for metals in orogenic gold deposits, Otago Schist, New Zealand: *New Zealand Journal of Geology and Geophysics*, v. 55, p. 137-149.

Lawrence, D. M., Treloar, P. J., Rankin, A. H., Harbridge, P., and Holliday, J., 2013a, The geology and mineralogy of the Loulo Mining District, Mali, West Africa: evidence for two distinct styles of orogenic gold mineralization: *Economic Geology*, v. 108, p. 199-227.

Lawrence, D. M., Treloar, P. J., Rankin, A. H., Boyce, A., and Harbridge, P., 2013b, A fluid inclusion and stable isotope study at the Loulo mining district, Mali, West Africa: Implications for multifluid sources in the generation of orogenic gold deposits: *Economic Geology*, v. 108, p. 229-257.

Lebrun, E., Miller, J., Thébaud, N., Ulrich, S., and McCuaig, C., in review 2015a, Structural controls on an orogenic gold system: The world-class Siguiri gold district, Siguiri Basin, Guinea, West Africa: *Economic Geology*.

Lebrun, E., Thébaud, N., Miller, J., Ulrich, S., Bourget, J., and Terblanche, O., in review 2015b, Geochronology and lithostratigraphy of the Siguiri district: implications for gold mineralisation in the Siguiri Basin (Guinea, West Africa): *Precambrian Research*.

López-Moro, F. J., 2012, EASYGRESGRANT—A Microsoft Excel spreadsheet to quantify volume changes and to perform mass-balance modeling in metasomatic systems: *Computers & Geosciences*, v. 39, p. 191-196.

Masurel, Q., Thébaud, N., Miller, J., Ulrich, S., Hein, K.A.A., Cameron, G., Béziat, D. and Bruguier, O., in press 2015, Sadiola Hill: a world-class gold deposit in Mali, West Africa: *Economic Geology*.

McFarlane, C. R. M., Mavrogenes, J., Lentz, D., King, K., Allibone, A., and Holcombe, R., 2011, Geology and Intrusion-Related Affinity of the Morila Gold Mine, Southeast Mali: *Economic Geology*, v. 106, p. 727-750.

Milési, J. P., Feybesse, J. L., Ledru, P., Dommange, A., Ouedraogo, M. F., Marcoux, E., Prost, A., Vinchon, C., Sylvain, J. P., Johan, V., Teguey, M., Calvez, J. Y., and Lagny, P., 1989, Les minéralisations aurifères de l'Afrique de l'Ouest. Leurs relations avec l'évolution lithostructurale au Protérozoïque inférieur: *Chronique de la recherche minière*, v. 497, p. 3-98.

Milési, J.-P., Ledru, P., Feybesse, J.-L., Dommaget, A., and Marcoux, E., 1992, Early Proterozoic ore deposits and tectonics of the Birimian orogenic belt, West Africa: Precambrian Research, v. 58, p. 305-344.

Miller, J., Bourassa, Y., Fougerouse, D., Davis, J., Ulrich, S., Apau, D., Jessell, M., McCuaig, C. and Perrouty, S., in review 2015, Structural evolution of gold systems in the world class Ashanti Belt, Ghana : insights into the evolution of a world class gold district: Economic Geology

Miller, J. M., Davis, J., Baratoux, L., McCuaig, T. C., Metelka, V. and Jessel, M., 2013, Evolution of gold systems in Guinea, southern Mali and western Burkina Faso: AMIRA International Ltd P934A - West African Exploration Initiative - Stage 2 Final report, Appendix D1, p. 127-234, confidential.

Neumayr, P., Walshe, J., Hagemann, S., Petersen, K., Roache, A., Frikken, P., Horn, L., and Halley, S., 2008, Oxidized and reduced mineral assemblages in greenstone belt rocks of the St. Ives gold camp, Western Australia: vectors to high-grade ore bodies in Archaean gold deposits?: Mineralium Deposita, v. 43, p. 363-371.

Oberthür, T., Vetter, U., Davis, D. W., and Amanor, J. A., 1998, Age constraints on gold mineralization and Paleoproterozoic crustal evolution in the Ashanti belt of southern Ghana: Precambrian Research, v. 89, p. 129-143.

Parra-Avila, L. A., 2015, 4D Evolution of the Paleoproterozoic Baoulé-Mossi Domain of the West African Craton: PhD thesis, University of Western Australia

Parra-Avila, L. A., Bourassa, L., Miller, J., Perrouty, S., Fiorentini, M. L. and McCuaig, T. C., in review 2015, Age constraints of the Wassa and Benso Mesothermal Gold Deposits, Ashanti Belt, Ghana, West Africa: Journal of African Earth Sciences

Passchier, C. W., and Trouw, R. A. J., 2005, Microtectonics, Springer, 366 p.

Paton, C., Hellstrom, J., Paul, B., Woodhead, J. and Herdt, J. 2011. Iolite: freeware for the visualization and processing of mass spectrometer data. Journal of Analytical Atomic Spectrometry 26, 2508-2518.

- Pigois, J.-P., Groves, D., Fletcher, I., McNaughton, N., and Snee, L., 2003, Age constraints on Tarkwaian palaeoplacer and lode-gold formation in the Tarkwa-Damang district, SW Ghana: *Mineralium Deposita*, v. 38, no. 6, p. 695-714.
- Pitcairn, I. K., Teagle, D. A., Craw, D., Olivo, G. R., Kerrich, R., and Brewer, T. S., 2006, Sources of metals and fluids in orogenic gold deposits: insights from the Otago and Alpine Schists, New Zealand: *Economic Geology*, v. 101, p. 1525-1546.
- Price, R. E., and Pichler, T., 2006, Abundance and mineralogical association of arsenic in the Suwannee Limestone (Florida): Implications for arsenic release during water–rock interaction: *Chemical Geology*, v. 228, p. 44-56.
- Ramsay, J. G., and Huber, M. I., 1987, The techniques of modern structural geology: Vol.2: Folds and fractures: London, Academic Press.
- Ridley, J. R., and Diamond, L. W., 2000, Fluid chemistry of orogenic lode gold deposits and implications for genetic models: *Gold* in, 2000, p. 141-162.
- Robert, F., Poulsen, K. H., Cassidy, K. F., and Hodgson, C. J., 2005, Gold metallogeny of the Superior and Yilgarn cratons: *Economic geology*, v. 100, p. 1001-1033.
- Salier, B. P., Groves, D. I., McNaughton, N. J., and Fletcher, I. R., 2005, Geochronological and stable isotope evidence for widespread orogenic gold mineralization from a deep-seated fluid source at ca 2.65 Ga in the Laverton gold province, Western Australia: *Economic Geology*, v. 100, p. 1363-1388.
- Savage, K. S., Tingle, T. N., O'Day, P. A., Waychunas, G. A., and Bird, D. K., 2000, Arsenic speciation in pyrite and secondary weathering phases, Mother Lode gold district, Tuolumne County, California: *Applied Geochemistry*, v. 15, p. 1219-1244.
- Taylor, R., 2010, Ore textures: recognition and interpretation, Springer Science & Business Media.
- Tomkins, A. G., 2013, On the source of orogenic gold: *Geology*, v. 41, p. 1255-1256.
- Vaughan, D.J. and Craig, J. R., 1978, Mineral chemistry of metal sulfides: Cambridge University Press, 493 p.

Voicu, G., Bardoux, M., Stevenson, R., and Jebrak, M., 2000, Nd and Sr isotope study of hydrothermal scheelite and host rocks at Omai, Guiana Shield: implications for ore fluid source and flow path during the formation of orogenic gold deposits: Mineralium Deposita, v. 35, p. 302-314.

Wilkinson, J., Boyce, A., Earls, G., and Fallick, A., 1999, Gold remobilization by low-temperature brines; evidence from the Curraghinalt gold deposit, Northern Ireland: Economic Geology, v. 94, p. 289-296.

Zhao, H.-X., Frimmel, H. E., Jiang, S.-Y., and Dai, B.-Z., 2011, LA-ICP-MS trace element analysis of pyrite from the Xiaoqinling gold district, China: implications for ore genesis: Ore Geology Reviews, v. 43, p. 142-153.

CHAPTER 5: CONCLUSIONS

4D EVOLUTION OF THE SIGUIRI DISTRICT – IMPLICATIONS FOR THE WEST AFRICAN CRATON AND GOLD EXPLORATION

This thesis presents an integrated lithostratigraphic, geochronological, structural and geochemical study of the Siguiri district and of its hosting sedimentary basin, the Siguiri Basin. Eleven deposits from the district were studied as well as a number of key locations across the Basin. A wide variety of datasets, tools and analytical techniques were used, ranging from fieldwork and the taking of structural readings to in-situ LA-ICP-MS. The work was organised to: 1) characterise the Siguiri Basin lithostratigraphy and its tectonic context during the Eburnean orogeny; 2) determine the controls on gold mineralisation affecting the Siguiri district, 3) understand the evolution of the Siguiri district and its current architecture, and; 4) characterise the district mineralisation and footprint. The major findings of this thesis and their implications in the understanding of the West African Craton formation and for gold exploration are detailed below.

LITHOSTRATIGRAPHY AND TECTONICS

- The Siguiri district is hosted in three distinct sedimentary Formations. From east to west: the Balato, Fatoya and Kintinian Formations.
- The Kintinian Formation is stratigraphically on top of the Fatoya Formation, itself overlying the Balato Formation.
- The three Formations are mainly derived from granitic rocks dated at around ca. 2015 Ma.
- The Balato and Fatoya Formations and their facies association are characteristic of a basal regressive sequence, whereas the overlying Kintinian Formation display stacks of polymict conglomerate interpreted to be the product of debris flow events.
- However, comparison of the lithostratigraphy and geochronology of the Kintinian Formation with the rest of the West African Craton suggests that this Formation is part of the Lower Tarkwa Group, typically described as "late orogenic basin"-type sediments.
- The Kintinian stacks of polymict conglomerate were interpreted to represent an olistostrome and can be followed throughout the whole Siguiri Basin.
- The deposition of this olistostrome is interpreted to mark a change in the dynamics of the Siguiri Basin opening, and the onset of increased tectonic activity associated with the first phases of Eburnean compression.
- The peculiar shape of the Kintinian olistostrome highlights the early architecture of the Siguiri Basin and is controlled by N-S, NE-SW and WNW-ESE faults presumed to represent fundamental structures that controlled the location of the Siguiri district in the Basin.

DEFORMATION EVENTS

- Four deformation events were recognized to affect the sediments of the Siguiri district: a cryptic N-S compression (D_{1S}), an E-W to ENE-WSW compression (D_{2S}) that is interpreted as progressively evolving into a transpression (early- D_{3S}) and then into a NNW-SSE transtension (late- D_{3S}), and finally a NW-SE compression (D_{4S}).
- The D_{1S} deformation event is mainly characterized by F_{1S} recumbent folds with E-W to NW-SE and NE-SW striking axial traces. A discreet S_{1S} cleavage, shallowly to moderately dipping to the WSW was locally observed in the northernmost part of the Siguiri district.
- The D_{2S} deformation event is responsible for the N-S structural grain observed across the Siguiri district and Siguiri Basin. This event is characterised by F_{2S} upright folds with NNE-SSW to NNW-SSE striking axial planes that refolds F_{1S} folds and create fold interference patterns. While no axial planar cleavage was found associated with the F_{2S} folds, bedding parallel and en-echelon V_{2S} veins developed during flexural slip along these fold hinges.
- The early- D_{3S} deformation is responsible for the development (or reactivation) of N-S thrusts, E-W normal faults, NE-SW dextral shear zones and WNW-ESE sinistral shear zones.
- The N-S, E-W, NE-SW and WNW-ESE structures control the development of late- D_{3S} veining (V_{3S}) and the location of ore shoots across the Siguiri district.
- The D_{4S} deformation event overprinted all previously developed structural features, locally refolds V_{3S} veins and develops a sub-vertical NE-SW striking S_{4S} cleavage.
- The mineralised structures are often found to be discreet incipient structures developed as ten to fifteen meters wide sub-vertical areas of dense V_{3S} veining,

lacking structures marked by discrete planes of fabric development across which there is offset.

- Finite strain and paleo stress-field analysis indicate that the stress-field variations from D_{2S} E-W compression to early-D_{3S} transpression and then to late-D_{3S} NNW-SSE transtension may have had a regional origin.
- The homogenisation of the stress-tensor and reduced differential stress, responsible for these stress-switches, is interpreted to be a prerequisite for the development of orogenic gold mineralisation.

HYDROTHERMAL ACTIVITY, MINERALISATION AND GEOCHEMISTRY

- Hydrothermal activity in the Sigiri district was found to be polyphase and characterised by four distinct events, taking place during D_{2S}, D_{3S} and D_{4S} deformations.
- The first three hydrothermal events are mainly associated with the development of three generations of veins (V_{2S}, V_{3A} and V_{3B}) whereas the last event (syn-D_{4S}) is characterised by pervasive hydrothermal activity associated with a penetrative cleavage (S_{4S}).
- LA-ICP-MS was used to compare the different trace element signatures of the sulphides associated with these hydrothermal events and constrain their relative timing.
- Three of these four hydrothermal events are gold bearing: the pyrite lattice from V_{3A} veins contains up to 43.3 ppm of gold, V_{3B} veins contain native gold and the lattice of the arsenopyrite associated with these veins also contains up to 55.5 ppm of gold, and D_{4S} deformation is interpreted to fracture previously developed sulphides and precipitate gold in their fractures.
- High grade zones are typically associated with carbonatation, bleaching and minor albitisation of the host rock.

- Geochemical variations across the ore shoots of the Siguiri district show enrichments in: Ag, Au, As, Bi, Co, Mo, Sb, Se, SO₃, Te and W. CaO was found to mark the reaction front of the mineralising fluids and 3K/Al and Na/Al modal saturation indices were found to highlight the discreet ore shoots over distance up to 10 to 15 meters.
- Comparison between the timing of gold mineralisation in the Siguiri district and other gold deposits in the West African Craton, indicates that syn-D_{3S} gold is uncommon in the rest of the Craton whereas economic syn-D_{4S} gold could be found in the Siguiri Basin.

CONCLUDING REMARKS AND FUTURE WORK

In terms of academic research, this work improves the understanding of the Siguiri Basin formation and of its tectono-stratigraphic position in the evolution of the West African Craton throughout the Eburnean orogeny. This work identifies the fundamental structures which control the morphology of the Basin, the main lithostratigraphic Formations exposed and gives an interpretation of their environment of formation. In addition, this work also introduces the concept of stress-switch as a critical process and a pre-requisite (or cause) for orogenic gold mineralisation rather than as a passive effect of the fault-valve process.

In terms of gold exploration, this thesis highlights the necessity of using a multi-scale and multi-disciplinary approach to understand the genesis and controls affecting world-class orogenic gold districts. In the case of the Siguiri district, the new understanding of the early architecture of the Siguiri Basin emphasises the role it played as a first order control on the location of the Siguiri district. This conclusion emphasises the importance of understanding the overall tectonic history of a province to aid mineral exploration. Geochronology, geophysics and structural geology are crucial tools to be used during this first step. Down one scale to the Siguiri Basin to district scale, second and third order structures can be targeted through the use of geophysics, structural geology and to some extent, geochemistry. At a deposit scale,

field observations and geochemistry appeared to be the most important tools to target ore shoots in the Siguiri district.

However, several key questions remain to be answered. Even though a model is proposed, further work would be required to fully assess how the Siguiri Basin opened and how was the extension oriented. Multiple deformation events and cleavages were observed in the Siguiri district and even though the main events and most visible cleavages are now well constrained, further work would be required to assess the importance of the D_{1S} N-S compression in the Siguiri Basin and the development of its associated cleavage. The number of fluids responsible for the four hydrothermal events observed in the Siguiri district and their respective composition could not be constrained in this thesis but could be constrained by a fluid inclusion and stable isotope study. These studies could potentially also give an answer as to where the fluid(s) and the gold originated from, even though this question has been the subject of a still ongoing debate in the literature.

ELECTRONIC APPENDICES

TABLE 1: SHRIMP DATA FOR THE SIX GEOCHRONOLOGICAL SAMPLES.

TABLE 2: SUMMARY TABLE OF THE PAST PRODUCTION OF THE SIGUIRI DISTRICT. GOLD GRADE (IN G/T) AND GOLD EXTRACTED (IN T) FOR SOME OF THE MAIN DEPOSITS DISCUSSED IN THE TEXT ARE DETAILED.

TABLE 3: GEOCHEMISTRY AND XRD DATA. ANALYSES BELOW DETECTION LIMIT IN RED.

TABLE 4: SUMMARY TABLE OF THE METHODOLOGY USED FOR THE LA-ICP-MS ANALYSES.

TABLE 5: LA-ICP-MS AND EPMA (FOR Fe AND As) DATA. CERTIFIED SULFIDE STANDARD LAFLAMME Po726 WAS USED TO CONSTRAIN LA-ICP-MS RESULTS FOR Au AND S. ANALYSES BELOW DETECTION LIMIT OR MISSING (NAN) ARE HIGHLIGHTED IN RED.

TABLE 6: SUMMARY TABLE OF THE LIMITS OF DETECTION ASSOCIATED WITH THE GEOCHEMICAL DATA.